Removal of toxic industrial chemicals using novel adsorbent hollow fibres

Jeffs, Corinne

Award date:
2015

Awarding institution:
University of Bath

Removal of toxic industrial chemicals using novel adsorbent hollow fibres

Corinne Ailsa Jeffs

A thesis submitted for the degree of Doctor of Philosophy

University of Bath

Department of Chemical Engineering

February 2015

…….

Table of Contents

List of tables

List of figures

Acknowledgements

My thanks to all those who have assisted me with lab work during my thesis.

Thank you to Valeska, Gabriele, Anne, Ursula, John Mitchels, John Bishop, Fernando, Bob, Rich, Suzanne, Marianne and Dan for their kind assistance using lab equipment at Bath and Amy, Charlotte, Tanya, Barry, Paul and Sue for their help.

Thank you to Neil, Kadhum and Grazia at the University of Cardiff for their input into and extremely helpful comments on my first paper.

Thank you to James Nevell for helping me get started and keeping me company on long days in the lab, and to Olivier for his mathematical expertise.

Heartfelt thanks to Tom Richards for his patience, kindness, camaraderie and extremely dedicated hard work.

Thank you to my friends in and outside of the office who helped me through the years. Especially to Kah Peng, my desk neighbour and teaching buddy, for all the help and information he's given me; Hannah, for always caring for everybody and remembering all the birthdays; Will, for many cups of coffee and biscuits; and most of all to Ben for being my first friend in the department and helping me to settle in.

Thank you to my family for their ongoing support and a good glass of wine!

Many thanks for Martin and Corinne for all their help, friendliness and hard work over the years.

Thank you to Semali for giving me a chance.

Thank you to Sam. I wouldn't have made it without you.

I wish you all the best for the future.

Declaration of work done in conjunction with others

Some elements of the work in this thesis were carried out by my colleagues.

Thomas Richards spun and prepared some of the hollow fibres.

Martin Smith measured cyclohexane, octane and water isotherms at Dstl, Porton Down.

Kadhum Msayib and Grazia Bezzu measured nitrogen isotherms at the University of Cardiff, which were used to calculate BET surface areas.

Graphs of the above are indicated in the relevant Sections.

Abstract

The current military respirator provides protection from contaminants using a cartridge packed with adsorbent activated carbon particles treated with metal salts to provide protection from toxic gases. However, the user of this respirator is subject to a physiological burden as a result. One component of this burden is the pressure drop, which makes breathing through the respirator filter difficult, with the burden becoming more severe at higher breathing rates. This project investigates the reduction of pressure drop and hence burden in respirator cartridges by using adsorbent hollow fibres. These are made up of adsorbent powder held together with a polymer binder to replace the conventional adsorbent particles. Adsorbent hollow fibres have a number of advantages, including lower pressure drop, the ability to operate in any orientation, no special filling requirements and customisability against emerging threats, such as toxic industrial chemicals. Dynamic challenges were performed using ammonia, hydrogen sulphide and cyclohexane as candidate gases, as each typifies a particular category of toxic industrial chemicals. Adsorbent hollow fibres were customised by treating with metal salts, metal organic frameworks and pore forming agents, and by replacing the hollow fibre polymer binder with a novel microporous polymer. In addition, the pressure drop of these adsorbent fibres was compared to granular beds. Pressure drop was then modelled using the Hagen-Poiseuille equation, and the breakthrough time was modelled with the Wheeler-Jonas equation, enabling the prediction of pressure drop and breakthrough time for new designs of adsorbent hollow fibre cartridges.

Nomenclature and abbreviations

Acronyms

AC	Activated carbon
Dstl	Defence Science and Technology Laboratory
GAC	Granular activated carbon
IDLH	Immediately dangerous to life or health
LDF	Linear driving force
LES	Length of equilibrium section
LMTZ	Length of mass transfer zone
LUB	Length of unused bed
MOF	Metal organic framework
MTZ	Mass transfer zone
NMP	N-methyl pyrrolidone
PIM	Polymer of intrinsic microporosity
PES	Polyethersulfone
THF	Tetrahydrafuran
TIC	Toxic industrial chemical
WJ	Wheeler-Jonas

Roman letters

a_0	fraction of empty surface
a_1	fraction of surface occupied by adsorbate
b	a constant
B	structural constant of the carbon (K^{-2})
B_0	k_0/k'_1
B_1	B_0/RT
C	constant, dimensionless, >1 and dependent on temperature
c_{out}	breakthrough concentration
C_0	contaminant inlet concentration in air (g/cm^3)
C	adsorbate concentration
C_b	contaminant breakthrough concentration (g/cm^3)
C_s	concentration at saturation vapour pressure (g/cm^3)
C_{solid}	concentration in adsorbed phase
$C_{monolayer}$	concentration in adsorbed phase when monolayer is complete

d_L	liquid density of organic vapour (g/cm^3)
d_p	particle diameter (m)
k_0	velocity constant for adsorption on an empty surface
k'_1	velocity constant for desorption from a monolayer
k_c	mass transfer coefficient
k_v	overall adsorption rate coefficient (min^{-1})
K	adsorption constant
L	bed length (cm)
M	weight of carbon bed (g)
Mw	molecular weight of vapour (g/mol)
P	pressure
P_b	bulk density of carbon bed (g carbon/cm^3)
Q	volumetric flow rate (g/cm^3)
R	ideal gas constant
T	temperature (K)
T_g	glass transition temperature
T_m	melting temperature
t_b	breakthrough time to reach c_{out} (min)
t_s	stoichiometric time
u	superficial velocity (m/s)
v	total volume adsorbed
v_L	superficial velocity
v_m	volume of gas adsorbed to form a monolayer
V	concentration of adsorbate in the solid phase
W	adsorbate loading
W_e	equilibrium adsorption capacity (g/g carbon)
W_o	micropore volume (cm^3/g carbon)
x	P/P_0

Greek letters

B	affinity coefficient of organic vapour (-)
ε	voidage (m)
μ	fluid viscosity (Pa·s)
ρ	fluid density (kg/m^3)

1 Introduction

Nerve agents were first developed in Germany in 1936 and led to such notorious chemical weapons as tabun, soman and sarin. However, these were not extensively used during the Second World War, primarily due to fear of retaliation. While these nerve agents are relatively easy and cheap to synthesise and transport, they can have a great many negative implications for those deploying them. A particular problem associated with nerve agents was demonstrated by the use of sarin by Aum Shinrikyo on the Tokyo Underground in 1995. In synthesising sarin, they drew the attention of the authorities having purchased the necessary precursors (Tucker, 2007). Other issues of such agents include storage, particularly in the long term, and disposal. Due to these problems there is a fear that terrorist groups may resort to opportunistic attacks using readily available industrial chemicals, such as ammonia or chlorine, as weapons. These are known as toxic industrial chemicals (TICs).

Protection from toxic chemicals is achieved using respirators when exposure cannot be avoided. The military gas mask is an air purifying respirator containing a mechanical filter to remove particulates and an adsorbent bed containing a large amount of activated carbon granules treated with chemicals to improve performance. Smaller granules have a higher available surface area for adsorption, but greater pressure drop (Yang, 1997). As such they provide greater protection for longer at the cost of comfort. In the military, gas masks must often be worn for long periods of time. It is vital that users are able to remain effective in a number of tasks, but a large pressure drop in a respirator is associated with a high burden, making everyday tasks challenging for wearers.

This research focuses on developing and producing novel hollow fibre adsorbents to replace granular packed cartridges. These fibres are made of a polymer and an adsorbent. They do not obstruct gas flow, and as such do not result in such high pressure drop. This will reduce the strain on people wearing gas masks over long periods and help to improve their performance. Hollow fibres also do not require a special packing technique, making them easier to use than granules. They will operate in any orientation and are fixed in position, lowering the risk of bypass or leakage through the respirator inlet, particularly after mechanical stress. Fibres also weigh less than an equivalent volume of granules. This, coupled with the decreased pressure drop, will enable the development of novel respirator designs using longer cartridges that fall within weight and pressure drop constraints.

1.1 Aims and objectives

The overall aim of this project is to develop novel hollow fibre modules with low pressure drop for use in respirator filters. These will be tailored to remove toxic industrial chemicals, while following EU regulations for stability and performance.

The objectives are to:

1. Determine the optimal adsorbents for removal of the model gases ammonia, hydrogen sulphide and cyclohexane, and prepare selected adsorbent encapsulated hollow fibres.
2. Optimise the hollow fibre structure for the greatest adsorption uptake, fastest adsorption kinetics and lowest pressure drop.
3. Explore ways to enhance adsorption using additives, such as metal salts, metal organic frameworks and pore formers.
4. Investigate an alternative microporous polymer for use as the binder in hollow fibres.
5. Model pressure drop and breakthrough time for a candidate novel hollow fibre respirator filter using the data collected.
6. Develop performance indices that will allow comparison of adsorbent hollow fibre and conventional granular adsorbent performance relative to their weight and pressure drop.

1.2 Structure of report

Chapter 2 presents information relevant to the project with a detailed literature review in the areas of toxic industrial chemicals, respirators, adsorbents and structured adsorbents, chemical impregnation, polymers and pore formers. Chapter 2 also includes a review of the theory pertinent to the project, including adsorption, breakthrough curves, mass transfer and pressure drop.

Chapter 3 contains all of the experimental techniques used in this project.

Chapter 4 presents the screening of adsorbents for use in hollow fibres for removal of ammonia, hydrogen sulphide and cyclohexane. It also contains information regarding the optimisation of hollow fibre structure and pressure drop. These are then compared to packed beds of pellets.

Chapter 5 focuses on modifying hollow fibres to improve adsorption of hydrogen sulphide by including metal salts in the structure. It also explores the possibility of using novel metal organic frameworks. In addition, the use of pore former additives is explored.

Chapter 6 presents research into replacing the conventional PES polymer binder in hollow fibres with a novel polymer of intrinsic microporosity (PIM-1) and explores ways to enhance the adsorption kinetics of the hollow fibres.

Chapter 7 brings together the gathered results to allow modelling of pressure drop and breakthrough times for a novel respirator filter design.

Chapter 8 presents future work that could be carried out following this project, Chapter 9 contains the overall conclusion of the work, Chapter 10 the references and Chapter 11 the appendices.

2 Background information

2.1 Literature review

2.1.1 Toxic Industrial Chemicals

Toxic industrial chemicals (TICs) are chemicals commonly used through industry with a range of hazardous properties, such as being explosive, corrosive or poisonous. As industrial chemicals, they are easily available, and an attack using TICs could expose a huge number of people to a mixture of dangerous chemicals. As an example, industrial chlorine has been used against people on several occasions; such as by the German army in World War I, where chlorine was obtained as a side product of dye production; and the recent chlorine bombings in Iraq, where it is used for water purification.

Many security groups have considered the top TICs of concern, generally rating them according to a hazard index. This reflects factors such as the volume in which a chemical may be present in a country or area of concern, the chemical inhalation toxicity, and whether it can present an inhalation hazard in its physical state. As such the hazard rating of chemicals will vary from country to country. An example of different TICs of high concern is shown in Table 2.1. For example, hydrogen cyanide and formaldehyde are precursors to a number of pharmaceuticals, ammonia is a well-known component of fertiliser, hydrogen fluoride is a catalyst in alkylation processes (Aigueperse *et al.*, 2000), and even phosgene, a chemical weapon in World War 1, now finds use as a precursor in the production of thermoplastics (Schneider and Diller, 2000).

Table 2.1. Toxic industrial chemicals with high hazard ratings from NATO International Task Force 25 (ITF-25) (Hincal and Erkekoglu, 2006).

TISSUE IRRITANTS	SYSTEMIC POISONS
Ammonia	Arsine
Boron trichloride	Boron trifluoride
Fluoride	Diborane
Formaldehyde	Ethylene oxide
Phosphorus trichloride	Hydrogen fluoride
Phosgene	Hydrogen sulfide
Hydrogen bromide	Carbon disulfide
Hydrogen chloride	Cyanide
Chlorine	Tungsten hexafluoride
Nitric acid	
Sulfur dioxide	
Sulfuric acid	

The agency that determines whether respirators meet UK standards is the British Standards Institution (BSI). They split chemicals into 4 groups of threats known as ABEK, with each letter representing a different type of contaminant. A represents organic vapours and gases with their boiling point over 65 °C; B represents inorganic gases (not including carbon monoxide); E represents sulphur dioxide and acidic gases; K represents ammonia and its derivatives. In addition, there are AX filters (for gases with boiling point below 65 °C), Hg filters (for mercury) and NO filters (for nitrogen oxides, or NO_x). Obviously a detailed literature review of every toxic industrial chemical is beyond the scope of this work. As such a gas from three of these groups was selected as a representative 'model' gas for this research. These model gases are cyclohexane (A), hydrogen sulphide (B), and ammonia (K).

2.1.1.1 Ammonia

Ammonia is a colourless, basic gas, with a distinctive and very pungent odour. The NIOSH exposure levels are 25 ppm as a weighted average over 10 h, or 35 ppm over short term exposure, or15 minutes (NIOSH, 2010). It is toxic through all routes, and the gas is a severe irritant to the eyes, skin and respiratory tract. At extremely high concentrations (>5000 ppm), death can result from spasm, inflammation and oedema of the larynx (HSDB, 2006). Over 1 million tonnes of ammonia are produced in the UK annually, the majority of which is used in the agricultural industry as a fertiliser, though it is also involved in the synthesis of dyes, plastics, synthetic fibres and explosives (Pritchard, 2011).

Due to the basic nature of ammonia and its small molecule size of 3Å (Thompson, 1971), ammonia will only be effectively adsorbed onto sorbents with an acidic surface and very small pores. As activated carbon has a wide range of relatively large pore sizes such as 10-20Å (Yang, 1997) and does not have high surface acidity, it is relatively ineffective at adsorbing ammonia without further treatment (i.e., chemical impregnation, acidification etc.).

Predicting a good adsorbent for ammonia removal can be difficult. In general, greater adsorption is seen in materials with higher surface area and hence higher capacity on the surface for adsorption. However greater quantities of ammonia were adsorbed onto

carbons with lower surface areas in one study. This was attributed to smaller average micropore sizes and a higher density of surface oxygen groups, to which ammonia can hydrogen bond (Lee and Reucroft, 1999).

In general, ammonia adsorption on activated carbons is enhanced in the presence of water, as highly soluble ammonia dissolves in water on the large surface area of the carbon, forming ammonium ions. These can react with dissociated carboxylic groups on the carbon via Brønsted acid-base interactions (Bandosz and Petit, 2009). To enhance weak ammonia adsorption on carbon in dry conditions, a number of chemical impregnants on an adsorbent support can be used. Ammonia has been found to sorb effectively onto many metal salts, particularly copper (II) salts including copper oxide (Smith *et al*., 2010) and chloride (Petit *et al*., 2007). $ZnCl_2$ has also been used as an impregnant, which increases loading of ammonia (Petit *et al.*, 2007; Fortier *et al.*, 2008). Carbons have also been impregnated with sulphuric acid to lower their pH. (Guo *et al.*, 2009) showed that this improved ammonia uptake and was unaffected by humidity

Some zeolites may be more effective adsorbents for ammonia than activated carbons due to their acidic nature and the availability of Bronsted and Lewis acid sites (Valyon *et al*., 1998). At atmospheric pressures, adsorption of NH_3 on 13X and 4A zeolites was found to be superior to adsorption on activated carbon, alumina or silica gel (Helminen *et al.*, 2000). However, the presence of atmospheric water may interfere with ammonia adsorption. For example, ammonia adsorption on silica gel was reduced by the presence of water (Blomfield and Little, 1973).

2.1.1.2 Hydrogen sulphide

The second model gas selected was hydrogen sulphide (H_2S). This is a colourless gas with a distinctive rotten egg-like odour. H_2S has a number of physiological effects, one of which, making H_2S particularly dangerous is that it causes olfactory fatigue at 100 ppm and olfactory nerve paralysis at 150 ppm, meaning that people exposed to H_2S lose their sense of smell (Sullivan and Krieger, 1992). The other effects of H_2S include eye irritation, with conjunctivitis at 5 ppm. At 50-250 ppm, hydrogen sulphide will affect the entire respiratory tract, causing rhinitis, bronchitis, laryngitis, pharyngitis and pneumonia (Sullivan and Krieger, 1992). The effects become severe at 200 ppm, with death

occurring after exposure to 600 ppm for 30 minutes or 800 ppm immediately (Verschueren, 2001), making reliable face masks a necessity on exposure. A great deal of research into hydrogen sulphide removal has stemmed from its presence in natural gas (ATSDR, 2006). Hydrogen sulphide adsorption into packed beds is typically carried out on activated carbon or zeolites, and is influenced strongly by temperature, humidity and several characteristics of the adsorbent, namely; pore size, surface area and pH (Bagreev *et al.*, 2000).

In dry conditions 13X was found by Meeyoo *et al*. to have higher capacity for H_2S than activated carbon. However in humid conditions zeolites lose effectiveness, most likely as a result of adsorbate competition with water (Meeyoo *et al*., 1997), and activated carbons have greater effectiveness (Meeyoo *et al*., 1998). Under dry conditions only physisorption can occur in carbons, while under humid conditions water condenses into micropores and encourages dissociation of H_2S (Meeyoo *et al*., 1997). It follows that in dry conditions a zeolite should be used to remove H_2S, while in moist conditions (i.e. high atmospheric humidity) a microporous carbon is likely to be more effective.

As with ammonia, carbons can be chemically impregnated to improve hydrogen sulphide adsorption. However, impregnant may occupy carbon pore volume and surface area, limiting physisorption. While in many applications, a catalyst can be successfully used to remove H_2S, this is less applicable for a respirator, which must operate in atmospheric conditions. This is also due to the fact that many catalysts have specific operating requirements for optimal performance, such as temperature and pressure, and one specific application rather than broad spectrum toxic gas removal. One option is catalysing formation of sulphur from the H_2S, though this will block pores, minimising physisorption (Bagreev *et al.*, 2001b). Another option is to use the impregnant sacrificially. An example of a combination of chemical impregnants to remove H_2S is potassium iodide and sodium or potassium hydroxide, which work in tandem. The following reaction is catalysed by potassium iodide:

$$SO_2 + H_2O \leftrightarrow HSO_3^- + H^+$$

The resulting acid reacts with the potassium or sodium hydroxide to form elemental sulphur and water (Leatt, 2011; Choi *et al*., 2008) which are then adsorbed into

micropores (Bagreev *et al.*, 2005). Copper is also noted for its effectiveness in removal of many TICs (Alves and Clark, 1986; Smith *et al.*, 2010), and has been shown to effectively remove H_2S, with adsorption performance enhanced at higher levels of humidity (Huang *et al.*, 2006). An alternative option which avoids the use of heavy metals would be to use triethylenediamine (TEDA, also referred to as 1,4-diazabicyclo[2.2.2]octane, or DABCO). This is part of the current gas mask due to its effectiveness in removal of cyanogen (Alves and Clark, 1986), but has also been found effective at removal of H_2S, with unimpregnated carbon loading 203 mg H_2S/g carbon and 12% TEDA-impregnated carbon loading 324 mg H_2S/g carbon (Wu *et al.*, 2007).

2.1.1.3 Cyclohexane

The final model gas selected was cyclohexane, C_6H_{12}. Commercially, cyclohexane is used as a starting material for cyclohexanone and cyclohexanol, raw materials necessary for the production of nylon 6, 6 (Mirasol, 2010). The IDLH (Immediately dangerous to life or health) value for cyclohexane is 3000 ppm, based on animal toxicity, however NIOSH defines IDLH as 1300 ppm, as this is 10% of its explosive limit (1.3%) (CDC, 1994). Symptoms of exposure to high levels of cyclohexane include dermatitis, irritation to the eyes and respiratory system and drowsiness, at high concentrations leading to narcosis (unconsciousness due to exposure to narcotic) and coma (unconsciousness for over 6 hours) (HSDB, 2005). Cyclohexane is not toxic on the same scale as the other gases tested. However, due to volatility, large kinetic diameter of 6.9 Å and ease of testing, it is a useful simulant gas for many physisorbing organic contaminants that contain a six carbon ring (benzene, naphthalene etc).

In general, a typical microporous carbon should be able to effectively remove cyclohexane. However, detailed studies of specific impregnation and specific techniques to remove cyclohexane in the literature are limited. Zeolites are unlikely to be effective due to their small pore sizes, and also due to the effects of water, as increased humidity was found to reduce breakthrough time for VOCs in zeolite 13X (Tao *et al.*, 2004).

2.1.2 Respirators

Respirators can be tight or loose fitting depending on their application. Tight-fitting respirators form a seal with the face of the wearer, taking the form of a quarter, half or

full face mask. Loose fitting respirators cover the face completely but only have a partial seal, for example hoods or full suits. Air is pumped into loose-fitting respirators to maintain a slight positive pressure relative to the outside environment. This means that contaminants cannot enter due to the outward flow of gas (Rajhans, 2002).

There are several types of air purifying respirators available:

Mechanical filters: These consist of fibrous materials that trap particulates such as dust. They work by straining, if particles are halted if they are larger than the pores in the filter; or by depth filtration, if the particles stick to the surfaces within the filter medium. Mechanical filters have an associated pressure drop, resulting in increasing breathing resistance as the filter medium becomes more loaded (Rajhans, 2002).

Chemical respirators: Chemical-cartridge respirators consist of a cartridge attached to a face piece, containing materials that remove specific vapours or gases from air by adsorption, absorption or chemical reaction. One of the most common filtering mediums is activated carbon. Activated carbon alone is effective at adsorbing organic vapours (Zhao *et al.*, 1998), or it can be impregnated with chemicals that will allow it to be selective against other gases/vapours (Fortier *et al.*, 2008; Nickolov and Mehandjiev, 2004; Tamon *et al.*, 1996). Chemical respirators have a high pressure drop due to the use of granules/particles in the cartridge. The lifespan of chemical cartridges is difficult to determine, as they are affected by many factors, such as humidity and breathing rate (Rajhans, 2002).

Gas masks: Gas masks operate in a similar fashion to chemical-cartridge respirators; however they are designed to protect from higher concentrations of contaminants for longer, and contain a larger amount of sorbent. There are two types: a front/back mounted gas mask, in which a large canister containing a high volume of sorbent is attached to the wearer's body; and the chin-style, where a canister is attached to the face piece. This type of respirator is more commonly used in the military, where the type and conditions of contaminant exposure are likely to be unknown (Rajhans, 2002).

2.1.2.1 Respirators in industry

A wide range of respirators are produced for civilian users by companies such as 3M and Dräger. In an industrial setting, exposure to hazards should be avoided by taking appropriate safety measures. However, sometimes exposure to a toxic chemical may be unavoidable, in which case a respirator is necessary. In an industrial setting in which

workers are at risk to exposure from chemicals, vapours, dust or smoke, an industrial respirator must be used. In industrial settings, the particular chemicals and the approximate concentrations that workers are at risk of exposure to would generally be known. For example, workers at an ammonia plant could be exposed to a high concentration of ammonia, the specific concentration of which can be determined by an ammonia detector. As such, a suitable mask suitable to this particular risk can be used.

2.1.2.2 Respirators in the military

In contrast to industrial settings, military personnel could be exposed to extremely varied concentrations of a range of unknown gases at unknown concentrations, making the larger gas mask the most suitable respirator. An example of a military gas mask is the UK S10, shown in Figure 2.1a). It comprises full face protection with a seal around the face and a harness to allow it to be worn under a helmet. Air enters through a sorbent canister at the side, passes over the eye-pieces to prevent them misting up and then out through the outlet valve in the centre, resulting in a slightly negative internal pressure (Figure 2.1b)). The S10 is also fitted with a drinking tube, to allow the wearer to drink while wearing the gas mask for long periods of time. Figure 2.1c) shows the Scott General Service Respirator (GSR), which has recently entered service in the UK. The presence of two canisters as opposed to one means reduced pressure drop (due to lower flow rate over each) as well as offering the opportunity for the user to change canisters without having to hold their breath. The reduced canister size improves compatibility with weapon sights.

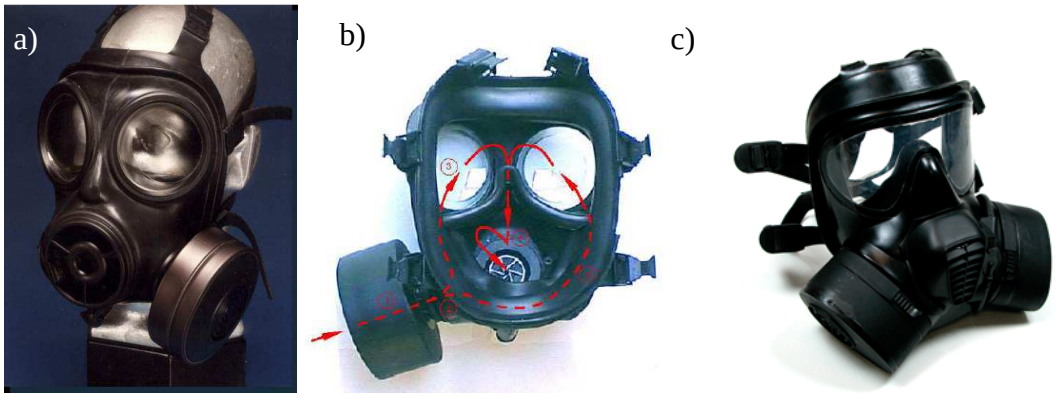

Figure 2.1. Examples of UK Gas masks: The S10 a) front view b) internal view with gas flow marked (Pelfrey, 2011) c) Scott General Service Respirator (GSR) (Scott-Safety, 2011).

In the S10 gas mask, the inhaled air initially passes over a glass fibre mechanical filter, which is pleated to increase the surface area to remove particulates. It then passes through a bed of impregnated granular activated carbon, where the toxic components of the

inhaled air are trapped by the carbon or by reacting with the chemical impregnant. A cross section of the filter is shown in Figure 2.2.

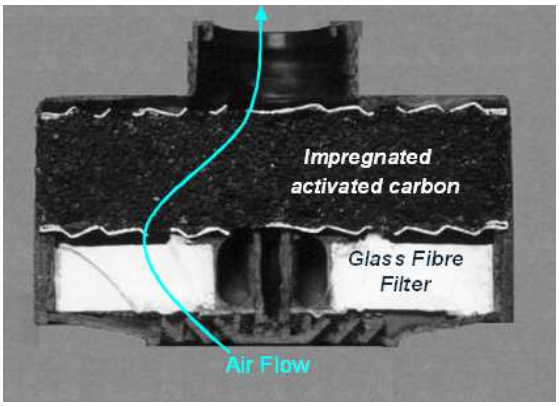

Figure 2.2. Interior of an S10 Gas Mask Cartridge (Smith, 2011).

Many current gas masks use carbons known as ASC/T or ASZM/T. ASC/T carbon is impregnated with copper (A), silver (S), chromium (C) and triethylenediamine (TEDA), while ASZM/T substitutes the chromium for zinc (Z) and molybdenum (M). The copper and silver components are effective for arsine and phosphine removal, and copper alone helps remove chlorine, hydrogen chloride, hydrogen fluoride and hydrogen sulphide (Doughty, 1996) among others. Chromium plays a role in hydrogen cyanide protection (Alves and Clark, 1986) this functionality being provided by zinc and molybdenum in ASZM/T. Amines improve removal of cyanogen chloride, with triethylenediamine (TEDA) the most effective of these. Amines are used in combination with chromium for maximum protection from cyanogen chloride (Tolles, 1989). TEDA is also effective for the removal of volatile methyl iodide (Schüth *et al.*, 2002) and H_2S (Wu *et al.*, 2007).

In order for gas masks to be effective, a complete seal around the face and a cartridge with a large quantity of very small adsorbent particles are required. These contribute to the physiological burden of wearing a gas mask. As an example, gas masks are very hot and can feel heavy after long periods of use, as well as making it more difficult to breathe. A high physiological burden is widely accepted as resulting in users tiring quickly and performing tasks more slowly and less effectively (Caretti *et al.*, 2001). As such, while it is necessary to develop gas masks that provide the greatest possible protection, it is also important for them to have low breathing resistance and weight. There are a variety of checks to ensure the efficacy and safety of respirators, with

components required to satisfy certain requirements in performance tests. The European standards are set out in BS EN 14387: “Respiratory protective devices - Gas filter(s) and combined filter(s) - Requirements, testing, marking” (BSI, 2008). These standards state the maximum allowed mass for a full face mask is 500 g, as well as giving standards for mechanical strength, temperature and flow resistance, pressure drop and particular requirements for capacity of canisters. The adsorbent hollow fibres presented in this report address several of the key issues associated with gas mask burden, and are discussed in the following Sections.

2.1.3 Adsorbents

While most solids can adsorb species from fluids, few are selective enough and have great enough capacity to be useful commercial adsorbents. An ideal adsorbent should strongly adsorb contaminants; have a high capacity for the target contaminant and good chemical, thermal and mechanical stability. Other useful characteristics are the ability to be regenerated after use and a low cost (Yang, 1997). One of the most important qualities of an effective adsorbent is a high specific surface area. As such, many commercial adsorbents are microporous. Micropores are defined by the International Union of Pure and Applied Chemistry (IUPAC) as having a diameter of < 20 Å, a mesopore as 20-500 Å and a macropore as > 500 Å (IUPAC, 2012). Key adsorbents of interest in this area include activated carbon, zeolites and metal organic frameworks (MOFs).

2.1.3.1 Activated carbon

Activated carbons are general purpose adsorbents, used in air purification systems, and in respirators (Ruthven, 2000). They are also used in industry for adsorbing organics in automobiles, decolourising sugar, water purification and solvent recovery. Activated carbons are a highly porous form of carbon, produced by chemically or physically activating carbonaceous material. They are made from char, which can be made from many precursors, such as coconut shells, peat, wood, bituminous coal (Bandosz, 2002), palm shells (Guo *et al.*, 2005) etc. These precursors are made up of 3D polymeric networks of cellulose and lignin. After pyrolysis at high temperatures water, CO_2 and a wide range of organic molecules are lost from the structure while heteroatoms such as O, H, Cl, N and S stay chemically bonded at the edges of aromatic macromolecules and are transformed into surface complexes (Rouquerol *et al.*, 1999). The char is then activated.

‘Chemical activation’ generally indicates that the carbonaceous precursor has been impregnated with a chemical (e.g., phosphoric acid, zinc chloride) prior to heat treatment and ‘physical activation’ applies to the precursor undergoing heat treatment in a mildly reactive atmosphere, such as steam or CO_2. The conditions of preparation can be altered to obtain particular pore structures and mechanical strength (Baker, 1992). The surface groups of the carbon play a major role in its chemical reactivity and hence its use as an adsorbent.

In comparison to other adsorbents, activated carbon has a very large BET surface area of approximately 300-2500 m^2/g, with pores in the range of 10-25 Å diameter (Yang, 1997). The surface of activated carbon is non-polar, or sometimes slightly polar. This means it can be used to separate without interference from moisture, and is effective for adsorption of non- or weakly-polar molecules (Yang, 1997). They are typically effective in removal of organics and can be chemically impregnated in order to adsorb a wider range of target contaminants, such as toxic industrial chemicals.

2.1.3.2 Zeolites

Zeolites are crystalline aluminosilicates made up of $[AlO_4]^{5-}$ and $[SiO_4]^{4-}$ tetrahedra. They occur naturally and have been known and mined for over 200 years (Dyer, 1988), and were first synthesised by Milton in 1959. At least 40 natural species of zeolites have been found, but a great many more can be synthesised. As of 2010, 194 unique zeolite frameworks had been classified by the International Zeolite Association structure commission (IZA-SC).

The stoichiometric formula for zeolites is:

$$M_{x/m}[(AlO_2)_x(SiO_2)_y]z\ H_2O$$

where *M* is the cation with valence *m*, *z* is the number of water molecules in each unit and *x* and *y* indicate the ratio of silica to alumina, and are integers such that $y/x \geq 1$. Some zeolites exist that contain no alumina ($y/x=\infty$), namely the silicalites. The M cations balance the charge of the $[(AlO_2)_x(SiO_2)_y]$ groups, which have a charge of -1 each. The *M* can be an alkali metal, with a matching charge of +1, or an alkali earth metal, which has a

charge of +2. For an alkali earth metal the attractive forces will be stronger, but the number of cations is halved. Larger cations have more electrons, which shield the positive nucleus and hence can diminish attraction (Yang, 1997). Adsorbed H_2O can be removed by heating and vacuum, making zeolites suitable for adsorption, and leaving a void fraction of 0.2-0.5 (Yang, 1997). The aluminosilicate skeleton has a regular, interconnected cage structure, the window size of which is controlled, from about 3–10 Å, by altering the type of cation. Unlike activated carbons, zeolites have very precise aperture sizes, and as such can be used as molecular sieves.

The Si/Al ratio in zeolites affects its properties in the ways illustrated in Table 2.2. Aluminium can be substituted with silicon, raising the Si/Al ratio and reducing the amount of cations necessary to counteract the charge from the aluminium. It is also possible to exchange cations with other alkali metals, or with H^+, which will affect the aperture size of the zeolite cages. The ability to swap cations gives rise to one of the most common uses of zeolites in water softening, as calcium and magnesium in hard water can be exchanged with Na^+ cations in the zeolite.

Table 2.2. Transition in zeolite properties from low to high Si/Al ratios, adapted from (Bekkum *et al.*, 1991).

Si/Al ratio	Stability (°C)	Surface selectivity	Cation concentration	Structure
"Low" (1-1.5) e.g. 13X, 5A	≤700	Hydrophilic	High	4, 6 and 8 rings
"Intermediate" (2-5) e.g. clinoptilolite		Transition at Si:Al ratio of 8-10 (Ruthven, 2000)		
"High" (10-100) e.g. ZSM-5	≈ 1300		Low	5 rings
Infinite e.g. silicalite		Hydrophobic	None	

A variety of topologies are known and classified by the International Zeolite Association. 13X, 5A, clinoptilolite and ZSM5 are commonly used zeolites for removal of toxic gases such as ammonia (Helminen *et al.*, 2001), carbon monoxide (Dangi *et al.*, 2010) and hydrogen sulphide (Garcia and Lercher, 1992). Although activated carbon is more commonly used in respirator canisters than zeolites, the potential of these zeolites to

remove a wide range of TICs that are not well sorbed by activated carbons, such as hydrogen sulphide (Bagreev *et al.*, 2000), makes zeolites an interesting option for use in a respirator filter. However, a potential drawback of zeolites is their relatively high affinity for water, even when the Si:Al ratio is high (van Bekkum, 2001).

2.1.3.3 Metal organic frameworks

Metal-organic frameworks (MOFs) are crystalline materials made up of a metal ion covalently bonded to an organic linker, which can have very high surface area (Yaghi *et al.*, 2003). As such an almost infinite number of MOFs potentially exist. At present, MOFs have not been widely introduced into industry although large scale production of some MOFs has been achieved. Projected applications of MOFs include catalysis, gas adsorption, gas separation, hydrogen storage, CO_2 capture, drug delivery and nanoreactors, which are reviewed in Férey (2008). MOFs are generally produced as a powder and in small quantities but this is no use in a respirator or many other industrial applications due to high pressure drop. Many groups are working on immobilising MOFs in various ways, including thin films of MOFs (Zacher *et al.*, 2009; Gascon *et al.*, 2008), MOF monoliths (Küsgens *et al.*, 2010), MOF paper (Kusgens *et al.*, 2009), silica-MOF composites (Ameloot *et al.*, 2010) and MOF-graphite oxide composites (Petit and Bandosz, 2009).

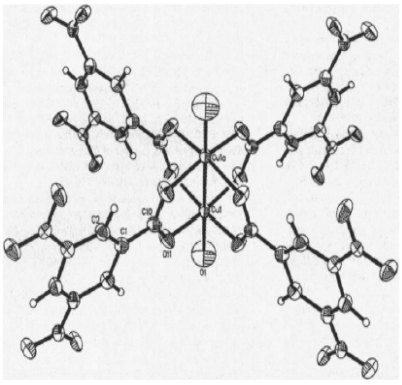

Figure 2.3. Cu-BTC dicopper (II) tetracarboxylate building block, known as a "paddlewheel" (Chui *et al.*, 1999).

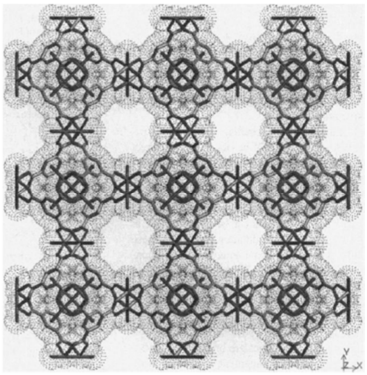

Figure 2.4. Cu-BTC framework (Chui *et al.*, 1999).

One of the most frequently studied MOFs is made up of copper and benzene tricarboxylate (Cu-BTC), which is also known as H-KUST1, Cu_2BTC_3 or MOF-199. The building block is visible in Figure 2.3 and its framework structure in Figure 2.4. While a great deal of the papers recently published on MOFs focus on their use in catalysis and

hydrogen storage, some papers have been published concerning their use in removal of toxic chemicals. Peterson *et al*. (2009) showed that Cu-BTC has a high adsorption capacity for ammonia through chemical interactions with its structure. Britt *et al.* (2008) tested six "benchmark" metal-organic frameworks with a variety of toxic chemicals, including ammonia, carbon monoxide sulphur dioxide and chlorine, and compared them with un-impregnated activated carbon. They showed that MOFs were promising adsorbents of all of the chemicals tested except for carbon monoxide, and determined that pore functionality was important in adsorption of toxic chemicals. Peterson (2008) found the greatest adsorption capacities for ammonia, sulphur dioxide and cyanogen chloride in MOFs with unsaturated metal sites. As such, Cu-BTC with its open metal sites has great potential for adsorption of several toxic chemicals.

There are a range of methods of synthesis, but solvothermal syntheses at temperatures greater than 100 °C are widely used (Férey, 2008). Other methods include electrochemical synthesis (Mueller *et al.,* 2006) and microwave synthesis (Jhung *et al.*, 2005). These methods usually result in small amounts of powder but some groups have shown the potential to produce some MOFs on a larger scale by mechanochemical means (Yuan *et al.*, 2010; Pichon and James, 2008). Producing MOFs on a larger scale will be fundamental for their wider use in industry. However, one area of concern is the general stability of MOFs on exposure to water (Gul-E-Noor *et al.*, 2011; Greathouse and Allendorf, 2006; Li and Yang, 2007). Most of the MOFs are unstable in the presence of humidity and this will limit the industrial applications of this material.

2.1.4 Structured adsorbents

In industry, powders cannot generally be used in adsorbent packed beds due to the prohibitively high pressure drop and particle lifting or crushing, resulting in attrition. The structured design of the adsorbent is very important and will vary depending on the process in which it is to be employed. A range of structures exist through the literature with several aims in mind. Some are made as a means of suspending adsorbents for use as such or in mixed matrix membranes. Different structures have different advantages and disadvantages, but important qualities will always include:

- Adsorbent loading within the volume of the structure
- Pressure drop per unit length of the structure

- External surface area per volume
- Void volume
- Channelling and dispersion characteristics.

(Rezaei and Webley, 2009)

There are trade-offs between these qualities. For example, the external surface area of an adsorbent will heavily govern its performance, but higher surface areas are usually associated with lower adsorbent volume (Rezaei and Webley, 2009). Also, an adsorbent structure with high voidage may result in improved adsorption kinetics, but this high voidage results in a lower bed density, and so lower loading in the structure (Rezaei and Webley, 2010). Several different types of structured adsorbents are reviewed in the Sections below.

2.1.4.1 Bead and granular adsorbents

At their most basic, commercial adsorbents for use in packed beds exist in a variety of forms. They can be either pure adsorbent, comprising a power, granule or flake, or suspended with a binder to form a pellet or sphere, with size typically ranging from 50 μm to 1.2 cm (Seader *et al.*, 1998). These particles may be chemically impregnated before use, such as in respirator filters. In many industrial processes, sorbent packed beds, comprised of the particles described above, are used to remove contaminants from a gas stream. Adsorbent geometry and the structure of the adsorbent bed are important, with the best adsorption kinetics in those with a small pellet size (the mass transfer resistance varies as a square of the particle size). However, the smaller the pellet size, the greater the drop in pressure. If pressure drop becomes very high, this can cause the bed to become fluidised, resulting in particle attrition (McCabe *et al.*, 2005). In addition there may be lifting or crushing of the particles of the bed, particularly for smaller particles, and the distribution of the gas can be uneven, resulting in bypass and poor exposure to the bed. There can also be an additional drawback of slow regeneration rates and as such high energy costs (McCabe *et al.*, 2005). As such, when adsorbent particles are used in a packed bed, the size of the particles must be a compromise between pressure drop considerations and adsorption kinetics (Rousseau, 1987). If pressure drop becomes too high, a more intensive use of energy is required to force gas through the packed bed.

2.1.4.2 Monoliths

Monoliths are commonly used as an alternative low pressure drop structure. They are composed of a single piece of material made up of interconnected cells or channels, with several ceramic monoliths shown in Figure 2.5. These channels can be prepared in a range of shapes, although square is the most common, it being the easiest to form. However, hexagonal and circular channels will have better adsorption kinetics (Crittenden *et al.*, 2005). Monoliths are generally made from ceramics, metals or plastics but have also been produced from carbon (Crittenden *et al.*, 2005) and porous glass (Barascu *et al.*, 2012). Monoliths may be inactive, such as metallic monoliths, and then have an active component added, for example by coating or growing a film, typically a process used for catalytic monoliths. Alternatively, the active material, such as carbon adsorbent, may be extruded directly into a monolith, which is commonly used for adsorption. Monoliths are generally most useful in situations where high flow rates and low pressure drop are required. One of the most well-known uses of monoliths is as catalytic converters in cars.

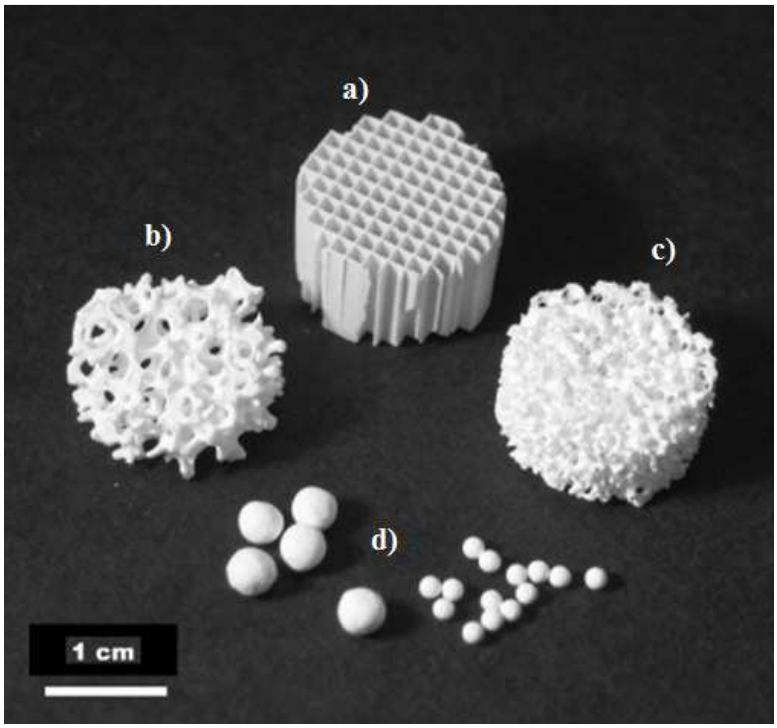

Figure 2.5 Different types of monoliths and pellets: a) a honeycomb monolith, b) a 20 pores per inch (ppi) foam monolith and c) a 45 ppi foam monolith and d) 3.3 and 1.5 mm pellets. Image taken from Patcas *et al.* (2007).

In comparison to a packed bed, a honeycomb monolith has a large geometric surface area with an open structure. They offer advantages compared to an equivalent volume packed bed system due to their thin walls, high surface area, low-pressure drop and good mass

transfer performance (Williams, 2001b). Because they are composed of a single piece of material, they are more resistant to attrition and vibration than granular beds. They are also of a lighter weight than an equivalent size packed bed (Heck *et al.*, 2001). In addition, due to their open structure they can be used in environments high in dust, with little risk of plugging, as can be seen in granular beds.

However, there are several disadvantages to the monolith structure. There can be high mass transfer resistance within monoliths due to external film resistance and pore diffusion within the monolith walls. In order for optimum adsorption kinetics, walls must be as thin as possible, giving higher cell density and shortening the diffusion path length. This means that adsorbent loading may be very low per unit volume, due to the high resulting voidage in relation to a granular bed, with not all of the adsorbent in the structure of the monolith accessible to adsorbate passing through the channels. Also, manufacturing monoliths with high cell density is difficult and expensive, although the potential for very good mass transfer has been demonstrated by an ultra-high cell density biomorphic monolith prepared from a cuttlebone (Li *et al.*, 2009). This disadvantage is compounded by the issue that residence time in monoliths is lower than an equivalent packed bed, meaning longer beds are necessary (though this is not unfeasible due to the reduced pressure drop). Other disadvantages of the monolith structure are the lack of control over heat transfer and poor radial mixing (Heck *et al.*, 2001). A full comparison of honeycomb monolith and pellet separation performance can be seen in Li *et al.* (1998). Monoliths offer a great many advantages over packed beds, making them a good option for use in respirator cartridges. However, the purpose of this research is to investigate novel light-weight options for gas mask design, and the monolith structure is very rigid and inflexible, and often quite brittle.

2.1.4.3 Laminate adsorbents

Laminate adsorbents, or parallel passage contacts, as they are also known, are similar to monoliths, but rather than having channels, they have 1D slits. Similar to monoliths, laminate structures have lower pressure drop and better mass transfer characteristics than a packed bed (Ruthven and Thaeron, 1996), and the pressure drop is adjustable by increasing or reducing the gaps between sheets, with the diffusion pathways controlled by the thickness of these layers. However, in order to avoid gas channeling, these slits must be spaced extremely accurately. In practice, this is difficult and often expensive to

achieve, and as such this type of adsorbent structure is not commonly used in separation processes, despite its potential advantages (Rezaei and Webley, 2010). The cost issues and the risk that mechanical stress could affect the precise spacing make laminate structures unsuitable for use as an adsorbent structure in respirator cartridges.

2.1.4.4 Foams

An example of an adsorbent foam structure is shown in Figure 2.5. Sometimes they are classed as monoliths, as they are also composed of a single piece of ceramic. Foams offer superior heat transfer and radial mixing to the honeycomb monolithic structure, although have higher pressure drop and lower mass transfer coefficients (Patcas *et al.*, 2007). Foams have high external surface area and large porosity compared to a packed bed. This porosity is so high that adsorption per unit volume can be rather poor in adsorbent foams, and they also retain some of the tortuousity of packed beds, reducing their adsorption performance (Rezaei and Webley, 2010). Current adsorbent foams are not seen as suitable for use in respirator canisters due to the issue of poor adsorption loading per unit volume, and potentially higher pressure drop than a monolith structure (Patcas *et al.*, 2007).

2.1.4.5 Adsorbent fabric

These are fabrics that are coated or impregnated with adsorbents, or made from adsorbent fibres, such as activated carbon cloth, which can be self-supporting (made from 100% carbon and no binder). These are prepared by coating organic binder in carbon, and then pyrolysing it so that the binder becomes activated carbon. As a result, adsorbent fabrics offer a flexible method of gas separation that can be orientated in a number of configurations with lower pressure drop than an equivalent granular bed. Two of the most commonly used are parallel sheets or spiral-wound structures. Adsorbent fabrics also have low attrition, and good mechanical strength, and can have favourable mass transfer compared to granule beds (Rezaei and Webley, 2010). Activated carbon cloths are used in defence applications, for example in protective clothing and in filters, such as escape hoods (Chemviron, 2013), with examples of the cloth shown in Figure 2.6. However, research showed poor loading on adsorbent fabrics compared to a bed of granules (Golden *et al.*, 2005), and they are already used in defence applications. As such they are not a novel option for use in a gas mask cartridge, where good adsorbate loading for a range of gases is vital, although could perhaps be incorporated alongside another option or into the structure of the novel mask.

Figure 2.6. Left: Zorflex activated carbon cloth. Right: Zorflex Knitted Cloth (Chemviron, 2013).

2.1.4.6 Hollow fibres

Hollow fibres were originally developed as membranes because of their high surface area per unit volume and because they avoid some of the problems associated with pressure drop (Pan and McMinis, 1992). The commercial applications of hollow fibres membranes include filtration and separation processes such as haemodialysis and water purification (Haslego, 2010). PES hollow fibre membranes have been used and studied by many scientists, however, adsorbent hollow fibres were first developed by (Perera and Tai, 2009). These are made up of a polymer binder with an adsorbent material held within, similar in configuration to a monolith, but rather than being a single piece of material, fibre bundles are prepared by combining a number of individual fibres into the desired overall shape. Tai, in an early use of hollow fibres, incorporated HiSiv3000 (UoP Honeywell, US) adsorbent powder into adsorbent fibres to remove VOCs from gas streams. An example of a typical zeolite fibre module is shown in Figure 2.7.

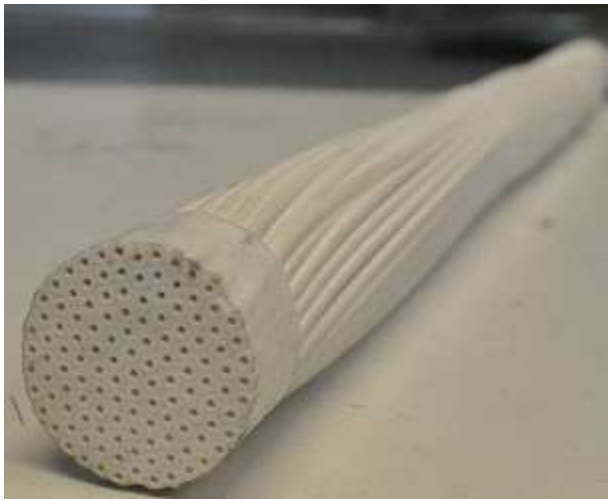

Figure 2.7. Zeolite hollow fibre module prepared by Thomas Richards at the University of Bath.

Hollow fibre modules can make efficient use of space with high external surface areas of up to 15,000 $m^2 m^{-3}$ for the fibre structure itself (Cheremisinoff, 2002), without including surface area provided by the incorporated adsorbent. This is in comparison to, for example, 7600 $m^2 m^{-3}$ for a packed bed of 0.794mm diameter spheres (Richardson *et al.*, 2002). As their overall structure is very similar to that of a monolith, i.e., a collection of channels arranged parallel to gas flow, many of their properties are likely to be similar, in comparison to granular beds. They will have higher voidage than a granular bed, with thinner walls reducing diffusion path length and so improving mass transfer in hollow fibres (Bhandari *et al.*, 2010). In contrast to monoliths, the separate fibres bundled together enable the module to be flexible, meaning that it can be bent or curved into a specific shape. This makes them ideal for novel respirator designs. Channel and wall size can also be adjusted relatively simply. In addition, a range of adsorbents can be incorporated into the adsorbent hollow fibre structure to produce novel composite fibres with the potential to remove a wide spectrum of TICs. Adsorbent hollow fibres present a novel design option for respirator cartridges, as they have rarely been used in adsorbent beds. They also have a number of benefits compared to a granular bed, such as decreased pressure drop, potentially improved mass transfer properties and the potential to incorporate a range and mixture of adsorbents.

2.1.4.7 Preparation of adsorbent hollow fibres

Preparing adsorbent hollow fibres by dry-wet spinning is a complex process with a variety of controlling parameters. These include the dimensions of the spinneret, the extrusion rate through the spinneret, the length of the air gap, the temperature of the coagulant bath, the composition of the coagulant bath, the composition of the coagulating bore fluid, as well as the concentrations of polymer, solvent and coagulant.

When the polymer concentration is high, vitrification, gelation or crystallation may occur (Machado *et al.*, 1999). High polymer concentrations also reduce porosity and flux in membranes, but low polymer concentrations, or below the critical point in the ternary diagram, result in a weaker structure due to poor polymer connectivity (Baker, 2004). For the adsorbent hollow fibres in this research, highly porous structures will be necessary to allow full access to adsorbent, as such, low polymer concentrations are desired.

When fibres rapidly coagulate, finger-like macrovoids are formed in the structure whereas when coagulation takes place slowly a porous sponge-like structure is formed (Kesting, 1971). If the concentration difference between the coagulating fluids (external bath and internal bore) is great, the fibre will coagulate more rapidly. (Xu and Alsalhy Qusay, 2004), showed that spinning fibres into a coagulating bath of water using a bore fluid of 90% solvent to 10% water resulted in a porous inner layer, where delayed liquid-liquid demixing had occurred, and a dense outer skin as a result of instantaneous liquid-liquid demixing. For membranes, a hollow fibre without macrovoids is preferable as this results in a mechanically more stable structure (Liu *et al.*, 2003).

A longer air gap in hollow fibre extrusion for membrane formation was found to increase the pore size in the outer skin due to the slower demixing. The longer the air gap, the larger the pore size in the outer skin (Liu *et al.*, 2003). The air gap also affects the thickness of the polymer. When extruded through a spinneret, polymer molecules may experience die swell. This means that as the polymer is compressed through a small space, the spinneret, it will begin to reform, or swell, to its original shape (Qin *et al.*, 2000). With no air gap, the fibre is likely to coagulate before die swell can occur fully. With a longer air gap, die swell is likely to be counteracted by gravitational effects (Qin and Chung, 2004).

Extrusion rate through the spinneret also affects the outer skin. With increasing shear rate, the outer skin becomes thicker and denser due to greater molecular orientation (Chung *et al.*, 2000). Polymers near the wall of the mould, in this case the spinneret, straighten out, packing more densely, while polymer near the centre remains coiled, packing more loosely (ToolingU, 2012). As a result, these fibres have higher tensile strength but lower flux (Chung *et al.*, 2000).

Hollow fibres can be tailored, with spinning conditions affecting the final qualities of the fibre and a great variety of potential configurations possible, with combinations of different adsorbents, spinning conditions and so forth. Characterising fibre behaviour as an adsorbent of a variety of TICs can inform future respirator design and enable further innovations that will not only provide better protection against a wide variety of TICs but lower the burden on the wearer. As such these were considered the optimal adsorbent structure for use in respirator cartridges and are the focus of this study.

2.1.5 Chemical impregnation

Activated carbon impregnated with copper, silver and chromium salts, and triethylene diamine is used in current UK military respirators. In order to enhance adsorption of specific contaminants, adsorbents can be impregnated with particular chemicals. Impregnated adsorbents could be used for single pass filtration, in which the impregnated chemical is irreversibly altered during adsorption. Examples of single pass filtration are the current military gas mask, and removal of H_2S by impregnation of carbon with caustics (Bagreev *et al.*, 2000). In some cases regeneration of the impregnants may be possible, allowing reuse, for example Sulfusorb activated carbon (Calgon) may be regenerated by heating (Calgon, 2006). Alternatively, the impregnant may be a catalyst, and convert the contaminant to a non- or less toxic alternative indefinitely, such as the catalytic converter in cars, the conversion of hydrogen sulphide to elemental sulphur (Kerr and Johnson, 1960) or sulphur trioxide (Meeyoo *et al.*, 1998) and the oxidation of carbon monoxide to carbon dioxide (Singh *et al.*, 2009).

Obviously, the most economical choice would be the catalytic impregnant, as this never/very infrequently requires replacement. However, in a respirator application, the conversion of one specific chemical to another, albeit slightly less toxic, is not safe for the user of the respirator. As such, complete, sacrificial adsorption is required. Whether or not the material can be regenerated is a complicated issue that must be considered in terms of cost and benefit. For example, because gas masks give no sign of when they are exhausted, it would be necessary to regenerate, at cost, at fixed time intervals, when the cartridge is unlikely to have been fully saturated. This, coupled with shipping costs for used and regenerated cartridges may make it more economical to simply dispose of used cartridges. There is an environmental argument to be made for recycling used cartridges despite the cost, and this must be considered on a case-by-case basis. This report will focus on producing single pass cartridges as user safety is the main focus, although recycling would be an interesting and useful option to have available in future if a good method of determining the level of bed saturation can be found, such as with residual service life indicators (RSLIs).

Depending on the qualities of the impregnating chemical, the carbon and the data available surrounding each of these, a range of different impregnation techniques are available. During impregnation, there are a great many interactions between the surface

groups of the carbon involved and the chemical in question, which are difficult to accurately model. Key impregnation techniques (Haber *et al.*, 1995) include:

Excess soaking impregnation – in this very common and straightforward method, the adsorbent and dissolved impregnant are mixed and then dried, with the impregnating material remaining on the adsorbent surface. Some of this will have ion exchanged onto the surface and be strongly held while the remainder is weakly adsorbed, resulting in a large particle size distribution.

Dry impregnation and incipient wetness impregnation – these two techniques are quite similar; for dry impregnation, the amount of impregnant introduced is equal to the pore volume of the adsorbent support, and as such the pore volume of the adsorbent must be known. For incipient wetness, the quantity of impregnant added is empirically determined to be that at which the adsorbent support appears wet, without needing to know the precise pore volume.

Selective reaction impregnation – the adsorbent is dipped in an excess of impregnant solution for a set time period and then removed. This is suitable when a strong bond with the surface of the adsorbent support is formed.

Percolation impregnation – impregnant solution is percolated through a bed of the adsorbent support and the effluent analysed to determine the extent of impregnation (Haber *et al.*, 1995; Radovic and Rodriguez-Reinoso, 1997).

There are more specific options available such as chemical deposition of metal carbonyl vapours (Omata *et al.*, 1990), physical vapour deposition (Potoczna-Petru and Krajczyk, 1995), and electrochemical (Polcaro *et al.*, 1993) or aerosol methods (Atkinson *et al.*, 2011). Detailed analysis of impregnation is not relevant to this report, as such only incipient wetness and excess soaking will be used, as the simplest methods to determine the viability of fibre impregnation.

It should also be noted that impregnating an adsorbent can result in decreased adsorption performance, particularly as the available surface area is reduced by the presence of the metal salt (Nakamura *et al.*, 2002).

2.1.6 Polymers

High temperature polymers are used in many industrial applications. A polymer is a series of monomers bonded covalently into a macromolecule. These exist in nature (cellulose, wool etc), and are also produced artificially (nylon, PVC etc.). However, those produced artificially from petrochemicals are generally referred to as plastics, from the Greek *plastos*, meaning suitable for moulding. In order to select a suitable polymer for use in adsorbent hollow fibres for TIC removal, it is important to consider their properties. Because polymers have a wide variety of structures and properties, they can offer a great deal of flexibility in hollow design over, for example, ceramics.

Linear polymers are those made up of many subunits in a single chain, with van der Waals bonding between chains. Branched polymers have side-chains connected to the main ones, resulting in lower packing efficiency and density. Cross-linked polymers have linear chains that are joined in several positions by covalent bonds. Thermoset plastics are cross-linked and degrade on heating, while thermoplastics are not cross-linked and melt on heating. Depending on how the complex polymer chains are arranged, polymers can be amorphous (disordered chains) or (semi-) crystalline if there are crystalline sections among the amorphous material. Many polymers exist with unique properties depending on their constituent monomer. Important properties include tensile strength, elasticity, melting point (T_m) and glass transition temperature (T_g). The glass transition point is the temperature at which, as a polymer is heated, it loses glassiness (stiffness) and becomes rubbery (pliable). Polymers exhibit glassy behaviour at low temperatures as they are unable to change conformation and hence are brittle. They show rubbery behaviour at high temperatures, as the polymer is able to change its conformation, becoming more flexible.

The molecular weight of the polymer can have a significant effect on thermal stability. Polymers with long chains have high molecular weights: the higher the weight, the higher the melting temperature. A polymer with a Mw of 10,000 g/mol or higher will be a solid polymer, while 1000 g/mol corresponds to a waxy solid or soft resin, and 100 g/mol would be liquid or gas (Callister, 2007).

To be fit for purpose in adsorbent hollow fibres intended for respirator cartridges, a polymer must have several key properties:

- Solubility in common solvents
- Stability at the high temperatures required to dry adsorbents
- Good mechanical strength (ballistics proof)
- Good chemical resistance (to the wide range of TICs it must protect against)
- Low or reasonable price

A range of polymers commonly used in industrially established separation membranes, their morphology and the barrier thickness of the membrane produced are shown in Table 2.3 (Ulbricht, 2006). Of these commonly used polymers, those with the relevant data available were evaluated against the criteria listed above, and the details are shown in Table 2.4. These properties were used to select polymers for further research.

Table 2.3. Polymers commonly used in membranes, their morphology and their barrier thickness. Adapted from Ulbricht, 2006.

Polymer	Morphology		
	Barrier type	Cross-section	Barrier thickness (μm)
Cellulose acetates	Nonporous	Anisotropic	~0.1
	Mesoporous	Anisotropic	~0.1
	Macroporous	Isotropic	50–300
Cellulose nitrate	Macroporous	Isotropic	100–500
Cellulose, regenerated	Mesoporous	Anisotropic	~0.1
Perfluorosulfonic acid polymer	Nonporous	Isotropic	50–500
Polyacrylonitrile	Mesoporous	Anisotropic	~0.1
Polyetherimides	Mesoporous	Anisotropic	~0.1
Polyethersulfones	Mesoporous	Anisotropic	~0.1
	Macroporous	Isotropic	50–300
Polyethylene terephthalate	Macroporous	Isotropic track-etched	6–35
Polyphenylene oxide	Nonporous	Anisotropic	~0.1
Poly(styrene-*co*-divinylbenzene), sulfonated or aminated	Nonporous	Isotropic	100–500
Polytetrafluoroethylene	Macroporous	Isotropic	50–500
	Nonporous		~0.1
Polyamide, aliphatic	Macroporous	Isotropic	100–500
Polyamide, aromatic	Mesoporous	Anisotropic	~0.1
Polyamide, aromatic, in situ synthesized	Nonporous	Anisotropic/composite	~0.05
Polycarbonates, aromatic	Nonporous	Anisotropic	~0.1
	Macroporous	Isotropic track-etched	6–35
Polyether, aliphatic crosslinked, in situ synthesized	Nonporous	Anisotropic/composite	~0.05
Polyethylene	Macroporous	Isotropic	50–500
Polyimides	Nonporous	Anisotropic	~0.1
Polypropylene	Macroporous	Isotropic	50–500
Polysiloxanes	Nonporous	Anisotropic/composite	~0.1<1–10
Polysulfones	Nonporous	Anisotropic	~0.1
	Mesoporous	Anisotropic	~0.1
Polyvinyl alcohol, crosslinked	Nonporous	Anisotropic/composite	<1–10
Polyvinylidenefluoride	Mesoporous	Anisotropic	~0.1
	Macroporous	Isotropic	50–300

Table 2.4. Properties of commonly available polymers used in membranes, with unsuitable polymers and properties greyed out, data obtained from (Omnexus, 2013) except where otherwise indicated.

Polymer	Heat deflection temperature @0.46 Mpa (67 psi) °C	Glass transition temperature °C	Youngs modulus	Chemical resistance	Cost (€/kg)
Cellulose acetates	50 - 100	100 - 130	0.6 - 2.8	"Poor chemical resistance (attacked by alcohols, ketones and concentrated acids)"	1.6 - 4
Polyacrylonitrile	70-80		3.1 - 3.8		3 to 11
Polyetherimides	195-210	215	3	Attacked by ketones, strong alkalis and aromatic and halogenated hydrocarbons	10 to 25
Polyethersulfones	205 - 212	210 - 230	2.3 - 2.8	"Attacked by polar solvents such as Ketones, Chlorinated solvents and Aromatic hydrocarbons"	3 to 11
Polyethylene terephthalate	75 - 115	73 - 78	2.8 - 3.5	"Affected by boiling water, Attacked by alkalis and strong bases, Attacked at high temperatures (>60°C) by ketones, aromatic and chlorinated hydrocarbons and diluted acids and bases"	1.6 - 4
Polyphenylene oxide (Boedeker, 2013)	129		2.4		
Poly(styrene-*co*-divinylbenzene), sulfonated or aminated	90 - 110	90	3 - 3.5	Poor chemical resistance, especially to organic solvents, Brittle at room temperature, Highly flammable	Less than 1.6
Polytetrafluoro ethylene	70 - 120		0.4 - 0.8		3 to 11

Polyamide	150 - 190		0.8 - 2	Poor resistance to acids, halogenated hydrocarbons and halogens	1.6 - 4
Polycarbonates, aromatic	110 - 150	115 - 170	2.07 - 2.23		3 to 11
Polyethylene (Goodfellow, 2013)	55-95	68 - 82	0.3 - 0.6		Less than 1.6
Polyimides	240 - 360	250 - 340	1.3 - 4	Attacked by concentrated acids and alkalis	More than 25
Polypropylene (Homopolymer)	100 - 120	-10	1.1 - 1.6	Attacked by highly oxidizing acids, swell rapidly in chlorinated solvents and aromatics	Less than 1.6
Polysulfones	176 - 182	187 - 190	2.5 - 2.7	"Can be attacked by polar solvents such as Ketones, Chlorinated solvents, Aromatic hydrocarbons."	3 to 11
Polyvinylidene fluoride	70 - 150	-42 - -25	1.5 - 2	Attacked by ketones and strong bases	3 to 11

To quantify these key properties, a polymer was needed that was soluble in NMP, stable to ~ 150 °C, with glass transition temperature above this, to enable drying. In addition, a high Young's modulus of at least 2 GPa, good chemical resistance, and cost no higher than 11 €/kg in cost were required. High temperature resistance is the most important characteristic as high temperature is required to remove contaminants before use. Of the polymers commonly used in membranes, the ones with high enough temperature resistance are polysulfone, polyethersulfone, polyimide and polyetherimide. Polyimide and polyetherimide are both comparatively expensive and polyimide can have a low Young's modulus, making these two less preferable than PS and PES. Polysulfone and polyethersulfone are roughly the same in price and mechanical stability but polyethersulfone has a slightly higher thermal stability and glass transition temperature than polysulfone, enabling higher regeneration temperatures. As such, polyethersulfone was selected for the main polymer for use in adsorbent hollow fibres, although special fibres could be prepared from several other polymers which would bring unique characteristics to adsorbent hollow fibres.

2.1.6.1 Polyethersulfone

Polyethersulfone is a thermoplastic with good temperature (and flame) resistance, chemical resistance and mechanical properties (Solvay, 2011), with the structure shown in Figure 2.8. The ether and sulfone bridging moieties give polyethersulfone its high temperature stability, particularly the electronegative sulfone group. Solvay describes PES as being stable at 180 °C for 20 years, with max temperature of 191 °C. It shows good stability with a range of chemicals, although it is attacked by benzene and toluene, methyl ethyl ketone, 2-ethoxyethanol, 1,1,1-trichloroethane and as such would not be suitable protection from these potential TICs. In addition, the flexibility of this polymer, even in its glassy state, allows fibre modules to be shaped to fit the available space. These important factors facilitate many new possibilities for filter design.

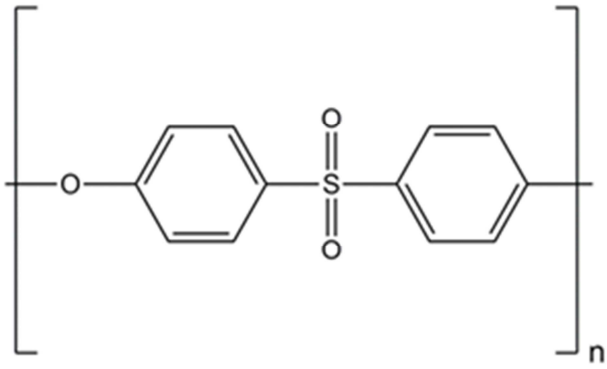

Figure 2.8. Polyethersulfone structure.

One potential problem for these fibre composites is that access to the adsorbent within may be blocked by the polymer binder (Nevell and Perera, 2011). This problem has been partially addressed by heating the fibres, which resulted in the rearrangement and shrinkage of PES (Barzin *et al.*, 2004).

2.1.6.2 Polymers of intrinsic microporosity

Many polymers are classified as nonporous, due to their flexible backbones, which enable efficient packing. However, it should be noted that all polymers have some free volume, with high amounts in some particular polymers such as poly(1-trimethylsilyl-1-propyne) (PTMSP). A novel family of polymers that have recently been developed at the University of Manchester by Peter Budd and Neil McKeown are known as polymers of intrinsic microporosity (PIM). PIMs are glassy polymers with rigid chains positioned in a contorted macromolecular structure. This particular configuration and lack of mobility

means efficient chain packing is impossible, which results in interconnected free volume in the polymer, making microporosity intrinsic to the polymer, rather than requiring any additional treatment to induce (Budd *et al.*, 2005b). As such, uniquely among these polymers, PIMs demonstrate high surface areas (Li *et al.*, 2011).

PIMs are prepared using bis-catechol 5,5′,6,6′-tetrahydroxy-3,3,3′,3′-tetramethyl-1,1′-spirobisindane and assembled by dibenzodioxane formation between three aromatic tetrol monomers with fluorine-containing compounds, with this process shown in Figure 2.9. The compounds are represented as A1-A3 and B1-B3 respectively in Figure 2.9 (Budd *et al.*, 2004b), with PIM-1 prepared from A1 and B1.

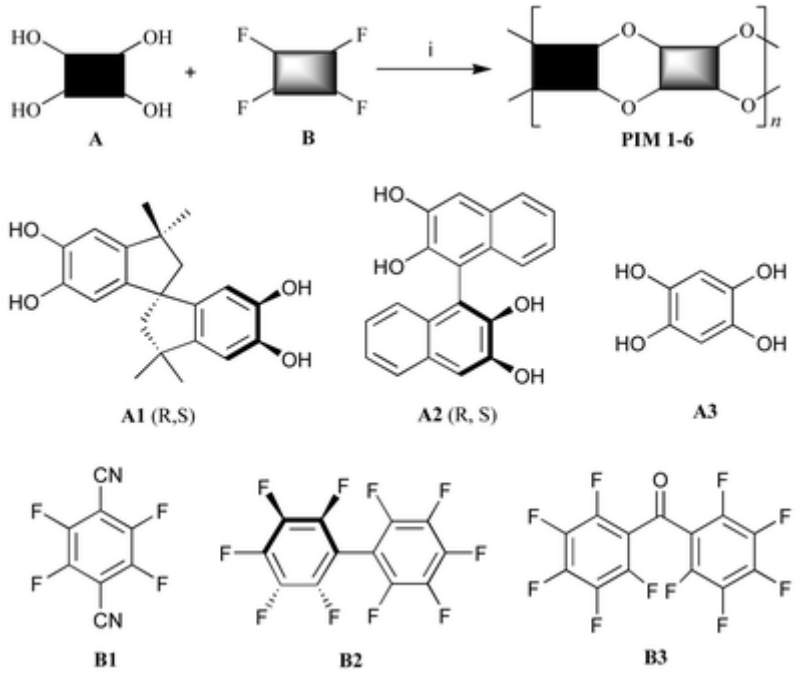

Figure 2.9. Compounds for synthesis of PIMs 1-6 (Budd *et al.*, 2004b).

The formed PIMs are soluble in polar aprotic solvents except for PIM-6, which is soluble in acidic solvents, and their apparent surface areas range from 430 m^2/g (PIM-6) to 850 m^2/g (PIM-1). PIM-1 is a fluorescent yellow powder (structure shown in Figure 2.10 (Budd *et al.*, 2004a)) with the highest surface area of the PIMs. It is thermally stable up to 370 °C, making drying and thermal regeneration feasible, and is soluble in common solvents, such as tetrahydrofuran, dichloromethane and chloroform. PIM-1 is also of particular note due to its high permeability and selectivity, exceeding Robeson's upper bound for oxygen/nitrogen selectivity and oxygen permeability (Budd *et al.*, 2005a). PIM-1 has several anticipated applications, including in the form of membranes, catalysis

and adsorbents for gas storage and water treatment, (McKeown and Budd, 2010), with network PIMs shown to selectively remove phenol from water (Budd *et al.*, 2003). PIMs have also been used in gas sensors (Rakow *et al.*, 2010). This could be applied to a respirator in the form of a residual life indicator, particularly in the case of an industrial respirator which is protecting against known gases. As such, of all the PIMs, PIM-1 was selected for experimental use in adsorbent hollow fibres.

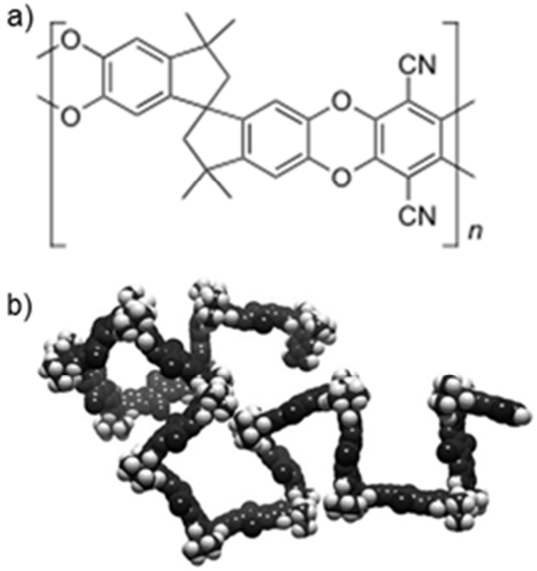

Figure 2.10. a) Chemical structure of PIM-1 b) molecular model of a single chain showing its contorted structure (Budd *et al.*, 2004a).

2.1.7 Pore formers

Adsorbent hollow fibre structure can be influenced by the use of additives, known as pore formers, in the polymer precursor mixture. These additives have a range of roles, and can enhance pore formation and improve the interconnectivity of pores. Commonly used additives include alcohols, water, polyvinylpyrrolidone and polyethylene glycol. Pores of particular sizes can also be introduced by pore formers by mixing them into the structure and are then removing them after the support has been formed. As an example, poly (alkylene carbonate) particles can be mixed into a fibre precursor mixture, and then burned off after the fibres have been formed, leaving behind pores the size of the particles (Empower-Materials, 2005). Alternatively, a hydrophilic pore former could be used, which would dissolve in water, leaving behind pores, although hydrophilic pore former could be difficult to use in adsorbent hollow fibres as it would be likely to hinder the

spinning process. Pore formers can also enhance adsorption performance by making parts of the binder porous, or tailor the support to improve adsorption of molecules it previously was not accessible to. Examples of pore former use in the literature are Williams (2001a), who added pore formers for mesopore formation, and Bagreev *et al.* (2001a), who used water to create very small pores.

2.2 Theory

2.2.1 Adsorption

Adsorption occurs when a solid surface becomes exposed to a particular gas or liquid. It is defined as "the enrichment of material or increase in the density of the fluid in the vicinity of an interface" (Rouquerol *et al.*, 1999). Molecules, atoms or ions in a gas or liquid diffuse to a solid surface where they may either chemically bond or be held by weak intermolecular forces. This occurs because the molecules on the surfaces of a solid are not fully surrounded by other molecules, and so are not fully saturated, while those on the inside are fully surrounded and hence saturated. As such those on the exposed surfaces are able to form additional bonds. The most effective solids for adsorption are those with more exposed surfaces, such as those that have a high surface area and are very porous.

The process of adsorption is exothermic (Gibbs Free Energy $\Delta F=\Delta H-T\Delta S$ with ΔS negative due to decrease in entropy) except in a few rare cases (e.g. molecular hydrogen on glass). The strength of the bond between the sorbate and sorbent can be determined from the heat of adsorption. Molecules may be adsorbed physically, by physisorption; or chemically, by chemisorption. Physical adsorption refers to adsorption where intermolecular forces, such as Van der Waals are involved. Chemical adsorption involves forces such as those made when chemical compounds are formed. The main features are in Table 2.5.

Table 2.5. Comparison of physical and chemical adsorption (Ruthven, 2000).

Physisorption	**Chemisorption**
Low heat of adsorption	High heat of adsorption
Non-specific	Highly specific
Mono or multilayer	Monolayer
Only occurs at relatively low temperatures	Can occur across a wide range of temperatures.
Rapid, reversible	May be slow, may be irreversible
No electron transfer	Bond formation through electron transfer

There are often considered to be three different stages to adsorption, although they all occur simultaneously throughout the adsorbent. Initially a monolayer of adsorbate molecules forms over the solid surface. As the adsorbate concentration increases, additional layers form and the amount physisorbed here may be limited by the pore volume. In addition, capillary condensation may occur as very small capillaries in the adsorbent are filled by condensed adsorbate (Richardson *et al*., 2002).

2.2.2 Adsorption equilibria

Adsorbent capacity is dependent on three factors: adsorbate concentration in the fluid phase, P, expressed in terms of pressure for a gas, adsorbate concentration in the solid phase (i.e. adsorbed adsorbate), C_s, and the temperature, T. By keeping one of these constant, the other two factors may be plotted to give adsorption equilibria. Plotting P against C_s with constant T gives an adsorption isotherm; plotting P against T and keeping C_s constant gives an isostere; plotting C_s against T, with constant P, gives an isobar. One of the most commonly used is the adsorption isotherm: $C_s = f(P)$ as T is fixed.

Isotherms generally form one of six shapes, which are classified by IUPAC as shown in Figure 2.11.

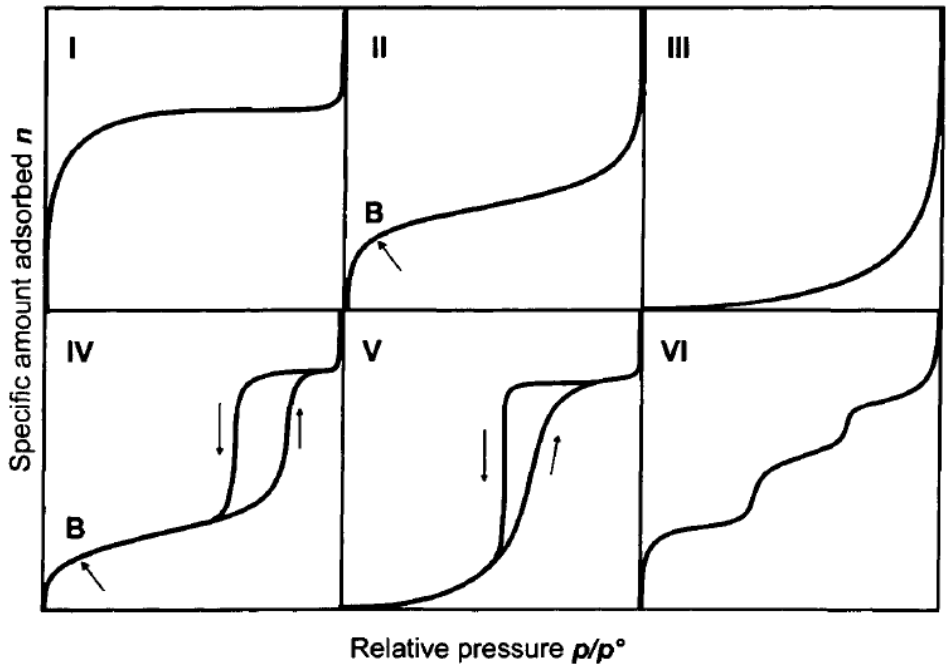

Figure 2.11. IUPAC main types of gas physisorption isotherms (Rouquerol *et al*, 1999).

Type I is typically seen in microporous solids, in which pores are completely filled at low relative pressure. The plateau of this isotherm indicates the formation of a monolayer.
Type II is associated with multi-molecular adsorption. If the 'knee' of the isotherm (point B) is sharp then the uptake from point B (quasilinear section) is generally considered as the completion of a monolayer (as in type I) and the beginning of the formation of a multilayer.

These two types show favourable adsorption, which a high uptake even at low pressures.Types I and II are the most common isotherms in separation processes (Yang, 1997).

Type III isotherms are seen in non-porous and macroporous solids, with weak interaction between adsorbate and adsorbent. Due to the weak interaction, there is little uptake at low relative pressure.
Type IV isotherms are seen in porous solids, with small pores in which capillary condensation occurs, resulting in hysteresis. The inflection point (B in Figure 2.11) indicates completion of the monolayer. These isotherms resemble type II isotherms, but with added hysteresis.

Type V isotherms resemble type III and are given by meso or microporous solids, with added hysteresis due to capillary condensation.

Hysteresis can occur during physical adsorption process, in which the quantity adsorbed is different when a gas is added to when it is removed. The exact causes of this are still not precisely defined. This phenomenon occurs in the multilayer regions for type IV and V types, where the upward adsorption branch of the hysteresis loop in Figure 2.11 is due to simultaneous multi-molecular adsorption and capillary condensation. However, during the downward desorption branch of the loop, only capillary condensation is occurring.

Type VI isotherms, also known as stepwise isotherms, are usually seen in adsorption onto a uniform nonporous solid surface. Each step corresponds to the formation of a layer on top of a previous layer.

At low concentrations, adsorbed molecules do not interact with one another on the surface of the adsorbent. As such, the concentration in the solid phase is proportional to the concentration in the fluid phase:

$$C_s = K_a P$$

This is Henry's Law, with K_a obeying the van't Hoff equation:

$$K_a = K_0 e^{-\Delta H/RT}$$

where ΔH is enthalpy change per mole of adsorbate transferring from gaseous to adsorbed phase (Richardson *et al.*, 2002) and R is the ideal gas constant. While this is the case for low concentrations, with no interaction between adsorbed molecules, at higher concentrations the adsorbent surface will become increasingly filled up. As the available surface decreases, rate of adsorption becomes proportional to the fluid concentration and the area available for it. In addition, some adsorbate will desorb for the adsorbent surface. The rate of desorption is proportional to the surface area occupied by adsorbate. For adsorption in a monolayer:

$$k_0 a_0 C = k_0(1 - a_1)C = k'_1 a_1$$

where

C is adsorbate concentration

a_0 is fraction of empty surface

a_1 is fraction of surface occupied by adsorbate

k_0 is velocity constant for adsorption on an empty surface

k'_1 is velocity constant for desorption from a monolayer

This can also be written as:

$$a_1 = \frac{B_0 C}{1 + B_0 C}$$

where $B_0 = k_0/k'_1$

This can also be expressed in terms of partial pressures for gases:

$$\frac{C_s}{C_{sm}} = \frac{B_1 P}{1 + B_1 P}$$

where

C_s = concentration in adsorbed phase

C_{sm} = concentration in adsorbed phase when monolayer is complete

$B_1 = B_0/RT$

P = partial pressure of adsorbate in gas phase

This is the Langmuir equation (Langmuir, 1918), which can be used to model isotherms, fitting a type I isotherm well. However, it assumes that adsorption only occurs in a monolayer, that there are no intermolecular interactions on the adsorbent surface, the adsorption energy is the same on the whole adsorbent and that there is no movement of molecules on the adsorbent surface. As such, not all adsorbent/adsorbate pairs follow this isotherm.

An alternative isotherm that allows for multilayer adsorption is the BET isotherm (Brunauer *et al.*, 1938). This is:

$$v = \frac{v_m c x}{(1 - x)(1 + (c - 1)x}$$

where

v = total volume adsorbed

v_m = volume of gas adsorbed to form a monolayer

$x = P/P_0$

c = constant, dimensionless, >1 and dependent on temperature

Using the relevant isotherm, adsorption characteristics can be determined from its shape. For example, the type I isotherm is favourable, due to high loading occurring at low adsorbate concentration, while type III is unfavourable due to poor loading until high adsorbate concentration. Irreversible adsorption can occur and is seen in an isotherm as a straight horizontal line, demonstrating the amount adsorbed is independent of concentration. An example of isotherm shapes and how favourable they are is shown in Figure 2.12.

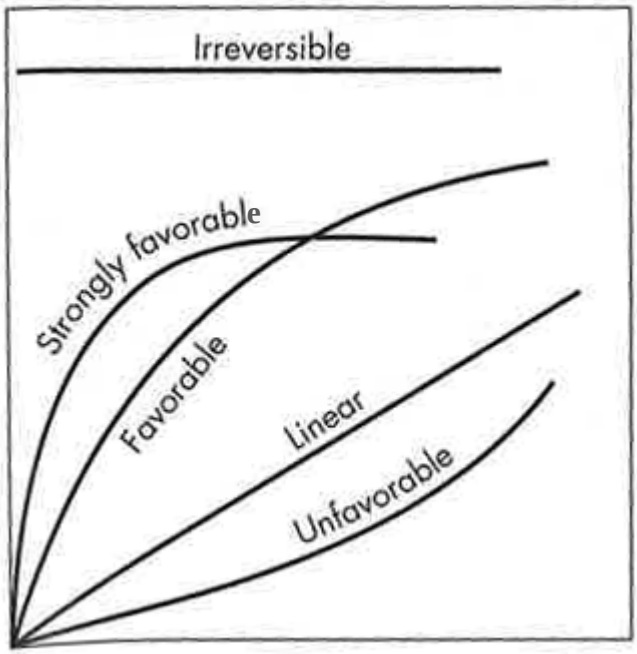

Figure 2.12. General isotherm shapes (McCabe *et al.*, 2005).

2.2.3 Adsorption breakthrough curves

In a column packed with activated carbon granules, air containing a contaminant that can be sorbed by the carbon, is pumped through the column from bottom to top. The contaminant will sorb onto and desorb from the carbon at the inlet until the sorption and desorption rates are in equilibrium, and the contaminant concentration in the gas that exits the first section is minimal. The top section will be in equilibrium and have reached its equilibrium capacity, and will be unable to remove more contaminant in the same conditions. Once the inlet carbon is exhausted, the next section will remove the

contaminant until it reaches equilibrium, and then the next section, and so forth. The section of the sorbent over which sorption is occurring is referred to as the mass transfer zone (MTZ), and the mass transfer zone moves up the column. It is preferable to have a short mass transfer zone, in order to make the most efficient possible use of the sorbent. As the MTZ moves up the column, it will eventually reach the end. At this point the concentration of the contaminant at the outlet will begin to rise, and when it becomes higher than a certain allowable limit, breakthrough is said to have occurred. When the section of adsorbent at the outlet reaches its adsorptive capacity, the concentration of the contaminant exiting the column will be the same as that entering, and equilibrium is said to have been reached. At this point the column is exhausted. This process is shown in Figure 2.13.

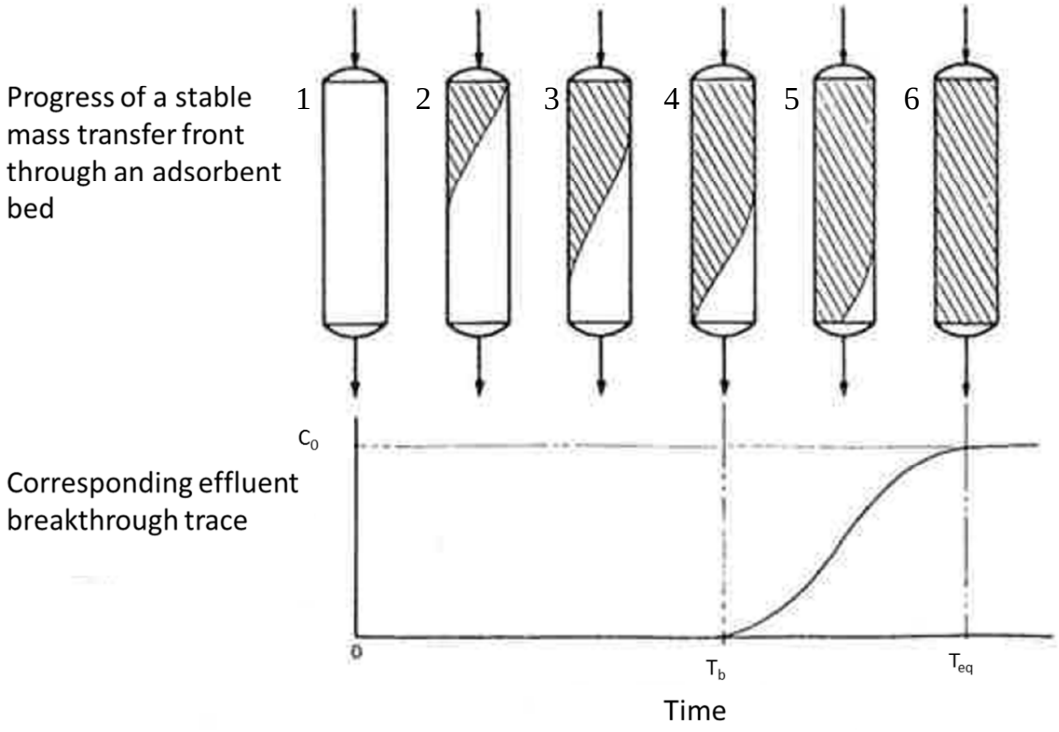

Figure 2.13. Progress of mass transfer zone and corresponding breakthrough curve, adapted from (Collins, 1967).

While the most important value determined from the breakthrough curve for a respirator application is the breakthrough time, as this indicates when the respirator is of no further use, several other key values can be determined which will aid in respirator design and breakthrough modelling. They can also allow a more detailed comparison between different adsorbents. These will be discussed in further detail below.

If flow rate became infinitely low, the length of the mass transfer zone becomes zero, and the concentration profile moves as an adsorption front. This is referred to as the stoichiometric front, and is indicated in Figure 2.14 by the line *wxyz*. It occurs at the stoichiometric time t_s and, if the breakthrough curve is symmetrical, when $C/C_0=0.5$. If the breakthrough curve is not symmetrical, then t_s is the point where the areas above and below the S-shaped curve (from point *w* onwards in Figure 2.14) are the same.

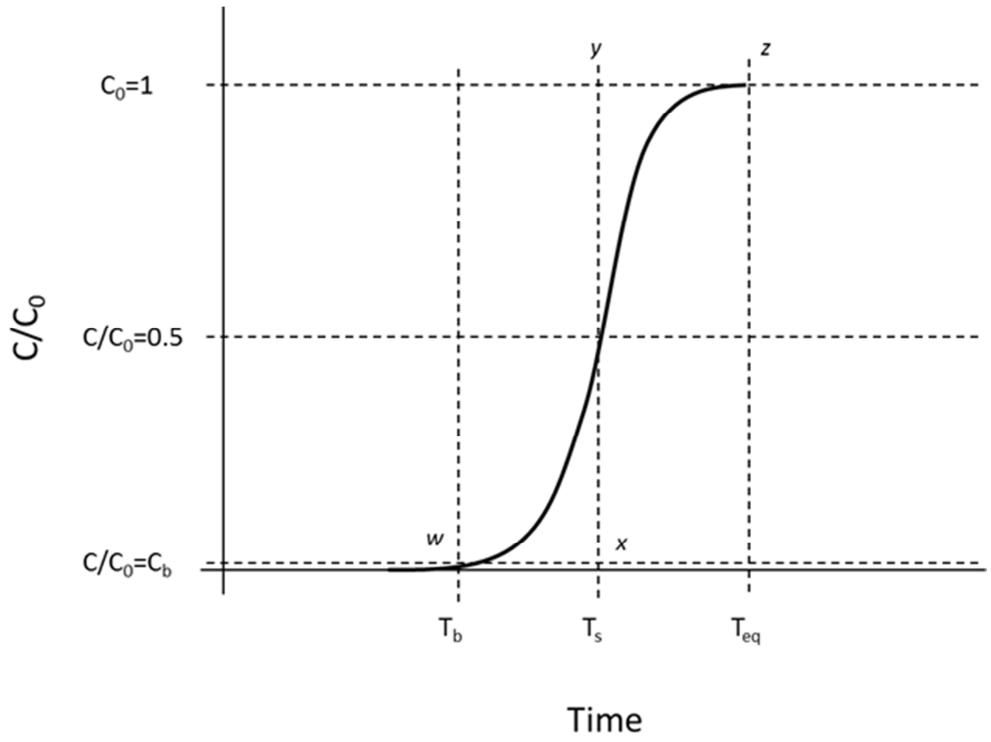

Figure 2.14. Graph demonstrating a breakthrough curve with relevant times and concentrations marked

The length of unused bed (LUB) is the amount of the bed not used for adsorption before breakthrough, which is indicated by the white area in adsorbent bed 4 in Figure 2.13. A smaller LUB indicates a sharper MTZ and more efficient use of the bed. The equation used to calculate the LUB is derived as follows:

At time t, the position of the stoichiometric front Ls is equal to the speed at which it is travelling multiplied by the time it took to reach that point.

$$L_s = v\ t$$

where v = velocity of mass transfer zone.

At the breakthrough time t_b:

$$L_s = v\ t_b \quad (1)$$

At the stoichiometric time t_s:

$$L_s = L = v\ t_s \quad (2)$$

(i.e. at the stoichiometric time, the stoichiometric front is at the end of the bed, hence it is at position L along the length of the bed, essentially the end of the bed). Therefore:

$$L - L_s = v\ t_s - v\ t_b$$

The length of unused bed is the area between the length of the bed and the position of the stoichiometric front at the stoichiometric time, as such;

$$\mathrm{LUB} = v\ (t_s - t_b) \quad (3)$$

By combining equations (2) and (3):

$$\mathrm{LUB/L} = v\ (t_s - t_b)/v\ t_s \quad (4)$$

and therefore LUB can be calculated using (Collins, 1967):

$$\mathrm{LUB} = L\ \frac{(t_s - t_b)}{t_s} \quad (5)$$

where

t_b = breakthrough time

t_s = stoichiometric time

LUB = length of unused bed

L = overall length of bed

The area of the bed that is used for adsorption before breakthrough is referred to as the equilibrium section, such that the length of the equilibrium section (LES) (McCabe *et al.*, 2005):

$$\text{LES} = L - \text{LUB} \quad (6)$$

The velocity of the MTZ, *u*, i.e. the speed at which the S-shaped MTZ travels along the bed, can be calculated by dividing the length of the bed by the stoichiometric time in a slight modification of the equation speed = distance over time:

$$u = \frac{L}{t_s} \quad (7)$$

To determine the length of the MTZ (LMTZ), the time period from the measurement of the initial detectable concentration to the inlet concentration C_0 must be recorded. This is expressed as Δt, which is equal to t_{eq}-t_b, the time required for the MTZ to travel its own length. Using *u* and Δt, the LMTZ can be calculated (Schweitzer, 1997).

$$\text{LMTZ} = u\Delta t \quad (8)$$

2.2.3.1 Factors affecting mass transfer zones

The rates of mass transfer and the pressure drop in an adsorbent bed are important. The rate of mass transfer is related to the resistance during transport from the bulk fluid phase and the adsorbent surface. When the adsorption rate is high, the length of the mass transfer zone is shorter and so the adsorbent is used more efficiently.

The shape of the mass transfer zone is heavily influenced by diffusion rate. Adsorbate molecules are carried by a gas flow, which forms a thin film around adsorbent particle surface. The transfer of the adsorbate and the carrier gas is by diffusion through this film. To reach the internal adsorbent surface, pore diffusion must occur. In addition, external bulk diffusion occurs transverse to the carrier gas flow (Schweitzer, 1997).

The length and rate of movement of the mass transfer zone are influenced by a number of factors (Schweitzer, 1997):

1. Adsorbent particle size: a greater surface area exists on smaller particles. A bed with smaller particles, although causing a higher pressure drop, will be more efficient, with a sharper MTZ than one with larger particles.

2. Adsorbent bed length: the bed must be longer than the length of the MTZ for efficient adsorption. If the MTZ is more than double the length of the bed, breakthrough will be instantaneous. Increasing bed depth will increase capacity significantly. Ideally, the longest possible bed should be used, allowing for pressure drop. To allow the MTZ to reach a steady-state, the bed should be approximately three times longer than the mass transfer zone, as demonstrated in Figure 2.15.

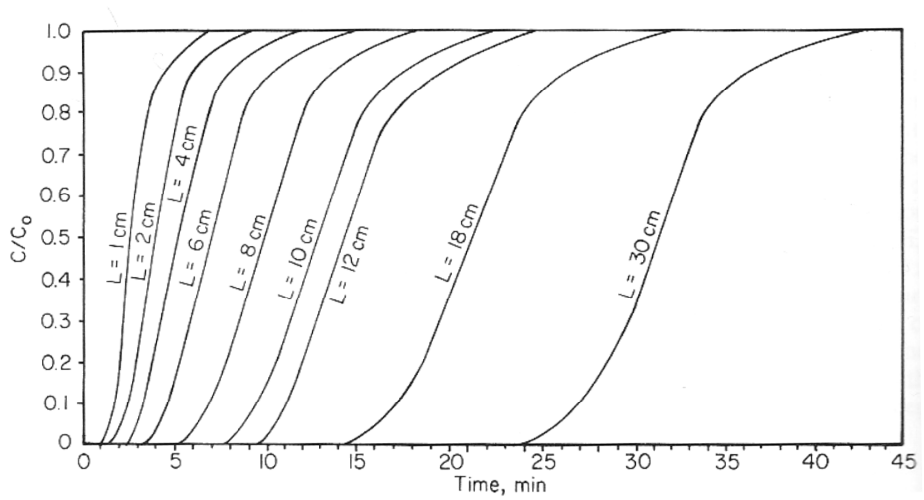

Figure 2.15. Breakthrough curves reaching steady-state at longer bed lengths (Schweitzer, 1997)

3. Gas velocity: this affects the length of the MTZ and the speed at which it travels. When superficial gas velocity is altered, the flow regime can vary between laminar and turbulent, changing the rate-controlling steps. In laminar, the rate controlling step is bulk diffusion, in turbulent it is pore diffusion (Schweitzer, 1997).

4. Temperature: physical adsorption capacity decreases as temperature increases. All diffusion rates will increase and so MTZ will be shorter, with a faster rate of movement. The shorter MTZ is less significant than increased movement speed, in gas-phase adsorption.

5. Adsorbate concentration: with increasing concentration, the rate of MTZ movement will increase and so Δt will decrease.

6. Concentration of other adsorbates: any gas or vapour can be adsorbed to some extent on any adsorbent. These gases compete for surface area and/or pore

volume, and so they will lower adsorption capacity. Moisture will interfere with polar adsorbents. The presence of moisture increases the rate of movement of the main adsorbate MTZ and will increase its length.

2.2.4 Modelling breakthrough curves

Gas masks may be challenged with a range of gases at different concentrations and flow rates. It is impossible to test for every possible challenge to a respirator. As such, models are necessary to predict breakthrough curves in a range of conditions. A number of methods to model breakthrough have been developed. Two of the most commonly used are the Linear Driving Force (LDF) equation and the Wheeler-Jonas equation. The Wheeler-Jonas equation is commonly used to predict the service life of respirators, while the LDF equation is more frequently used in the design of adsorbers (Grévillot *et al.*, 2011).

The Linear driving force (LDF) equation is based on a model of mass transfer within adsorbent particles. The breakthrough curve can be determined using this equation:

$$t = \frac{MW_e}{Qc_0} - \frac{1}{k_q}\left(1 + \frac{1}{1-R}\right) ln\left(\frac{1 - c_b/c_0}{(c_b/c_0)^R}\right) \qquad (9)$$

where

t = time

M = weight of module (g)

W_e = equilibrium loading of module

Q = flow rate

c_0 = initial concentration

c_b = breakthrough concentration

$$R = \frac{1}{1 + K\ C_0}$$

k_q = intraparticle mass transfer coefficient (min^{-1})

For spherical pellets, k_q is given by:

$$k_q = \frac{15D_e}{r^2} \qquad (10)$$

where

D_e = effective intraparticle diffusion coefficient

r = radius of spherical particle.

The focus of this research is on adsorbent hollow fibres, meaning an adjustment would need to be made to determine k_q. Patton *et al.* (2004) applied the LDF model to adsorption in monoliths, determining k_q for hollow cylinders. This could theoretically also be applied to hollow fibres. The first term of the LDF equation is the same as for the Wheeler-Jonas equation, and gives the stoichiometric time, with the second term explaining the spreading around the stoichiometric time. However, the LDF equation also includes the Langmuir coefficient K, so taking into account the curvature of the isotherm as well as the mass transfer coefficient, k_q. A higher K value from the Langmuir isotherm will result in a shorter mass transfer zone. Also, the curve given will be asymmetric, as a result of R.

The Wheeler-Jonas equation gives a model of breakthrough curves based on the mass balance between the contaminant, amount adsorbed and amount passing through the bed. It assumes plug flow, physisorption, and pseudo first order reaction kinetics (Bell *et al.*, 2012). The Wheeler-Jonas equation has been found to apply in a range of situations, including streams containing water vapour (Lodewyckx and Vansant, 1999), non-linear flow patterns (Suzin *et al.*, 2000) and chemisorption of inorganic gas molecules (Lodewyckx and Verhoeven, 2001 and 2003).

The Wheeler-Jonas equation is:

$$t_b = \frac{M.W_e}{Q.c_0} - \frac{W_e.p_b}{k_v.c_{in}}.\ln\frac{c_0 - c_b}{c_b} \qquad (11)$$

(Jonas and Rehrmann, 1973; Wheeler and Robell, 1969)

where

t_b = breakthrough time to reach c_{out} (min)

M = weight of carbon bed (g)

W_e = equilibrium adsorption capacity (g/g carbon)

Q = volumetric flow rate (g/cm^3)

p_b = bulk density of carbon bed (g carbon/cm^3)

k_v = overall adsorption rate coefficient (min^{-1})

c_0 = initial concentration (g/cm^3)

Most of these parameters are readily available, but two of them must be calculated: W_e, the adsorption capacity and k_v, the overall rate coefficient.

W_e can be calculated from Dubinin-Radushkevich equation:

$$W_e = W_o\, d_L \exp\left[\frac{-BT^2}{\beta^2}\log^2\left(\frac{c_s}{c_0}\right)\right] \qquad (12)$$

(Wood and Lodewyckx, 2003)

where

W_e = adsorption equilibrium capacity

W_o = micropore volume (cm^3/g carbon)

d_L = liquid density of organic vapour (g/cm^3)

B = structural constant of the carbon (K^{-2})

T = test temperature (K)

B = affinity coefficient of organic vapour (-)

c_s = concentration at saturation vapour pressure (g/cm^3)

While W_e is relatively simple to calculate, k_v is more challenging to model. This is because it is affected by a wide range of parameters and depends on the interactions between specific gases and adsorbents. There are a range of methods for calculating k_v, based on theoretical diffusion models and some data. This presumes dependence of the adsorption rate constant k_v on the linear velocity (Jonas and Rehrmann, 1974), molar polarization, linear airflow velocity and breakthrough fraction (Wood and Stampfer, 1993), airstream velocity, the affinity constant of the organic vapour tested, and the mean diameter of the carbon particles (Lodewyckx and Vansant, 2000). One of the most recent equations also takes into account the square root of the molar equilibrium capacity of the

test gas in the carbon, and gives good correlation with experimentally determined rate coefficients (Wood and Lodewyckx, 2003):

$$k_v = 800\,\beta^{0.33} {v_L}^{0.75} {d_p}^{-1.5} \sqrt{\frac{W_e}{M_w}} \qquad (13)$$

where

M_w = molecular weight of vapour (g/mol)

d_p = average diameter of carbon particle (cm)

β = affinity coefficient of organic vapour (-)

v_L = superficial velocity

When k_v can be calculated using the Wood and Lodewyckx (2003) equation above, it suggests surface diffusion is the limiting step in adsorption. When this equation does not apply, it suggests there is a different limiting step, for example chemical interactions between carbon, impregnants and adsorbed gas. As such, for the purposes of this work and the likely interactions for ammonia and hydrogen sulphide, empirical data was sought. k_v can be calculated from a single breakthrough experiment, using (Busmundrud, 1993):

$$k_v = b\frac{L}{v_L} = b\,\frac{M}{Q\,p_B} \qquad (14)$$

where

b = a constant

L = length of bed

v_L = superficial velocity

M = wt adsorbent

Q = volumetric flow rate

p_b = bulk density of granular bed

Alternatively, if multiple breakthrough experiments are carried out, W_e and k_v can be extrapolated from a graph of breakthrough time against bed weight, or 1/flow rate against bed weight. This gives a straight line, with W_e equivalent to the slope and k_v to the intercept (Wood and Moyer, 1989). This has been shown to be more accurate in determining W_e and k_v than the Busmundrud method by (Lodewyckx *et al.*, 2004).

While the Wheeler-Jonas equation was designed to predict physisorption on GAC, it has been shown to have a greater scope with and without minor modifications. For instance, it can be used to predict breakthrough times when humidity is present in the gas stream (Lodewyckx and Vansant, 1999), also it can be used in the case of pulsating flow, as would be used to model breathing in a respirator (Suzin *et al.*, 2000). Several groups have demonstrated that the Wheeler-Jonas equation could be applied for chemisorption as well as physisorption (Verhoeven and Lodewyckx, 2001).

The Wheeler-Jonas equation can be used to plot a full breakthrough curve, as well as obtain breakthrough time:

$$t = \frac{\rho_b q_0}{c_0}\left[\frac{z}{u} - \frac{1}{k_v} ln\left(\frac{c_0 - c}{c}\right)\right] \quad (15)$$

where

z = position in the bed

t = time

c = concentration at z and t

u = empty column gas velocity

The stoichiometric time can be calculated, assuming an infinite k_v in the ideal case of no axial dispersion and ideal mass transfer kinetics. This gives:

$$t_s = \frac{M.W_e}{Q.c_0} \quad (16)$$

This does not take into account curvature of the isotherm, which is known to affect the shape of the adsorption front (Yang, 1997). t_s occurs when the exit concentration is half the feed concentration, meaning the Wheeler-Jonas is most applicable when the isotherm is linear and for a symmetrical breakthrough curve. In addition, the curve is constant, and does not change shape as it travels through the bed, meaning entrance effects are not taken into account. It also does not take into account mass transfer kinetics or axial dispersion, which spread the adsorption front (Grévillot *et al.*, 2011).

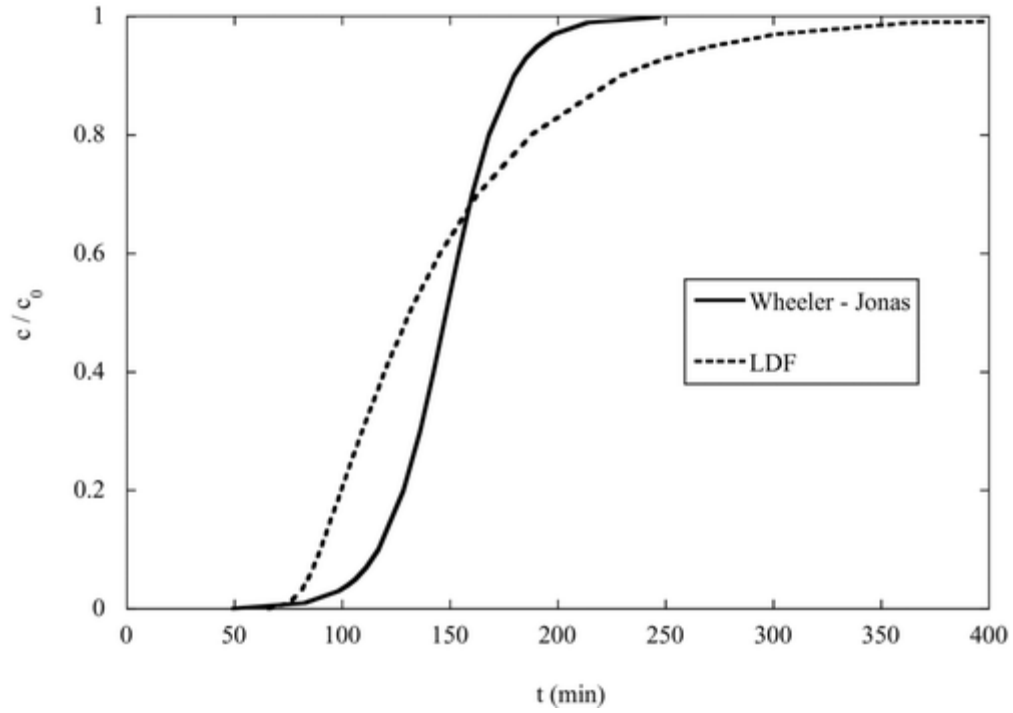

Figure 2.16. Comparison of the Wheeler-Jonas and LDF breakthrough curves with same t_s = 148 min. (K = 8 m3 g^{-1}, R = 0.038, c_0 = 500 ppm) (Grévillot *et al.*, 2011).

Figure 2.16 shows a comparison of the two breakthrough models. The Wheeler-Jonas equation can be used for any isotherm, while the Linear Driving Force equation requires a K value from a Langmuir isotherm, meaning that the isotherm for the material and adsorbate of interest need to fit a Langmuir isotherm model. In addition, an intraparticle diffusion coefficient needs to be calculated. While the LDF has been applied to monoliths (Patton *et al.*, 2004), in terms of practicality the Wheeler-Jonas equation is the simplest option for modelling the experimental results. This is especially true for some of the TICs due to the difficulties in obtaining isotherms in some cases, such as ammonia.

2.2.5 Mass transfer and transport resistances

Mass transfer occurs due to a difference in chemical potential, as a molecule will move from area of higher concentration (inlet gas stream) to lower concentration (adsorbent). Mass transfer will cease when there is a uniform concentration (at equilibrium). A large mass transfer resistance can lead to full use not being made of the adsorbent module due to slow access to adsorption sites.

There are three main types of mass transfer resistances during adsorption:

1) Film transport, related to the diffusion of adsorbate through a hydrodynamic boundary layer around the pellet or within hollow fibre bore (mass transfer coefficient k_c).
2) Resistance to diffusion through the adsorbent macropores (Maxwellian or Knudsen depending on pore size vs mean free path of adsorbate molecules).
3) Resistance to diffusion on the surface of the pores (micropore resistance, diffusivity coefficient, as adsorbed molecules move to adsorption sites).

Adding together Maxwell/Knudsen and surface diffusion coefficients gives an effective diffusion coefficient D_e. This, with mass transfer coefficient, k_c, allows the overall mass transfer coefficient, k, for the process to be found with resistance defined as 1/k (Seader *et al.*, 2010). The relative importance of the steps above depends on the adsorbent, adsorbate and conditions (temperature, pressure etc.) (Crittenden, 1998).

For physical adsorption, the rate controlling step is the intraparticle transport of gas once it is within the porous adsorbent structure, rather than the adsorbate-adsorbent attachment, which is very quick. Smaller pellets and thinner fibres have a shorter diffusional path, which will enhance adsorption uptake due to a reduction in mass transfer resistance as well as increased surface area (though there is a trade off with pressure drop). The macropore resistance depends upon the thickness of the wall, and so will be comparable between adsorbent hollow fibres and pellets of similar size. Similarly, the micropore resistance will depend on the adsorbent used, its cage/pore sizes and affinity towards the adsorbate.

In industry, when crystalline adsorbents such as zeolites are used they must be suspended in a ceramic or polymeric binder to withstand pressure changes and minimise the attrition associated with extremely small particle size. Generally they are bound with a binder, such as clay, to make a pellet containing macro and micropores. After passing through the boundary layer, the molecules of adsorbate diffuse into the complex structure of the adsorbent pellet, which is composed of an intricate network of fine capillaries or interstitial vacancies in a solid lattice. Zeolite crystals have uniform windows and channels, thorough which adsorbate may travel and reach larger meso or macropores. These intercrystalline cavities can form a network through the structure, while the binder,

typically clay, also contains micropores. This results in additional resistance of zeolite intracrystalline diffusion, and can lead to a molecular sieving effect (Ruthven, 2000).

For materials using a binder, such as polymer in adsorbent hollow fibres, there is the possibility of added resistance if access to adsorbent is blocked. This is referred to as "occluded" sieves (Bhandari *et al.*, 2010). This means that rather than diffusion being through the porous structure of the interconnected pore network of the adsorbent, it will be through the polymer. In this case, the solution diffusion mechanism is more dominant.

Research suggests that hollow fibre membrane modules have faster mass transfer than a granular module, in the case of gas absorption (Wickramasinghe *et al.*, 1992) and several inherent advantages over a granular bed shape, especially that of inherently higher surface area. Bhandari *et al.* (2010) have investigated the different significance of the various resistances in adsorbent hollow fibres compared to adsorbent pellets, with resistances in a pellet shown in Figure 2.17. For example, macropore resistances are lower in fibres than pellets due to the thin walls of hollow fibres compared to pellets. Obviously, if pellet size is decreased to match the thin walls of the fibres, pressure drop will increase accordingly.

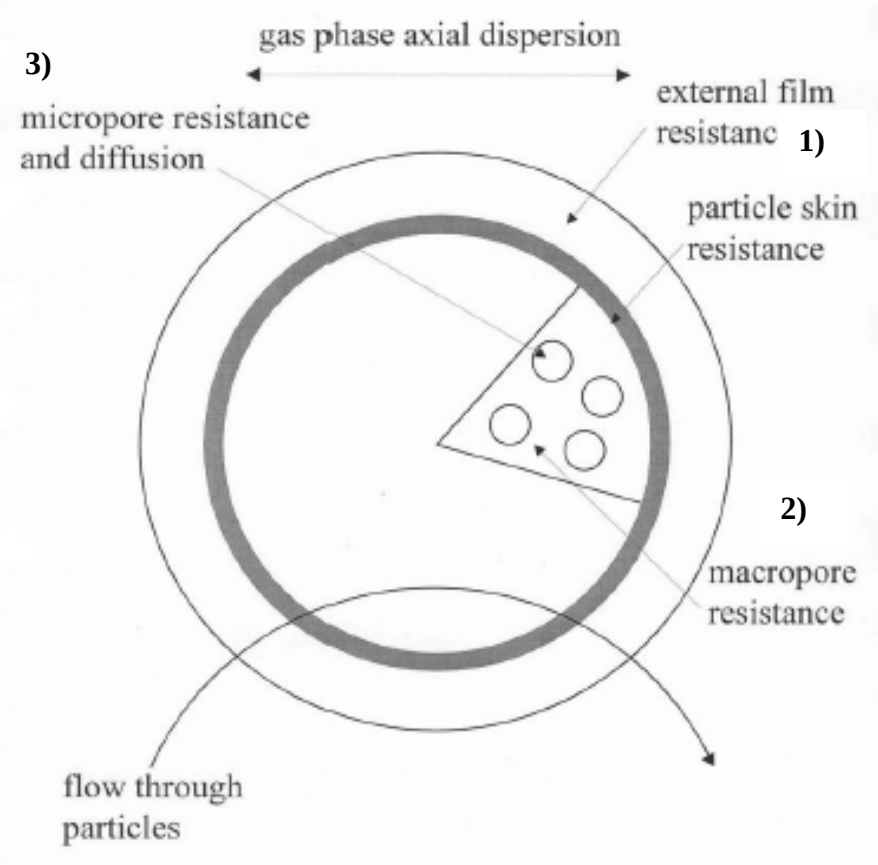

Figure 2.17. Adsorption resistances in a particle (Crittenden, 2010).

2.2.5.1 Transport in polymers

Due to the potential for adsorbent to become occluded by binder, particularly polymers, as mentioned in Section 2.2.5, it is important to consider how transport through the binder will affect mass transfer. Several examples of transport are demonstrated in Figure 2.18. In the case of most polymers, solution diffusion will be taking place, while other mechanisms of gas flow will occur throughout the macrostructure of the hollow fibre or pellet.

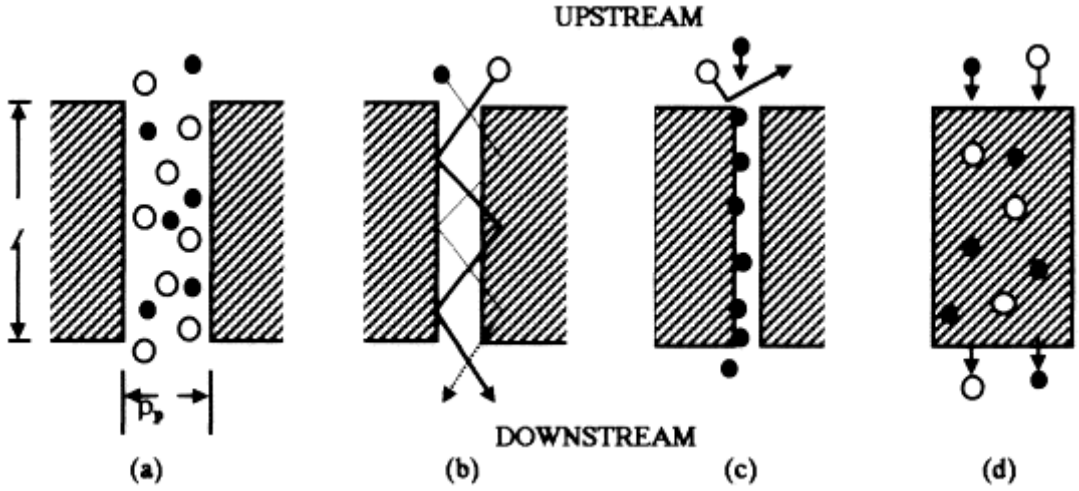

Figure 2.18. Gas molecule transport in porous structures by: a) viscous flow, b) Knudsen flow, c) molecular sieving, d) solution diffusion (Stern and Trohalaki, 1990).

How gas flows depends on the size of the pores in relation to the free-path of the gas molecules. For viscous flow through a large pore, the rate of flow is inversely proportional to viscosity of the gas, while in Knudsen flow, where mean free-path is greater than the size of the pore, flow rate is inversely proportional to square root of molecular mass of the diffusing species. Meanwhile, molecular sieving is extremely selective compared to these other methods. In solution diffusion, the adsorbate species permeating the polymer interact with the polymer matrix, essentially dissolving in it. This results in mass transport along a chemical potential gradient.

Transport behaviour will vary for different chemicals in different polymers, largely affected by free volume within the polymer as well as the mobility of its chains. This segmental mobility is tied with the glass transition temperature of the polymer, both being affected by how much crosslinking there is in the polymer, as well as its crystallinity and saturation (George and Thomas, 2001). As such, in general polymers with greater segmental mobility and hence low glass transition temperatures have greater diffusivity than those with lower segmental mobility (Brown and Park, 1970), although the PIMs are an exception. Unsaturated polymers tend to have greater segmental mobility, hence greater diffusivity (Auerbach *et al.*, 1958). Also, lower diffusivity has been observed with polymers with lower molecular weight (Berens and Hopfenberg, 1982).

The rate of diffusion through the polymer will also vary according to the adsorbate molecule. A small molecule such as ammonia is likely to have higher diffusivity than a large molecule, such as cyclohexane, and larger adsorbate molecules, such as longer chain length alkanes, are reported in the literature to have lower diffusivity (Kim *et al.*, 1993).

2.2.6 Pressure drop

Pressure drop, ΔP, describes a drop in pressure between one point and another as a result of frictional forces. It is dependent on fluid flow rate and fluid viscosity, with high velocity and viscosity resulting in a higher pressure drop. While pressure drop can be measured, it is important to model pressure drop at flow rates that would be difficult to test in the lab in order to inform design decisions. As an exam3c ple, breathing at 85 L/min with no respirator results in a 150 Pa pressure drop. In a WW2 gas mask, there was an 800 Pa pressure drop at this flow rate, while in the M17 (used by US pre-1959) and M40 (used by US 1959-1992) were 450 and 500 Pa respectively (Borrelli, 2007). Testing pressure drop at 85 L/min would be beyond the scope of this study; as such a pressure drop model will be used to investigate the effects at higher flow rates.

In order to determine pressure drop, the type of flow (laminar or turbulent) must be determined by calculating the Reynolds number. For flow through a granular bed, this takes voidage into account:

$$Re^{pb} = \frac{\rho u d_p}{\mu(1-\varepsilon)} \tag{17}$$

where

u = superficial velocity (m/s)

ρ = fluid density (kg/m^3)

d_p = particle diameter (m)

ε = void space (m)

μ = fluid viscosity (Pa·s)

Laminar flow exists when $Re^{pb} < 10$, turbulent ≥ 2000 (Rhodes, 2008; Richardson *et al.*, 2002).

To determine the type of flow in a cylindrical pipe:

$$Re = \frac{\rho u d}{\mu} \quad (18)$$

where d is the diameter of the pipe.

Flow is assumed to be laminar when Re < 2300, transient when 2300 < Re < 4000 and turbulent when Re > 4000.

2.2.6.1 Modelling pressure drop

There are a range of equations that can be used to model pressure drop. Each equation is most accurate in particular cases. Three commonly used equations are the Hagen-Poiseuille, Carman-Kozeny and Ergun equations. The Hagen-Poiseuille equation applies for the laminar flow of a fluid in a circular channel (Hagen, 1839). The Carman-Kozeny equation applies for the laminar flow of a fluid through a packed bed of solids (McCabe *et al.*, 2005) . The Ergun equation applies for turbulent flow of fluid through a packed bed of solids, when Carman-Kozeny no longer applies. (Richardson *et al.*, 2002).

The Hagen-Poiseuille equation is as follows, with this particular example from Feng *et al.* (1998):

$$\frac{\Delta P}{L} = \frac{32\mu}{d^2}\left(\frac{v}{\epsilon_0}\right) \quad (19)$$

where

ΔP = pressure drop (Pa)

L = bed length (m)

v = average superficial velocity based on empty cross section of adsorber

ε_0= is the fractional volume of the adsorber used for gas flow

d = fibre inner diameter (m)

μ = fluid viscosity (Pa·s)

The Carman-Kozeny equation, as given by McCabe *et al.* (2005) is:

$$\Delta P = L\,\frac{180\,u\,\mu}{{\varphi_p}^2 {d_p}^2}\frac{(1-\epsilon)^2}{\epsilon^3} \tag{20}$$

where

ΔP = pressure drop (Pa)

L = bed length (m)

μ = fluid viscosity (Pa·s)

ε = void space

u = superficial velocity (m/s)

d_p = particle diameter (m)

φ_p = sphericity of the particles

The Ergun equation (Ergun, 1952) is:

$$\Delta P = L\left(\frac{150u\mu(1-\varepsilon)^2}{\varepsilon^3 d_p^2} + \frac{1.75(1-\varepsilon)\rho u^2}{\varepsilon d_p}\right) \tag{21}$$

where

ΔP = pressure drop (Pa)

L = bed length (m)

μ = fluid viscosity (Pa·s)

ε = void space

u = superficial velocity (m/s)

d_p = particle diameter (m)

ρ = fluid density (kg/m^3)

With this knowledge, pressure drop can be calculated using a variety of models. For the calculation of pressure drop through hollow fibres while the flow remains laminar, the Hagen-Poiseuille model is the most suitable, and has been used for this purpose by Bhandari *et al.* (2010). For a packed bed system, the Ergun and Carman-Kozeny equations could both be applied, with the Ergun equation giving a more accurate result in turbulent flow (Rhodes, 2008).

2.3 Conclusion

The idea behind the respirator is old, and little has changed over time. There are a number of aspects of the current military gas mask that could be improved. Main areas to focus on include reducing the respirator burden, namely its size, weight and breathing resistance (pressure drop). Other areas for improvement include resistance to ageing, a residual life indicator and minimising leaks, as well as improving performance with TICs (Pelfrey, 2011; Smith, 2011). Following a review of current literature and theory, adsorbent hollow fibres are seen as having the potential of addressing several of the issues with granular filters in respirators for a number of reasons, given below:

1. Low pressure drop results in easier breathing and so reduced physiological burden and greater comfort for the wearers, particularly if wearing over long periods of time.

2. Low mass transfer resistance in fibres results in shorter mass transfer zones result in more efficient use being made of adsorbent, when only a low weight can comfortably be carried.

3. High voidage means lighter weight, so a greater volume/length of hollow fibre has an equivalent weight to granules.

4. The even distribution of adsorbent powder within the fibre structure and the uniform shape of hollow fibres minimise the risk of gas channelling and bypass.

5. Fibres can operate in any orientation (respirator user lying down, standing up, moving) while granular beds risk gas bypass if operated horizontally.

6. No special packing equipment is required to fill a cartridge with fibres, while special equipment is required for efficient packing of granules.

7. Fibres can have multifunctional layers, making it possible to incorporate a variety of adsorbents required to tackle acid and basic gases simultaneously.

8. The polymers in adsorbent hollow fibres are strong, as would be required to withstand rough treatment of respirators (such as ballistics testing).

9. The flexible shape of adsorbent hollow fibres enables novel designs of respirator where the filter does not necessarily need to be in a cartridge separate from the mask.

In order to address a range of TICs:

- Adsorbent composite fibres made up of a mixture of activated carbon and zeolites will be investigated. This will take advantage of the respective strengths of both types of adsorbent.
- Methods to enhance the adsorption of difficult to remove TICs such as H_2S will be explored, primarily by impregnating the adsorbent fibres with metal salts and metal organic frameworks, which have greater affinity for H_2S than untreated activated carbon or zeolite.
- A novel intrinsically microporous polymer, PIM-1, will be explored as a potential adsorbent binder for adsorbent hollow fibres. This will offer an improvement in surface area compared to a conventional polymer binder.
- The breakthrough times of adsorbent fibre modules exposed to a range of flow rates will be modelled using the Wheeler-Jonas equation. This will allow an impression to be gained of breakthrough times at very high flow rates.
- The pressure drop that different size adsorbent fibre modules will cause at human breathing rates, from 5-150 L/min, will be investigated. A model will be used to understand pressure drop at very high flow rates.

3 Materials and Methods

During this research, a number of experimental procedures were used repeatedly throughout work in different Chapters. Rather than repeat the experimental procedures each time they are used, the protocol is recorded in this Chapter and can be referred back to for Chapters 4, 5, 6 and 7. Any specifics of the experiment will be explained in the Chapter itself.

The process of adsorbent hollow fibre production, wet phase inversion, is similar to that used in the production of membrane hollow fibres; a polymer, such as polyethersulfone, is dissolved in a solvent, such as N-methyl-pyrrolidone. At this point, the mixture would undergo phase inversion and be prepared into adsorbent hollow fibres. The key difference for adsorbent hollow fibres is that an adsorbent powder, such as an activated carbon powder, is mixed into the polymer/solvent mixture before phase inversion. This results in an adsorbent hollow fibre, with the polymer holding together the adsorbent, which is distributed throughout the fibre structure.

While this particular example is a simple process, it has the potential to offer a diverse range of adsorbent hollow fibres depending on a number of factors in the spinning process. Using a different adsorbent or mixture of adsorbent powders results in completely different adsorbent hollow fibres. The ratio of polymer to solvent in the polymer/solvent mixture and the ratio of polymer to adsorbent will affect the adsorbent hollow fibre structure. There are a range of other factors in fibre preparation, which will also be explored in this Chapter.

3.1 Materials

The materials used in this research and the companies from which they were purchased or received are given in a table below.

Table 3.1. A list of the materials used in this research and the suppliers

Material	Company	Country
3000P polyethersulfone	Solvay	Brussels
N-methyl-pyrrolidone	Sigma-Aldrich	UK
Tetrahydrofuran	Sigma-Aldrich	UK
Copper (II) oxide powder	Fisher Scientific	UK
AbScents1000 zeolite powder	Honeywell UOP	US
HiSiv1000 zeolite powder	Honeywell UOP	US
13X zeolite powder	Zeochem	Switzerland
5A zeolite powder	Zeochem	Switzerland
Clinoptilolite zeolite powder	Zeochem	Switzerland
ZSM-5 zeolite powder	Alfa Chemicals	UK
NaY zeolite powder	Zeochem	Switzerland
LiLSX zeolite powder	Zeochem	Switzerland
NV5 activated carbon powder	Eurocarb	UK
HTS activated carbon powder	Eurocarb	UK
RGE activated carbon powder	Eurocarb	UK
SAC activated carbon powder	Eurocarb	UK
BPL activated carbon powder	Chemviron	UK
“Avon” activated carbon powder	Avon	UK
Silicone sealant	Bostik	UK
Wyoming sodium bentonite	RS Minerals	UK
800 ppm hydrogen sulphide in nitrogen gas	BOC Gases	UK
800 ppm ammonia in nitrogen gas	BOC Gases	UK
1000 ppm cyclohexane in nitrogen gas	BOC Gases	UK
Benzene tricarboxylic acid	Sigma-Aldrich	UK
Copper (II) sulphate	Sigma-Aldrich	UK
Ethylene glycol, anhydrous, 99.8%	Sigma-Aldrich	UK
Methanol, anhydrous, 99.8%	Sigma-Aldrich	UK
Copper (II) chloride	Sigma-Aldrich	UK
Sodium hydroxide pellets	Sigma-Aldrich	UK

Octane liquid, reagent grade, 98%	Sigma-Aldrich	UK
Cyclohexane liquid, anhydrous, 99.5%	Sigma-Aldrich	UK
Licowax SP	Clariant	Switzerland
Licowax C Micop	Clariant	Switzerland
Licowax PE 520 FG	Clariant	Switzerland
PIM-1	Dstl	UK

3.1.1 Pore formers

Three pore formers purchased from Clariant are listed in the table above. Licowax SP (säure powder) is a montan wax acid. This is made up of a mixture of "montanic acids" (C22 - C36 carboxylic acids) and esters (Broehmer, 2013), with drop forming point of 84 °C. Licowax C Micropore C is bis stearyl ethylenediamine, an amine found in lipsticks, sunscreen, and eye shadow, with drop forming point of 142 °C, melting point of 144 °C and decomposition of >200 °C. Licowax PE 520 fine grain is polyethylene wax, with a drop forming point of 120 °C (Clariant, 2012). By Clariant designations, Licowax SP has a particle diameter of < 500 μm, Licowax C micro powder has particle diameter of < 50 μm and Licowax PE 520 has particle diameter of < 125 μm (Clariant, 2012).

3.2 Methods

3.2.1 Adsorbent hollow fibre module manufacture

There are several separate steps in preparing an adsorbent hollow fibre module for testing. These are explained in chronological order in the Sections below.

3.2.1.1 Preparation of the adsorbent hollow fibre precursor mixture

Polymer/solvent/adsorbent mixtures, referred to as the adsorbent fibre precursor mixtures, were prepared by dissolving 3000P polyethersulfone (PES) polymer in N-methyl-pyrrolidone (NMP) solvent. This was prepared in a ratio of 1 polymer: 4 solvent, for example 80 g of NMP was added to 20 g of PES. These proportions were found to sufficiently dissolve the PES and form a heterogeneous mixture. The mixture was stirred on rollers at 8 rpm for 24 hours until the polymer was completely dissolved. This mixture was then stirred using an electric stirrer while the adsorbent powder was gradually added in small portions over 24-48 hours in order to ensure full mixing. For some organophilic adsorbents, such as activated carbon and AbScents1000, additional NMP was added as

required to ensure that all of the adsorbent could be suspended within the mixture and reduce its viscosity in order to make spinning possible. After the initial screening process of this report, a ratio of 1 polymer to 4 adsorbent was used, as this presented a reasonable compromise between the high adsorbent loading necessary for efficient use of the module volume (i.e., the polymer proportion of the fibre does not contribute to adsorption), and the necessary proportion of polymer to ensure the adsorbent fibre structure was mechanically strong enough to be formed into cartridges. At this stage, additives, such as pore formers could be included in the mixture. Once the adsorbent powder was successfully suspended, the adsorbent fibre precursor mixture was further mixed on rollers at 8 rpm for 24 hours to ensure adequate mixing and a suitable viscosity for spinning. The final stage of the preparation of the adsorbent hollow fibre precursor was vacuuming. For 30 minutes prior to spinning, the adsorbent mixture was exposed to a vacuum in order to remove any bubbles that formed in the mixture during the mixing process, as these may cause the fibre to break during spinning. Some fibres were prepared by Thomas Richards at the University of Bath. These ones are listed in Appendix 5.

3.2.1.2 The adsorbent hollow fibre spinning process

The prepared homogeneous adsorbent fibre precursor mixture was transferred to a stainless steel feed vessel which was pressurised with compressed air. The pressure ranged from 0.5 to 5 barg depending on the viscosity of the adsorbent fibre mixture, with a typical value of 1 barg. When exposed to pressure, the precursor mixture was pressurised into a multi-annular spinneret, as shown in Figure 3.1, with a view from above shown in Figure 3.2. Multi-annular spinnerets consist of a hollow tube in the centre of an orifice with a liquid, in this case a 1:1 mixture of water and NMP, injected through the tube to form a bore and maintain the tubular shape of the fibre until it was fully coagulated. As explained in Chapter 2, if the bore fluid contains a higher proportion of water, coagulation is rapid, reducing the porosity of the inner layer, and if the bore fluid contains a higher proportion of solvent, in this case NMP, the coagulation will be too slow and the tubular shape of the fibre will not be maintained. The 1:1 mixture was selected to ensure gradual coagulation of the inner layer of the adsorbent fibre, enhancing its porosity but ensuring the tubular structure was maintained during the spinning process.

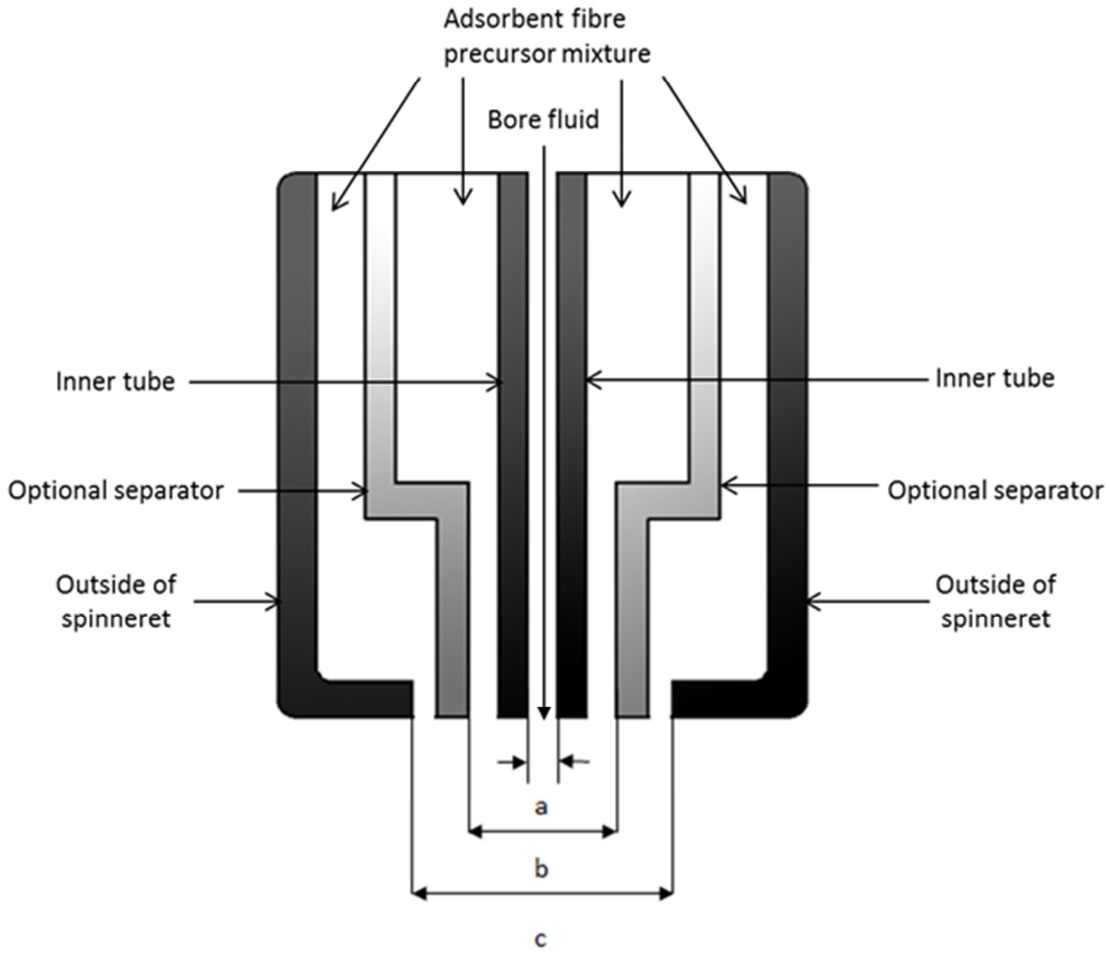

Figure 3.1. Diagram of the spinneret showing the structure in dark grey and the optional separator layer in light grey. The label *a* indicates the tube diameter of 0.8 or 0.6 mm depending on the tube used, *b* indicates the diameter of the optional separator, *c* indicates the outer diameter of the spinneret.

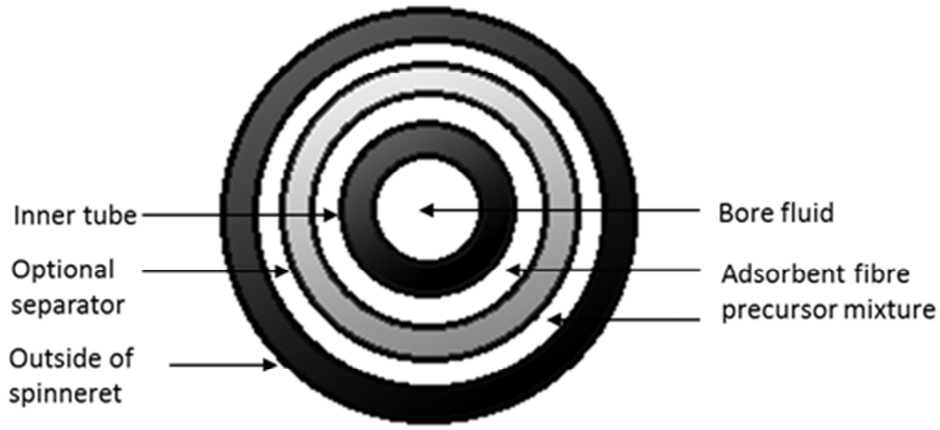

Figure 3.2. Diagram of the spinneret viewed from above with the structure in dark grey and the optional separator in light grey.

Two inner tube sizes were available for this research, 0.8 mm (referred to as ‘standard’ bore) and 0.6 mm (referred to as ‘small’ bore). The outer diameter of the spinneret was 2 mm and an additional layer could be produced by inserting a separator between the two. The separator had a diameter of 1.4 mm. The precursor mixture can pass through the multi-annular spinneret in three different ways. Firstly, with no separator, the mixture can be pushed through to form a thick single layer fibre. Secondly, with the separator in, the mixture can be extruded through both layers to produce a double-layer fibre. Thirdly, with the separator in, the mixture can be pushed through the inner layer only, producing a thin single layer fibre.

The pressurised adsorbent fibre precursor was pushed through the spinneret in one of the methods explained above and entered a water bath filled with tap water, shown in Figure 3.3. It is possible to introduce an air gap between the spinneret and the water; however, as was explained in Chapter 2, a shorter air gap (or no gap) enhances the surface area of the adsorbent hollow fibre. As a high surface area was desired, no air gap was used and the adsorbent fibre precursor mixture was passed straight into the water, where the solvent in the mixture exited into the water. This resulted in coagulation, forming the adsorbent hollow fibre. The newly formed adsorbent fibre moved through the initial water bath fibre as described above, and was then passed through a second, separate water bath. This maintained a steep concentration gradient between the amount of solvent in the fibre and in the water bath, and removed additional solvent from the fibre structure.

Water was used as the external coagulation due to the large quantity required to fill the adsorbent fibre spinning bath. The use of water as the external coagulant will result in rapid removal of the solvent from the adsorbent fibre mixture due to the steep water/solvent concentration gradient, and result in rapid coagulation. This forms a dense layer, as explained in Chapter 2. While this is unlikely to significantly lower the adsorption performance of adsorbent hollow fibres, as contaminants will enter the fibres through the bores, and have limited exposure to the outer layer, it is possible that the adsorption performance could be better in fibres with a more porous outer layer. As such, the potential to prepare fibres using a water/solvent mixture as the external coagulant, and so lowering the concentration difference between the fibre and the external bath, will be discussed in Section 3.2.1.3.

The prepared fibre was then attached to automated rollers, which ensured that the fibre was pulled through the water baths at a regular speed and avoided mechanical dragging, which could damage the fibre. After wrapping around the roller, the fibre was then collected in a third water bath. This maintained the concentration gradient between water and solvent and drew the remaining solvent out of the fibre. The fibre remained in the final bath for 72 hours and the water in this bath was refreshed every day to maintain the concentration gradient and remove small quantities of residual solvent from the adsorbent fibres. The hollow fibres were then removed from the collection bath and allowed to dry in ambient conditions for 48 hours before regeneration and characterisation.

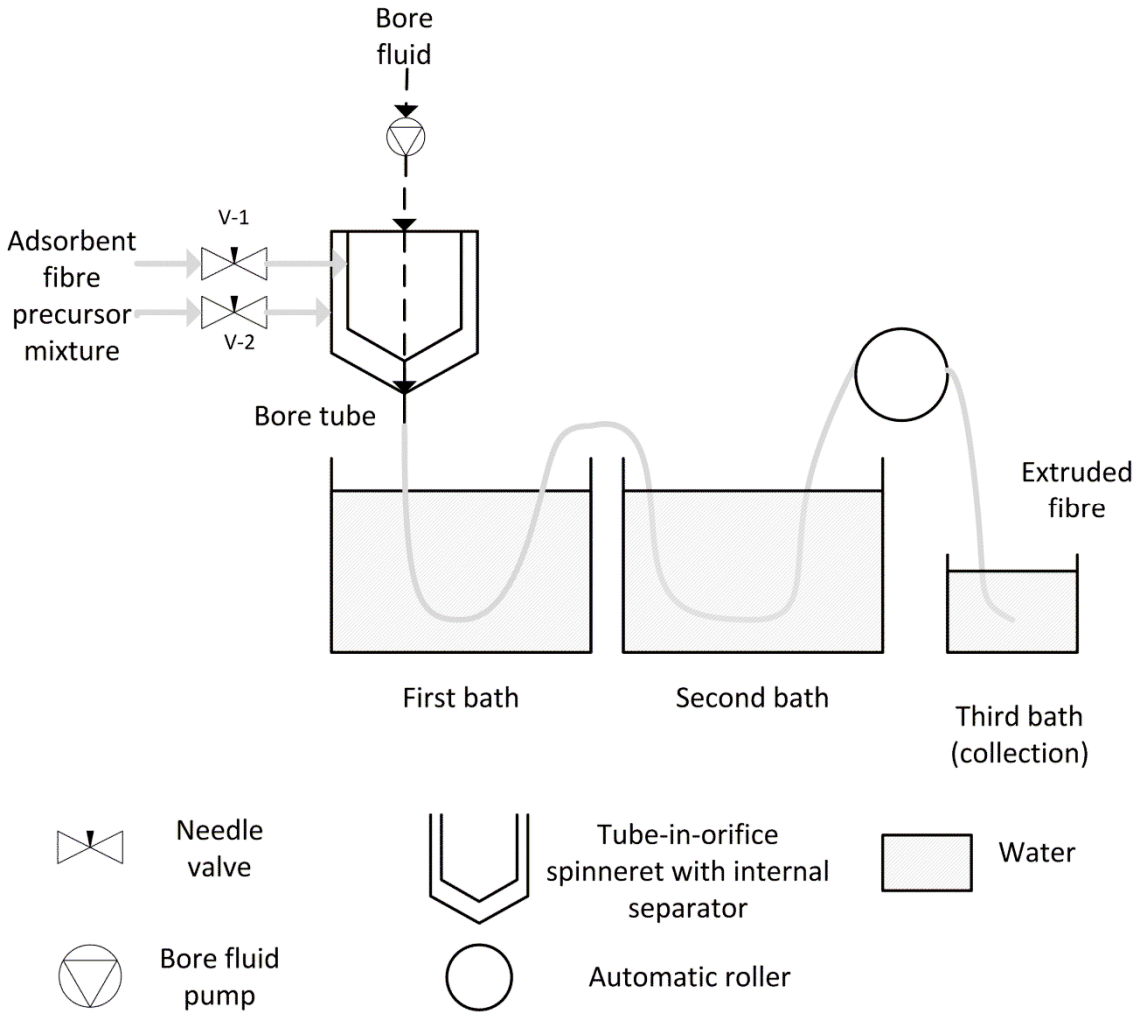

Figure 3.3. Schematic diagram of the adsorbent hollow fibre spinning apparatus.

3.2.1.3 Spinning into solvent as the external coagulating fluid

The feed vessel was pressurised with compressed air and the same spinneret and bore fluid were used as in the spinning method described in Section 3.2.1.2. However rather than passing through two water baths filled with tap water and over rollers into a

collection bath, the adsorbent hollow fibres were spun into a single bath filled with a 1:1 solvent/water mix. After being allowed to coagulate, the fibres were moved to a water bath to remove additional solvent. The fibres remained in the water bath for 72 hours and the water in this bath was refreshed three times over this period to maintain a steep concentration gradient between water and solvent and remove additional solvent from the fibres. After this washing step the adsorbent hollow fibres were removed and allowed to dry in ambient conditions for 48 hours before regeneration and characterisation.

3.2.1.4 Spinning process for PIM-1 fibres

To spin PIM-1 fibres, the process described in Section 3.2.1.3 (spinning fibres into solvent as the external coagulating fluid) was used. However, it was carried out inside a fume cupboard, and PIM-1 was dissolved in tetrahydrafuran (THF) solvent rather than NMP.

3.2.1.5 Preparation of adsorbent hollow fibre modules for dynamic adsorption challenge and pressure drop testing

In order to be used in respirator filters, a number of fibres must be packed into a module. For dynamic adsorption challenge and pressure drop testing, the modules were stainless steel cylinders of 2 cm in diameter and lengths in 5 cm intervals from 5 to 25 cm. To pack these modules, fibres were cut to 0.5 cm longer than the required length (e.g. 5.5 cm, 10.5 cm, etc.). The lumen at one end of each fibre was blocked with a small quantity (approximately 1 mm) of silicone and left to dry for 24 hours. Adsorbent fibres were then bundled into a cylindrical shape fitting the desired test module, with all the blocked ends together on the same side. A large quantity of silicone was then pressed into the blocked end and around the side of the fibre. This sealed the interstitial spaces of one end of the fibre bundle without deeply blocking the lumen. After drying for 24 hours, approximately 0.2 cm was cut from the sealed end, to expose the bores of the fibres while keeping the interstitial spaces between fibres sealed. The other (unsealed) end was then cut so that the fibre was the required length. These fibre modules were regenerated by heating to 190 ºC for 24 hours while dried compressed air was passed over the module. This stage helped to remove water and residual solvent from the adsorbent fibres and shrink the polymer, improving access to the adsorbent within the fibre, as discussed in Chapter 2. The fibre test module was then completed by inserting the regenerated fibre bundle into the

stainless steel module. If the fit was not tight, the sealed end of the fibres was wrapped in PTFE gas tape to prevent gas bypass.

After heating, in general a double layer fibre had an outer diameter of approximately 3 mm and single layer had an outer diameter of approximately 2 mm. Thick single layer fibres also had a diameter in the region of 3 mm. The disparity between fibre diameter and spinneret diameter is due to the spinning conditions, the type of adsorbent/s used, die swell, and the fact that the fibres shrink slightly when heated.

3.2.2 Adsorbent pellet manufacture

Conventional respirator canisters contain adsorbent pellets or granules. In order to compare the adsorbent hollow fibres to a conventional pellet bed of the same composition, pellets containing the same adsorbent powder in the same proportion as an adsorbent fibre were prepared. Details are given below for the manufacture of adsorbent pellets containing AbScents1000 zeolite and a 50:50 mixture of AbScents1000 and NV5 activated carbon powder using a hand press. A photograph of the hand press used is shown in Figure 3.4.

Figure 3.4. The hand press used to prepare adsorbent pellets. The dough was placed inside the tube to the left and pressed through a die at the base of the hand press. Pressure was exerted by turning the handle.

To prepare 80%wt AbScents1000 pellets, 20 g of Wyoming sodium bentonite powder was thoroughly mixed with 87.9 g of AbScents1000 powder (80 g dry weight) and 105 g

of tap water was added. This was formed into dough and allowed to mature for two days. The mature dough was placed into a metal tube and then the handle of the press was turned, compressing the dough through a stainless steel extrusion die. The die used is shown in Figure 3.5. It was 2 cm in diameter and had a number of circular cavities 1.2 mm in diameter. The dough was formed into cylindrical extrudates 1.2 mm in diameter and of varying short lengths. These were dried at 5 °C for two days and then fired in a kiln using the following temperatures: first they were heated to 180 °C over 18 hours and then to 550 °C over ten minutes. This temperature was maintained for 20 hours. The extrusions were broken into pellets and sieved, keeping what remained between 0.3 mm and 2.8 mm sieves, and then heated to 165 °C to remove water from the adsorbent.

Figure 3.5. The extrusion die used to prepare adsorbent pellets. The dough was pressed through this die to form long cylindrical extrusions which were cut into pellets.

3.2.3 Adsorption testing

3.2.3.1 Dynamic toxic gas breakthrough studies

Respirator filters are exposed to toxic gases under dynamic conditions as the wearer breathes. As such, dynamic adsorption tests, in which the adsorbent modules were challenged with a flow of ammonia, hydrogen sulphide or cyclohexane gases were carried out in order to determine the level of protection that the adsorbent hollow fibres and adsorbent pellets could provide. A gas detector was used to measure the external concentration of toxic gas over time. This can be used to plot a breakthrough curve, which enables important values such as breakthrough time and loading to be calculated, as discussed in Chapter 2. A Tiger PhoCheck photoionisation detector (PID) was used to measure the concentration of the toxic gas at the outlet of the adsorbent module. The PID contains a bulb that emits UV light, which breaks gas molecules into positively charged ions. The ionised gas is electrically charged, producing an electric current. The current is

amplified, read, multiplied by a factor to calculate the concentration and then displayed as the output of the PID. As a result, PIDs are not selective detectors and the identity of the test gas must be known in order to obtain accurate results.

From these tests, the breakthrough time can be observed. In addition, breakthrough loading, (the weight of toxic gas adsorbed at the breakthrough time), can be calculated. After regeneration, the adsorbent hollow fibres were weighed and then dynamically challenged with toxic gases in the adsorption apparatus shown in Figure 3.6. The test gases H_2S or NH_3 were provided at 800 ppm dilution and cyclohexane was provided at 1000 ppm in air. As discussed in Chapter 2, BSI regulations refer to breakthrough times after exposure to challenge concentrations of 1000 ppm (BSI, 2008). H_2S and NH_3 concentrations were only 800 ppm. This is because initial experiments used electrochemical detectors (ECDs) rather than a PID. The principle behind an ECD is a reaction between a specific test gas and a chemical in the detector that results in a current, read by an ammeter, multiplied by a factor and displayed as a concentration. As such ECDs are generally specific to one test gas. This type of sensor has a limit to the concentration it can read, and the sensors used initially could only measure up to 800 ppm. As such, NH_3 and H_2S, which were measured with an ECD, were limited to this concentration. An additional downside to ECDs is that the chemical inside the detector can become exhausted very quickly when exposed to high concentrations of the test gas, resulting in incorrect concentration readings. Cyclohexane was initially measured using a flame ionisation detector (FID). These are typically used to measure concentrations of VOCs, and operate by passing a sample of the test gas through a hydrogen flame. The ions formed during the combustion of the VOC are then detected and measured. Similar to the PID, the FID is not a selective detector, though it is capable of reading high concentrations of test gas. When the PID became available, cyclohexane dynamic challenges were performed using the PID, for consistency with the other gases.

To begin the dynamic gas breakthrough studies, the test gas cylinder was opened and set to 5 bar pressure. Test gas passed through a mass flow controller (MFC), and the test module was challenged at a flow rate, set at one value between 1 and 3 L/min. The gas outlet concentration of the module was measured by a gas detector, as described in the above paragraph. The effluent gas was then removed by the ventilation system. As the application of these fibres will be a respirator filter, the module was tested under 1 bar of

pressure (atmospheric conditions). Gas concentration was recorded in ppm every 10 seconds and was plotted as the concentration divided by the initial concentration (C/C_0) over time to determine the breakthrough time, as determined by BSI regulations, which was when the test gas reached 25 ppm for ammonia and 10 ppm for hydrogen sulphide and cyclohexane. Equilibrium time was also recorded. This was the time when gas concentration reached initial concentration, $C/C_0=1$. When equilibrium was reached, test gas flow was stopped and the sensor was purged with air to remove any residual toxic gas. The adsorbent fibre bundle was then removed from the stainless steel case and its weight was recorded. This weight was compared with the equilibrium loading value calculated from the breakthrough curve to ensure consistent results.

A schematic diagram of the dynamic adsorption test apparatus is shown in Figure 3.6.

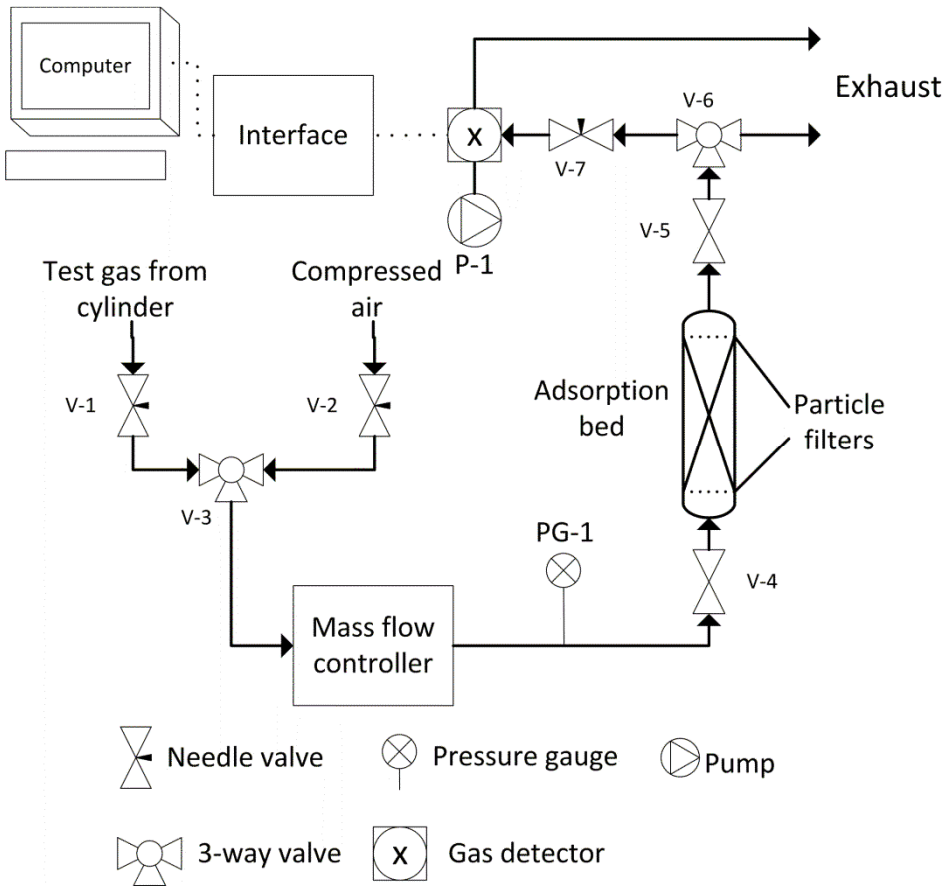

Figure 3.6. Schematic diagram of the dynamic adsorption apparatus.

In Figure 3.6, the test gases available were 800 ppm NH_3 in nitrogen, 800 ppm H_2S in nitrogen, and 1000 ppm cyclohexane in air. V-1 allowed test gas to enter the apparatus while V-2 allowed purge gas (compressed air) to enter the apparatus. V-3 enabled either of these two lines to be isolated. The mass flow controller (MFC) enabled control of the

influent gas flow rate, which could be varied from 0.5 L/min to 5 L/min with the apparatus available. Pressure gauge PG-1 was included prior to the test module to ensure no backpressure in the test module. The test module was a bundle of fibres in stainless steel casing, as described above, with a particle filter at each end. Valves 4 and 5 allowed the adsorption bed to be isolated for weighing. Valve 6 split the test gas, passing some to the exhaust and some to the needle valve V-7. This valve controlled the flow that was passed over the gas detector. The detector had an inbuilt pump, P-1, necessitating the control of the flow rate entering the sensor. The sensor connected to a PC, allowing data to be collected. After test gas had passed over the sensor, it went to exhaust.

PID has a built-in pump giving an outlet flow rate of 285 ml/min. When incorporated in-line, the same flow rate must be provided at the inlet to avoid damaging the pump.
Needle valve V2 enabled control of the flow rate to ensure that the correct flow rate passes over the PID while the rest goes to vent.

3.2.3.2 Dynamic water vapour breakthrough studies

Respirator canisters, as well as removing toxic gases, must contend with ambient moisture in the air that passes through them. As such, the amount of moisture adsorbed on adsorbent fibre modules was investigated in dynamic water vapour breakthrough studies. Fibre modules were loaded into the humidity apparatus, shown in Figure 3.7.

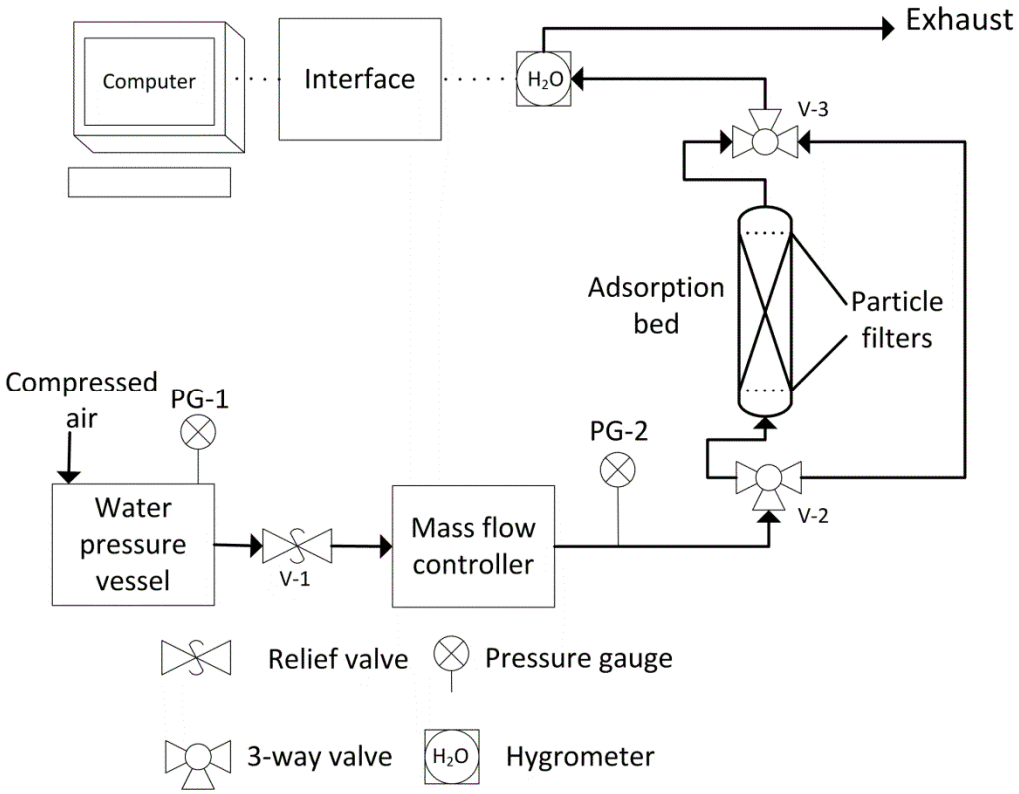

Figure 3.7. Schematic diagram of the dynamic water vapour apparatus.

1 L/min of compressed air passed through a pressurised water tank, measured by PG-1, to increase its humidity. This challenge gas passed through a relief valve, V-1, allowing humid air to exit the water pressure vessel once it was completely pressurised. The mass flow controller set the flow rate to 1 L/min and PG-2 ensured atmospheric pressure in the apparatus. The water vapour could then be passed over the fibre module or diverted to a bypass line using V-2 and V-3. This test ensured the level of humidity was stable before going through the test module. Test gas exiting the module passed over a chilled mirror dew point hygrometer, which detected % relative humidity and dew point at the test module outlet. Finally, test gas passed to exhaust.

Chilled mirror dew point hygrometers measure humidity content by passing the air stream over a chilled mirror and then detecting the level of condensation on the surface of the mirror. This data was passed to PC for analysis. The initial humidity level in the compressed air inlet was 30% by default and the amount of water taken up by the fibre was recorded.

3.2.4 Synthesis of metal organic frameworks

3.2.4.1 Solvothermal synthesis of CuBTC using ethylene glycol

Metal organic frameworks could potentially be used to adsorb toxic gases, as discussed in Chapter 2. As such, a small quantity of the MOF CuBTC was synthesised for characterisation and for impregnation onto adsorbent hollow fibres. The impregnation process is described in Section 3.2.5. CuBTC synthesis was adapted from Schubert *et al.* (2012). 3.64 g benzene tricarboxylic acid and 4.15 g of copper sulphate were dissolved in 82 g of ethylene glycol. This was sealed and heated at 110 ºC for 8 hours with stirring under autogeneous pressure. A blue precipitate of copper benzenetricarboxylate with complexed ethylene glycol was formed, which was washed with methanol and filtered to remove residual copper sulphate and substitute the ethylene glycol solvent in the structure with the lower boiling point methanol. The blue powder was then dried in a vacuum oven at 85 ºC, forming 1.416 g of deep purple dry copper benzenetricarboxylate powder product.

3.2.5 Impregnation of adsorbent hollow fibres and granules with metal salts and metal organic frameworks

In order to customise adsorbent hollow fibres further, they can be impregnated with various compounds. These can enhance the adsorption performance for specific toxic gases, as discussed in Chapter 2. Metal salts are commonly used impregnants on granules, although the impregnation of adsorbent hollow fibres with metal salts is novel and has not previously been explored. In addition, metal organic frameworks could prove effective as impregnants, as some work, discussed in Chapter 2, has covered ways to suspend MOFs in granular beds. While MOFs have been incorporated into hollow fibre membranes, they have not previously been impregnated on to adsorbent hollow fibres. In this work, the adsorption performance of MOFs impregnated on to adsorbent hollow fibres is compared with that of impregnated metal salts to determine whether the more expensive and water sensitive MOFs present a viable alternative impregnant.

Several techniques of impregnation are suitable for adsorbent hollow fibres, and for this work excess soaking impregnation was employed. In this process, an impregnating solution was prepared by suspending the solid impregnant in a suitable solution, such as methanol. The prepared adsorbent hollow fibre bundle was inundated with the

impregnating solution and left uncovered to allow it to dry, on a mixer, to ensure even distribution of the impregnating solution.

3.2.5.1 Impregnation of copper (II) oxide onto adsorbent hollow fibres by a 3 step chemical reaction

The potential of copper (II) oxide as an impregnant to enhance adsorbent hollow fibre removal of H_2S by chemisorption was explored. Because CuO is insoluble, excess soaking impregnation of CuO powder onto adsorbent fibres would not be possible. As such, CuO is impregnated by a reaction, using $CuCl_2$ as a starting material. By impregnating this soluble salt onto the fibres, adding NaOH to convert it to $Cu(OH)_2$ and finally by heating this copper salt, CuO will be formed on the hollow fibres.

$$CuCl_2 + 2\,NaOH \rightarrow Cu(OH)_2 + 2\,NaCl$$

$$Cu(OH)_2 \xrightarrow{heat} CuO + H_2O$$

The fibres used were 20%wt PES 40%wt AbScents1000 and 40%wt NV5 activated carbon fibres, which weighed 12.145 g. For impregnation, 10% wt of CuO was selected, which was 1.215 g, or 0.0153 moles. This % wt was chosen to ensure that a large enough quantity of impregnant was present so that results would be clear, while avoiding an excessively high % wt of impregnant, which can reduce surface area and thus negatively affect adsorption (Fortier *et al.*, 2008). Using the molecular weights in Table 3.2, the correct weights for the precursor copper salts and sodium hydroxide can be calculated.

Table 3.2 Molecular weights of materials involved in CuO impregnation.

Material	Mw
CuO	79.5
NaOH	40.0
$CuCl_2$	134.5
$Cu(OH)_2$	97.5

2.05 g $CuCl_2$ was dissolved in water and impregnated onto the fibres by excess soaking as described above. Then 1.22 g of NaOH in an excess of distilled water was added to form 2.06 g of $Cu(OH)_2$. This was washed with water to remove NaOH and NaCl (but not insoluble $Cu(OH)_2$) then heated to 190 ºC, resulting in the oxidation of $CuOH_2$ into CuO.

After impregnation and drying, the fibres weighed 13.48 g, showing a weight gain of 1.34 g. This was higher than the expected gain of 1.22 g, and was most likely due to a small amount of NaCl or NaOH remaining after the washing step. This small quantity was not

expected to interfere with adsorption, and could potentially enhance it due to the interaction between H_2S and NaOH.

3.2.5.2 Impregnation of the metal organic framework benzene tricarboxylate onto adsorbent hollow fibres by excess soaking impregnation

In order to compare the adsorption performance of adsorbent fibres, fibres were impregnated with a metal salt, CuO, and a metal organic framework, CuBTC. The CuBTC was a sample of the MOF powder synthesised in Section 3.2.4. For a fair comparison, approximately 10 %wt of MOF was used, with 1.24 g of CuBTC impregnated on to composite adsorbent 20 %wt PES 40 %wt AbScents1000 and 40 %wt NV5 activated carbon fibres weighing 12.00 g. The MOF powder was dissolved in an excess of methanol and the fibres were soaked in the mixture, as described in Section 3.2.5. Once the methanol had dried in atmospheric conditions, the fibres were dried further in a vacuum oven at 85 °C for 72 hours, resulting in a final impregnated adsorbent fibre weight of 12.33 g and therefore a loading of 0.32 g of CuBTC (2% loading). This is significantly below the intended 10% loading weight and was due to the poor adherence of the MOF to the adsorbent fibre, with some of the CuBTC powder remaining behind, unattached. This poor impregnant loading has been observed previously by Küsgens *et al.* (2010), who attempted to impregnate monoliths with CuBTC. They addressed this problem by including the metal organic framework in the monolith dough before extrusion. This sort of solution is impossible for adsorbent hollow fibres due to the preparation process involving immersion in water, which will break down the CuBTC (Gul-E-Noor *et al.*, 2011; Greathouse and Allendorf, 2006; Li and Yang, 2007). As such, the 2% loading weight was taken into account when calculating adsorbate loading and comparing adsorption performance of copper salt and copper MOF impregnants. This will be explored in Chapter 5.

3.2.6 Pressure drop testing of granular beds and adsorbent hollow fibre modules

The pressure drop in a respirator canister is important to consider as a high pressure drop results in high breathing resistance for the user and contributes to a high respirator burden, as discussed in Chapter 2. The pressure drop will be different for adsorbent hollow fibres modules and granular beds, but will also vary depending on the bore

diameter of the adsorbent hollow fibres. An adsorbent fibre module with smaller bore diameter will have a higher pressure drop than a larger bore diameter due to the higher superficial velocity through smaller bores and greater friction against the inner wall of the bore. In order to observe the trend fully, ideally the pressure drop in adsorbent fibres of different bore diameters should be tested. However, large bore fibres cannot be spun with the current spinning apparatus. As such, a monolith with circular bores, prepared at the University of Bath by Yuan-Yao Li (1998) was tested to represent a 'large' bore module. The shape of the circular bore monolith is similar enough to a fibre module that the flow results should accurately reflect an equivalent hollow fibre module.

The pressure drop in adsorbent fibre modules over a range of flow rates was determined experimentally with a u-tube manometer, shown in Figure 3.8, and compared to the pressure drop determined from the same volume granular beds. The pressure drop ΔP can be calculated by using the equation below, assuming the density of nitrogen to be negligible compared to density of water:

$$\Delta P = h_m \rho_m g$$

where

ΔP = pressure drop (N/m^2)

h_m = height difference between liquid levels on manometer (m)

ρ_m = density of water (kg/m^3)

g = acceleration due to gravity (9.81 m/s^2)

The manometer was connected to the module as shown in Figure 3.8. A nitrogen cylinder (BOC gases) provided the test gas through needle valve V-1.

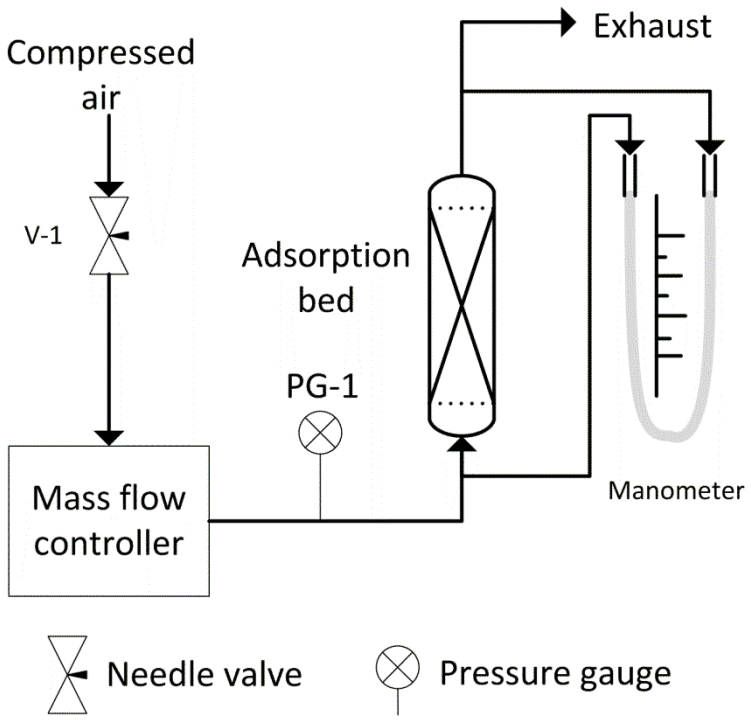

Figure 3.8. A diagram of the adsorbent fibre or granule module attached to the U-tube manometer in order to determine pressure drop.

A mass flow controller was used to set flow rates at 0.5 L/min intervals from 0.5 to 5 L/min. At each flow rate, the pressure drop was allowed to equilibrate for one minute, confirmed by PG-1, and then the difference in liquid levels h_m was measured. Test nitrogen gas passed to exhaust. The module diameter was kept constant at 2 cm and the module lengths tested were 5, 10, 15, 20 and 25 cm long. These modules were packed with either 1 mm average diameter NV5 carbon granules, 0.8 mm or 1 mm bore adsorbent hollow fibres (‘small’ and ‘standard’ bore respectively), or a monolith with a circular bores of 1.2 mm diameter.

Longer length hollow fibre beds were tested by placing several shorter length hollow fibre modules in sequence and this was compared to an equivalent length single module to ensure there was no difference in pressure drop. Bore size was measured using the graphical manipulation programme ImageJ. Ten measurements were taken for each test module and average bore sizes were calculated from the data obtained.

3.2.7 Characterisation

A number of characterisation techniques were used to investigate the adsorbent hollow fibres prepared as well as the MOFs synthesised in 3.2.4.

3.2.7.1 Scanning Electron Microscopy

Fibres were characterised by scanning electron microscopy (SEM). Fibre samples were prepared by freezing in liquid nitrogen for one minute and sectioning. Samples of each fibre were then mounted on a sample tray using double sided adhesive carbon discs and coated with gold using an Edwards S150B Sputter Coater to aid in obtaining quality micrographs. Prepared samples were then examined with a JEOL JSM6480LV scanning electron microscope with a working distance of 12-14 mm and an accelerating voltage of 15 kV.

3.2.7.2 Energy Dispersive X-ray Analysis

To determine the presence of elemental composition of the adsorbent hollow fibres and identify the metal salts impregnated on to commercial activated carbons, energy dispersive X-ray analysis (EDX) was carried out using the JEOL JSM6480LV scanning electron microscope. Samples were prepared as in Section 3.2.7.1, although no coating was used, as all fibres undergoing EDX were carbon. This is sufficiently conductive without further treatment. Sections of each image were selected for analysis, with at least three sections selected in each case.

3.2.7.3 X-Ray Diffraction

X-Ray powder diffraction (pXRD) was used to determine the crystalline structure of the synthesised CuBTC MOF and determine whether this crystalline structure was maintained in the adsorbent fibres impregnated with the MOF. Samples were prepared by grinding in a mortar and pestle and mounted in a Bruker D8 powder diffractometer. The sample was then exposed to x-rays between 5° and 70°. This work was kindly carried out by Gabriele Kociok-Kohn in the Department of Chemistry.

3.2.7.4 Nitrogen adsorption isotherms

Nitrogen adsorption analyses were used to investigate the nitrogen adsorption isotherms of the adsorbent hollow fibres and metal organic framework. They were also used to determine the surface areas of polymer and adsorbent powders. Nitrogen isotherms in Chapter 6 were measured on a Coulter SA3100 instrument across a pressure range of 0.001 to 780 mmHg, at the University of Cardiff by C. Grazia Bezzu and Kadhum J. Msayib, while those in Chapter 5 were measured on a Micromeritics Surface Area and

Pore Analyser (ASAP) at the University of Bath, with assistance from Valeska Ting and Fernando Acosta. The majority of samples were degassed at 190 °C, while those containing PIM-1 were degassed at 150 °C. The tests were performed at 77 K. In all cases, a sample of powder or a short length of chopped fibre was tested.

3.2.7.5 Organic/water adsorption isotherms

Octane, cyclohexane and water sorption analyses were used to determine the octane, cyclohexane or water adsorption isotherms of the adsorbent hollow fibres, polymers and metal organic frameworks. They were also used to determine the adsorption kinetics of cyclohexane and octane on adsorbent powder, fibres and polymers. These tests were carried out on a Dynamic Vapour Sorption (DVS) Advantage 2 instrument (Surface Measurement Systems Ltd) over a range of 0.03-0.95 relative pressure at Dstl, Porton Down, by Martin Smith. The material to be tested, (water, cyclohexane or octane), was loaded into the DVS instrument as a liquid before being vaporised over the sample. To minimise error and maintain consistency in the adsorbent hollow fibre analyses, 2 x 1 cm lengths of fibre were rested diagonally in the sample tray for testing. The sample mass was typically 30-50mg; all isotherms were determined at 298K.

3.2.7.6 Organic/water uptake rate testing

Using the DVS Advantage 2 Instrument and octane, cyclohexane and water test vapours, the rate at which the test gas was taken up by the adsorbent sample could be recorded. This gave an impression of the adsorption kinetics of the sample for the test vapours. Using data collected for the adsorption isotherms, described in Section 3.2.7.5, the time vs. change in mass (*dm*) were plotted to give a graph of the uptake mass of the test vapour over time. Unlike the fibres, which were positioned in the same manner in the sample tray for each test, the depth of adsorbent powder sample in the sample pan can affect its uptake time. This meant that the uptake speed results were not quantitatively comparable between powder samples. As such this technique was used as a method to determine the adsorption uptake rate of adsorbent hollow fibre samples only.

3.3 Practical issues in adsorbent hollow fibre testing

There are a number of practical issues to be considered before testing adsorbent hollow fibres. These include; the way the heated fibres are stored; how the fibres are oriented in dynamic testing; and the sensor used to test outlet test gas concentration.

3.3.1.1 Storage of adsorbent hollow fibres

It was important to find an efficient method of storing adsorbent hollow fibres to prevent them losing capacity by adsorbing atmospheric water. Adsorbent hollow fibre storage was tested using the hydrophilic adsorbent LiLSX. 82% LiLSX fibres were stored by vacuum packing or in a capped tube for one week before dynamic challenge with 800 ppm 1 L/min ammonia to determine the effectiveness of the method of storage (Figure 3.9).

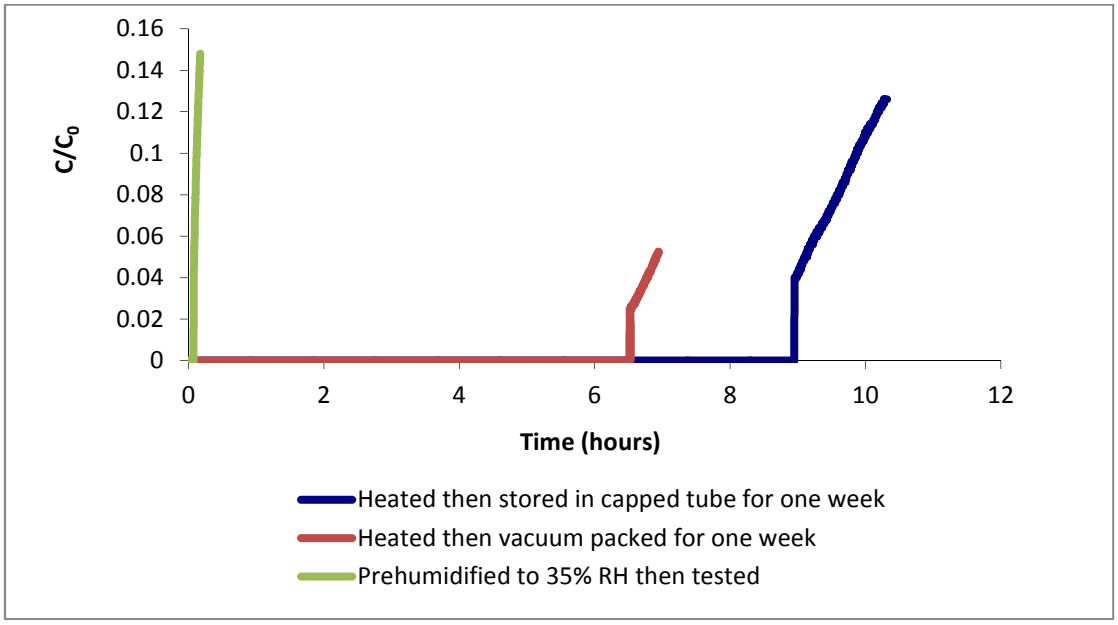

Figure 3.9. Dynamic 800 ppm 1 L/min ammonia challenge on 82% LiLSX fibres following different methods of storage.

It is clear from Figure 3.9 that prior exposure to 35% RH will significantly reduce ammonia adsorption on LiLSX. Vacuum packing the fibre greatly enhanced ammonia breakthrough time, but storage in a capped tube resulted in even higher breakthrough time for the same batch of fibres. This is most likely due to a poor seal in the vacuum packing, possibly due to a fault with the equipment or technique used in vacuum packing. Packing in a capped tube is simple, and so avoids both of these problems.

To confirm this, hydrophilic silica gel was stored in two tubes. One tube was closed, the other was left open and measurements were periodically taken over 120 hours. The fibre bundle in the unsealed tube gained over 2% of its mass in weight in atmospheric water while the fibre bundle in the closed tube maintained a constant weight.

These results demonstrate that hydrophilic adsorbent hollow fibres can be stored in a capped tube without adsorbing any moisture, while vacuum packing was not satisfactory for this. As such, all fibres were stored in a capped tube after heating, and allowed to cool for at least 24 hours before testing.

3.3.1.2 Orientation of test modules

Test modules were sealed at one end to prevent gas bypassing the fibres. This sealed end could be at the gas inlet, forcing gas to enter through the bores only, or at the outlet, allowing gas to travel through the bores and into gaps between fibres, though they are blocked at the outlet from leaving through any part of the fibre except the bore. The two options were compared by dynamic hydrogen sulphide challenge, using open end at the inlet to sealed end at outlet, and modules with both ends sealed to minimise the risk of bypass after the initial potting, with the result shown in Figure 3.10.

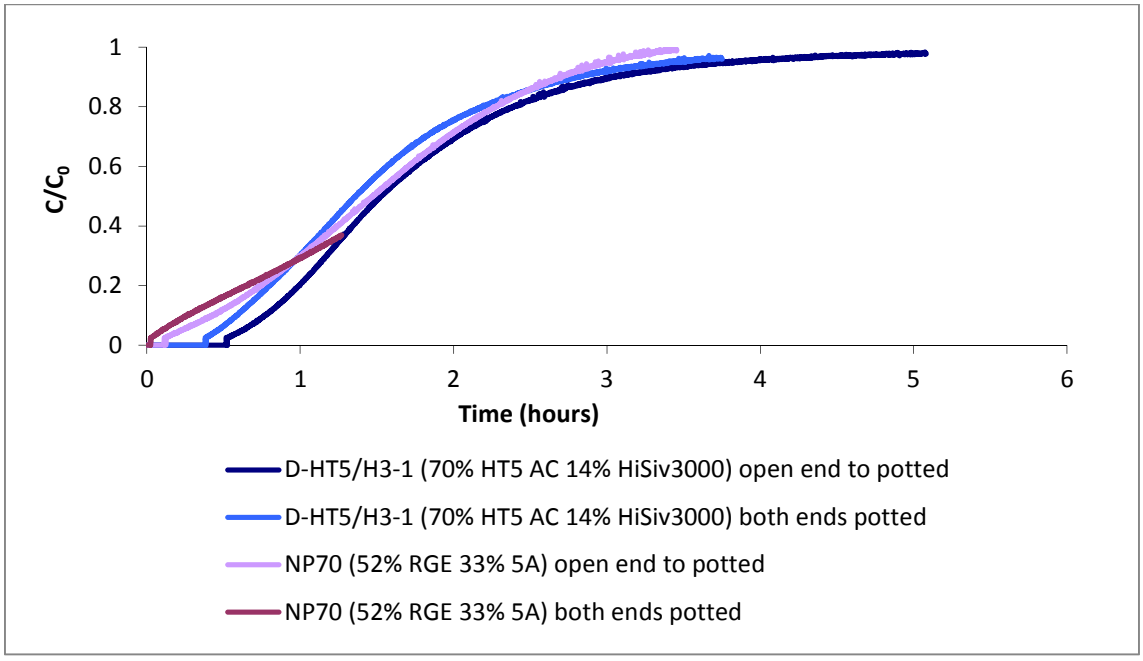

Figure 3.10. Breakthrough curves of 5 cm open and sealed fibre modules challenged in dynamic conditions with 800 ppm hydrogen sulphide at 1 L/min.

A very small improvement in breakthrough time was observed by aligning modules from open end to sealed end compared to potting both ends for both the fibres tested. For the HT5 fibres, breakthrough loading increased from 0.35% for the both ends sealed fibre to 0.47% for the open end to sealed, and for the RGE fibres, from 0.02% for both ends sealed to 0.12% for open end to sealed end. This trend matched expectations, although the improvement is very small, just 0.1%wt or approximately 1 mg each. However, the available surface area for just the bores is 55.00 cm^2 compared to 235.62 cm^2 for the outer structure, making the surface area for the whole structure 285.62 cm^2, a five-fold increase over that of the bores. The reason for such a small increase could be due to the outer layer of the fibres being very thick, with low porosity and poor kinetics for adsorption. Examples of this are shown in SEMs in Figure 3.11, with Figure 3.11a) demonstrating a thick layer of polymer blocking pores, while Figure 3.11b) shows a very thick outer skin on double layer fibres. This is likely to impede adsorption onto the exterior of the fibres.

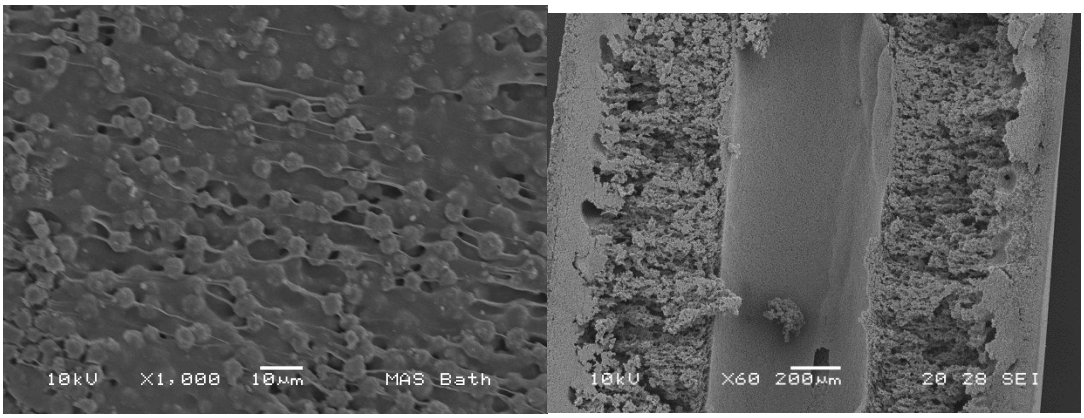

Figure 3.11. a) The outer wall of LiLSX fibres x1000. b) The bore of Avon carbon/5A fibres.

3.3.1.3 Consistency of toxic gas sensor measurements

In order to investigate the consistency of breakthrough curves from different sensors, the same breakthrough test was carried out with different sensors in the same conditions. The sensors were a Detcon EC sensor, a Dräger EC sensor and a Phocheck PID. 80% AbScents1000 fibres were challenged with 1 L/min 800 ppm ammonia and the outlet concentration was monitored with the three different types of sensors used over the course of the project. The breakthrough curve recorded by each sensor is shown in Figure 3.12.

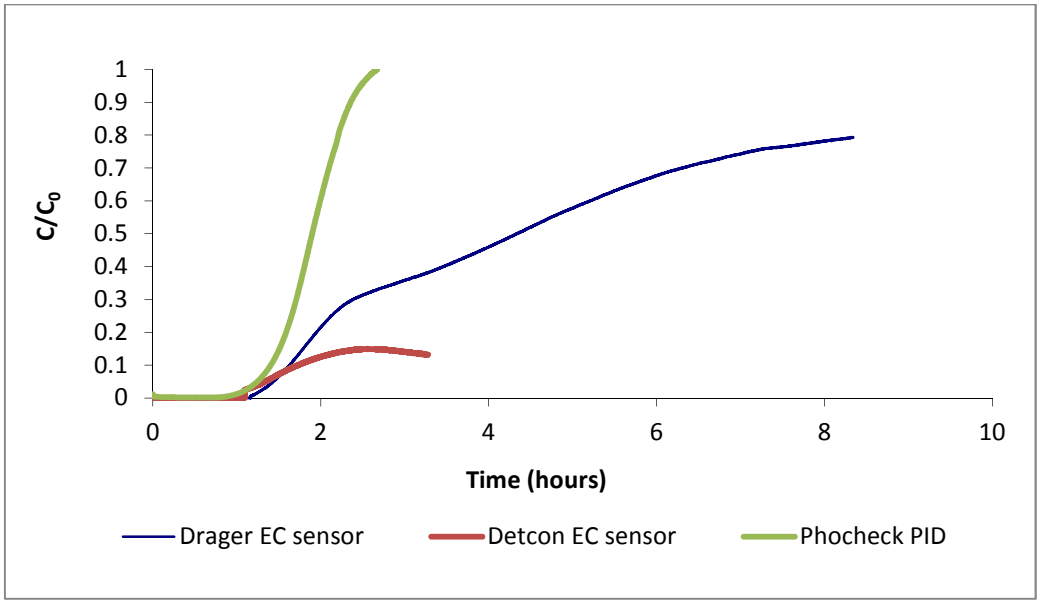

Figure 3.12. 800 ppm 1 L/min ammonia breakthrough challenge on AbScents1000 fibres. EC = electrochemical, PID = photoionisation detector.

The Dräger and Detcon brand sensors demonstrated unusual breakthrough curve shapes, while the PhoCheck PID measured a more typical shape. However, the breakthrough times were very similar for the three. This suggests that the PID is the most accurate sensor for recording the full breakthrough curve, with equilibrium time and loading. It also suggests that while breakthrough time from the EC sensors is consistent with the PID, equilibrium times/loadings etc. from the EC sensors were not valid. This is as a result of the high concentrations tested and exhaustion of the EC sensors. As such, the PID sensor was used for breakthrough tests, and equilibrium or curve data collected with EC sensors were discarded.

3.4 Conclusion

This Chapter has described the methods and materials used during this thesis. Due to the reuse of these experimental protocols through Chapters 4, 5, 6 and 7, this Chapter is intended as a reference point to the basic method, to be supplemented with the specifics provided in each of these Chapters to fully explain the experiments.

Practical issues in preparation and testing of adsorption fibres were considered:

- Satisfactory storage of these heated fibres to prevent adsorption of atmospheric water was shown to be in a capped tube.

- The optimum orientation of these fibres was shown to be with the sealed end of the fibres positioned at the gas outlet to allow some adsorption on the fibre exterior walls and ensure gas exits only through the fibre bores.
- The most reliable sensor for obtaining a full breakthrough curve was shown to be a Phocheck PID, but the EC sensors gave consistent breakthrough times.

4 Adsorbent screening and development of adsorbent fibre structures for use in respirators

4.1 Introduction

In this Section, a range of adsorbents are tested with the three TICs of interest to enable selection of optimum adsorbents for further study. The effects of the fibre structure, bed length and flow rate are also investigated. Adsorbent hollow fibres are then compared to granule and pellet beds. In addition, an overview of problems encountered during composite fibre preparation is given.

4.1.1 Selecting and screening suitable adsorbents for removal of TICs

As discussed in the literature review, a variety of adsorbents could be used in hollow fibres to remove NH_3, H_2S and cyclohexane. Candidate adsorbents include zeolites 13X, 5A, clinoptilolite, NaY, LiLSX, ZSM5, HiSiv1000 and AbScents1000, and several commercial activated carbons. A range of these adsorbents were spun into fibres and bundled into modules by the techniques shown in Section 3.2. The adsorbent hollow fibres were then tested under dynamic adsorption conditions by the experimental methods shown in Section 3.2.3.1 to determine the breakthrough times for a challenge concentration of NH_3, H_2S or cyclohexane. Using the breakthrough times and loadings, and taking into account how such adsorbents would be likely to behave when exposed to humid conditions, several adsorbents were selected for more detailed analysis.

While a range of adsorbents were tested, by no means was this screening exhaustive; a great range of adsorbents would potentially make very effective adsorbent hollow fibres for any target gas of choice, and could be tested in future work.

4.1.2 Fibre structure testing

Adsorbent hollow fibres were prepared by extruding adsorbent/polymer solution through a spinneret as described in Section 3.2.1. They can be made with three different structures: a thin single layer, a double layer, or a thick single layer fibre.

A thin single layer fibre will have a small diameter, and a higher voidage compared to the thick single and double layer fibres. This means a greater number of thin single layer fibres can be packed in to a module, increasing the number of channels through which gas

passes. In addition, the thin layer of the fibre will minimise gas diffusion path lengths. However, thin fibres are more difficult to bundle, quite fragile to axial force as well as easy to compress.

Double layer fibres have a larger diameter than the thin single layer fibres. This is made by using a spinneret with a divider, making two separate layers of adsorbent fibre rather than one. Less individual fibres will fit into a module than for the thin single layer, and the module will have lower voidage than its single layer equivalent. These fibres are easy to bundle and form stronger but more brittle modules, which do not tend to compress as much as the single layers.

Spinning parameters were selected based on the literature reviewed in Chapter 2. Zero air gap was used as previous research at Bath on adsorbent hollow fibres had indicated that a large air gap decreased the fibre porosity. This resulted in a thick wall becoming a larger proportion of the overall fibre structure, which lowered permeability (Nevell, 2009). This seemed to be a more significant effect than observed in the literature, where larger pore sizes were observed on the outside of the fibre with a large air gap (Liu *et al.*, 2003). It is suggested that this is as a result of the greater weight of adsorbent hollow fibre precursor mixture than a polymer-only hollow fibre, particularly when large proportions of adsorbent were used, enhancing the gravitational effect. A fibre composition of 80% adsorbent to 20% polymer was used as a trade-off between keeping the polymer proportion low to increase the active adsorbent proportion of the fibre as well as to enhance fibre porosity while maintaining a high enough proportion to keep the fibres strong enough to bundle. The extrusion rate was not controlled as no method of measuring this was available. As such it is possible that there could be a shear effect resulting in thicker walls of less viscous fibre precursor mixtures (typically zeolites) compared to the more viscous precursor mixtures (typically carbons). A water coagulation bath filled with tap water at room temperature was used, with a 50/50 water/NMP mix of bore fluid, which was determined effective from previous experience within the group. Bore fluid flow rate was varied to match the fibre extrusion rate. If the bore fluid moved too slowly, the fibre structure collapsed and if it moved too fast, holes formed in the adsorbent fibre structure. As such the optimum bore fluid pump speed for each fibre to ensure the optimum fibre structure was recorded for each fibre spun.

Thick single, thin single and double fibres were prepared and compared by cyclohexane and octane adsorption analyses to determine the optimal fibre structure for the fastest adsorption rate, determined by the methods described in Section 3.2.7.6. Breakthrough tests with ammonia and cyclohexane were carried out to compare different fibre types and the pressure drop in different fibre structures was measured to enable an optimum fibre structure to be determined. For a full comparison, a 'large bore' (i.e. 1.2 mm circular bore) monolith with circular channels was tested and compared to the fibres to examine pressure drop, as no larger spinneret than 1 mm was available.

4.1.3 The effect of adsorbent fibre module length and challenge gas flow rate on the adsorption properties

Using two adsorbents selected from breakthrough screening and humidity tests, three different fibres were prepared: one of one adsorbent, one of the other adsorbent and one hybrid fibre made of a 50/50 mixture of the two. Three lengths (10, 15 and 20 cm) of fibres were challenged with 1 L/min 800 ppm ammonia in double and single layer configuration, focusing on the optimal bore selected from pressure drop and cyclohexane uptake testing. These results were used to determine mass transfer zones and examine trends in the adsorption properties of the adsorbent hollow fibre module as length was increased.

Using cyclohexane, the effect of changing the flow rate on the breakthrough curves and adsorption properties was explored in more detail. Three different flow rates were tested for each fibre, to enable modelling (see Chapter 7). Initially flow rates of 1, 2 and 3 L/min were used but in some cases 3 L/min resulted in instant breakthrough. In these cases, flow rates of 1, 1.5 and 2 L/min were tested and compared.

Adsorbent fibres may take up very large quantities of cyclohexane, making tests extremely slow, expensive and impractical to complete. As such in some cases, the tests were curtailed at the breakthrough point so that enough gas would be available to complete all of the tests. Though adsorption characteristics such as the mass transfer zone, length of unused bed and equilibrium time could not be found in these cases, the breakthrough time and loading are the most important factor in respirator design. These

values will also enable use of modelling to predict further breakthrough times, and potentially the full breakthrough curve.

Cyclohexane adsorption isotherms were performed on the hybrid fibre and its individual components to examine whether there were any synergistic or antagonistic effects when two different adsorbents were mixed in one adsorbent hollow fibre structure.

4.1.4 Adsorption breakthrough curves for adsorbent hollow fibre modules compared to adsorbent particle modules

Gas flow through a granular bed will follow a tortuous path between granules, becoming turbulent at low flow rates while gas flow through an adsorbent hollow fibre module will be through the bores. As a result, in the case of beds packed with small particles, contaminants were exposed to the full outer surface of the adsorbent granules, resulting in potentially greater adsorption. In comparison, for adsorbent hollow fibres only the inner surface of the bore and potentially the outer wall will come into direct contact with contaminants before diffusion.

There are disadvantages to granular beds, such as the potential for gas to be channelled, and avoid sections of the granular bed, and for the higher pressure drop as a result of the greater friction. Granular beds will nevertheless, be expected to adsorb more before breakthrough than an equivalent volume hollow fibre module, in part due to lower voidage and higher density, as discussed in Section 2.1.4. As such steps must be taken to make fibres more accessible to contaminant gases.

The different adsorption behaviour on granular beds and adsorbent hollow fibres will be investigated by comparing 80% AbScents 1000 hollow fibres with a pellet module of the same composition by dynamic adsorption. Ammonia and cyclohexane were the challenge gases used for these tests. In addition, hybrid 50/50 NV5/AbScents1000 adsorbent fibres and pellets were compared by the same methods. The morphology of the pellet and fibres were assessed using SEM. The method by which the pellets were produced can be seen in Section 3.2.2.

4.2 Results

4.2.1 Selecting suitable adsorbents for use in adsorbent hollow fibres for NH_3, H_2S and cyclohexane removal

Adsorption screening trials were performed in order to select candidate adsorbents for hollow fibre development. A variety of different adsorbents were dynamically tested by the method described in Section 3.2.3.1 with 800 ppm NH_3 and H_2S in nitrogen gases and 1000 ppm cyclohexane in nitrogen gas at 1 L/min. The results are summarised in Table 4.1 - Table 4.3 below, where t_b = breakthrough time and t_{eq} = equilibrium time. The breakthrough curves shown in Appendix 1.

Table 4.1. Adsorbent fibre screening trials: summary of experimental results of 800 ppm 1 L/min ammonia challenge, ordered from highest to lowest breakthrough loading by %wt.

Fibre name (composition)	Adsorbent wt (g)	t_b (h)	t_b loading %wt	t_{eq} (h)	t_{eq} loading %wt
NP60 (81% NaY 19% PES) chopped (too thin and fragile to bundle)	3.81	5.18	4.54%	12.69	5.97%
NP68 (82% LiLSX 18% PES)	8.06	8.95	3.69%	15.86	5.11%
NP66 (42% 13X 42% ZSM5 16% PES)	7.39	7.21	3.24%	18.43	6.09%
NP65 (82% ZSM5 18% PES)	2.62	1.71	2.17%	7.40	5.07%
NP64 (55% Avon carbon 28% 5A 17% PES)	6.53	1.84	0.94%	8.36	2.84%
Chopped 80% copper (II) oxide 20% PES fibres	6.23	1.66	0.89%	4.25	1.55%
D-H1-2 (80% AbScents1000 20% PES)	6.54	1.15	0.58%	2.64	0.95%
DM1 (86% TZP2524 mesoporous silica 14% PES)	8.96	0.40	0.13%	0.00	0.00%
EUR20 (80% NV5 carbon 20% PES)	3.21	0.12	0.12%	0.71	0.24%
NP10(5) (81% HiSiv3000 19% PES)	7.55	0.16	0.07%	0.97	0.17%
NP47 56% HiSiv3000 25% HiSiv1000 19% PES)	7.87	0.10	0.04%	4.11	0.49%
NP58 (45% NV5 carbon 29% HiSiv3000 26% PES)	0.00	0.10	0.02%	0.94	0.05%
NP67 (42% Clinoptilolite 42% 5A 1 % PES)	7.95	0.00	0.00%	5.75	1.27%

The highest ammonia breakthrough times and loadings were on NaY fibres, (5.18 hours and 4.54%wt) and LiLSX fibres (8.95 hours and 3.69%wt). The NaY and LiLSX fibres also had the highest equilibrium loading, with 5.97%wt and 5.11%wt respectively. The high silica AbScents1000 and ZSM5 fibres had lower breakthrough times and loadings of 1.15 hours and 0.68%wt and 1.17 h and 2.17%wt respectively. The HiSiv3000, NV5 carbon, clinoptilolite and mesoporous silica fibres all had lower than 0.5%wt breakthrough loading. ‘Avon carbon’ (which was impregnated with an unspecified metal

salt) fibres, and CuO impregnated fibres both had greater than 0.5%wt loading for ammonia, demonstrating the potential for copper oxide and other impregnants to enhance ammonia adsorption. A key trend observed in breakthrough and equilibrium times was that materials with a low Si:Al ratio had greater ammonia breakthrough and equilibrium loadings than those with higher Si:Al ratios. This is due to the hydrophilic, polar nature of the low Si:Al ratio zeolites, as explained in Chapter 2. The lower the Si:Al ratio, the greater the loading of polar materials that would be expected. However, it is important to consider that as well as ammonia, a high uptake of water would be expected on these zeolites, as discussed in Section 2.1.1.1.

Table 4.2. Adsorbent fibre screening trials: summary of experimental results of 800 ppm 1 L/min dynamic hydrogen sulphide challenge, ordered by breakthrough loading.

Fibre name (composition)	Adsorbent wt (g)	t_b (h)	t_b loading %wt	t_{eq} (h)	t_{eq} loading %wt
NP64(3) (55% Avon carbon 28% 5A 17% PES)	8.29	2.00	1.60%	7.84	3.87%
NP65 Chopped (82% ZSM5 18% PES)	3.43	0.42	0.82%	1.40	1.07%
CJ1 (42% 5A 42% 13X 16% PES)	6.65	0.58	0.57%	4.39	2.48%
NP67 (40% 5A 40% Clinoptilolite 20% PES)	7.44	0.60	0.54%	6.23	2.95%
D-HT5/H3-1 (70% HT5 activated carbon 14% HiSiv3000 16% PES)	7.39	0.53	0.47%	5.08	1.59%
NP70 (52% RGE activated carbon 33% 5A 15% PES)	6.77	0.13	0.12%	3.46	1.49%
NP68 (82% LiLSX 18% PES)	9.60	0.13	0.09%	2.94	0.97%
DM1 (86% TZP2524 mesoporous silica 14% PES)	8.82	0.03	0.02%	0.11	0.03%
NP10 (5) (81% HiSiv3000 19% PES)	8.47	0.02	0.01%	0.48	0.05%
NP58 (48% NV5 activated carbon 25% HiSiv3000 17% PES)	6.86	0.01	0.01%	0.37	0.05%
MW3 (82% HiSiv3000 18% PES)	8.72	0.01	0.01%	0.13	0.03%
NP20(9) (82% Clinoptilolite 18% PES)	7.95	0.01	0.00%	0.63	0.10%
NP72 (70% SAC460 carbon 15% 5A 15% PES)	7.24	0.00	0.00%	0.62	0.13%
NP47 (56% HiSiv3000 25% HiSiv1000 19% PES)	8.53	0.00	0.00%	0.17	0.04%

For all the adsorbents tested except for the impregnated carbon, breakthrough times of less than 0.6 hours and breakthrough loadings below 1%wt of hydrogen sulphide were observed. The highest breakthrough time and loading of 2 hours and 1.6%wt loading was observed on metal salt impregnated carbon fibres, suggesting that presence of a metal impregnant may be necessary to improve breakthrough time and loading for H_2S dynamic challenge. It should also be noted that despite their poor breakthrough loadings of 0.57 and 0.54% respectively, the 5A/13X and 5A/clinoptilolite fibres had equilibrium loading weights of 2.48 and 2.95%, respectively. This suggests that these materials have the capacity to adsorb H_2S, but too slowly to give adequate protection in a respirator, where fast kinetics and higher breakthrough time are important. However, the affinity for moisture that these zeolites have should be taken into consideration, particularly given the slow uptake of H_2S that would have to compete with rapid uptake of water (van Bekkum, 2001).

Table 4.3. Adsorbent fibre screening trials: summary of experimental results of 1000 ppm 1 L/min dynamic cyclohexane challenge, ordered by breakthrough loading.

Fibre name (composition)	Adsorbent weight (g)	t_b (h)	t_b loading %wt	t_{eq} (h)	t_{eq} loading %wt
EUR20 (80% NV5 carbon 20% PES)	5.09	0.54	2.15	?	18.75
D-A-1 (80% AbScents 1000 20% PES)	6.27	0.15	0.50	3.62	5.83
D-C-1 (80% Chemviron BPL 20% PES)	5.40	0	0	?	12.40
D-H3-1 (80% HiSiv 3000 20% PES)	/	0	0	0	0.00
D-Z-1 (80% ZSM-5 20% PES)	/	0	0	0	0.00

In the case of D-A-1 80% AbScents1000 adsorbent hollow fibres, the experiment was carried out using a photoionisation detector (PID), showing a complete breakthrough curve and the equilibrium loading calculated from the breakthrough curves closely matched that calculated from weighing the fibres (5.82 and 5.83%wt, respectively). As is apparent from the breakthrough curves for cyclohexane dynamic tests shown in Appendix 1, there was a problem with the FID sensor used, which was detecting greater outlet concentration than the initial concentration. As such, all equilibrium loadings in the Table above were calculated from the final weight of the fibres when the test was stopped. This

is as opposed to using the (incorrectly shaped) breakthrough curve by the method shown in Appendix 3.

Overall, the highest breakthrough loading, 2.15%wt, was observed on NV5 carbon fibres, followed by AbScents1000, with 0.5%wt breakthrough loading. However, the breakthrough times were low in both of these cases, at 0.54 and 0.15 hours respectively. Despite these breakthrough times and loadings, significantly higher equilibrium loadings were observed, with the NV5 carbon fibres increasing from 2.15%wt breakthrough loading to 18.75%wt equilibrium loading. This was most likely due to the large size of the cyclohexane molecule, resulting in slow adsorption, particularly in the case of the fibres prepared from Chemviron BPL carbon, which had 12.4%wt equilibrium loading. For HiSiv3000 and ZSM-5, negligible breakthrough times and loading were observed, possibly due to pore size being too small to allow entrance of the bulky cyclohexane molecule.

Overall, 4.54%wt breakthrough loading of ammonia and 2.15%wt breakthrough loading of cyclohexane were the highest breakthrough loadings observed. However, the highest breakthrough loading for hydrogen sulphide was 1.6%wt on an impregnated carbon and 0.82%wt on a fibre prepared from untreated material. These screening tests have highlighted that metal impregnation of the selected fibres can increase breakthrough time and loadings of H_2S. Using these results, adsorbents for a composite fibre were selected considering an optimal combination for high breakthrough time and loading of ammonia and cyclohexane. This composite will then be treated with impregnants to increase breakthrough time and loading of H_2S. This will be explored in more detail in in Chapter 5.

Though the highest ammonia loadings were observed on low Si:Al ratio zeolites, these are likely to be significantly affected by the presence of water (van Bekkum, 2001). Excluding these, as a respirator must operate at a range of ambient humidities, the best options for ammonia adsorption are the high Si:Al ratio zeolites ZSM-5 and AbScents1000.

For cyclohexane, the greatest breakthrough time and loading (0.54 hours and 2.15%wt) was seen on NV5 carbon, followed by AbScents1000 zeolite (0.15 hours and 0.5%wt).

Negligible breakthrough times were recorded for ZSM-5, Chemviron BPL and HiSiv3000. As such, in order to prepare a hybrid fibre with a high breakthrough time and loading for ammonia and cyclohexane over a range of humid conditions, and the potential to be impregnated with metal salts in order to sorb hydrogen sulphide, NV5 carbon (for cyclohexane) and AbScents1000 (for ammonia and cyclohexane) were selected for further study. Adsorbent fibres were prepared using these two adsorbents in a 50:50 ratio. In future this ratio could be varied to tailor fibres to particular requirements.

It should be noted that 80% adsorbent NV5 fibres were difficult to spin. The polymer/adsorbent precursor mixtures were extremely viscous, tending to block the spinneret, and the fibres were very brittle. The NV5 powder was examined with a scanning electron microscope and compared to AbScents1000 powder. The scanning electron micrographs are shown in Figure 4.1. There is a large distribution of carbon particle sizes, up to nearly 50 μm in length. This is as opposed to the relatively small and regular particles of AbScents1000. The difficulty spinning and fragility of the fibre were speculated to be associated with the large particles of the activated carbon powder, which are held in the fibre structure by thin strands of polymer. While these may coat the smaller AbScents1000 particles and hold them securely, the larger carbon particles will be held only loosely, and form mechanically weak fibres. Problems associated with the use of a large proportion of NV5 activated carbon in the adsorbent fibres were not encountered during preparation of the hybrid AbScents1000/NV5 activated carbon hybrid fibre.

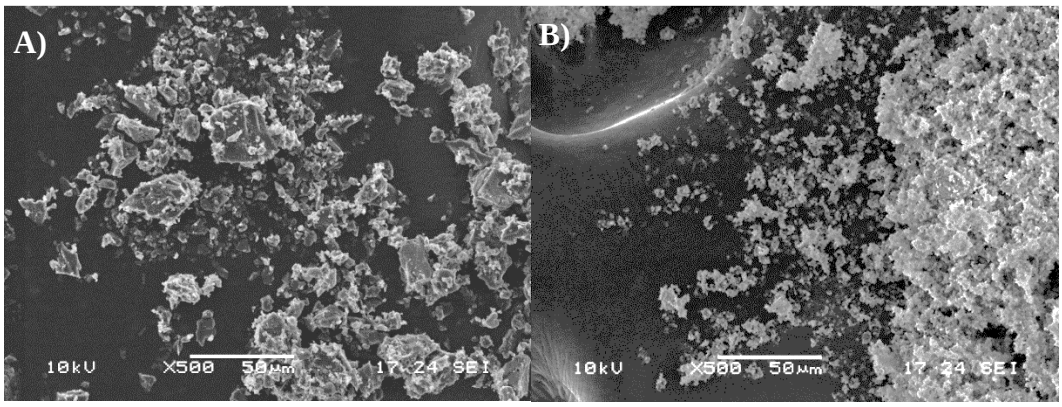

Figure 4.1. A) NV5 carbon powder B) AbScents1000 zeolite powder.

4.2.1.1 The effects of humidity on hydrophilic and hydrophobic adsorbent fibres

Respirators must operate effectively over a wide humidity range, whether a tropical rainforest or a desert. As such, water vapour isotherms and humidity breakthrough tests were performed on the adsorbents selected after screening, NV5 and AbScents1000.

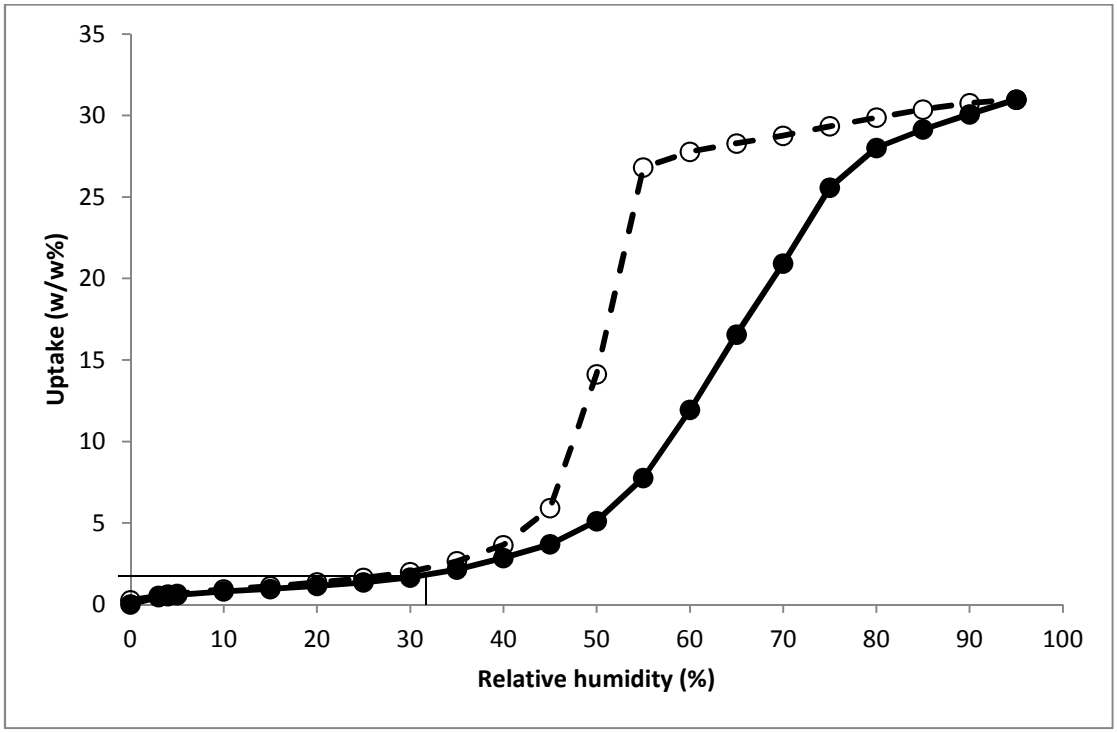

Figure 4.2. NV5 fibre water isotherm, with adsorption shown as the solid line and filled circles, and desorption shown as dotted line with empty shapes. The vertical and horizontal lines mark the %RH used in the dynamic test below (characterised at Dstl).

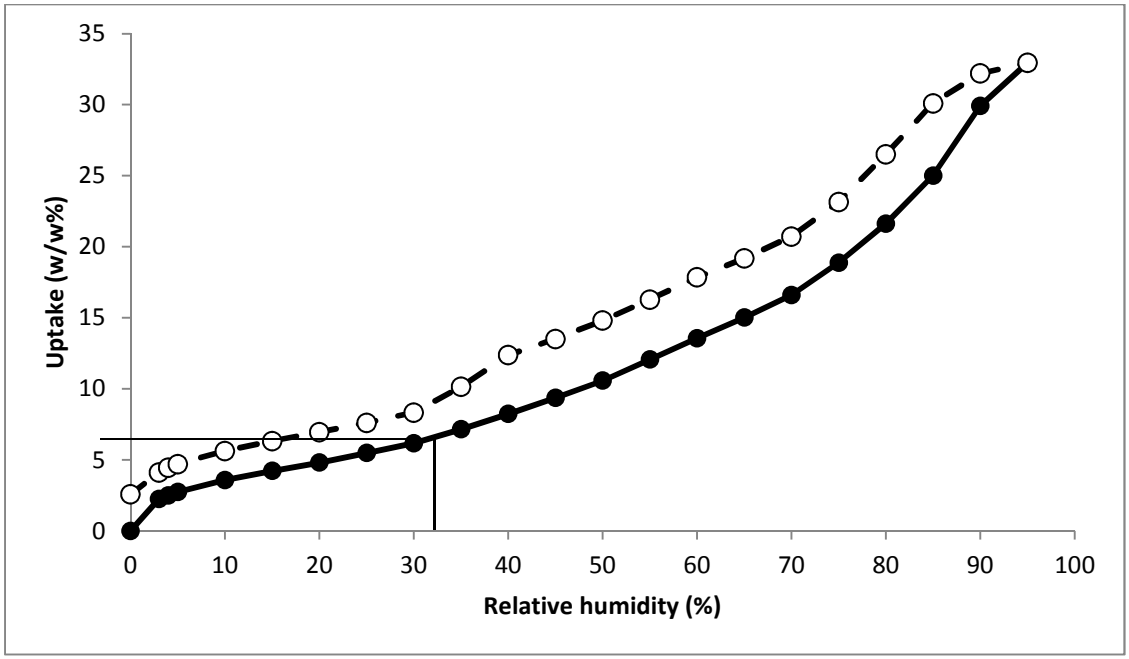

Figure 4.3. AbScents1000 water isotherm, with adsorption shown as the solid line and filled circles, and desorption shown as dotted line with empty shapes. The vertical and horizontal lines mark the %RH used in the dynamic test below (characterised at Dstl).

The water adsorption isotherm for NV5 carbon (Figure 4.2) demonstrated a characteristic type V isotherm for water adsorption on carbon, with little adsorption at low pressure and more at high pressure. This was followed by hysteresis as a result of capillary condensation, and loading of 30%wt. The equilibrium loading of the NV5 carbon at a relative humidity of 35% was negligible, which corresponds to the values observed in the water isotherm. The water adsorption isotherm for AbScents1000 (Figure 4.3) exhibited a type IV isotherm, again with hysteresis due to capillary condensation, and eventual loading of 33%wt. AbScents1000 is marketed as a hydrophobic zeolite, which does not agree with this isotherm. The equilibrium loading of 4.6%wt calculated from the breakthrough curve was approximately the same loading as that on the water isotherm at 34% RH (Figure 4.3).

Detailed humidity testing is beyond the scope of this investigation. However, the combination of a zeolite and a carbon in the hybrid fibre are expected to complement each other for adsorption. In general carbons are less adversely affected by humidity than zeolites, and may adsorb some soluble gases (such as ammonia) more effectively in humid conditions, while zeolites perform effectively in dry conditions (Meeyoo *et al.*,

1998). Similarly, synergistic combinations of adsorbents could be incorporated in future to ensure optimal adsorption across a wide humidity range.

4.2.2 Optimising adsorbent hollow fibre structure: layers, thickness and bore size

Different adsorbent hollow fibre structures were compared on the basis of their thickness, their bore size and the number of layers. The different fibre types were bundled into cylinders with 2 cm diameter, and as such different numbers of fibres were packed. Details of the average number of fibres in a module and the resulting voidage/bore volume are shown in Table 4.4. It should be noted that the calculated maximum number of fibres was determined by dividing the area of the module by that of an individual fibre. This number is unlikely to be reached in practice as there will be small gaps between fibres and around the edges of the module. However it should be noted that in some cases, more standard bore thin single layer fibres than the calculated maximum were fitted into a module. This was due to their thin walls; they can easily be compressed, albeit with decreased bore diameter.

Table 4.4. Adsorbent hollow fibre parameters.

Layers	Bore	Fibre outer diameter (mm)	Bore diameter (mm)	Calculated max no. fibres	Average number of fibres	Lumen area (mm^2)	Voidage
Single	Small	2	0.8	100	80	44	0.14
	Standard	2	1.0	100	80	51	0.16
Double and thick single	Small	3	0.8	44	40	22	0.07
	Standard	3	1.0	44	40	34	0.10

Table 4.4 demonstrates that the voidage was highest for single layer fibres with standard bore and lowest for double layer fibres with small bore.

4.2.2.1 Scanning electron microscopy

The structure of adsorbent hollow fibres was examined by SEM. Figure 4.4, Figure 4.5 and Figure 4.6 show SEMs of cross sections of the different fibre types.

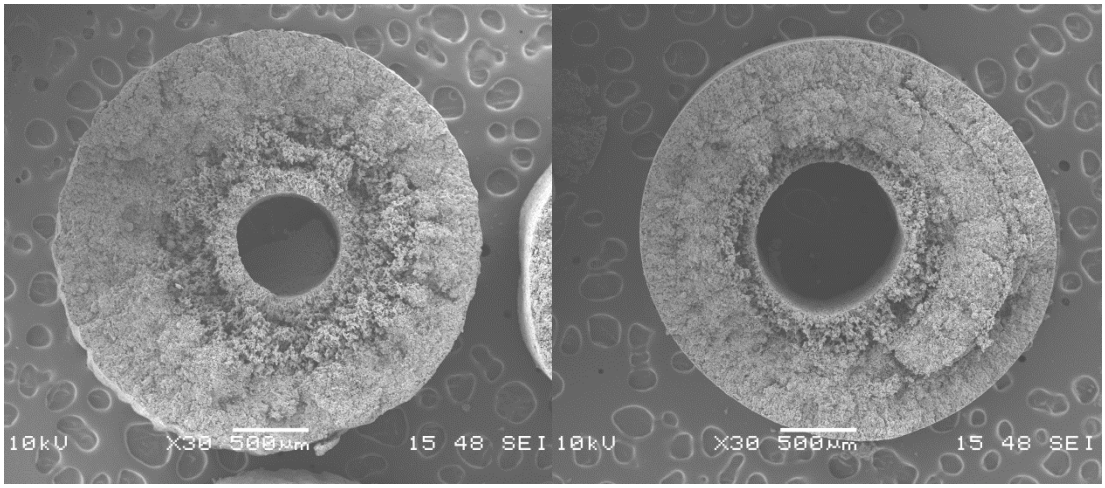

Figure 4.4. 20% PES 80% HiSiv3000 adsorbent fibre cross sections. Left: double layer 'small bore'. Right: double layer 'standard bore'.

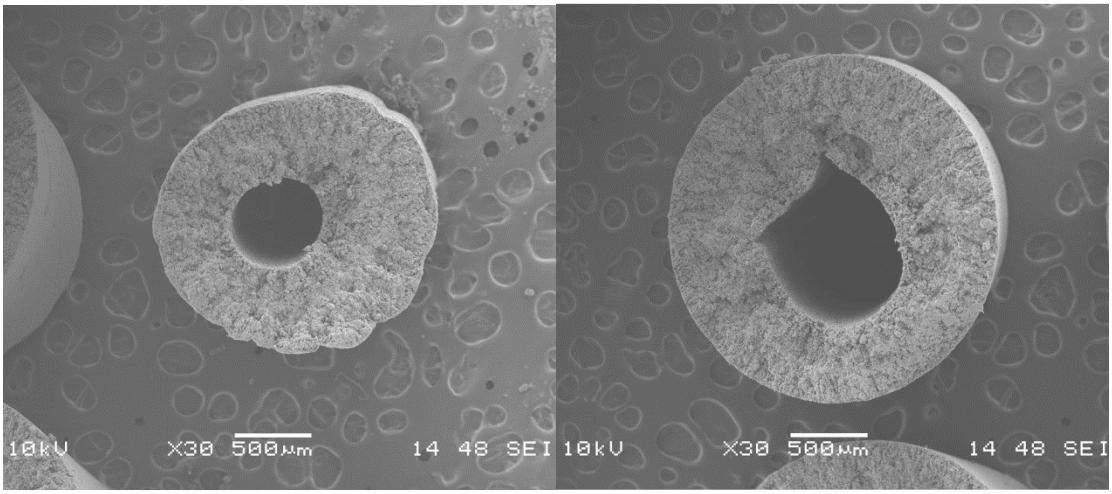

Figure 4.5. 20% PES 80% HiSiv3000 adsorbent fibre cross sections. Left: single layer 'small bore'. Right: single layer 'standard bore'.

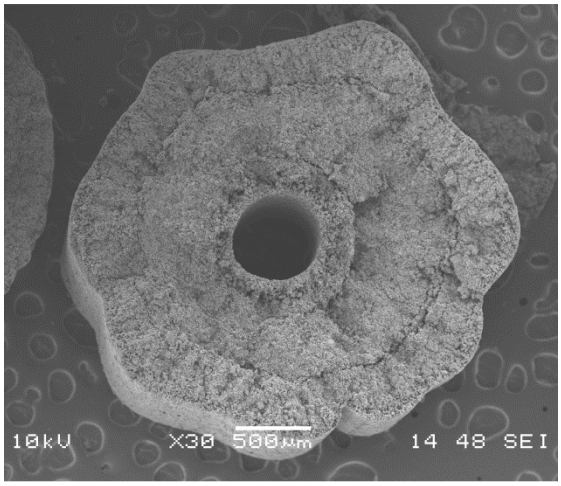

Figure 4.6. 20% PES 80% HiSiv3000 adsorbent fibre cross sections. Thick single layer 'small bore' fibre.

Double layer fibres (Figure 4.4) showed two distinct layers: an open macrovoidal layer around the bore and a less open outside skin layer. This skin is likely to have high resistance to gas flow, as suggested in Section 3.3.1.2. The thin single layer fibres (Figure 4.5) had a uniform macroporous structure with no thick skin apparent from the cross section. The thick single layer fibre (Figure 4.6) showed three distinct sections. The outer and inner sections, which were both exposed to the water in the spinning process, and the middle section, which was not exposed to water until it diffused through the fibre. This means it took longer for the solvent to leave this part of the fibre. All the fibres spun had a spongy structure with no large finger-like macrovoids. This suggests that coagulation took place slowly in all of the adsorbent hollow fibres (Kesting, 1971).

Single layer fibres remain flexible and elastic compared to the more brittle double layer fibres. This is due to their open structure and lack of a solid outer wall. The double and thick single layer fibres have less flexibility, due to their thick, wall layer on the outside, though this does protect them from compression, which the single layer fibres are prone to. It should be noted that there is some deformation to the bore of the single layer standard bore fibre. This was the case for several of the single layer standard bore fibre samples examined under SEM, and is likely due to the thin and very porous wall surrounding the bore, making it more likely to deform.

Further details of each fibre structure were observed by SEM. Figure 4.7 shows the transition between 'inner' and 'outer' layer in more detail. The differences between inner and outer layer are due to the coagulating fluids. The outside of the fibre is exposed to tap

water in the spinning bath. As the concentration gradient is very steep, NMP is rapidly drawn from the outer layer, causing the fibre to coagulate quickly and more densely. The inside of the fibre is exposed to the bore fluid, which is a 50/50 mixture of tap water and NMP. As the concentration gradient is not so steep, the NMP leaves the structure gradually, meaning the coagulation occurs less quickly and resulting in a more open structure (Xu and Alsalhy Qusay, 2004). Obviously, this open structure may be replicated by spinning into a bath of 50/50 NMP/water. This is unpractical on the large scale, but was explored as a possibility to enhance the porosity of the fibre outer wall in Chapter 6.

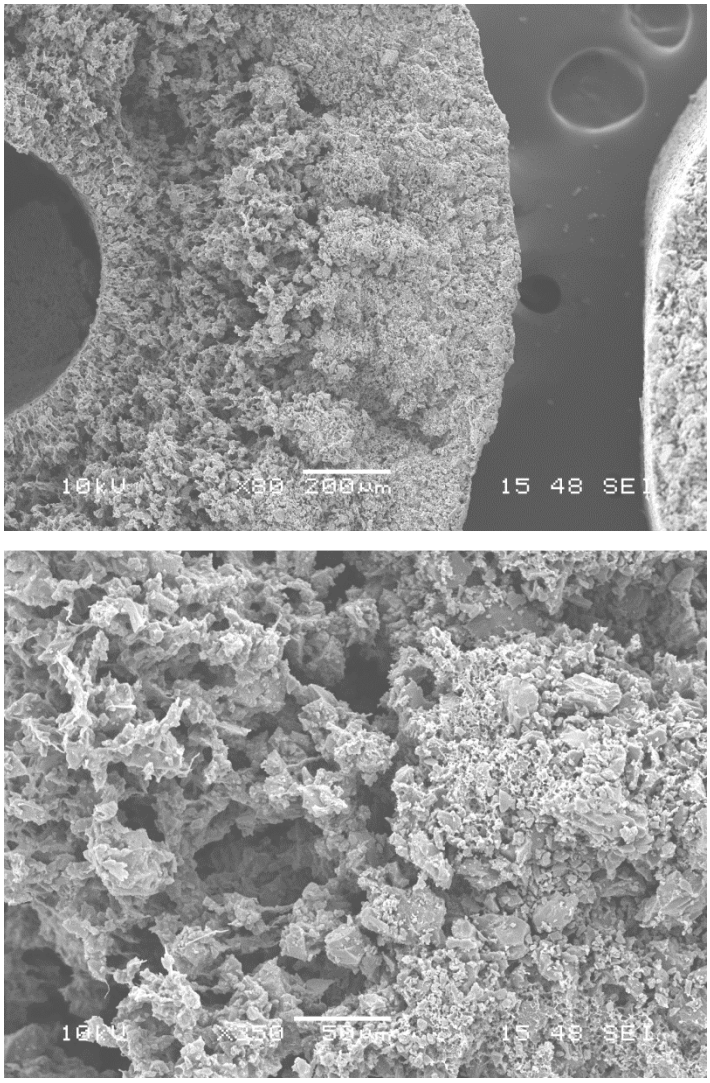

Figure 4.7. Double layer small bore fibre layer transition x 80 (top) and x 350 (bottom) of 20% PES 80% HiSiv3000 fibres.

A similar process occurs in the thick single layer small bore fibre (Figure 4.8). The outer skin rapidly coagulates and the inner skin slowly coagulates as described above. As these fibres are so large, the section between the two does not initially coagulate at all. The

dense structure suggests that it eventually coagulates rapidly, presumably when the fibre is in the collection bath filled with tap water.

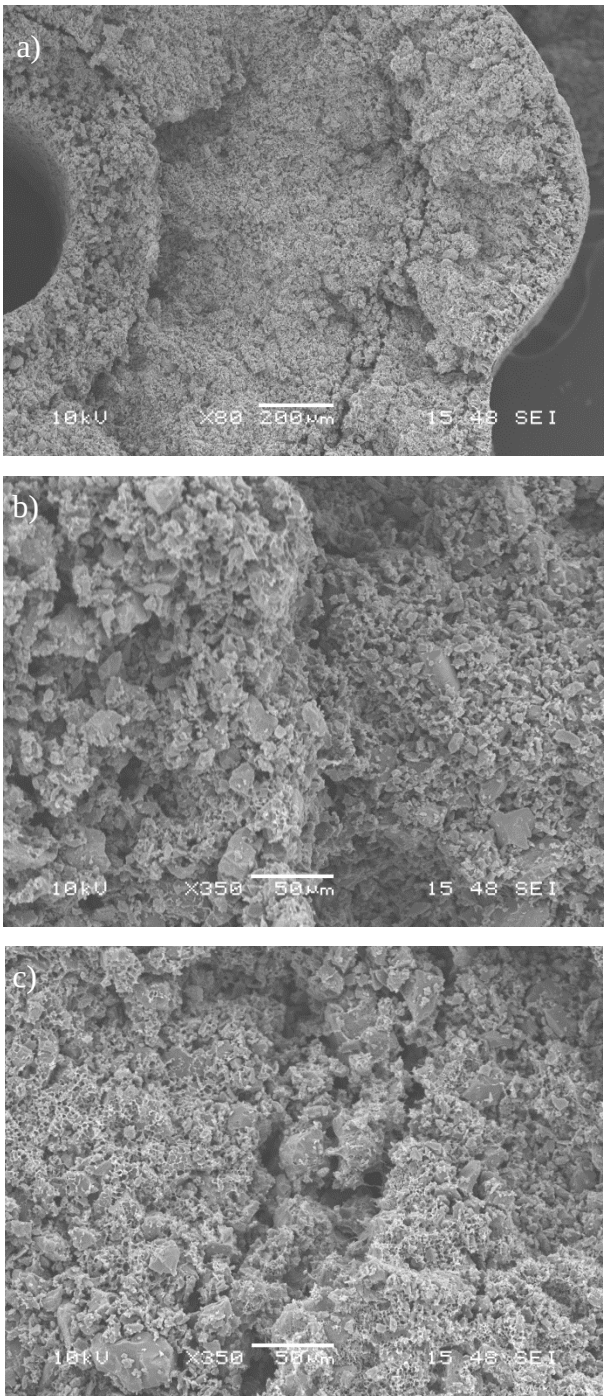

Figure 4.8. a) Thick single layer small bore 20% PES 80% HiSiv3000 fibre x 80 and zoomed in on the layer transitions – b) inner x 350 and c) outer x 350 (bottom).

The fibre walls were examined by SEM, shown in Figure 4.9. The top image shows the lumen wall of the fibre, which was exposed to 50/50 NMP/water during the spinning process. The bottom image shows the outer wall of a hollow fibre, which was exposed to

tap water during the spinning process. The key difference is that the lumen wall has a regular series of pores with no completely covered areas, allowing gas easy access. Meanwhile, the outer wall shows small pores and sections that are clogged by the polymer, due to the rapid coagulation on exposure to water. This lowers the porosity and may hinder adsorption kinetics.

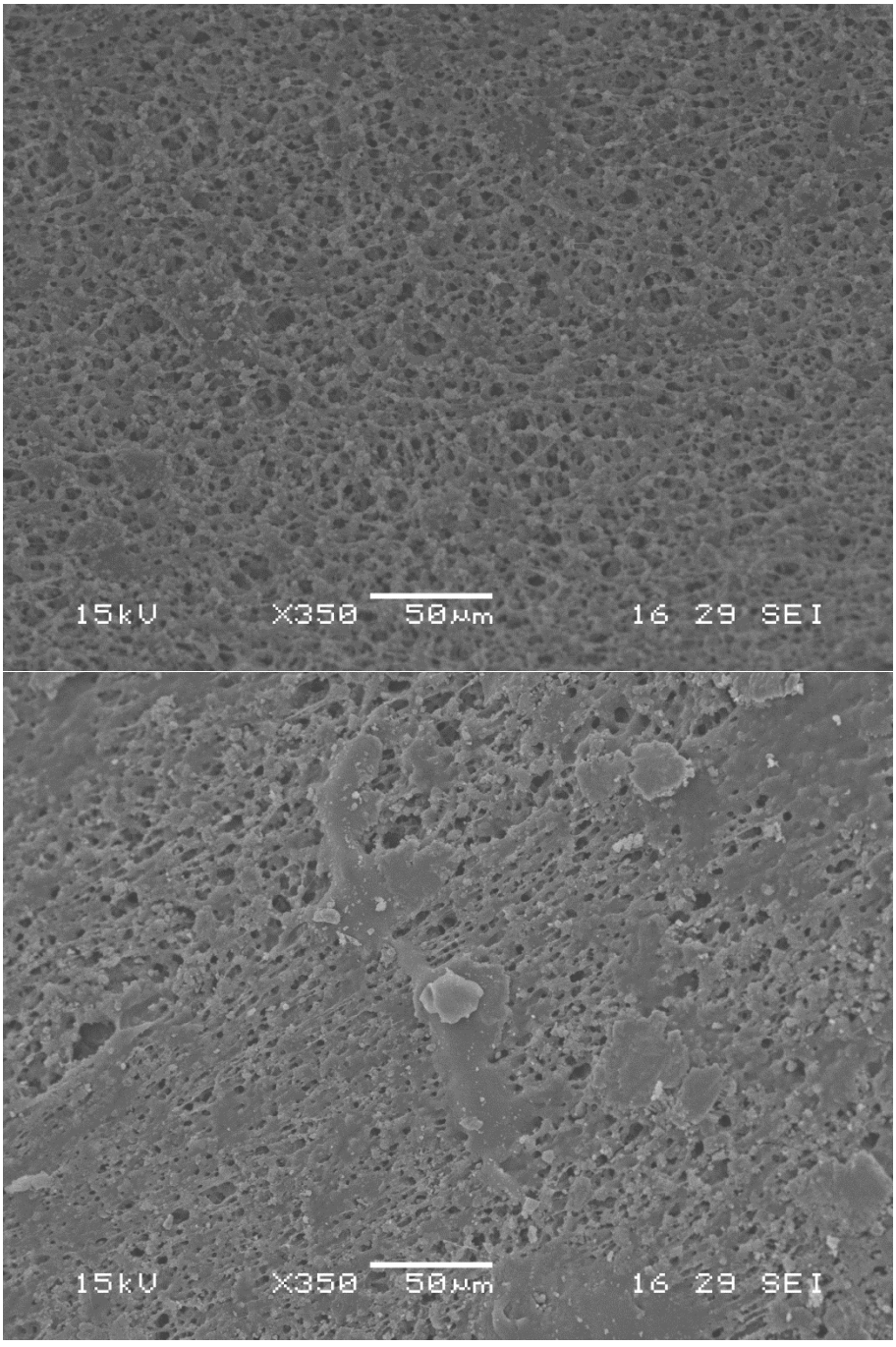

Figure 4.9. SEM images of hybrid NV5/AbScents1000 fibre, sections from the inside wall of the fibre bore (top) and outer wall of the fibre (bottom) x350.

4.2.2.2 Cyclohexane uptake testing

Different fibre structures are likely to have different rates of gas uptake. These were investigated by measuring the adsorption kinetics of the first point in a cyclohexane isotherm, a process described in Section 3.2.7.5. A graph of cyclohexane uptake (w/w%) compared to time is shown in Figure 4.10.

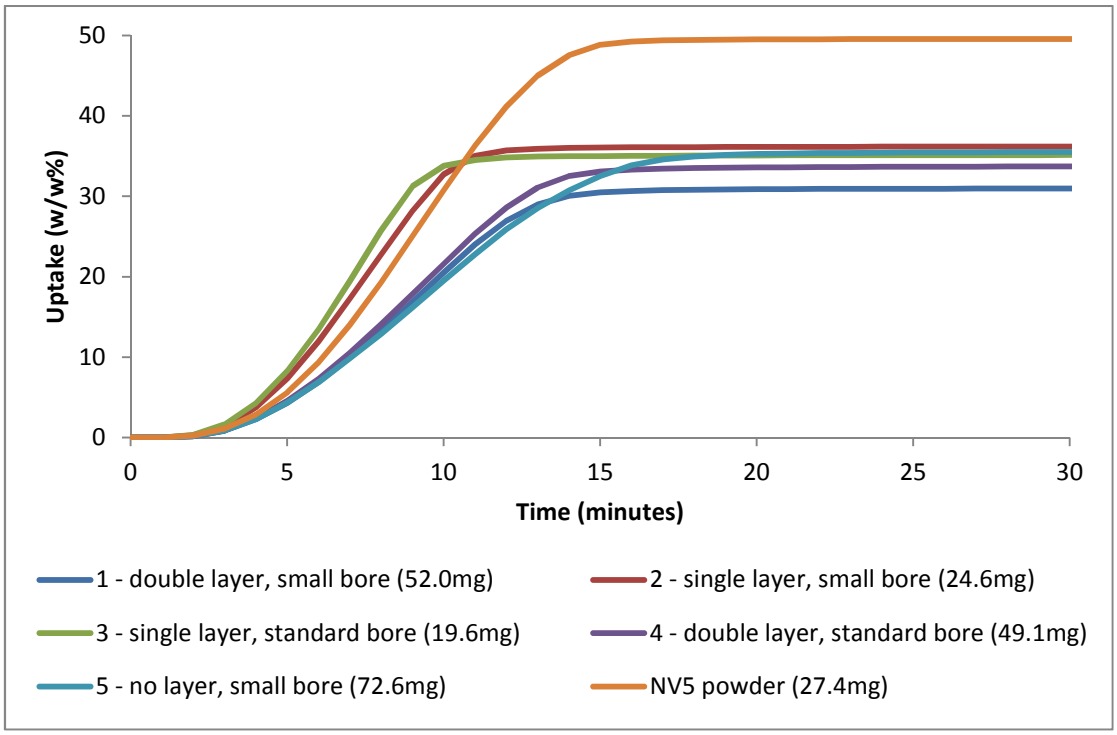

Figure 4.10. Initial uptake in cyclohexane vapour sorption for differently structured 20% PES 80% NV5 carbon hollow fibres (characterised at Dstl).

The fibres had slightly lower uptake than the powder per weight. This is due to the polymer content of the fibres. All the fibres would be expected to have the same % wt uptake. However, it was slightly lower in both double layer fibres. This could be because the thick outer skin layer observed in the double layer fibres blocked access to some of the adsorbent carbon.

The most rapid uptake was seen in both thin single layer fibres, which was faster even than the adsorbent powder. This is most likely associated with the thin fibre walls and inherently high surface area of the fibre structure, allowing easy access for the cyclohexane adsorbate. In addition, the final uptake w/w% was reached more rapidly by the single layer fibres than the double (10 minutes compared to 15 minutes). This is also likely to be associated with the thick outer skin in the fibres, as well as lower surface area, allowing slow cyclohexane diffusion into the structure. This data suggests that

cyclohexane adsorption kinetics are fastest in a single layer NV5 carbon fibre, regardless of the bore size.

4.2.2.3 Pressure drop due to fibre bore size

The pressure drop was measured in double and single layer hollow fibres with 'small' and 'standard' bore size. In order to fully investigate the effect of bore size on pressure drop, monoliths with 'large' circular bores were tested in addition to the hollow fibres. This was necessary as only two different inner tube sizes were available for hollow fibre preparation. Also, to test pressure drop at longer fibre lengths, several modules were put together in sequence. To confirm that there was no difference between a single fibre module and several smaller modules combined in series, both were tested and the pressure drops compared. The results are shown in Figure 4.11.

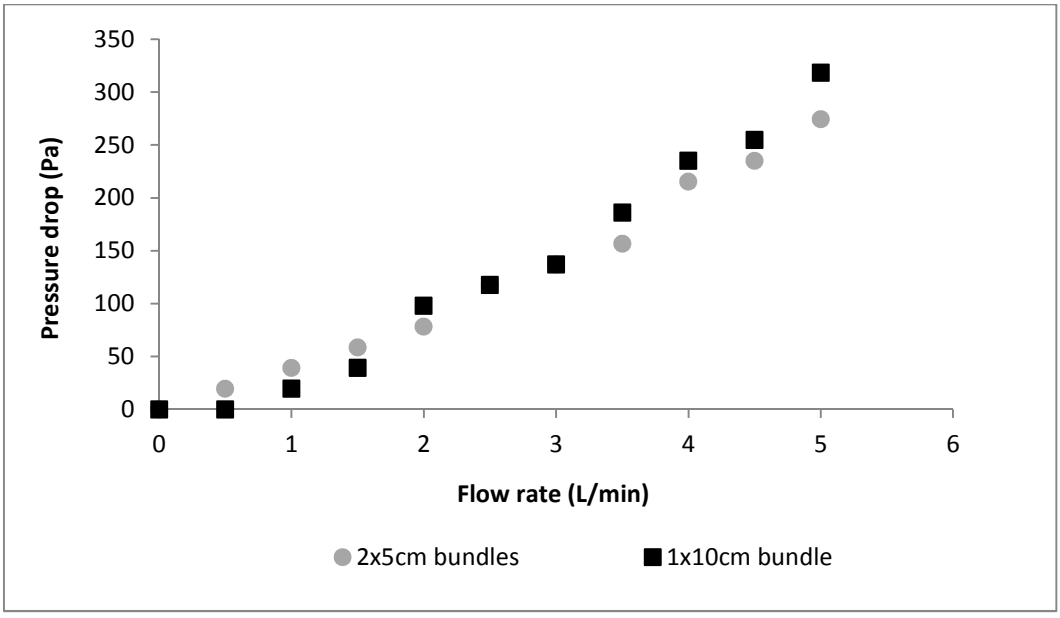

Figure 4.11. A comparison of pressure drop in a single 10cm fibre bundle compared to 2 x 5 cm fibre bundles set up one after the other.

No clear differences were observed between the single 10 cm bundle and the two 5 cm bundles, so it was assumed that the pressure drop measured from a number of shorter bundles was equivalent to that of a single bundle of their total length. As such, pressure drop in 20 and 25 cm hollow fibre modules was determined from no more than two shorter length hollow fibres put together.

Pressure drops across various modules over 0-5 L/min flow of compressed air are shown in Figure 4.12 to Figure 4.15. The pressure drop increased as the length of fibres/monolith/granular bed and the flow rate of the gas increased. The highest pressure drop was across the granular beds and the lowest was across the large bore monoliths. For the hollow fibres, the highest pressure drop was in those with the smallest bore size, while the lowest pressure drop was in the monoliths with the large bore. It should be noted that the empty column had some pressure drop in itself. However, the value was so low that it was assumed not to significantly affect results, and it was not taken into account.

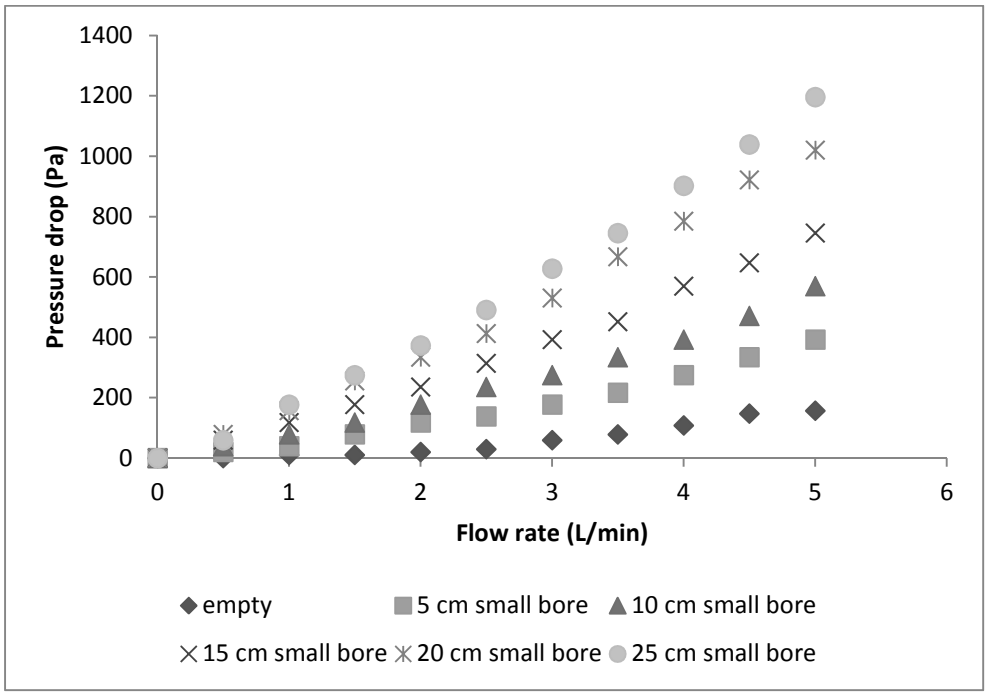

Figure 4.12. Pressure drop for 0.8 mm double layer small bore hollow fibres from 0-5 L/min flow rates.

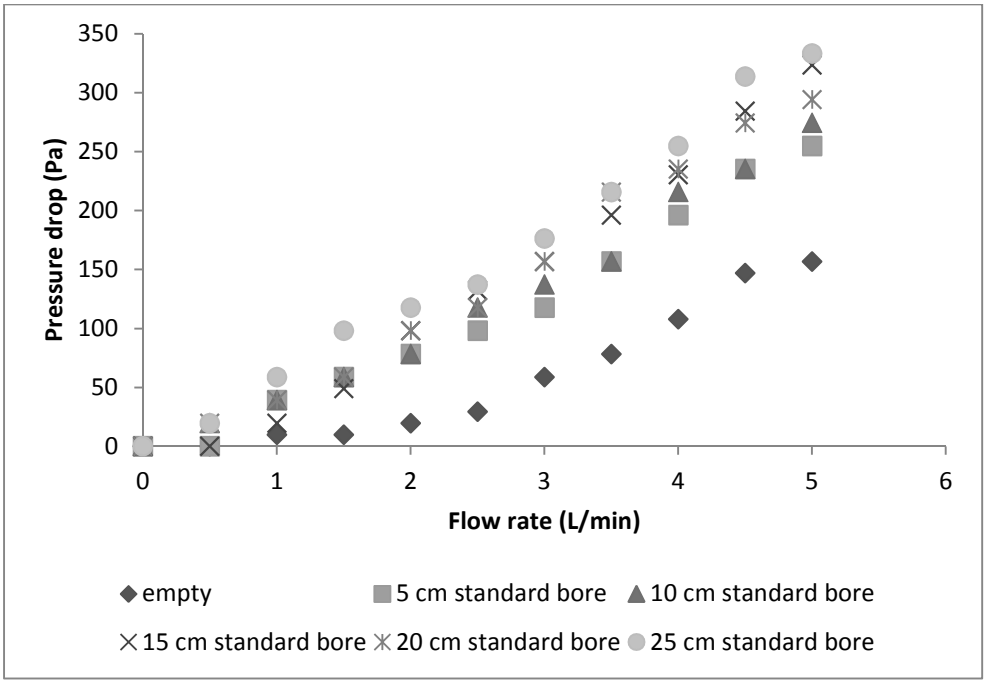

Figure 4.13. Pressure drop for 1 mm double layer standard bore hollow fibres from 0-5 L/min flow rates.

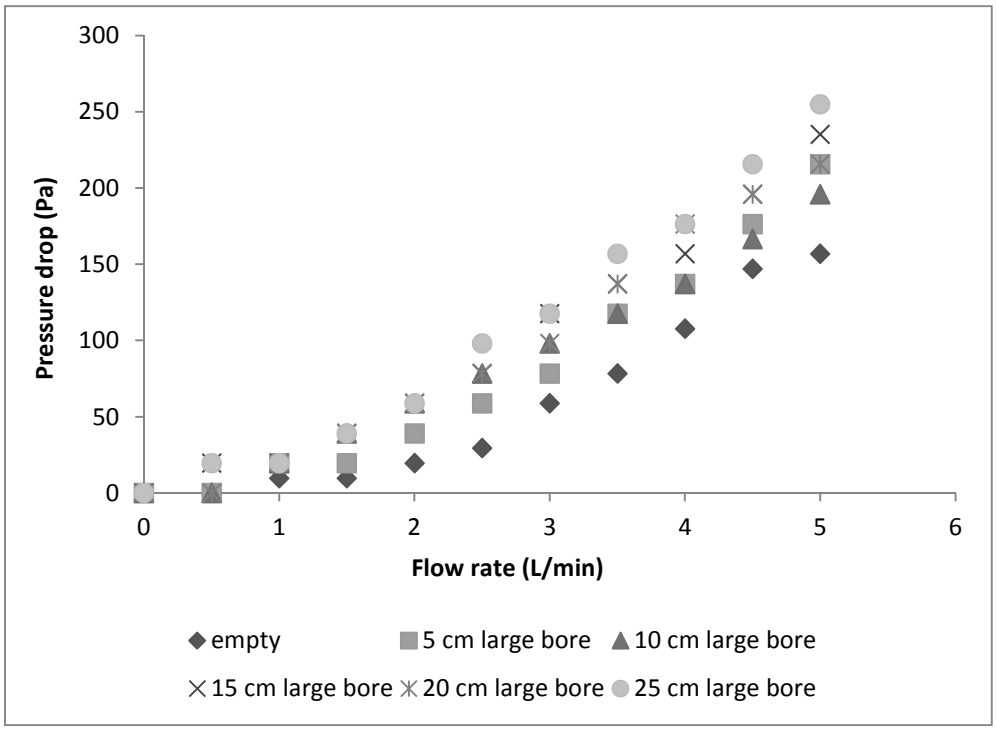

Figure 4.14. Pressure drop for 1.2 mm large bore monoliths from 0-5 L/min flow rates.

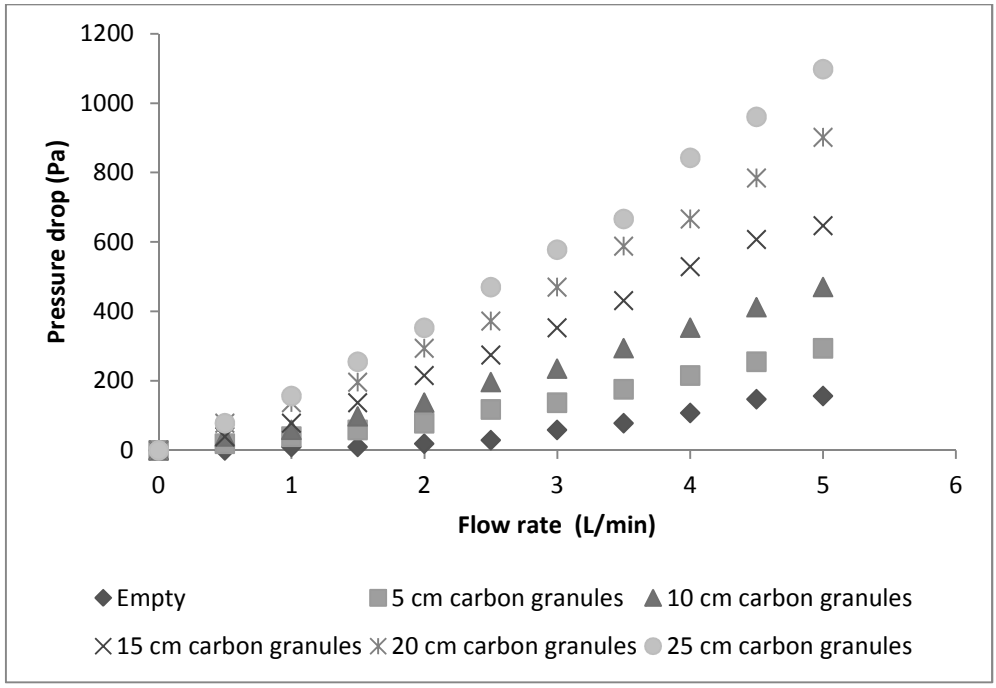

Figure 4.15. Pressure drop for 1 mm carbon granules from 0-5 L/min flow rates.

Pressure drop theory dictates that a larger channel size will result in lower pressure drop (Poiseuille, 1846; Hagen, 1839) and this was observed to be the case with some of these results. The granular beds used had higher pressure drop than 1 mm and 1.2 mm bore fibres at each flow rate, demonstrating hollow fibres to be superior in terms of pressure drop in these instances. However, the 0.8 mm bore fibres had greater pressure drop than the packed bed, highlighting the importance of the bore size in this case. The pressure drop in hollow fibres and granular beds is explored in greater detail in Chapter 7.

4.2.2.4 Pressure drop as a function of length

In order to standardise the data, pressure drop values were divided by the length of the module to obtain $\Delta P/L$ in Pa/m. These are shown in Figure 4.16 to Figure 4.19.

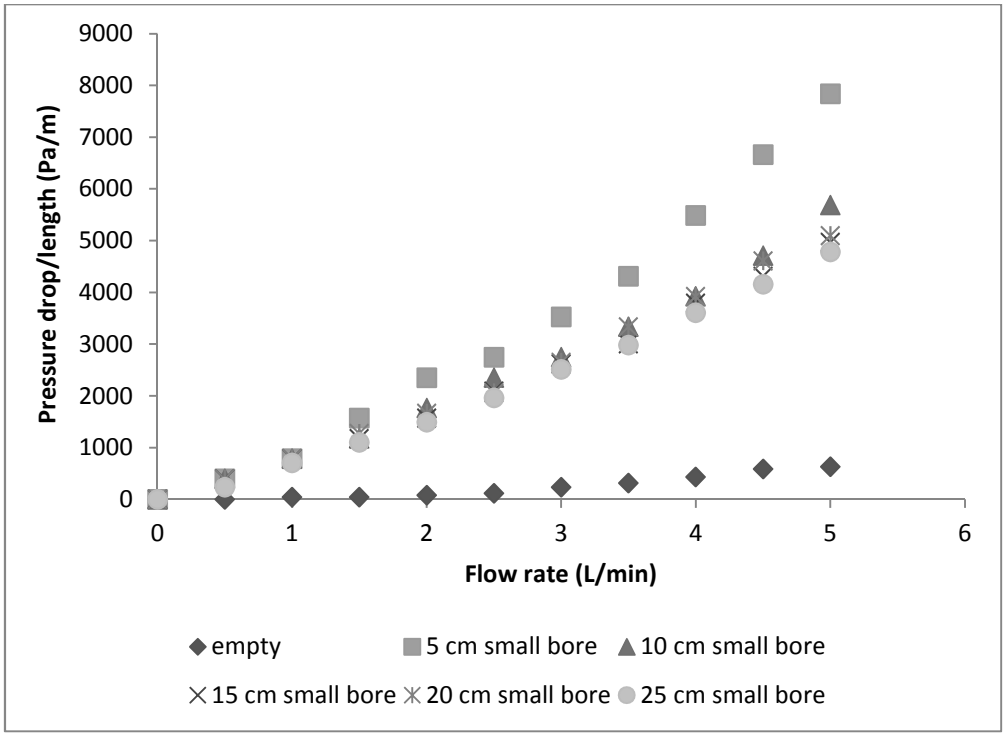

Figure 4.16. Pressure drop/length for 0.8 mm small bore hollow fibres.

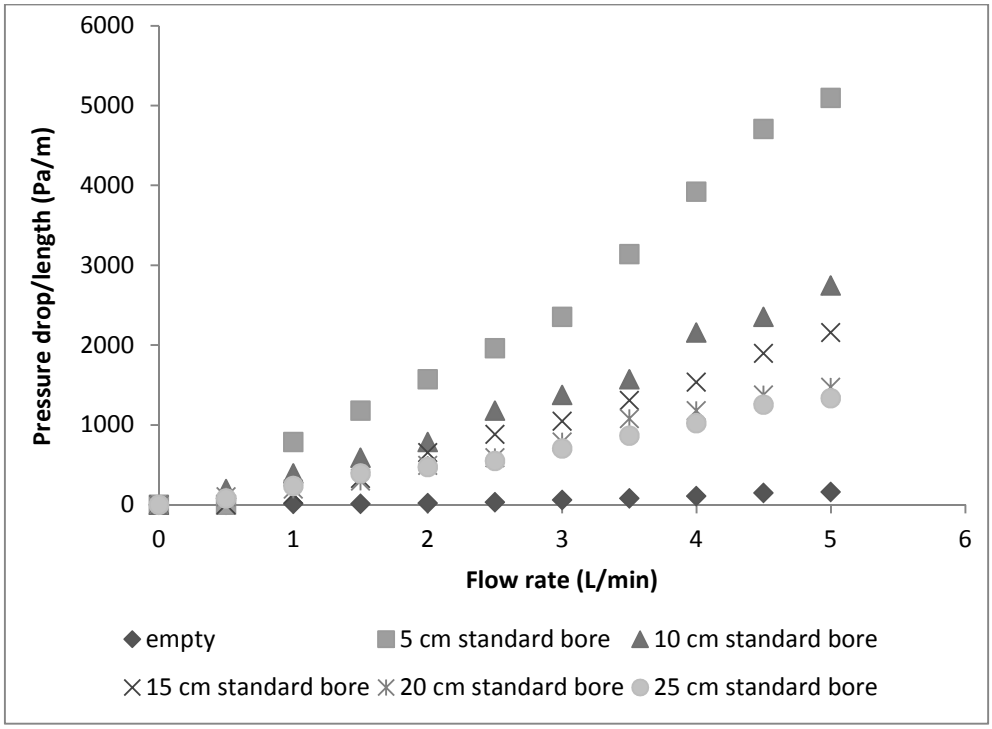

Figure 4.17. Pressure drop/length for 1 mm standard bore hollow fibres.

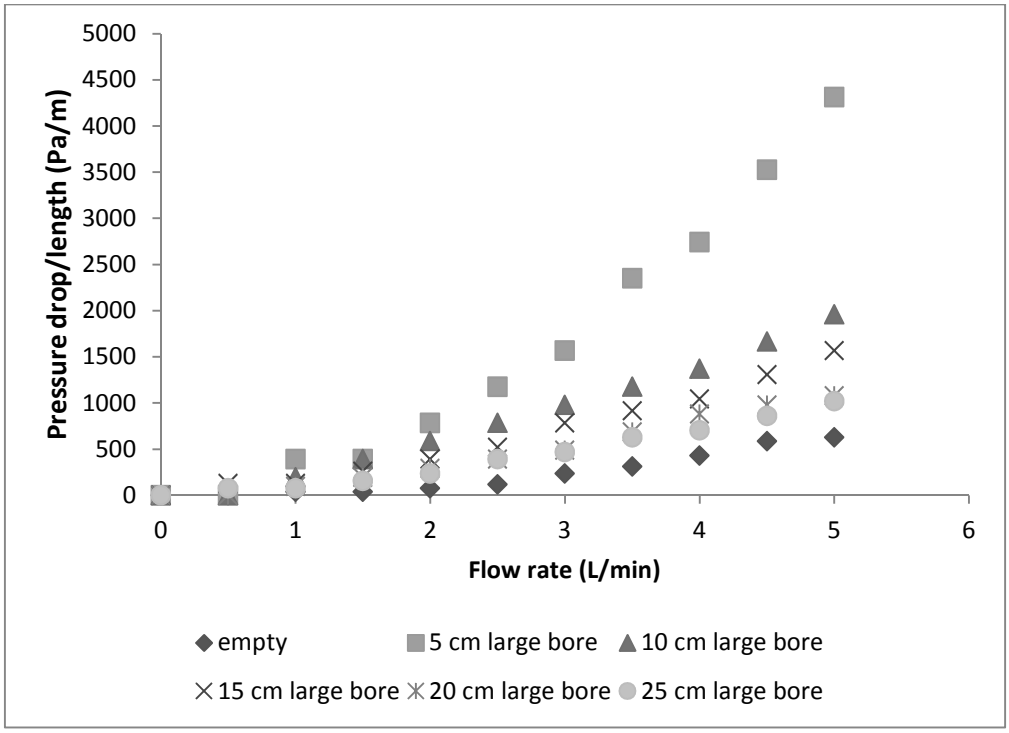

Figure 4.18. Pressure drop/length for 1.2 mm large bore monoliths.

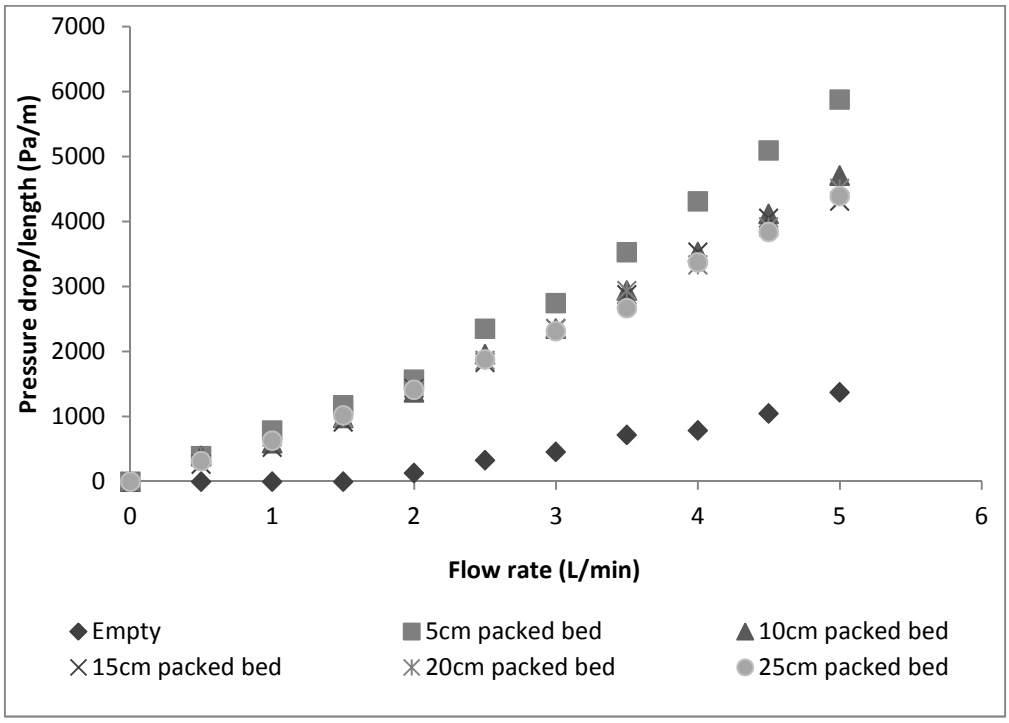

Figure 4.19. Pressure drop/length for 1 mm carbon granule granular bed.

Given how pressure drop models can be used to calculate ΔP/L, it was anticipated that the lines for pressure drop as a function of length should overlap for each set of data. However, as can be seen in the figures above, this was not the case. In every case, the shorter beds had the highest the ΔP/L and the longest beds had the lowest ΔP/L. As length

reached a certain point, the ΔP/L curves began to overlap. For small bore, 15, 20 and 25 cm ΔP/L overlapped; for the standard bore, 20 and 25 cm overlapped; for the large bore, 20 and 25 cm overlapped; for the granular bed, 10, 15, 20 and 25 cm overlapped. These overlaps suggest that there may be some form of entrance effect that ceases to be significant for modules as they approach a certain length. When steady state flow is reached, ΔP will begin to normalise. This will allow the pressure drop of modules at the length at which ΔP/L stabilises to be modelled by various methods, which is explored in Chapter 6.

These entrance effects could be due to the gas inlet diameter compared to the bed diameter (Figure 4.20a) or to the bed diameter and the fibre inner diameter (Figure 4.20b), particularly at high flow rates and shorter lengths of beds. Due to the speed of gas flow, it is possible that it does not fully disperse through the beds until it is some distance through, or not at all. It is possible that this could be mitigated with a disperser initially or by using a longer column to allow fluid flow to normalise.

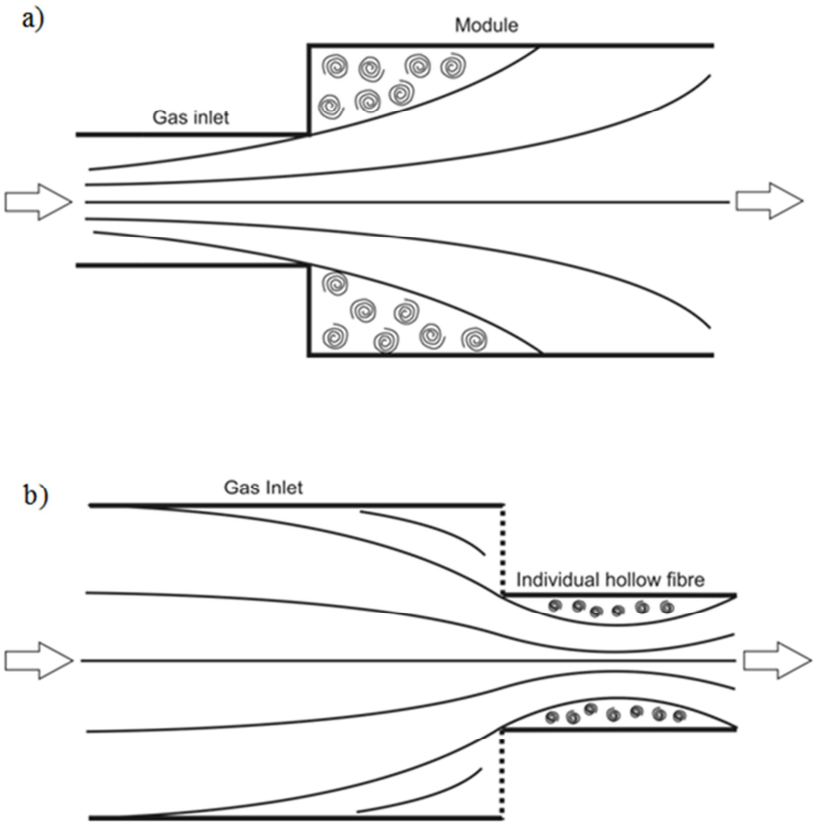

Figure 4.20. a) Example of flow in a sudden expansion, b) Example of flow in a sudden contraction and resulting vena contracta.

To determine whether entrance effects were caused by a sudden expansion, of the gas inlet into the 2 cm diameter module, or a sudden contraction, of the 2 cm bed into the inner bore of the hollow fibres, pressure drop was measured for a 5 cm hollow fibre module at the top (20 cm from gas inlet, sudden contraction only) and bottom (0 cm from gas inlet, sudden expansion followed by sudden contraction) of a 25 cm stainless steel module.

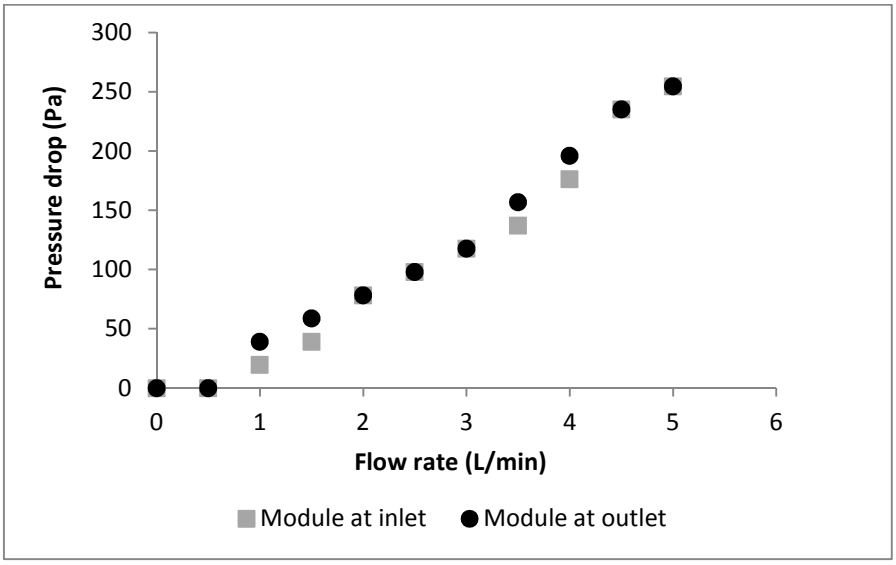

Figure 4.21. A comparison of pressure drop in 5 cm long hollow fibre modules situated at the top and bottom of a 25 cm long column to test for possible entrance effects.

Figure 4.21 shows little difference between the module at the gas inlet and at the outlet. From this data it was possible to determine that any entrance effects are likely to instead be due to the sudden contraction of fluid flow into the bores of the fibres, which occurred in both cases, as opposed to the sudden expansion.

According to Massey and Ward-Smith (1998), one would expect entrance effect to occur for a distance approximately 8x the diameter (i.e. 2 cm x 8 = 16 cm for the module, 6.4 mm for small bore fibres, 8 mm for standard bore fibres, 9.6 mm for large bore fibres). While 6.4 mm seems small, it is over 10% of the length of a 5 cm column, and for the larger bore, 9.6 mm makes up 20% of the length of a 5 cm column.

4.2.3 Testing fibres of different lengths and diameters with ammonia

Single layer and double layer 80% AbScents1000 fibres were dynamically challenged with 800 ppm ammonia at 1 L/min and the results are shown in Figure 4.22.

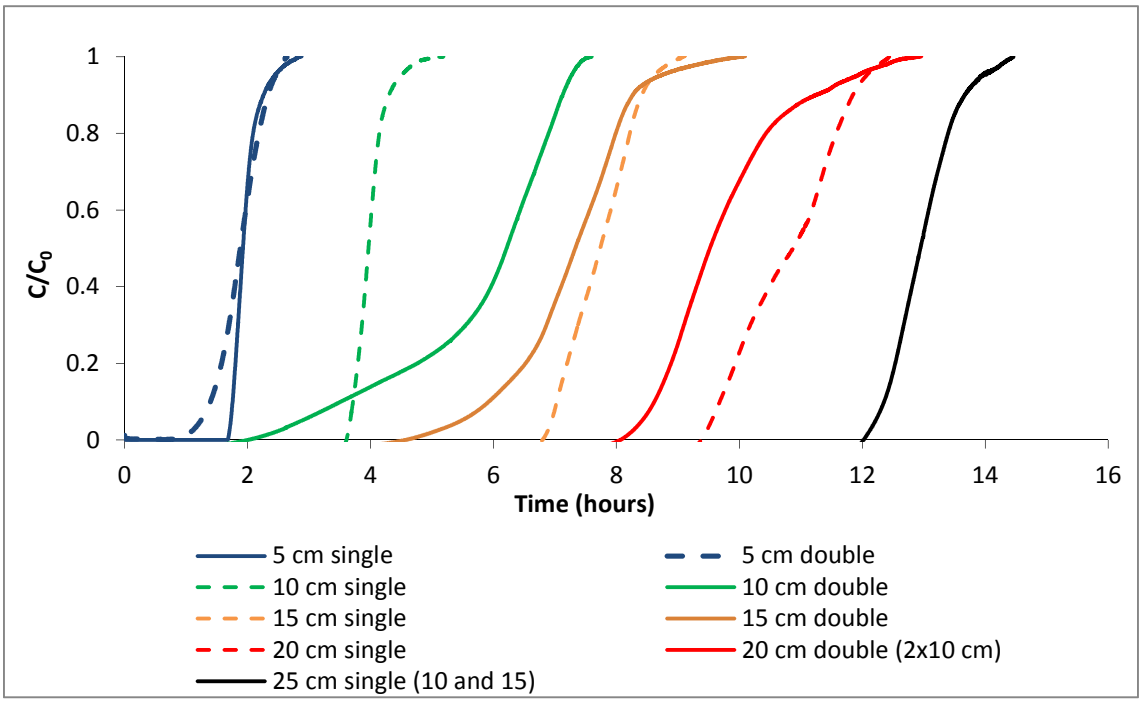

Figure 4.22. Breakthrough curves for 800 ppm 1 L/min ammonia challenge on single and double layer AbScents1000 fibres, showing double layer fibres with solid lines and single layer with dotted lines. (The lengths are paired by colour except for 25 cm single, for which a double layer test was not carried out).

Increasing breakthrough time as length increased was clearly observed for single and double layer fibres, as shown in Figure 4.22. In all cases, the single layer fibres had longer breakthrough time and sharper breakthrough curves than their equivalent double layer. This improvement was even more marked when considering weight (Table 4.5) with single layer fibres showing higher breakthrough and equilibrium loading than double layer fibres.

Table 4.5. Dynamic breakthrough data for single and double layer 80% AbScents1000 fibres tested with 1 L/min 800 ppm ammonia.

Fibre	Weight (g)	t_b (h)	t_b loading (%)	t_{eq} (h)	t_{eq} loading (%)	t_s (h)	LUB (%)	MTZ (cm)
10 cm single	9.13	3.65	1.35%	5.19	1.45%	4.00	8.71%	3.85
15 cm single	14.42	6.91	1.63%	9.08	1.78%	7.74	10.77%	4.22
20 cm single	18.40	9.49	1.76%	12.44	1.95%	10.80	12.12%	5.47
10 cm double	11.15	2.62	0.79%	7.60	1.73%	5.81	54.96%	8.58
15 cm double	16.08	5.22	1.09%	10.09	1.50%	7.26	28.12%	10.07
20 cm double	21.56	8.32	1.31%	12.96	1.50%	9.73	14.51%	9.53

The same trend can be observed for the ammonia dynamic challenge on hybrid fibres, shown in Figure 4.23. There were far longer breakthrough times observed on single layer fibres modules despite their higher voidage. Table 4.6 shows the breakthrough data and clearly demonstrates that the single layer fibres had significantly higher breakthrough loading per weight than the double layer fibres. These were relatively consistent across all weights for the single layer fibres; whereas an increase in breakthrough loading was seen in double layer fibres, indicating an entrance effect. MTZ was also consistent in the single layer fibres, except in the case of the 15 cm length, which is most likely an anomalous result. In this case it was difficult to determine the correct equilibrium time of the sample, meaning LUB and MTZ may be miscalculated.

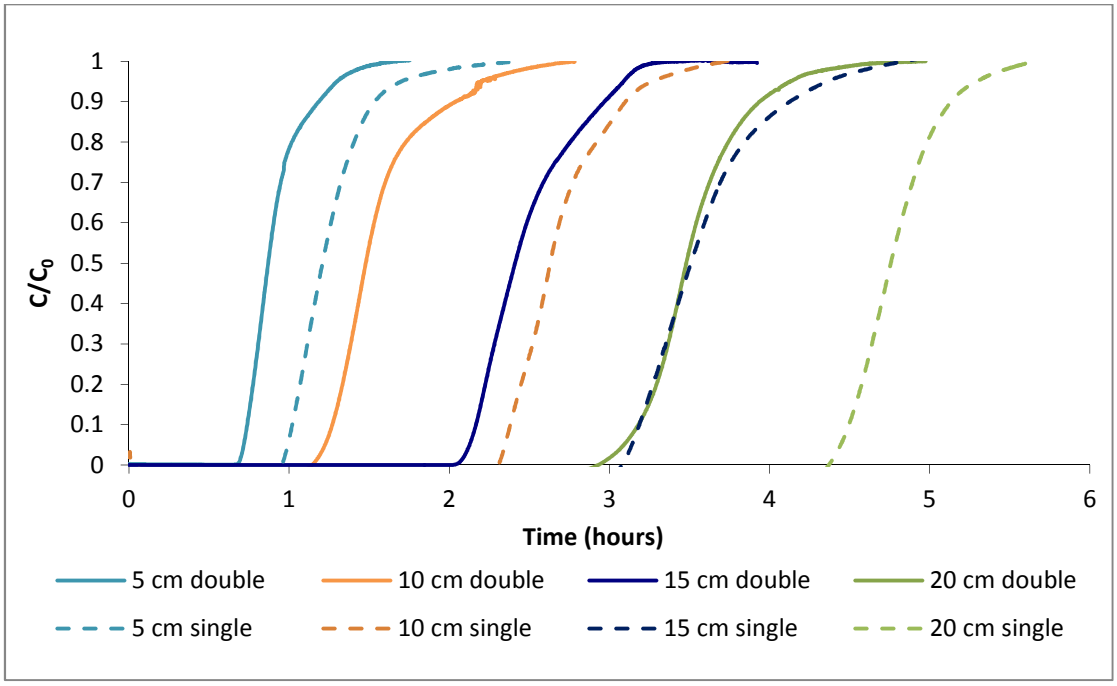

Figure 4.23. Breakthrough curves for 800 ppm 1 L/min ammonia challenge on single and double layer AbScents1000/NV5 hybrid fibres, showing double layer fibres with solid lines and single layer with dotted lines. The lengths are paired by colour.

Table 4.6. Dynamic breakthrough data for single and double layer 80% AbScents1000/NV5 hybrid fibres tested with 1 L/min 800 ppm ammonia.

Fibre	Weight (g)	t_b (h)	t_b loading (%)	t_{eq} (h)	t_{eq} loading (%)	t_s (h)	LUB (%)	MTZ (cm)
5 cm single	3.97	0.98	0.84%	1.10	1.05%	1.26	22.00%	5.86
10 cm single	8.65	2.34	0.91%	1.33	1.03%	2.69	13.30%	5.21
15 cm single	11.82	3.12	0.90%	1.94	1.01%	3.59	12.96%	7.13
20 cm single	16.04	4.43	0.94%	1.54	0.99%	4.80	7.72%	5.18
5 cm double	4.84	0.69	0.47%	1.11	0.61%	0.89	22.29%	6.02
10 cm double	8.47	1.21	0.48%	2.24	0.61%	1.56	22.35%	10.04
15 cm double	14.20	2.12	0.50%	2.22	0.58%	2.49	14.81%	7.91
20 cm double	18.57	3.04	0.55%	2.76	0.63%	3.53	13.79%	10.93

Single layer and double layer 80% NV5 fibres were dynamically challenged with 800 ppm ammonia at 1 L/min and the results are shown in Figure 4.24.

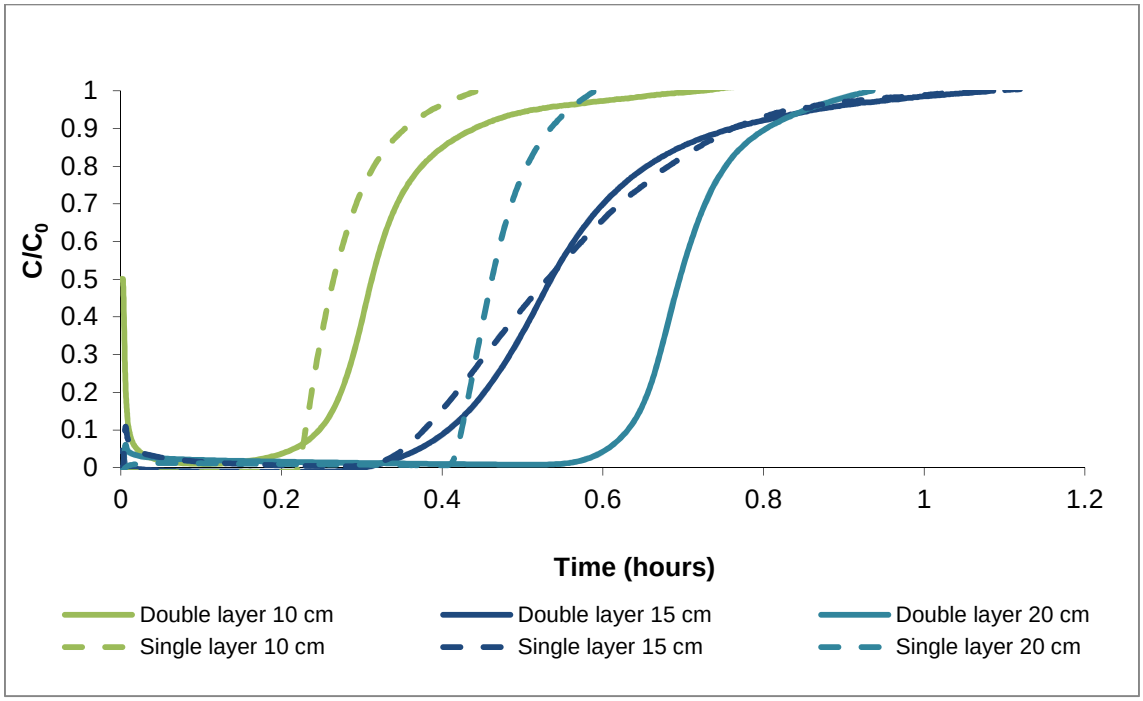

Figure 4.24. Breakthrough curves for 800 ppm 1 L/min ammonia challenge on single and double layer 80% NV5 hybrid fibres, showing double layer fibres with solid lines and single layer with dotted lines. The lengths are paired by colour.

As is apparent from Figure 4.24, all NV5 fibres had low breakthrough time. The times are very similar between single and double layer fibres except in the case of the 20 cm long fibres, with breakthrough occurring for double layer at 0.6 hours and for the single at 0.4 hours. The data in Table 4.7 shows low but fairly consistent breakthrough and equilibrium loading and long, unstable mass transfer zones at all lengths, demonstrating that NV5 is a poor adsorbent for ammonia. Despite the apparently large difference between the breakthrough times for single and double layer 20 cm fibres, the loading at breakthrough differs by only 0.04%.

Table 4.7. Dynamic breakthrough data for single and double layer 80% AbScents1000/NV5 hybrid fibres tested with 1 L/min 800 ppm ammonia.

Fibre	Weight (g)	t_b (h)	t_b loading (%)	t_{eq} (h)	t_{eq} loading (%)	t_s (h)	LUB (%)	MTZ (cm)
10 cm single	8.50	0.23	0.09%	0.44	0.11%	0.28	19.49%	7.85
15 cm single	11.57	0.34	0.10%	1.12	0.16%	0.56	38.51%	14.00
20 cm single	16.92	0.42	0.08%	0.59	0.09%	0.47	11.47%	5.58
10 cm double	7.86	0.19	0.08%	0.72	0.14%	0.33	4.22	42.21%
15 cm double	12.43	0.35	0.09%	1.09	0.15%	0.56	5.61	37.41%
20 cm double	16.77	0.59	0.12%	0.94	0.14%	0.70	2.41	16.07%

4.2.4 Testing fibres at different flow rates with cyclohexane

A range of flow rates, from 1-3 L/min, were tested for each type of fibre bundle with cyclohexane. Due to the high price of cyclohexane gas canisters and the low quantities available, some tests were only run to the breakthrough point. This was to ensure that the breakthrough time was found for all samples, at the cost of the complete breakthrough curve for some samples. As such, in some cases, a full comparison of equilibrium times, mass transfer zones and length of unused beds is not available. While this lack of information is unfortunate, the breakthrough time and loading are the most important pieces of information for single pass respirator applications. Figure 4.25 - Figure 4.27 show the breakthrough curves as cyclohexane flow rate was increased for the adsorbent hollow fibres, while Table 4.8 – Table 4.10 show the values associated with these curves.

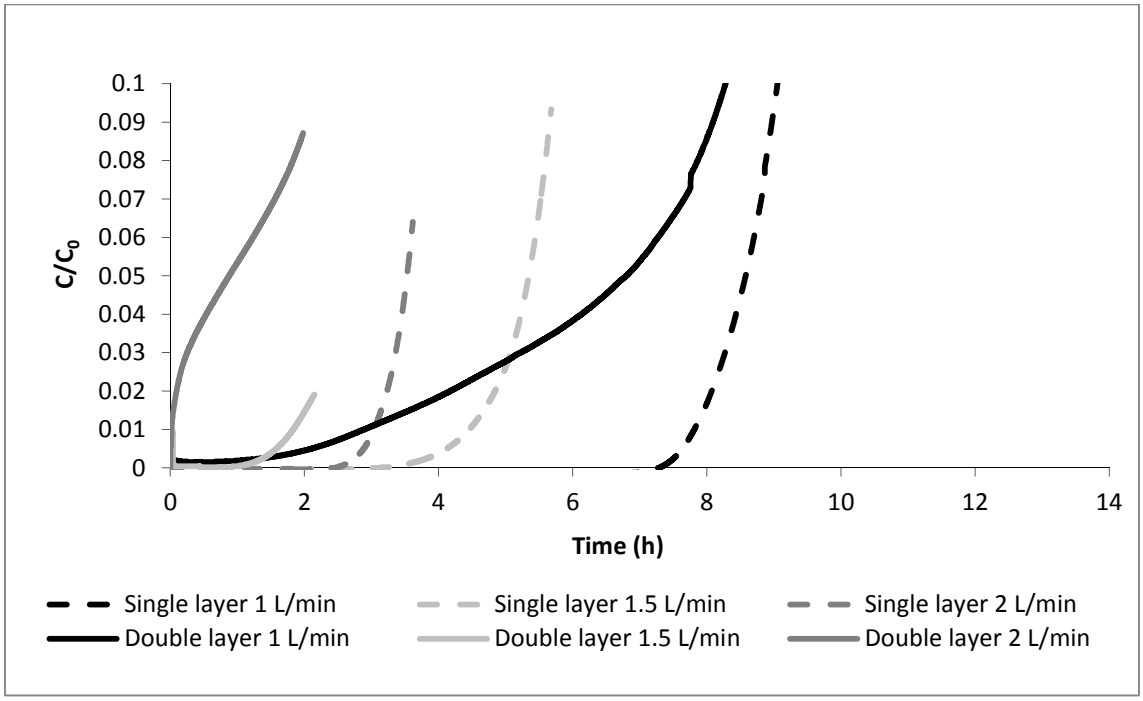

Figure 4.25. Breakthrough loading for 1000 ppm cyclohexane on 80% NV5 carbon 20% PES fibres, double and single layer, as flow rate was increased, shown for up to 100 ppm outlet concentration.

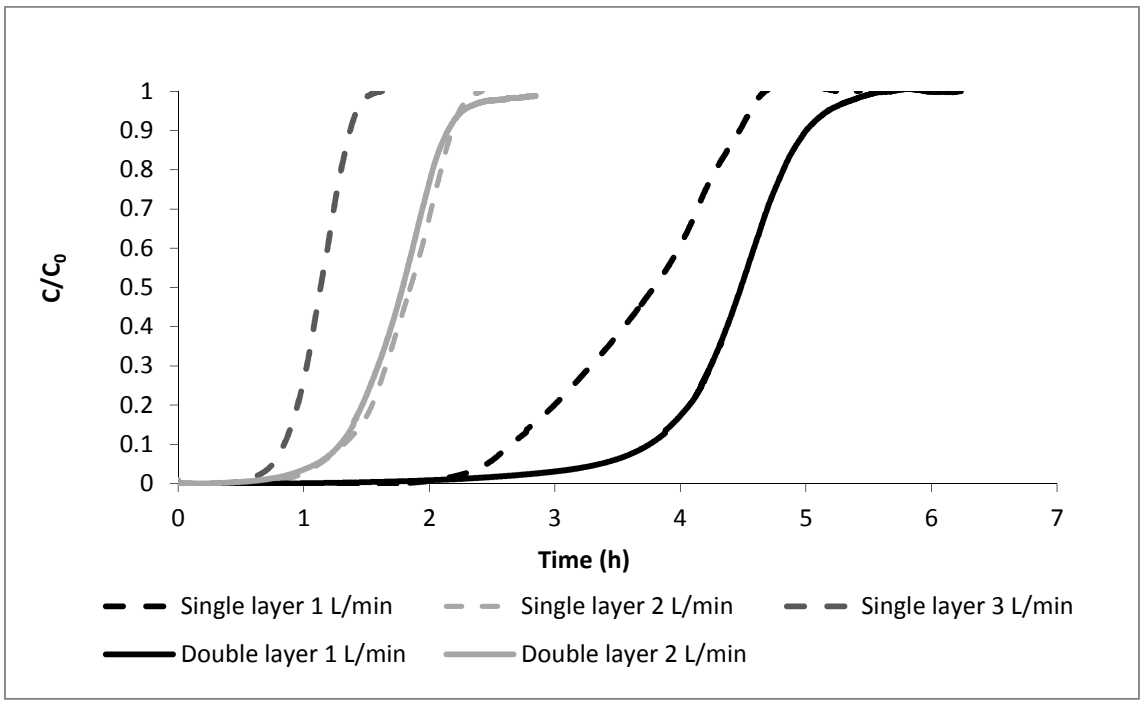

Figure 4.26. Breakthrough curves for 1000 ppm cyclohexane on 10 cm 80% AbScents1000 20% PES fibres, double and single layer, as flow rate was increased. The double layer fibre at 3 L/min is not shown as this test broke through instantly.

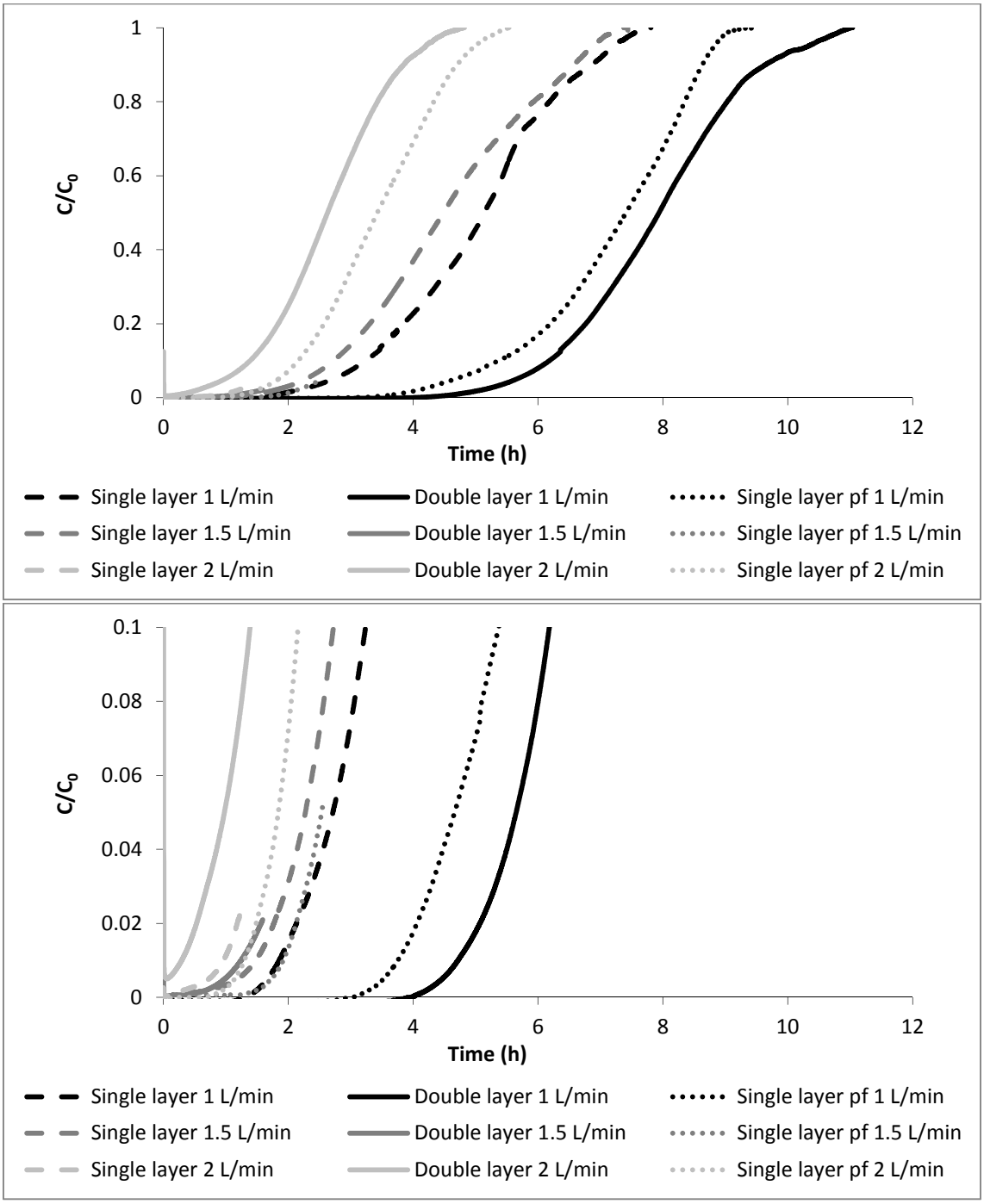

Figure 4.27. Top: breakthrough curves for 1000 ppm cyclohexane on 40% NV5 carbon 40% AbScents1000 20% PES fibres, double and single layer, as flow rate was increased. Bottom: The above graph shown up to 100 ppm outlet concentration.

Figure 4.25 shows the poor kinetics for cyclohexane adsorption on double layer NV5 carbon fibres compared to single layer fibres, with a gradual rise in concentration beyond the breakthrough point of 10 ppm ($C/C_0 = 0.01$) significantly before the equivalent single layer fibres. For AbScents1000 fibres, shown in Figure 4.26, at 1 L/min the double layer fibres had a sharper breakthrough curve and longer breakthrough time than the single layer but at a flow rate of 2 L/min, both fibres had very similar breakthrough curves,

while at 3 L/min, the double layer fibres broke through instantly while the single layer fibres did not. It should also be noted that in all cases, the single layer fibres had lower adsorbent weight than the double layer, meaning that in each case the single layer fibres had superior breakthrough loading (shown in Table 4.8). For the hybrid fibres (Figure 4.27), at 1 L/min the double layer fibres significantly outperformed the single layer fibres, with breakthrough times of 4.72 and 1.86 hours respectively. However, similar to the results for the AbScents1000 fibres, as flow rate increased to 1.5 L/min, the single and double layer fibres were approximately equal in breakthrough time, and at 2 L/min, the single layer fibre outperformed the double layer. In all cases, the single layer hybrid fibres with 1% SP pore former gave a higher breakthrough time than the single layer fibre without pore former.

Table 4.8. Dynamic breakthrough data for single and double layer 80% NV5 fibres tested with 1 L/min 1000 ppm cyclohexane. S indicates single layer fibres, D indicates double layer fibres.

S or D	Flow rate (L/min)	Weight (g)	t_b (h)	t_b loading (%)	t_{eq} (h)	t_{eq} loading (%)	t_s (h)	LUB (%)	MTZ (cm)
S	1	8.82	7.76	18.08%	12.59	24.38%	10.48	25.98%	2.30
	1.5	8.00	4.46	17.12%					
	2	8.48	3.04	14.67%					
D	1	7.16	2.88	8.23%	13.28	30.00%	10.47	72.46%	4.96
	1.5	10.86	1.83	5.18%					
	2	7.78	0.02	0.10%					

Table 4.9. Dynamic breakthrough data for single and double layer 80% AbScents1000 fibres tested with 1 L/min 1000 ppm cyclohexane. S indicates single layer fibres, D indicates double layer fibres.

S or D	Flow rate (L/min)	Weight (g)	t_b (h)	t_b loading (%)	t_{eq} (h)	t_{eq} loading (%)	t_s (h)	LUB (%)	MTZ (cm)
S	1	8.83	2.07	4.82%	5.36	8.48%	3.65	43.24%	4.51
	2	9.12	0.83	3.71%	2.42	8.09%	1.80	53.95%	8.87
	3	8.00	0.55	4.22%	1.63	8.61%	1.12	50.87%	9.60
D	1	10.53	2.11	4.11%	6.22	8.54%	4.39	51.82%	4.68
	1.5	10.56	1.56	4.53%					
	2	10.19	0.68	2.73%	2.85	7.06%	1.75	61.18%	12.38

Table 4.10. Dynamic breakthrough data for single and double layer 80% AbScents1000/NV5 hybrid fibres tested with 1 L/min 1000 ppm cyclohexane. S indicates single layer fibres, D indicates double layer fibres.

S or D	Flow rate (L/min)	Weight (g)	t_b (h)	t_b loading (%)	t_{eq} (h)	t_{eq} loading (%)	t_s (h)	LUB (%)	MTZ (cm)
S	1	6.83	1.86	6.23%	7.81	15.12%	5.03	63.09%	11.82
	1.5	10.17	1.49	4.48%					
	2	9.19	0.96	4.28%					
D	1	9.94	4.72	9.74%	1.62	16.32%	7.91	40.36%	3.99
	1.5	9.76	1.24	3.89%					
	2	8.42	0.29	1.41%	1.07	12.76%	2.62	88.86%	17.30

NV5 and hybrid fibres showed a decrease in breakthrough loading as the flow rates increased. However, the AbScents1000 fibres did not show any clear pattern in breakthrough loading as the flow rate increased. Looking at breakthrough time corrected for weight, a slightly clearer pattern can be observed, although the reason for this discrepancy is uncertain. For the NV5 fibres, single layer were greatly superior to double layer in terms of breakthrough time. Single layer fibres at 1 L/min had 18%wt breakthrough loading compared to 8%wt on double layers. There was also a sharper downwards trend for the double layer fibres, dropping from 8%wt loading to 0.1%wt at 2

L/min, compared to 18%wt to 15%wt for the single layer fibres. This same trend was observed on the hybrid fibres. At 1 L/min the double layer hybrid fibre had higher breakthrough loading than single layer fibres with and without added pore former. At 1.5 L/min, it had slightly lower breakthrough loading than both single layer fibres. At 2 L/min, it was even further apart, with 5.8%wt on single layer with pore former, 4.3%wt on single layer without pore former and 1.4%wt on the double layer fibres. It should be noted that, as expected, though the breakthrough loading values decreased as flow rate increased, the equilibrium loading changed very little at different flow rates. For example the cyclohexane loadings for AbScents1000 single layer fibres at 1, 2 and 3 L/min were 8.5, 8.1 and 8.6%wt.

The higher breakthrough loadings on single layer fibres confirm these results for ammonia seen previously (Section 4.2.3). The decrease in breakthrough loading as flow rate increased was most likely as a result of the higher superficial velocity through the fibres. More single layer fibres were packed into a bundle than double layer, meaning that more surface area was available and hence the superficial velocity was lower for single layer fibres as flow rate increased than for double layer fibres. As can be observed in Figure 4.28, the difference becomes greater as flow rate increases (i.e. the two lines are not parallel), meaning a more pronounced drop in breakthrough loading is observed as flow rate increases for double layer fibres than single layer.

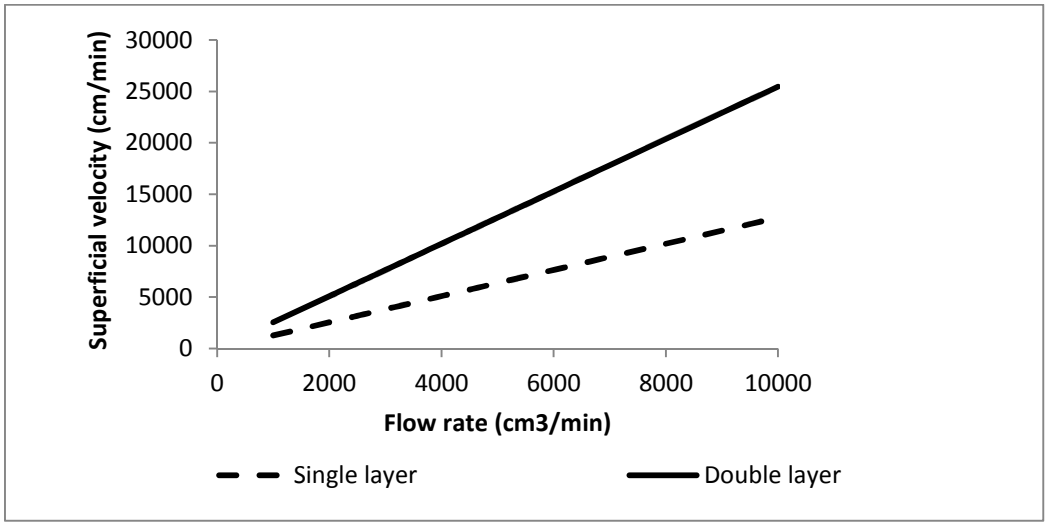

Figure 4.28. Superficial velocity in 2 cm diameter circular hollow fibre beds, assuming 100 single layer fibres or 50 double layer fibres in a bundle, with 1 mm bore diameter.

The decrease in breakthrough loading as flow rate increased was most likely as a result of entrance effects, particularly as the modules tested were only 10 cm long. A 2 cm x 10 cm module has a volume of 31.4 cm^3, meaning a flow rate of 2 L/min will pass through this very quickly, and most likely without the opportunity for flow to fully develop, as observed in the ΔP/L calculations, shown in Section 4.2.2.4. This was also reflected in the length of mass transfer zone. This should be unaffected by velocity, as velocity is not used in its calculation. For single layer AbScents fibres, the length of mass transfer zone increased as flow rate increased from 4.5 cm, at 1 L/min, to 9.6 cm at 2 L/min. For double layer hybrid fibres, LMTZ was 4.0 at 1 L/min and 17.3 cm at 2 L/min. For double layer AbScents fibres, LMTZ increased from 4.7 cm to 12.4 cm as flow rate increased from 1 to 2 L/min. The MTZ in some cases was longer than the length of the bed. It was not possible to predict the flow rate at which instant breakthrough would occur using Figure 4.25 - Figure 4.27 as the relationship between breakthrough loading % and flow rate is not linear.

4.2.5 Adsorption performance of adsorbent hollow fibres compared to granular beds

This Chapter has demonstrated that adsorbent hollow fibres have favourable pressure drop compared to an equivalent volume granular bed. However, an empty cartridge would have even lower pressure drop than a fibre bed (albeit providing no protection). In order to be suitable for use in respirator cartridges, adsorbent hollow fibres must show good adsorption characteristics that are comparable with a granular bed.

First, AbScents1000 pellets were prepared with the same adsorbent composition as the fibres (80% adsorbent) by the method described in Section 3.2.2. These were tested as 5 cm long modules, which were dynamically challenged with 800 ppm ammonia at 1 L/min. The results are shown in Figure 4.29 and Figure 4.30, with data calculated from the graphs in Table 4.11.

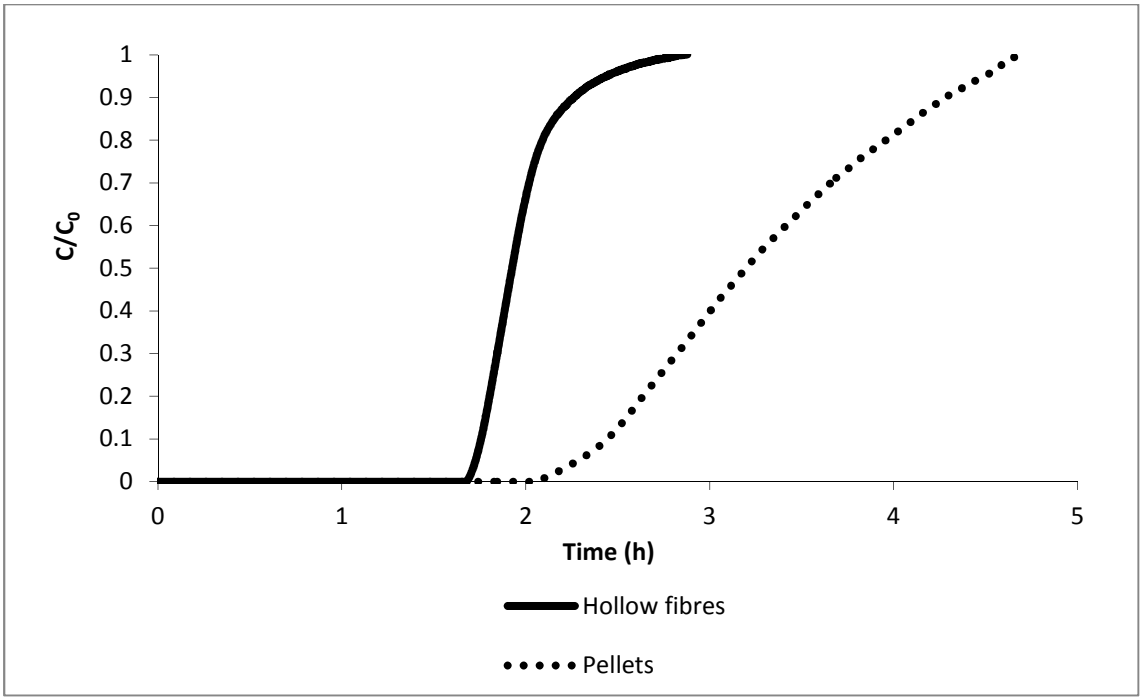

Figure 4.29. Breakthrough curves of 5x2 cm adsorbent 80% AbScents1000 hollow fibre and granular bed module challenged with 800 ppm 1 L/min NH_3.

Table 4.11. Breakthrough and equilibrium time and loadings for 5x2 cm adsorbent hollow fibre and granular bed modules challenged with 800 ppm 1 L/min NH_3.

	Hollow fibre module	*Pellet module*
Adsorbent weight (g)	4.79	8.86
Breakthrough time (h)	1.72	2.45
Breakthrough loading (% wt)	1.21	0.93
Equilibrium time (h)	2.88	5.12
Equilibrium loading (% wt)	1.37	1.24
Mass transfer zone (cm)	2.91	4.00
Length of unused bed (cm)	0.65	1.32

Figure 4.29 shows that the fibre module had a far sharper breakthrough curve than the pellet module. This translated to a shorter mass transfer zone and length of unused bed of the adsorbent hollow fibres, displayed in Table 4.11. This indicates more efficient use was made of the adsorbent hollow fibre module, with a shorter adsorption front traveling through the fibre. Meanwhile the AbScents 1000 pellets took longer to reach equilibrium, displaying a longer mass transfer zone and greater proportion of the adsorbent left unused. For the pellet module, the 1.63 cm length of unused bed constitutes over a quarter

of the length of the module, compared to 0.65 cm for the fibre module. As has been discussed previously and is shown in Table 4.11, fibres have a higher voidage and so a lower density than an equivalent volume granular bed. Therefore, in order to standardise by weight, C/C_0 was plotted against time/weight (in hours/gram), and this is shown in Figure 4.30.

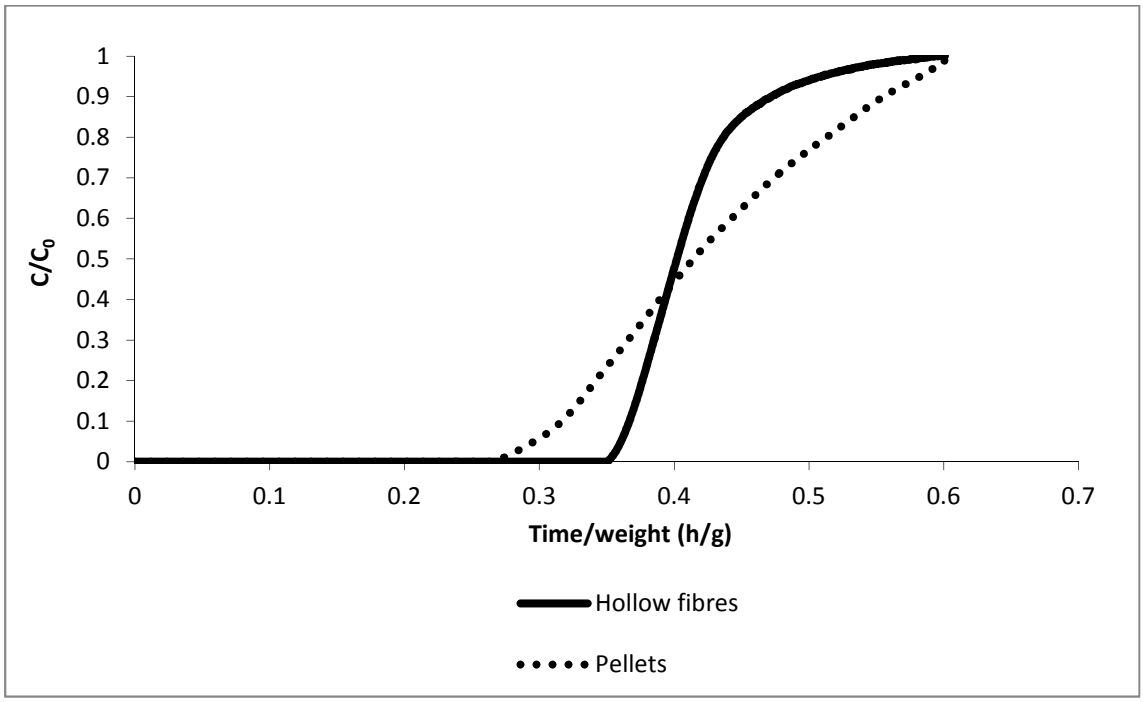

Figure 4.30. Breakthrough time/weight curves of 5x2 cm single layer 80% AbScents1000 hollow fibre and 80% AbScents1000 granular bed module challenged with 800 ppm 1 L/min NH_3.

In this case, the adsorbent hollow fibres were seen to have greater breakthrough time per unit weight than the equivalent volume of pellets, although lower equilibrium loading (0.07 g ammonia in fibres, 0.11 g in the granular bed). Due to their low density, it can be concluded that adsorbent hollow fibres present a favourable alternative to pellets when weight is a limiting factor, but a less favourable option when volume is more limited. This is particularly the case because, as seen in Section 4.2.2.4, fibres suffer from entrance effects more severely than a granular bed. As such a certain bed length will be required to ensure fully developed flow in the adsorbent hollow fibres.

A 10 cm bed of hybrid 80% NV5/AbScents1000 pellets was also tested. This was prepared by the same methods as the AbScents1000 pellets, and tested against an

equivalent volume fibre. Ammonia and cyclohexane challenges were carried out and compared. The breakthrough curves obtained for ammonia challenges are shown in Figure 4.31 and Figure 4.32, and for cyclohexane challenges in Table 4.12.

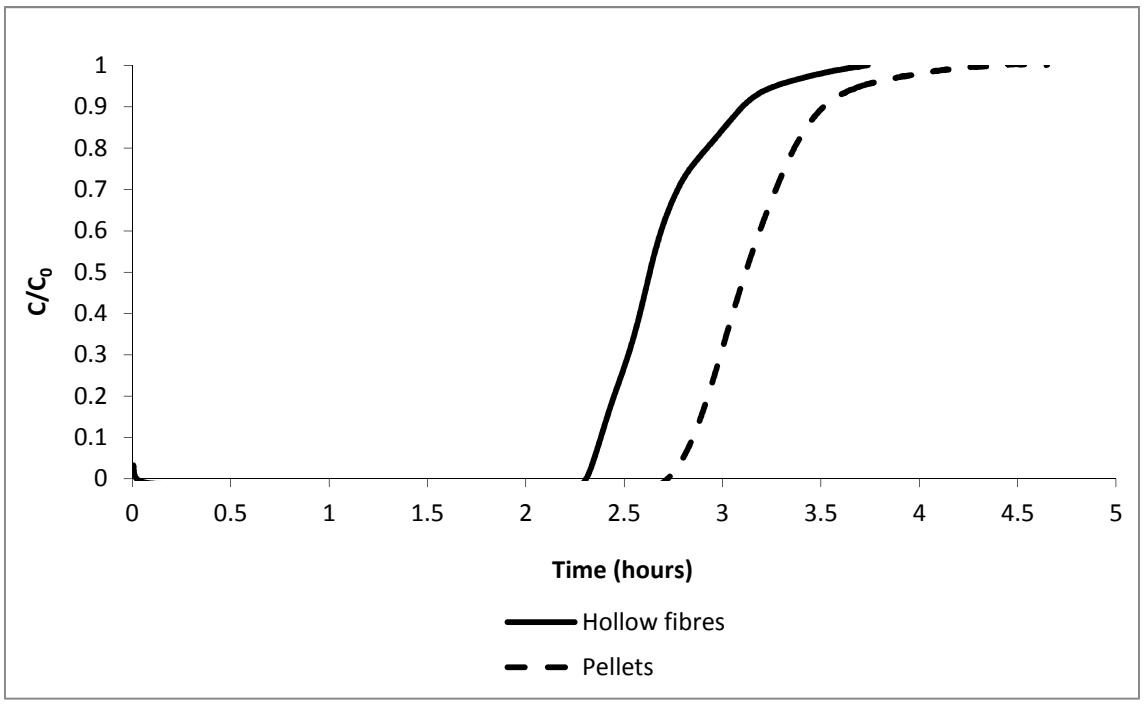

Figure 4.31. Breakthrough curves of 10x2 cm hybrid 80% NV5/AbScents1000 single layer adsorbent hollow fibre and granular bed module challenged with 800 ppm 1 L/min NH_3.

Similar to before, Figure 4.31 shows that fibres had a lower breakthrough time than an equivalent volume bed of pellets. However, if this is corrected for weight, it can be seen in Figure 4.32 that fibres had significantly greater breakthrough time/weight adsorbent than the granular bed.

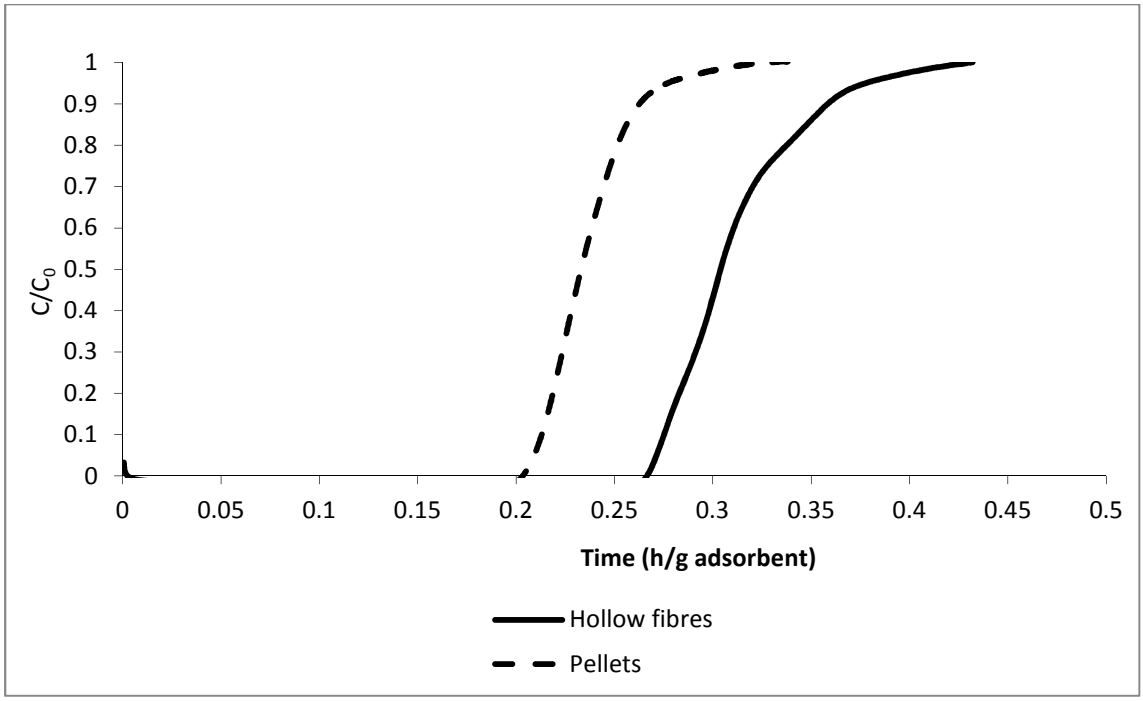

Figure 4.32. Breakthrough time/weight curves of 5x2 cm single layer 80% hybrid NV5/AbScents1000 hollow fibre and granular bed module challenged with 800 ppm 1 L/min NH_3, corrected for adsorbent weight.

However, in this case the mass transfer zone of the pellets is shorter than that of the fibres, with a 5.2 cm MTZ for hybrid hollow fibres compared to a 2.5 cm MTZ for the granular bed. This suggests that there may be some diffusion impedance due to the PES binder in the adsorbent hollow fibres compared to the clay in the pellets. Alternatively, this may be associated with the time required for development of the mass transfer zone in fibres, with entrance effects distorting the value for MTZ calculated. A 5.2 cm MTZ on a 10 cm bed can only be completed once, whereas the 2.5 cm MTZ on the pellet bed can repeat four times.

1000 ppm 1 L/min cyclohexane dynamic challenge was also carried out on the 10 cm hybrid fibre and pellet modules. As is clearly shown in Table 4.12, when challenged with 1000 ppm cyclohexane the adsorbent hollow fibres had significantly lower breakthrough time and breakthrough loading than the pellets. This contradicts the results observed when the fibres and pellets were challenged with ammonia, and suggests there may be fundamental differences in how the two contaminants were adsorbed.

Table 4.12. Breakthrough data after 1000 ppm 1 L/min cyclohexane challenge on 10 cm modules of hybrid fibres and hybrid pellets.

	Weight (g)	Breakthrough time (h)	Breakthrough loading (g)	Breakthrough loading (%)
Pellets 10 cm	13.10	12.54	2.57	19.66%
Hybrid fibres 10 cm double layer	9.94	4.72	0.97	9.74%
Hybrid fibres 10 cm single layer	6.83	1.86	0.43	6.23%

To determine why the fibres had greater breakthrough time per weight for ammonia than the granular beds, and why the reverse was the case for cyclohexane adsorption on the same fibres and pellets, scanning electron micrographs were taken for an AbScents 1000 pellet and hollow fibre. It is apparent in Figure 4.33 that the pellet had a relatively closed macrostructure. By contrast, the adsorbent hollow fibre had a very open macrostructure with smaller zeolite crystals held within, shown in Figure 4.34. These macrovoids and channels were present throughout the fibre structure and on the inner and outer walls, as can be seen in Figure 4.35. The macrovoids were formed as the fibres coagulated; the inner skin layers are highly porous due to the use of a mixture of NMP/water in the bore fluid, while the less porous outer skin is due to spinning into a water bath with no solvent. The macrovoidal structure of the adsorbent hollow fibres, seen in the low magnification image in Figure 4.34, suggests that they should exhibit rapid adsorption kinetics. This was observed for ammonia but not for cyclohexane.

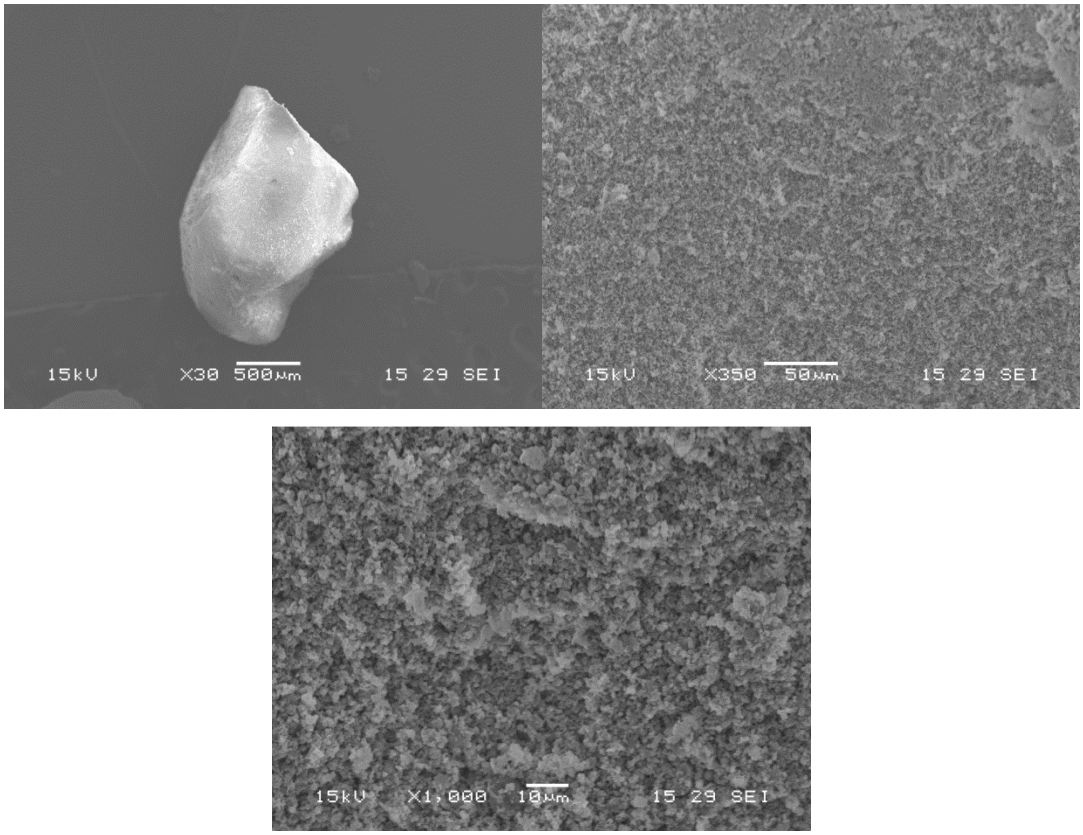

Figure 4.33. SEM images of the surface of a AbScents 1000 adsorbent pellet, x30 (top left) and x350 (top right) and x1000 (bottom).

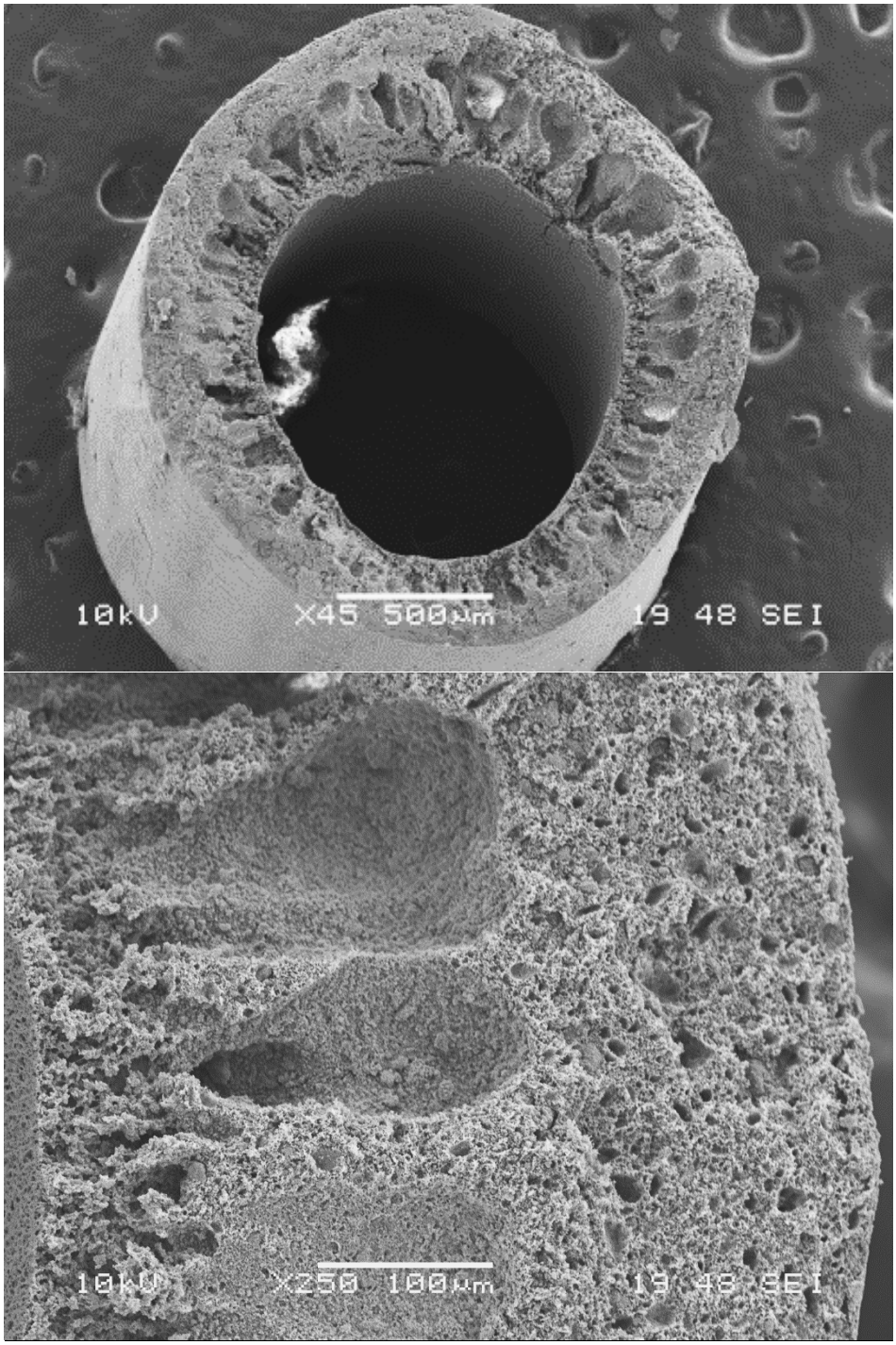

Figure 4.34. SEM images of adsorbent hollow fibre containing AbScents 1000– x45 cross section (top) and x250 cross section (bottom).

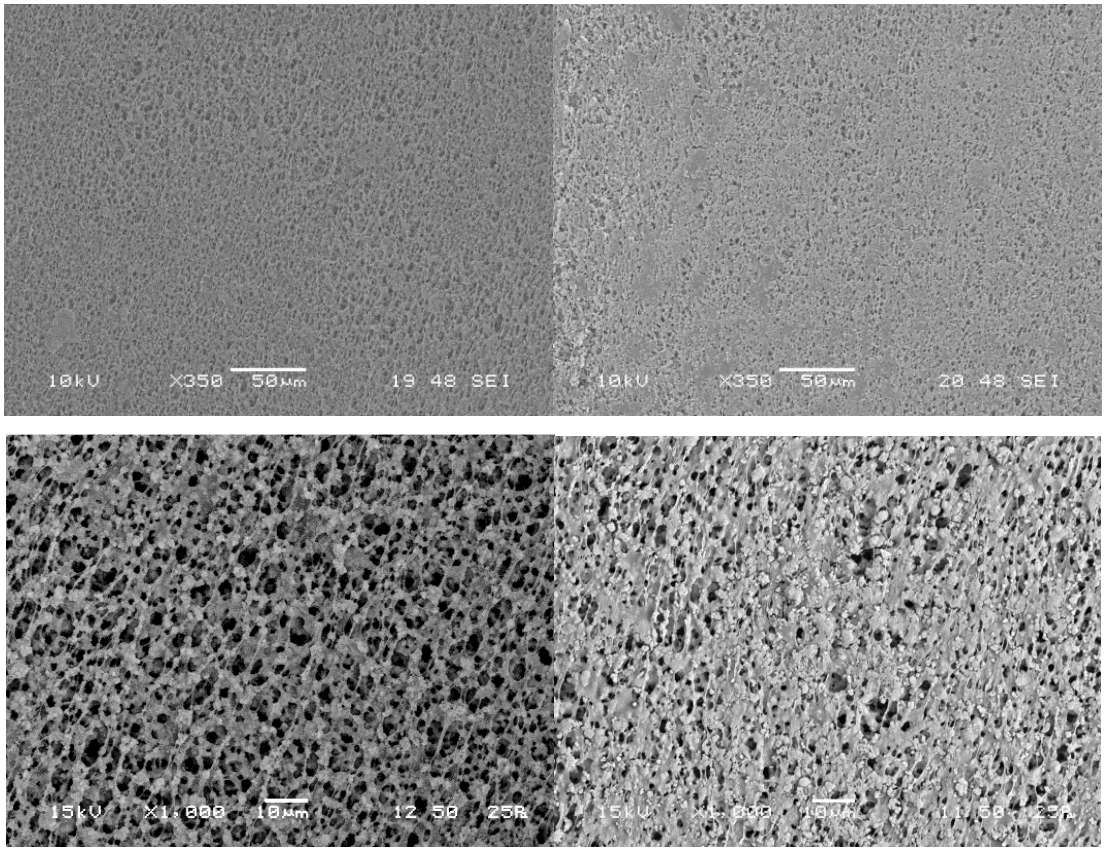

Figure 4.35. x350 and x1000 scanning electron micrographs of adsorbent hollow fibres containing AbScents 1000 – inner surface of fibre (upper and lower left) and outer wall of fibre (upper and lower right).

To investigate the poor performance of adsorbent hollow fibres with cyclohexane further, cyclohexane isotherms were measured for the pellets and fibres. Cyclohexane uptake of the components of AbScents and AbScents/NV5 hybrid pellets are shown in Figure 4.36.

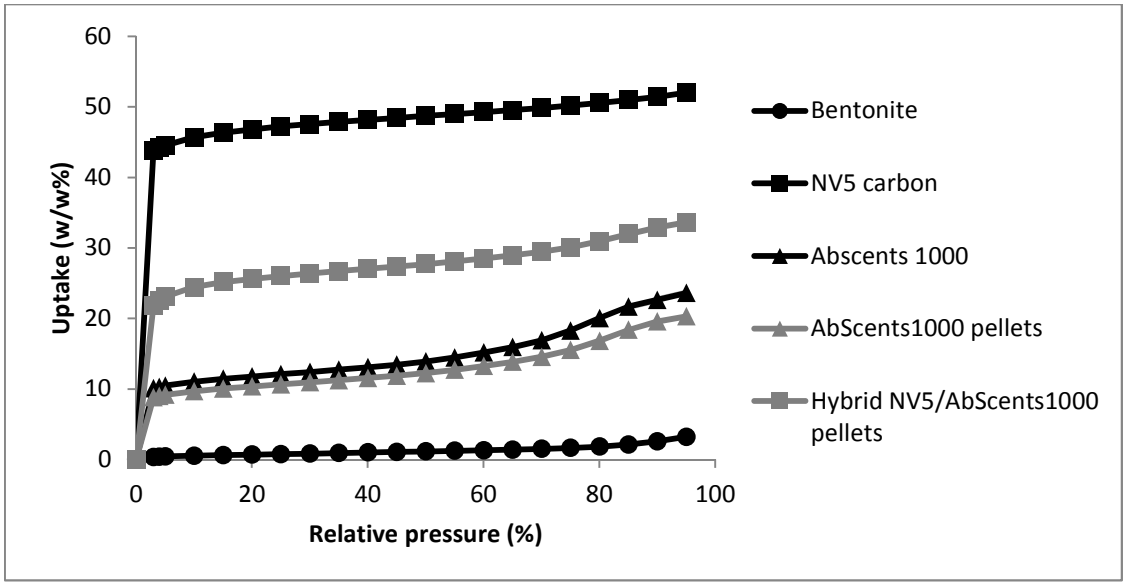

Figure 4.36. Cyclohexane uptake isotherms of bentonite, NV5 carbon and AbScents1000 powders compared to hybrid NV5/AbScents1000 and AbScents1000 only pellets (characterised at Dstl).

AbScents1000 pellets had very similar uptake to the AbScents1000 powder, while the hybrid pellets had uptake between that of the NV5 carbon and AbScents 1000 powder, as anticipated. Wyoming bentonite had negligible uptake of cyclohexane. A 'weighted average' cyclohexane isotherm was calculated for the pellets. This was done by taking a proportion of the isotherms for each component in the pellet. For example, for the hybrid pellet, 20% of the uptake values for bentonite would be added to 40% of the uptake values of AbScents1000 and 40% of the uptake values of NV5, to give the 'weighted average' isotherm. These are shown in Figure 4.37.

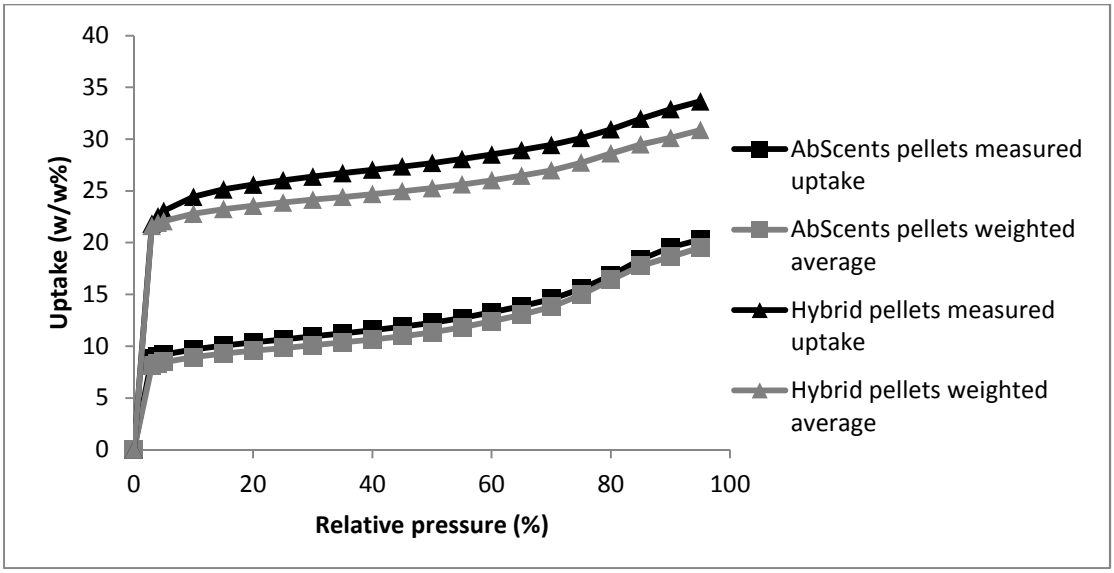

Figure 4.37. Cyclohexane uptake isotherms of 20% bentonite: 80% AbScents1000 pellets and on 20% bentonite 40% AbScents1000 and 40% NV5 carbon pellets, compared to weighted average uptake isotherms for their components (characterised at Dstl).

In both cases, there was good agreement between the weighted averages of the pellet and its constituents. The AbScents1000 pellets and powder overlapped, suggesting that there was no interference to adsorption as a result of the presence of bentonite binder. The hybrid pellets had slightly higher uptake than the weighted average of their components, but the difference was very small and most likely as a result of several small errors in the constituent data which are amplified due to the use of several sets of data points (i.e. bentonite and AbScents1000 and NV5 carbon). The initial point is very similar for the two, at 21.6%wt for the weighted average and 21.8%wt for the fibre, and, at highest relative pressure, only 3%wt uptake difference, at 33.6%wt for the fibre, and 30.9% for the weighted average.

The pellets were then compared to the fibres with the same adsorbents. The only differences between the pellets and fibres were the binder used; PES in the fibres and bentonite in the pellets; and the preparation temperature; heating to 190 °C with dry air flow for the fibres and sintering at 550 °C with CO_2 flow for the pellets. This is shown in Figure 4.38.

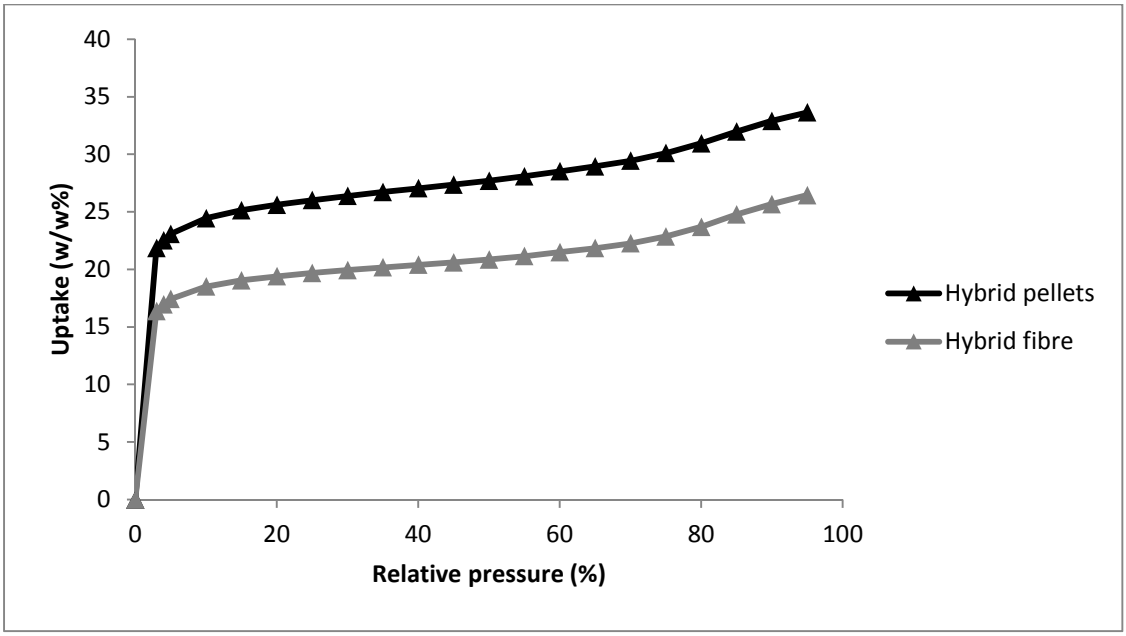

Figure 4.38. Cyclohexane uptake isotherms of 20% bentonite: 80% AbScents1000 pellets and on 20% bentonite 40% AbScents1000 and 40% NV5 carbon pellets, compared to their equivalent PES fibres (characterised at Dstl).

The hybrid fibre had lower uptake than the pellets at all points, up to 26%wt uptake on fibres and 33%wt on the pellets at 100% relative pressure. If the fibre uptake was compared to a weighted average of its components (which was very similar to the line for the pellets, as PES had the same low uptake as bentonite), it was below by several %wt. This is most likely as a result of the PES binder. While bentonite is a porous clay, PES is a nonporous polymer which, as is evident from the SEMs in earlier Sections, such as 3.3.1.2, covers up the adsorbent and thus reduces the potential equilibrium loading of the fibres. Obviously this is a disadvantage in a respirator application, where efficient use needs to be made of the available space.

4.3 Discussion

During this Chapter, NH_3, H_2S and cyclohexane adsorption was tested on a range of adsorbents to select candidate adsorbents to use in adsorbent hollow fibres for more detailed investigation. Low Si:Al ratio zeolites such as 13X had the highest and fastest uptake of NH_3 with moderate to poor uptake on the high Si:Al ratio zeolites. This was most likely due to the greater amount of cations in high Al zeolites, which attract polar molecules such as ammonia, as well as greater acidity in zeolites with lower Si:Al ratios, to which the basic ammonia is attracted (Shirazi *et al.*, 2008). However a problem with this is the rapid uptake of water, which is a polar molecule (van Bekkum, 2001). The poor

performance of materials after water uptake was observed, particularly in Section 3.3.1.1. Figure 3.9 showed very poor ammonia uptake on LiLSX after prehumidification to 35% RH. As a result, the optimum candidate adsorbents for ammonia that could operate reasonably across a range of humidity values were ZSM-5 and AbScents1000.

For hydrogen sulphide, poor uptake was seen on most adsorbents. While hydrogen sulphide is a polar molecule with two electron pairs, sulphur is far less electronegative than oxygen, making it not particularly polar. This means it will not compete strongly with water to adsorb on zeolites. H_2S is also weakly acidic, and so will not adsorb particularly well on acidic zeolites or carbons. Further, H_2S does not sorb well on carbons in dry conditions (Meeyoo *et al.*, 1998), which was also observed in these experiments. The highest sorption uptakes were seen on carbons impregnated with metal salts. This is because H_2S can chemisorb onto metal salts, reacting to form sulphides or elemental sulphur. In addition, activated carbon provides a large surface area for the metal salt to cover (Yang, 1997), thus improving the impregnant exposure to the H_2S. It is important to consider what the products of this may be however, as elemental sulphur formed in basic environments (caustic carbons) was found to fill micropores and block further adsorption (Bagreev *et al.*, 2005). Metal salt impregnation is used in the current respirator to provide protection from many different contaminants, and its use in adsorbent hollow fibres to enhance adsorption of H_2S will be explored more thoroughly in Chapter 5.

For cyclohexane, the highest adsorption uptake was seen on activated carbons, due to the high surface area provided for physisorption. However, the carbons did not necessarily have good adsorption kinetics; poor breakthrough loading was observed on Chemviron BPL carbon (0%wt) compared to high equilibrium loading (12.4%wt). This was due to the large size of the cyclohexane molecule. This size makes cyclohexane a useful simulant for bulky molecules containing a cyclic ring, which may not be adsorbed well by zeolites with small pores, such as 3A, with its ~ 3 Å opening compared to the ~ 5.7 Å kinetic diameter of cyclohexane.

Taking into account the screening results, AbScents1000 and NV5 carbon were selected for further testing and for use in preparation of a hybrid adsorbent that will take up ammonia and cyclohexane well. This provided a suitable candidate fibre for further testing throughout this Chapter, and modelling, in Chapter 7. The hybrid was anticipated

to provide reasonable adsorption across a range of humidity, given the tendency of carbon to sorb well at higher humidity while zeolites can sorb well at lower humidity (Meeyoo *et al.*, 1998). Obviously these sorbents do not provide the best overall adsorption, and only a handful of readily available sorbents were tested. These are merely intended to provide a candidate fibre and enable the investigation of adsorption of a limited number of model TICs on adsorbent hollow fibres. Future work could expand on the range of adsorbents tested for further optimisation in this regard.

As fibres can be prepared to different size specifications, fibre structures were also investigated in this Chapter. At present, adsorbent fibres are not currently commonly used as such, making comparison of the results found in this report with results from literature difficult. However, superficially at least, the shape of an adsorbent hollow fibre module resembles a honeycomb monolith structure, in that it is a parallel passage adsorbent contactor, or a group of channels through which contaminated gas passes from inlet to outlet. As such comparisons were made with literature values for this type of monolith.

Fibre modules with 1 mm bores and the monolith modules with 1.2 mm bores were found to have lower pressure drop than the 1 mm particle size granular beds, due to their higher voidage and hence lower density. The larger the bore of the fibre, the lower the pressure drop, due to the lower superficial velocity and residence time through the structure. However, the 0.8 mm bore fibres were found to have greater pressure drop from 0.5-5 L/min flow rate. Similar results were found by Águeda *et al.*, (2011), who calculated a large theoretical decrease in pressure drop as channel size was increased. Águeda *et al.*, also predicted improved mass transfer characteristics in monoliths with smaller channels, though with the downside of higher pressure drop and also of a higher cost in producing monoliths with smaller channels. This cost issue does not exist for adsorbent hollow fibres and it is possible to produce fibres with very small bore diameters, though obviously with accordingly higher pressure drop. Another group, An *et al.*, (2013), found that breakthrough time was improved by increasing the number of channels, increasing the channel size and decreasing the sample diameter. They also determined that these three factors had a combined effect. For this report, only the effect of increasing the number of channels was tested, in the form of double vs single layer fibres. Their discovery that increasing channel size improved breakthrough time contradicted the result of Blanco *et al.*, (2000), although, for the reasons above, this is most likely due to the

overriding effect of increasing the number of channels and decreasing the wall thickness, that Blanco *et al*. did not take into account. Also, it should be noted that An *et al.*, tested activated carbon fibre–phenolic resin composites with honey comb structure, which had far smaller channels (0.051 mm to 0.10 mm) than Blanco *et al*., (1.3 to 2.6 mm), and that Águeda's channel sizes are more in line with the fibre diameters. Overall, An *et al*. concluded that the best monolith structures for adsorption of CO_2 had high voidage and thin walls, hence the improvement with increasing channel number and size (thus increasing voidage). The cyclohexane uptake results in this Chapter (Section 4.2.2.2) agree with the uptake advantages of thin walls. As a result of this, standard bore fibres were selected to produce candidate fibres for more thorough testing because, while small bore fibres may have improved mass transfer properties, the pressure drop in small bore fibres was roughly the same as that in a granular bed of 0.8 mm granules.

Single layer fibres had lower pressure drop than double layer fibres with equivalent bore size. This is in line with the work of An *et al.,* (2013), as in single layer fibres voidage is higher and density is lower. In addition, gas velocity is lower and residence time higher, as there are more channels for gas flow. However, higher pressure drops than predicted were observed in 5 to 15 cm long adsorbent hollow fibres at all flow rates. This is most likely due to entrance effects or wall effects as a result of the aspect (or length to diameter L/D) ratio. It is commonly accepted that when L/D ratio for a granular bed exceeds 30-40, wall effects may be neglected (Ren *et al.,* 2005). However, in the case of adsorbent hollow fibres, the aspect ratios of 5, 10, 15, 20 and 25 cm long fibre modules with 2 cm diameter respectively are 2.5, 5, 7.5, 10 and 12.5, all of which are below the value of 30. While this applies to granular beds, it is uncertain how this would apply to adsorbent hollow fibre modules and could be an interesting subject for further investigation, particularly in comparison to granular beds. This may be a problem in respirator design, and suggests that a 2 cm diameter module would not be ideal unless it was at least 20 cm in length, which would be difficult to incorporate into a face mask. Alternatively a gas distributor could be incorporated at the inlet of the adsorbent hollow fibre cartridge, although these have an associated pressure drop. They are not typically used with granular beds as the tortuous structure acts as a distributor. However, it should be noted that the external dimensions of an S10 gas mask cartridge (i.e. measured on the outside of the cartridge) are length 5.5cm by diameter 11.5 cm, giving an aspect ratio of 0.48, which is very low. As such, eliminating wall effects may not be necessary for a gas mask,

though the potential of achieving this with fibres due to their low pressure drop presents an interesting opportunity, which will be further explored in Chapter 7. Also, obviously, custom masks and storage would need to be developed for novel fibre cartridges with distributors.

The results of An *et al*. also suggest that single layer fibres should be superior to double layer fibres for adsorption of CO_2, given their thinner walls and higher voidage. Whether this will apply to other gases is unclear, as such double layer fibres were dynamically tested alongside single layers. Breakthrough testing was performed so that the adsorption performance of two different voidage fibres could be compared. These results show that for adsorption of ammonia, AbScents1000 and hybrid AbScents1000/NV5 carbon single layer fibres consistently had higher breakthrough times and loadings, and shorter MTZs than their equivalent double layer fibres. In contrast, when flow rates were increased for cyclohexane dynamic challenge of double and single layer fibres, the single layer fibres were not better than the double layer fibres. A clear trend could be seen from low to high flow rates, with single layer fibres superior to double as flow rate increased due to the lower superficial velocity and greater residence time through the greater number of bores. However, double layer hybrid fibres had higher breakthrough loading than single layer with and without pore former at 1 L/min, the lowest flow rate, with 9.74%wt uptake on double layer and 6.23%wt on single layer. As this was only seen for one result, it is possible that it may be anomalous, or due to the low weight of that particular single layer hybrid fibre module (6.83 g compared to 8-10 g for the other single layer hybrid fibres). These results contrast with results from a paper by Blanco *et al.*, (2000), who found that by decreasing the diameter of square monolith channels from 2.6 to 1.3 mm they could use shorter monolith lengths to achieve adsorption, as molecules could reach the adsorbent walls more rapidly. However, they used square monoliths with square channels, and in changing the size of the channels, they also changed the size of the walls, resulting in a monolith of 5 x 5 bores with 2.6 mm compared to 11 x 11 bores of 1.3 mm. This is not directly comparable with fibres, as it would be like comparing double layer standard bore fibres with single layer small bore fibres, (two variables have been changed), and demonstrates a potential advantage of fibres over monoliths in this regard.

In all cases where they could be calculated, MTZ and LUB increased as flow rate increased. This is expected, as increasing gas velocity will lengthen MTZ and increase the

speed at which it travels (Schweitzer, 1997). The increase in MTZ velocity was also observed to be the case, one example being an increase from 0.02 cm/min, for 1 L/min flow rate, to 0.15 cm/min, for 3 L/min gas flow rate, for single layer AbScents1000 fibres, a 7.5 times increase for a 3 x flow rate increase. This expected change in LMTZ makes it difficult to determine whether there were entrance effects as a result of the increasing flow rate in a 10 cm long bed, though given the pressure drop results, this is most likely the case.

The adsorption performance of hollow fibres modules was compared with granular beds of pellets. These were made of the same adsorbent in the same composition as the fibres, apart from the PES polymer, which was replaced by Wyoming bentonite. For ammonia adsorption, pellets had greater breakthrough times than fibres, but when corrected for weight, the fibres showed better breakthrough performance, with shorter MTZ and LUB than an equivalent volume pellet bed, (2.91 cm MTZ length on fibres compared to 4.00 cm MTZ length on granular beds, 5 cm overall length). There were also roughly equal equilibrium loadings between granular beds and fibres, of 1.37%wt on fibres and 1.24%wt on granular beds. However, for cyclohexane adsorption, the pellets significantly outperformed the fibres in terms of breakthrough time and loading (a full test could not be completed, so hybrid pellet MTZ, LUB and equilibrium loading were unknown, although the breakthrough loading for the pellets was higher than the equilibrium loading of either double or single layer hybrid fibres). The principle difference between pellets and fibres was the binder, however the isotherms showed that there was no major difference between cyclohexane loadings on the PES and bentonite. The fact that the fibres had lower cyclohexane loading than the sum of their parts suggests that the PES polymer may be blocking access to some of the adsorbent, slightly lowering the cyclohexane equilibrium uptake of the fibres compared to the pellets. By comparison, ammonia equilibrium loadings were the same for pellets and fibres. This would suggest poor interconnectivity in the polymer matrix, or pores in the hollow fibre PES structure that the cyclohexane molecule in particular could not easily access, that it could in the bentonite.

SEM images indicated that the adsorbent hollow fibres were more macroporous structures than the pellets. While this would suggest fibres have a better structure, cyclohexane isotherms indicated that the weight uptake of pellets matched one calculated from their constituent parts, while the weight uptake of fibres was lower than predicted, with 26%wt

uptake on fibres and 33%wt at the highest relative pressure, when the two should be approximately identical. This is most likely as a result of the PES binder. While a macroporous structure allows rapid access to the adsorbent, some PES covers adsorbent and does not allow gas to diffuse into the structure, blocking access to some of the adsorbent structure. This is particularly likely to be associated with the thick skin at the external surface of the hollow fibres due to instantaneous liquid-liquid demixing, observed in SEMs. The spongy structure with few macrovoids is as a result of slow coagulation (Xu and Alsalhy Qusay, 2004), which was unexpected given the use of a pure water coagulation bath. It is likely that the additional presence of adsorbent in the hollow fibre structure slows the coagulation, as the adsorbent will take up some water itself. In addition, the lack of an air gap is most likely to have resulted in smaller external pores (Liu *et al.*, 2003). In addition, high shear rates may have increased the density of the external skin (Chung *et al.*, 2000). The bentonite, a porous clay, is far simpler to understand as it is not affected by the many spinning parameters. Bentonite pellets have a less macroporous structure than the adsorbent hollow fibres, slowing access to the adsorbent, but as it is porous it eventually allows all the contaminant into the structure, resulting in the higher %wt uptake seen in isotherms. This is obviously a disadvantage for fibres, as optimal use is not being made of the volume available, and ways to improve this are investigated in Chapter 6.

4.4 Conclusions

Following dynamic tests on a range of adsorbents with three candidate TICs (NH_3, H_2S and cyclohexane), AbScents1000 and NV5 carbon were selected as suitable adsorbents to be studied further. This selection helps to minimise issues associated with relative humidity and its effect on adsorption and to maximise capacity for each contaminant.

Fibre structure was considered:

- Cyclohexane uptake tests showed the fastest uptake of cyclohexane was on single layer fibres except in one case (hybrid AbScents1000/NV5 fibres at the lowest flow rate, 1 L/min).
- Ammonia adsorption was faster, with higher breakthrough time and loading and shorter MTZ, on single layer fibres.

- Pressure drop testing demonstrated that 1 mm bore fibres had significantly lower pressure drop than 0.8 mm bore fibres and granular beds.

Fibres were compared to pellets with the same adsorbent content:

- After breakthrough challenge, fibre modules had lower breakthrough loading by volume but higher breakthrough loading by weight.
- Cyclohexane isotherms of the equivalent AbScents1000 pellets matched predicted pellet isotherms, while fibres had slightly lower uptake values than would be expected. This suggests that the PES binder interferes with maximum cyclohexane loading in the fibres.

5 Modifications to adsorbent hollow fibres to enhance performance

5.1 Introduction

In the previous Chapter, adsorbent hollow fibres were shown to have a lower pressure drop than granular beds and similar adsorption %wt loading in most cases but with poor adsorption of H_2S. In general, adsorbent hollow fibres had lower breakthrough times than granular beds of equivalent volume, albeit due to their lower density and as such lower amount of adsorbent. Modifications were therefore considered that could enhance the adsorbent hollow fibre adsorption capability. UK S10 respirator cartridges contain activated carbon granules impregnated with copper, among other metal salts, to provide protection from a range of potential contaminants. As such, this Chapter investigates techniques for impregnating adsorbent hollow fibres with metals. This had a particular focus on removal of H_2S, as this was not adsorbed well by AbScents1000 or NV5 carbon.

As well as modifying fibres using impregnants, pore forming substances can be used to form additional pores of a specific size in various materials and enhance adsorption kinetics for some contaminants. This Chapter also includes an investigation of the incorporation of pore formers into adsorbent hollow fibres and their effects on adsorption.

5.1.1 Metal salts

In the previous Section, the highest uptake of H_2S, 1.6%wt breakthrough loading, was seen on carbons impregnated with metal salts. Many carbon granular beds are impregnated with metal salts to enhance their adsorption of gases not typically sorbed by carbon. These gases include a range of toxic industrial chemicals such as NH_3 (Bandosz and Petit, 2009), H_2S (Bagreev *et al.*, 2000), SO_2 and HCN (Smith *et al.*, 2010). Metal salt impregnation is a widely studied field, which has been explored in depth in the literature review.

Several options for applying metal salts to adsorbent hollow fibres were explored:

- Impregnation of adsorbent with metal salt, (such as a commercially purchased impregnated carbon) and then preparing fibres from the impregnated adsorbent.

- Incorporation of metal salts into the fibre structure by mixing them into the fibre precursor mixture.
- Impregnation of the preformed fibres with metal salt.

Metal salt treated adsorbent hollow fibres were prepared by the three techniques described above. Their adsorption properties were tested by dynamic H_2S breakthrough studies and the fibres and metal salts associated with them were characterised by scanning electron microscopy and elemental analysis.

5.1.2 Metal organic frameworks

As well as modifying fibres with metal salts, the possibility of using novel adsorbents, such as metal organic frameworks, was also investigated. Some metal organic frameworks (MOFs) are reported to have great potential as adsorbents and as impregnants due to their high surface area and active metal sites (Peterson *et al*., 2009). However, consistent synthesis of MOFs is difficult, and buying them can be very expensive, particularly for use in one-shot applications, such as respirators. In addition, there are drawbacks associated with their stability, particularly on exposure to water (Gul-E-Noor *et al.*, 2011; Greathouse and Allendorf, 2006; Li and Yang, 2007).

A commonly used and simple to synthesise MOF, copper benzenetricarboxylate, CuBTC, was selected as a pilot. Obviously, due to its poor stability in atmospheric humidity, CuBTC may not be the best candidate for future use in a respirator. This is because respirators must operate under ambient conditions and last for as long as possible in potentially very humid environments. However, as more water-stable MOFs are developed (such as the MIL series), and can be produced in bulk, their use in respirators could be explored further. This Section is intended to determine whether MOF impregnation on adsorbent hollow fibres is a viable option in this application, given their potential flaws, rather than to explore the vast range of MOFs, their syntheses and affinities for specific TICs.

To determine the effectiveness of MOF impregnation, CuBTC was synthesised as a powder by the methods described in Section 3.2.4.1. This was suspended in methanol and used to impregnate adsorbent hollow fibres by incipient wetness impregnation, followed

by heating in a vacuum oven at 75 °C to remove the methanol. This was deemed the most suitable method for including MOF in adsorbent hollow fibres as the other techniques for including metal salts in fibres (described above) require the fibres to be spun into water, and most MOFs (including CuBTC) are not stable under water (Gul-E-Noor *et al.*, 2011; Greathouse and Allendorf, 2006; Li and Yang, 2007). The MOF impregnated fibres were examined by X-ray diffraction (Section 3.2.7.3) to confirm the successful synthesis of CuBTC. The fibres were then compared with CuO impregnated fibres. CuO has the same active metal as CuBTC but not the same crystalline structure and high surface area, to determine whether MOFs had superior H_2S removal capability compared to metal salts. Water isotherms were carried out on CuBTC powder to measure the moisture uptake and confirm the lack of stability in humid conditions.

5.1.3 Pore formers

An additional network of pores could be introduced into the fibre structure by adding a pore former and removing it after the fibres have been spun. This could help to improve adsorption kinetics (Kim and Lee, 1998; Liu *et al.*, 2003). Several different pore formers were obtained from the company Clariant (Switzerland). These were Licowax SP, Licowax C Microp PM (referred to as Micropore C) and Licowax PE 520 Fine Grain. Detailed information regarding these pore formers can be seen in Section 3.1.1.

These pore formers were all included in adsorbent hollow fibre precursor mixtures at the stage described in Section 3.2.1.1. The amount added was 1% of the total weight of the fibre (e.g. for a 20 g polymer / 80 g adsorbent precursor mixture, 1 g of pore former was added). These were then heated to 190 ºC to remove the pore former, and tested using breakthrough studies with ammonia and cyclohexane, and by cyclohexane uptake analysis.

5.2 Results

5.2.1 Fibres prepared using commercial impregnated activated carbons

Several commercial impregnated activated carbons were selected for testing, shown in Table 5.1. As the chemical impregnants of the Avon carbon were unknown due to their commercial nature, analysis was performed with SEM and EDX. The SEM micrographs

are shown in Figure 5.1. Crystals are visible on the carbon surface, suggesting a metal salt. This is corroborated by the elemental analysis. The EDX of 'Avon' carbon detected copper, oxygen and sulphur, with some trace amounts of aluminium and silicon. It is hypothesised that Avon carbon is impregnated with copper oxide which is known to enhance adsorptive behaviour for ammonia (Guo *et al.*, 2005), with the detected sulphur a side product of the carbon activation process.

Table 5.1. Descriptions and suppliers of the activated carbons investigated in this report.

Supplier	Activated Carbon name	Description
Avon	"Avon" (Avon, 2011)	Granules, impregnated, composition not given (approximately 0.8 mm average diameter with low variance)
Eurocarb	HTS 12x20	Respirator grade granules, H_2S specific, impregnated with copper oxide (0.85-1.68 mm particle size)
	RGE 12x20	Respirator grade granules, H_2S specific, impregnated with potassium hydroxide and potassium iodide (0.85-1.68 mm particle size)
	SAC 460 12x20	Biogas grade granules, impregnated with NaOH (0.85-1.68 mm particle size)

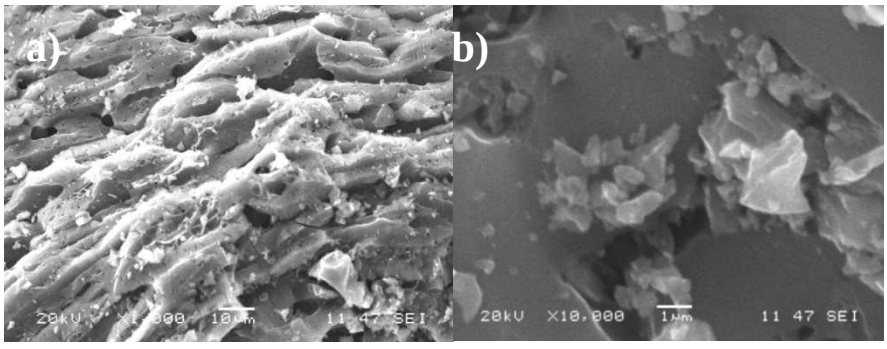

Figure 5.1. SEM images of activated carbon supplied by Avon a) x1000 b) x10000.

The commercial activated carbons 'Avon', HTS, RGE and SAC, were ground in a planetary ball mill and the resulting powders were spun into adsorbent hollow fibres by the methods described in Section 3.2.1.1. Due to difficulty spinning fibres from the

impregnated carbon powders, they were all mixed with a quantity of zeolite to ensure successful spinning while maintaining approximately 85% adsorbent. This difficulty in spinning carbon stemmed from strong adsorption of the solvent used to suspend them, resulting in precursor mixtures that were particularly thick with a tendency to clump, blocking the spinneret. The presence of zeolite made the fibres simpler to spin due to their small relative particle size. The zeolites themselves, as shown in earlier results, are unlikely to adsorb high quantities of H_2S, but should not block the impregnated carbon from doing so. 5cm fibre and granule modules were challenged with 1 L/min 800 ppm H_2S, and the results are shown in Figure 5.2 and Table 5.2.

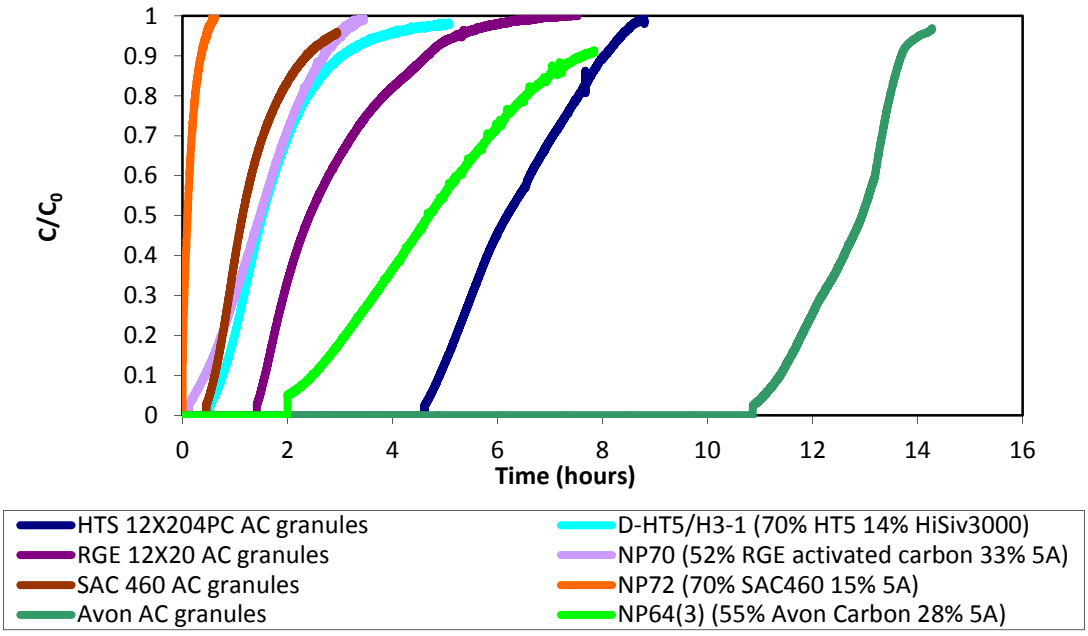

Figure 5.2. 1 L/min 800 ppm H_2S dynamic challenge on adsorbent hollow fibres prepared using impregnated carbon. Darker colours on the graph indicate granules while the lighter variant of the same colour indicates the respective fibre.

Table 5.2. Breakthrough and equilibrium times and loadings for 5 cm of carbon granules and their respective fibres after challenge under dynamic conditions with 800ppm H_2S at 1L/min, where a subscript g indicates granules and a subscript f represents fibres.

Adsorbent	Weight (g)	t_b (h)	t_b loading (% wt sorbent)	t_b loading (% wt carbon only)	t_{eq} (h)	t_{eq} loading (% wt sorbent)
HTS (CuO) $_g$	11.60	4.61	2.64	-	8.78	5.03
D-HTS/H3-1 (HTS/HiSiv3000) $_f$	7.39	0.53	0.47	0.57	5.08	1.59
RGE (KI/KOH) $_g$	11.60	1.42	0.81	-	7.15	1.60
NP70 (RGE/5A) $_f$	6.77	0.13	0.12	0.15	3.46	1.49
Avon carbon (CuO/H_2SO_4) $_g$	11.29	10.87	6.40	-	14.28	7.49
NP64(3) (Avon/5A/pf) $_f$	8.29	2.00	1.60	2.48	7.84	3.87
SAC (NaOH) $_g$	9.91	0.46	0.31	-	2.95	0.89
NP72 (SAC/5A) $_f$	7.24	0.00	0.00	0.00	0.62	0.13

As can be seen in Figure 5.2, the 'Avon' carbon granules had the highest breakthrough time, 10.87 hours, followed by HTS carbon granules, with 4.61 hours. The smaller particle size of the 'Avon' granules may explain this difference, although the higher equilibrium loading of the Avon granules, shown in Table 5.2, is most likely as a result of a different impregnant loading on the carbon. Precise knowledge of the compositions of these commercial carbons would be useful for a full comparison. However, these were difficult to obtain. RGE and SAC granules were less effective for adsorption of H_2S. Adsorbent hollow fibre breakthrough times followed the same trend from highest (Avon carbon fibres) to lowest (SAC carbon fibres), although they had significantly lower breakthrough times and loadings than their respective granules. The granules also had greater equilibrium loading than their respective fibres. There are several possible reasons for this. Firstly, polymer could be blocking adsorbent sites, as discussed in Chapter 4. Secondly, these differences could be associated with the fibre spinning process. Fibres

were spun into water, and the spun fibres remained in water for a number of days. This treatment may have also removed metal ion impregnants, particularly soluble ones, such as KI. To determine whether this was the case, EDX was carried out on Avon, RGE and SAC activated carbon fibres. Carbon, sulphur, calcium, oxygen, aluminium and silicon were detected for all the carbon fibres, and so were excluded from the table. The elements detected are presented in Table 5.3.

Table 5.3. Elements detected in fibres prepared from commercial impregnated activated carbon by energy-dispersive X-ray spectroscopy.

Activated Carbon Fibre	Impregnants	Fibre composition	Section of fibre	Elements detected
Avon	Unspecified	55% Avon carbon 28% 5A	All sections	Copper
RGE	KI, KOH	52% RGE 33% 5A	Inner bore	Potassium Chlorine
			Outer layer	Potassium Chlorine Sodium
SAC	NaOH	70% SAC 15% 5A	Inner bore	Chlorine Sodium
			Outer layer	Chlorine Sodium

Aluminium and silicon were present in 1:1 ratios in each case, consistent with the 1:1 Si:Al ratio of the 5A zeolite incorporated into each of these fibres (see Table 2.2). This also explains the presence of calcium, the cation in 5A (Yang, 1997). Chlorine was found on RGE and SAC carbons, which could be because fibres were left in tap water, and picked up some salt. This would also explain the presence of sodium, due to ion exchange. In addition, a lack of iodine was observed on RGE carbon hollow fibres. This was likely due to the spinning process. KI, KOH and NaOH are all highly soluble in water, and as such are likely to be lost when the fibre is exposed to water. This is a major drawback for fibres made from activated carbons with water soluble impregnants.

5.2.2 Incorporation of metal salts into adsorbent hollow fibre structures to enhance removal of H_2S and NH_3

Impregnation may block access to the inner structure of the adsorbent hollow fibres (especially for microporous carbons). As an alternative, metal salts were incorporated into 80% NV5 carbon adsorbent hollow fibre precursor mixture and spun. This required an insoluble metal salt to prevent loss during spinning process, as was observed in Section 5.2.1. The insoluble copper (II) oxide salt was therefore selected. This was incorporated at 1, 2 and 4% wt to avoid having a significant impact on the structure of the adsorbent hollow fibre during the spinning process. These fibres were challenged with 800 ppm H_2S at 1 L/min, with the breakthrough curves are shown in Figure 5.3. They were also examined by SEM, with images shown in Figure 5.4, Figure 5.5 and Figure 5.6.

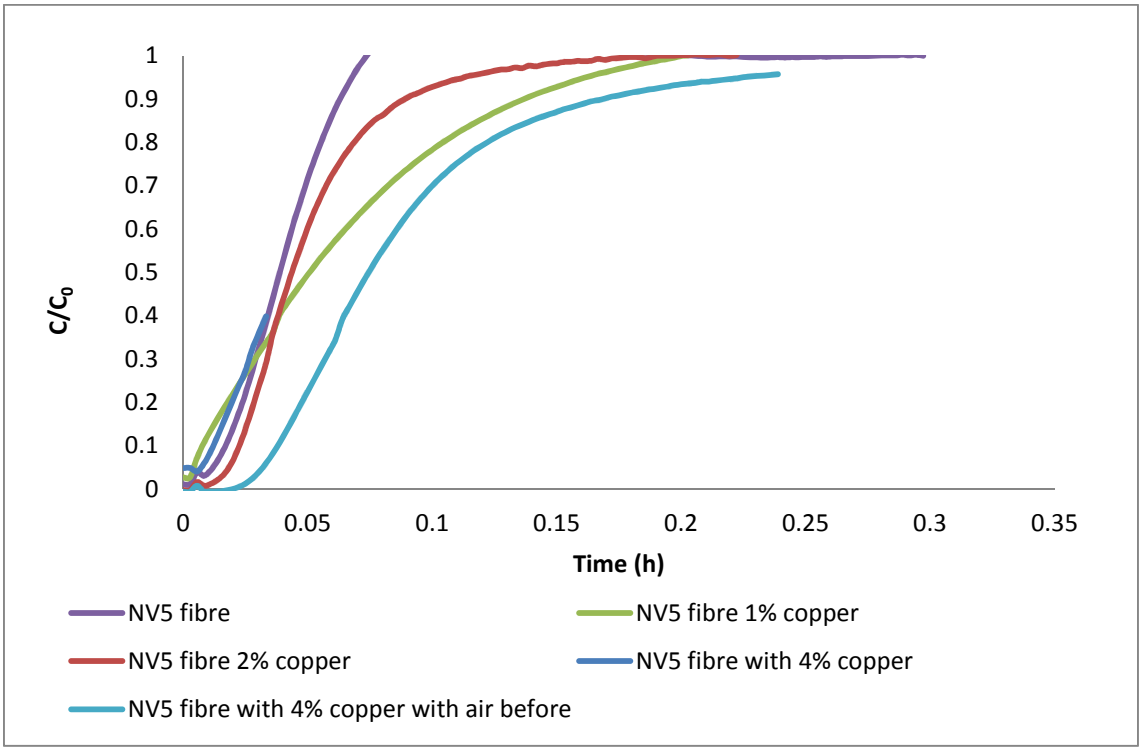

Figure 5.3. 1 L/min 800 ppm H_2S challenge on NV5 carbon fibres with incorporated CuO, one fibre was prehumidified with air at ambient humidity and room temperature.

There were no marked differences between breakthrough curves. A slight improvement was seen by exposing fibres to ambient air for 1 hour prior to testing. The low quantity of copper used in the studies most likely resulted in its poor distribution through the fibre. It is required on the fibre surface to react with toxic gases. If it is distributed on the inside of

the fibre structure it cannot do this. Further, presence of copper oxide particles in the fibre will reduce available surface area due to its non-porous nature, and could weaken the fibre structure. This means incorporating higher quantities would not be a viable option.

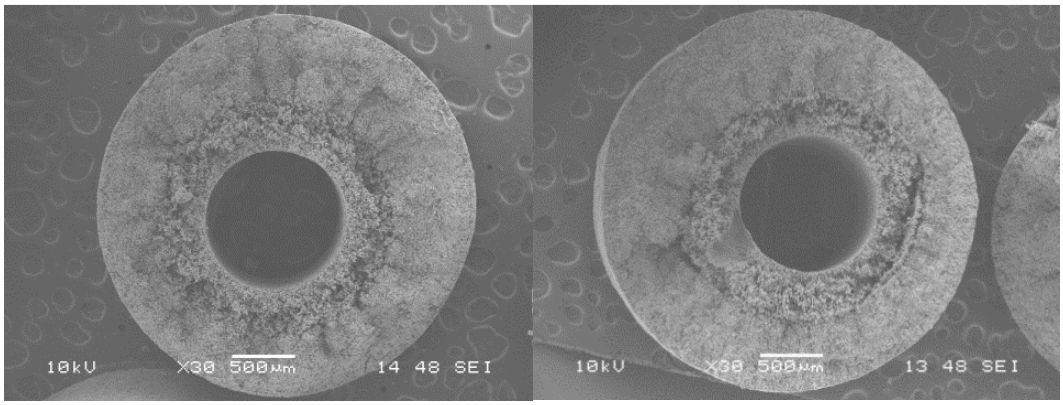

Figure 5.4. SEM of 2% (left) and 4% (right) NV5 carbon fibres

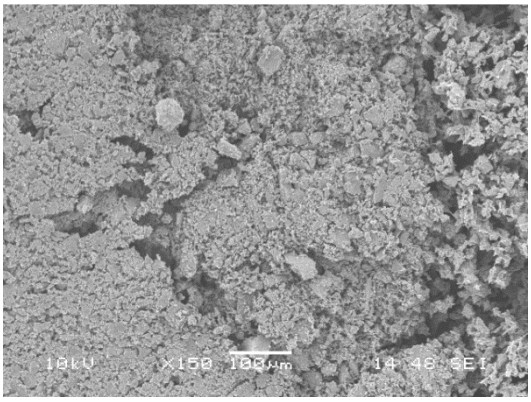

Figure 5.5. Copper particles in outer skin layers in 4% CuO NV5 fibres

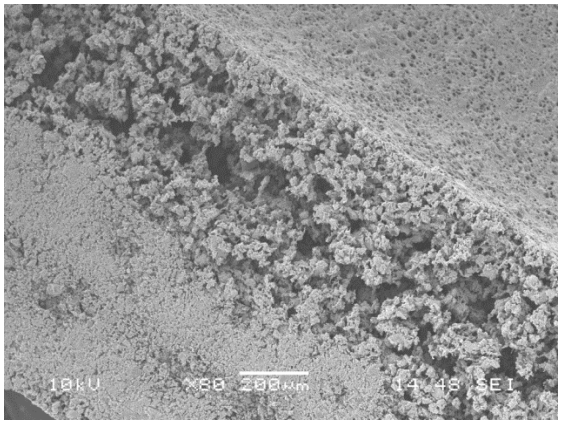

Figure 5.6. Bore of 4% copper oxide fibres.

At this magnification, clear differences were difficult to see between a cross section of fibre with incorporated copper and one without (Figure 5.4). At higher magnification, the

scanning electron micrograph showed ~ 50 μm particles, which can be seen in Figure 5.5. These may be too large to have a significant effect on adsorption properties of the fibre. This means performance may be improved by using nanoparticles, although this would greatly add to the cost (25 g of <10 μm CuO powder was available for £15.00 on Sigma Aldrich, while 25 g of <50 nm CuO nanopowder was available for £43.50). In addition, when examining the bore in Figure 5.6, no particles of copper oxide were visible. This suggests that the copper may not be distributed evenly through the structure.

5.2.3 Impregnating adsorbent hollow fibres with metal salts to enhance removal of H_2S and NH_3

5.2.3.1 Potassium hydroxide and potassium iodide

An additional alternative method to include metal salts in adsorbent hollow fibres would be to impregnate carbon or zeolite fibres after they have been spun. A number of unimpregnated carbon fibre samples with high polymer content were sent to the company Eurocarb (UK) for chemical impregnation for H_2S removal. They found that their usual process for impregnating granules damaged the fibres. As such they soaked EUR20 (20% polymer) fibres in a potassium iodide and potassium hydroxide bath, and sprayed EUR30 (30% polymer) fibres with the same mixture. These modules were challenged with 800 ppm 1 L/min H_2S and compared with 'NP70' fibres, which were made from 'RGE' carbon (KI and KOH impregnant), shown in Figure 5.7 and Table 5.4. At the recommendation of Eurocarb, the impregnated fibres they provided were pre-humidified with a 35% relative humidity airstream prior to testing.

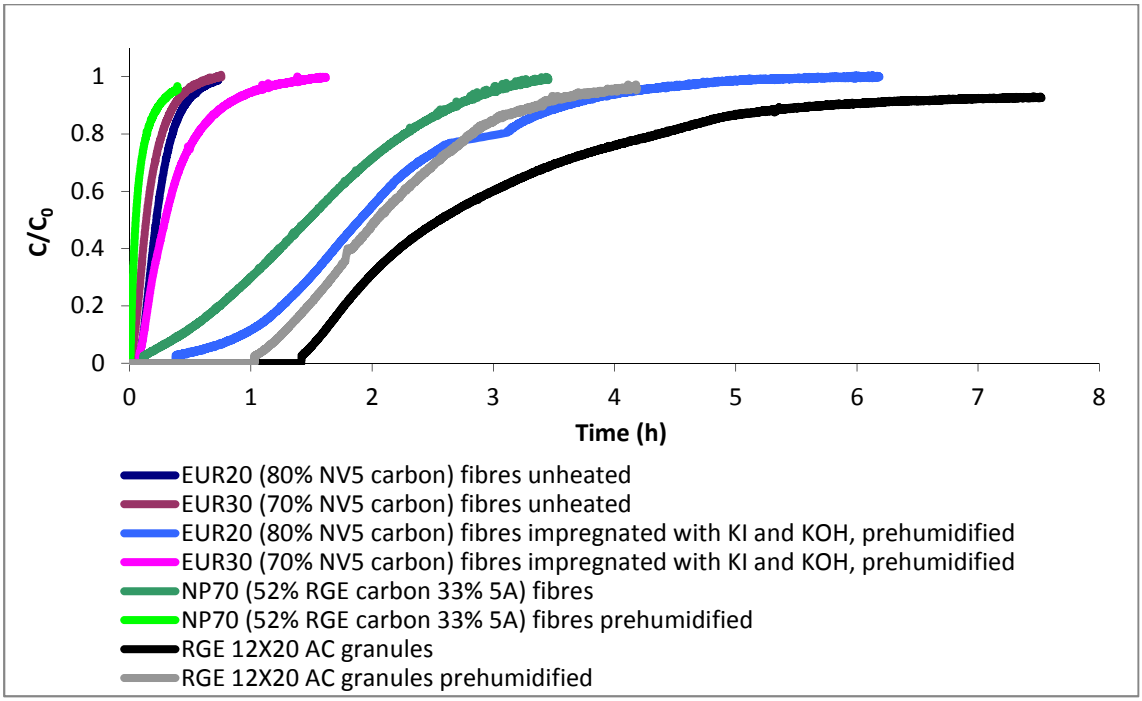

Figure 5.7. Breakthrough curves of 5cm KI/KOH impregnated and unimpregnated carbon fibres and granules, challenged with 800ppm H_2S at 1L/min under dynamic conditions.

Table 5.4. Breakthrough and equilibrium times and loadings on 5 cm impregnated and unimpregnated carbons fibres and granules after challenge with 800 ppm H_2S at 1L/min under dynamic conditions. The blue data bars compare relative values within each column.

Adsorbent	Adsorbent wt (g)	t_b (h)	Breakthrough loading (%wt)	t_{eq} (h)	Eq. loading (%wt)
EUR20 (80% NV5 carbon) unheated	5.29	0.08	0.10%	0.73	0.32%
EUR30 (70% NV5 carbon) unheated	5.11	0.02	0.03%	0.76	0.23%
EUR20 (80% NV5 carbon) impregnated with KI and KOH, pre-humidified (35% RH)	8.87	0.4	0.27%	6.19	1.69%
EUR30 (70% NV5 carbon) impregnated with KI and KOH, pre-humidified (35% RH)	4.5	0.08	0.12%	1.62	0.57%
NP70 (52% RGE carbon 33% 5A) pre-humidified (35% RH)	6.36	0.01	0.01%	0.4	0.41%
NP70 (52% RGE carbon 33% 5A)	6.77	0.13	0.12%	3.46	1.49%
RGE 12X20 AC granules	11.6	1.42	0.81%	7.15	1.60%
RGE 12X20 AC granules pre-humidified (35% RH)	8.28	1.03	0.83%	4.18	1.76%

The results in Table 5.4 indicate that the unimpregnated EUR20 and EUR30 fibres had negligible adsorption of hydrogen sulphide. When impregnated with KI and KOH, EUR20 showed an increase in breakthrough time and loading compared to the unimpregnated EUR20, from 0.08 hours to 0.4 hours, and 0.1% wt to 0.27%wt. Impregnated EUR20 also had a longer breakthrough time than NP70 fibres prepared from the RGE carbon. This was due to the presence of 5A in NP70 fibres. This zeolite was incorporated into the RGE carbon fibres, enabling them to be spun more easily but at the cost of water tolerance, which can be observed on Figure 5.7 for the pre-humidified NP70 fibres. RGE granules also showed a slight decrease in breakthrough time if pre-humidified. This is surprising, given the recommendation of the company. Some water is required in order to enable the reaction to take place with KI and KOH. However, it is possible that a very specific amount of water is required for this to occur optimally, which may be provided by the ambient humidity in the H_2S canister (~30%). It was also observed that the dry and pre humidified RGE granules had very similar equilibrium loadings to one another. These values were also very close to the loadings for the EUR20 soaked in KI and KOH and then pre humidified, as well as to the NP70 fibres. The lower breakthrough time and loading for the two fibres indicated some interference with adsorption kinetics, but the same overall capacity. The sprayed fibres had lower equilibrium loading, suggesting potential problems with the spraying impregnation process. This may be because the majority of the sprayed impregnants will be located on the outside of the fibre structure, while the majority of the gas will travel through the bores and into the structure. Despite this, in all cases, impregnated fibres had greater loading than unimpregnated fibres.

Overall, the technique of impregnation shows promise and with collaboration with Eurocarb, the process of impregnation could be refined and studied in greater detail with other chemicals and fibres.

5.2.3.2 Impregnation with copper salts

Copper (II) oxide showed promise in removal of H_2S in the previous Sections. As such, it was impregnated onto the adsorbent hollow fibres following spinning and NV5 granules for comparison. A three step technique, described in Section 3.2.5.1, was used to achieve this in both cases. These modules were challenged with 800 ppm 1 L/min H_2S.

Breakthrough curves are shown in Figure 5.8, Figure 5.9 and data extracted from the curves are shown in Table 5.5.

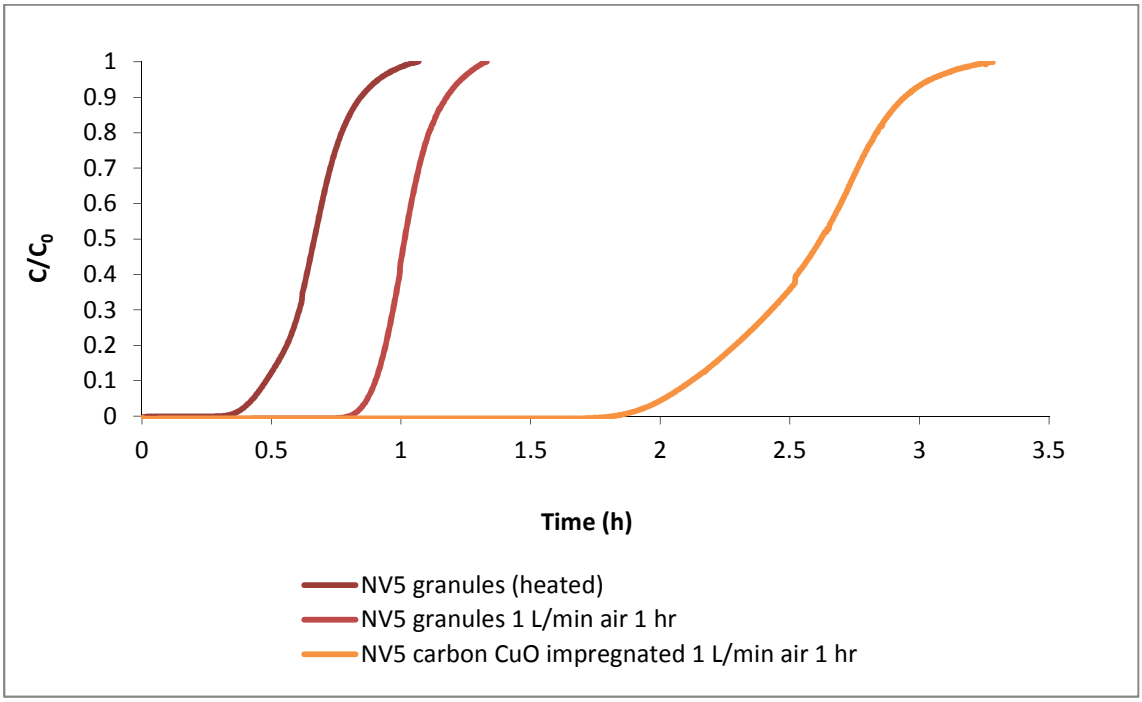

Figure 5.8. 800 ppm 1 L/min H_2S dynamic test on NV5 carbon granules with and without exposure to ambient air for 1 hour prior to challenge, compared to a 10% CuO impregnated granule module.

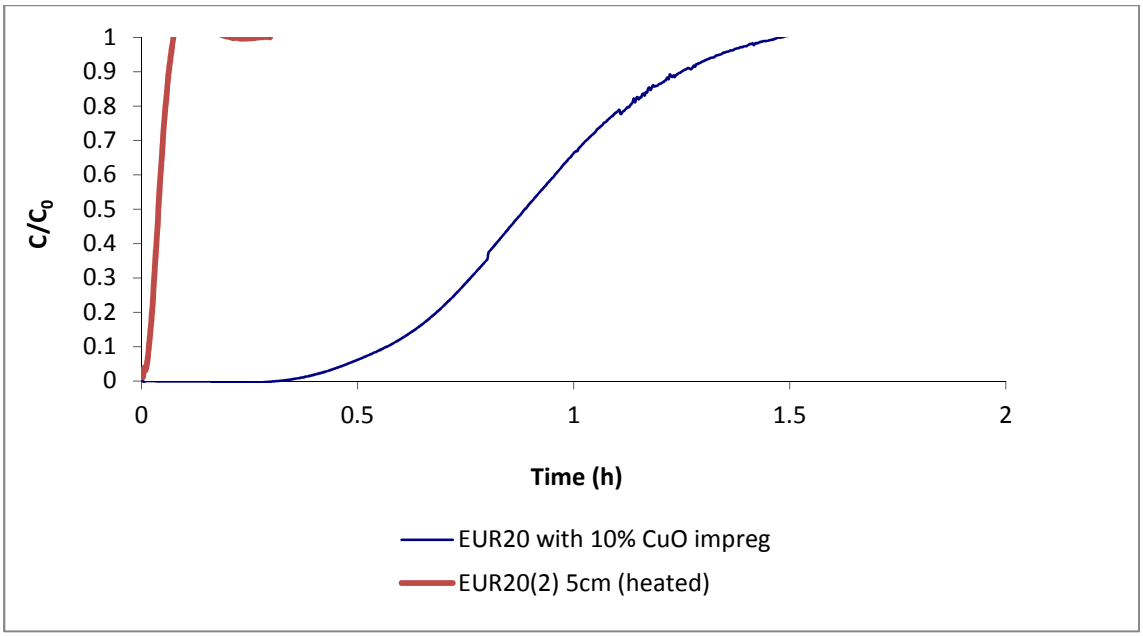

Figure 5.9. 800 ppm 1 L/min H_2S challenge on impregnated and virgin adsorbent hollow fibre.

Table 5.5. Adsorption data derived from Figure 5.8 and Figure 5.9.

Adsorbent	Adsorbent wt (g)	t_b (h)	t_b loading (%)	t_{eq} (h)	t_{eq} loading (%)
NV5 granules	7.18	0.37	0.34%	1.07	0.62%
NV5 granules with air prior	7.81	0.84	0.72%	1.33	0.87%
NV5 granules impregnated with 10% CuO and exposed to air prior	8.68	1.91	1.47%	3.28	1.97%
NV5 fibre module	4.93	0.00	0.00%	0.09	0.00%
NV5 fibres impregnated with 10% CuO and exposed to air prior	4.13	0.39	0.63%	1.53	1.45%

Figure 5.8 showed that prior exposure to compressed air (containing moisture) enhanced adsorption of H_2S, and so these conditions were used for the impregnated fibre modules also. Coating NV5 carbon granules with CuO significantly improved breakthrough time for H_2S, particularly after prior exposure to air (Figure 5.8), from 0.84 hours to 1.91 hours. The same was observed for fibres (Figure 5.9), with an increase from instant breakthrough to 0.39 hours. However, granular beds still had longer breakthrough time overall, with data shown in Table 5.5. This demonstrates the potential of impregnating carbon fibres with 10% CuO in order to significantly enhance adsorption of H_2S, increasing the breakthrough time from 0 hours to 0.4, and loading from 0% to 0.63% wt of adsorbent.

5.2.4 Encapsulation of metal organic frameworks in adsorbent hollow fibre structure

5.2.4.1 H_2S adsorption on MOF impregnated pellets

Initial MOF impregnation tests were carried out on pellets to determine whether CuBTC would effectively adsorb H_2S. CuBTC impregnated 13X pellets were prepared by soaking the pellets in the CuBTC as it was synthesised and filtering and drying as described in the Britt *et al.* (2008) synthesis method. One sample of these was tested with H_2S. Another was left in atmosphere overnight until the pellets were saturated (indicated by colour change to pale blue) and then challenged with hydrogen sulphide, 800 ppm 1 L/min. The results are shown in Figure 5.10.

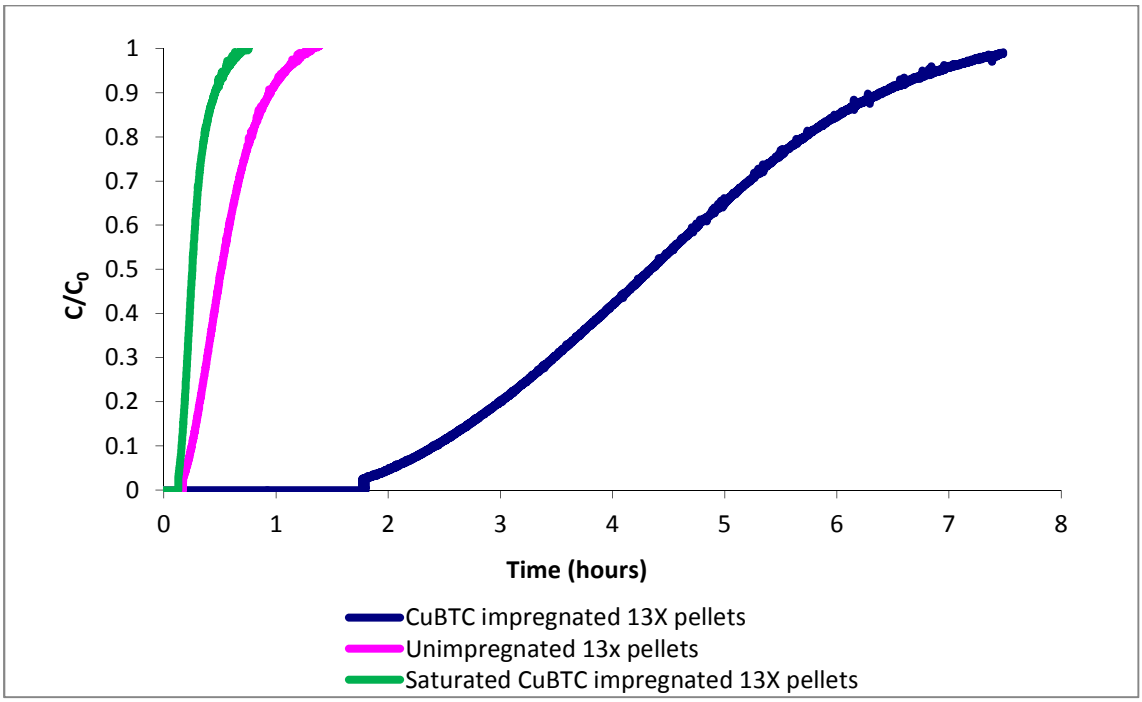

Figure 5.10. 800 ppm 1 L/min H_2S dynamic challenge on CuBTC impregnated 13X pellets.

13X pellets had H_2S breakthrough loading of 0.08%wt and equilibrium loading of 0.31%wt, while the impregnated beads had breakthrough loading of 1.07%wt and equilibrium loading of 2.62%wt. Significant improvement in adsorption was seen compared to unimpregnated 13X pellets, but the long breakthrough curve for the MOF impregnated beads suggests sub-optimal adsorption kinetics. However, as evidenced by breakthrough curve of the saturated beads, the presence of even ambient moisture over night was enough to significantly reduce the adsorption of H_2S.

Several colour changes were observed during this experiment. CuBTC impregnated 13X pellets changed from deep blue/purple to a light brown colour, indicating a chemical reaction with H_2S that formed copper (II) sulphide, an irreversible process. In addition, when the impregnated beads were initially left overnight to saturate, the top few layers of pellets changed light blue, indicating water adsorption, but those underneath remained deep purple, indicating they remained dry. To fully saturate, the pellets had to be spread out flat. This is potentially reassuring for storage in a respirator, particularly in a long, thin configuration. If the respirator was not in use and was simply exposed to ambient moisture, the top few millimetres of the adsorbent in the cartridge would fill with water but exert a protective effect on the adsorbent behind them. However, if the respirator was

in use, moisture would be pulled through the downstream adsorbent, saturating it and thus greatly reducing its adsorption performance.

5.2.4.2 Characterisation of synthesised MOF and adsorbent hollow fibres

To confirm successful synthesis of MOF powder in ethylene glycol, X-ray diffraction was performed. The result is shown in Figure 5.11.

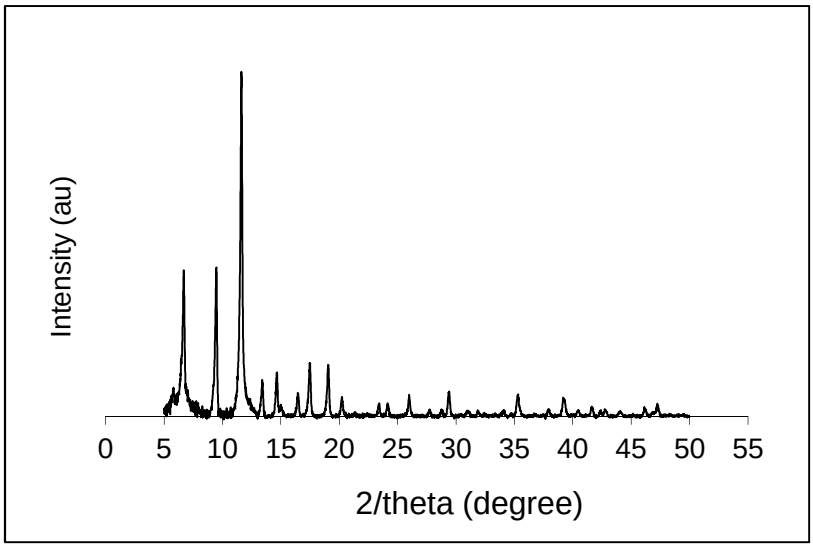

Figure 5.11. XRD of CuBTC synthesised in ethylene glycol

This graph was compared to XRDs of CuBTC from the literature, shown in Figure 5.12. The peaks are similar between the graphs, with two tall peaks at 7 and 10 º, one very tall peak at 12 º and then 5 or 6 noticeable but smaller peaks following this, between 14 and 26 º. The main difference between Figure 5.11 and Figure 5.12 is the fourth peak, which is very small in the CuBTC synthesised for this report. However, this is similar to the result of the MOF synthesised ultrasonically in (Loera-Serna *et al.*, 2012). From this it was concluded that the MOF powder had the correct crystalline structure and had therefore been synthesised successfully.

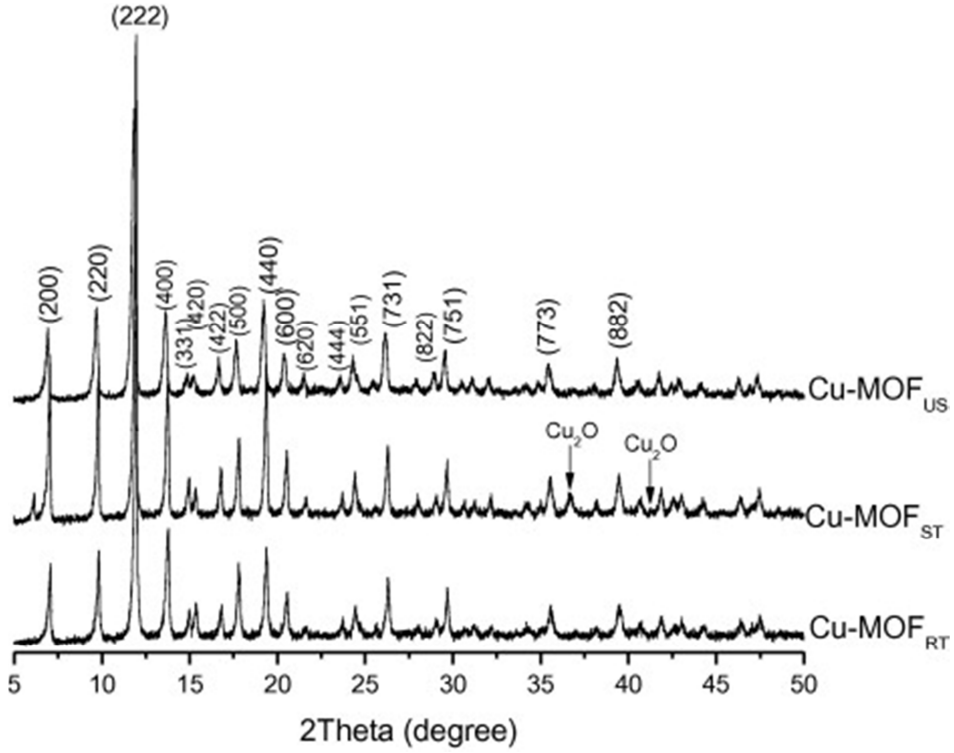

Figure 5.12. XRD of CuBTC synthesised in DMF/EtOH/H_2O. US = ultrasonic. ST = solvothermal. RT = room temperature (Loera-Serna *et al.*, 2012).

5.2.4.3 Effects of humidity on CuBTC

A water dynamic vapour sorption test was carried out on CuBTC powder, shown in Figure 5.13.

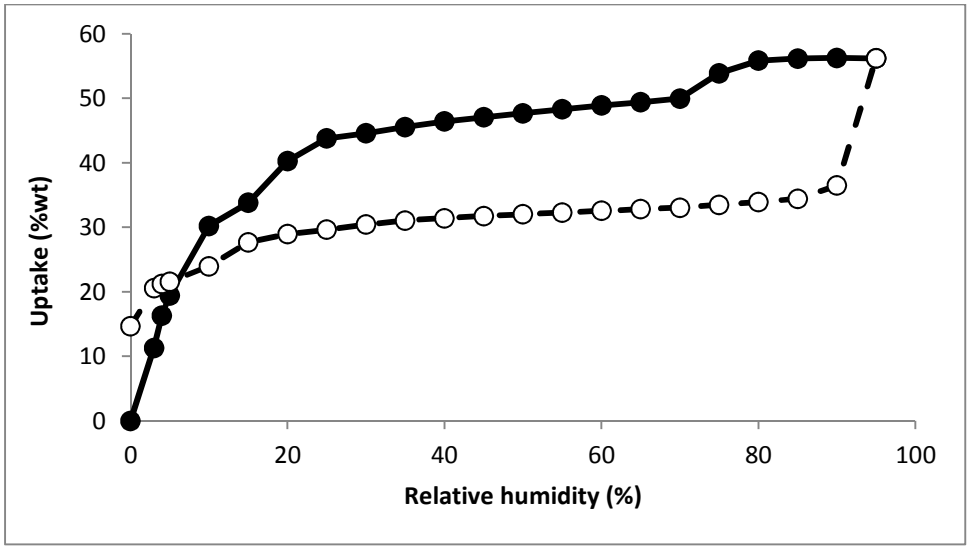

Figure 5.13. Dynamic water vapour sorption on CuBTC. Filled circles represent adsorption, empty circles and dotted line represent desorption (characterised at Dstl).

Rapid water uptake was seen on CuBTC powder as RH increased. This levelled off at 56% RH, followed by a rapid loss of weight during desorption, and a reversed hysteresis. The adsorption curve resembled that of a Type IV isotherm, with two steps, which would indicate the formation of a monolayer at 25% RH, with capillary condensation accounting for hysteresis. However in this case, the rapid weight loss (accompanied by a colour change) would indicate degradation of the adsorbent as the water was removed, following which it could not be regenerated.

In terms of practicality, the high initial water uptake suggests that water interference is likely to occur at ambient humidity, further verified by poor H_2S sorption on the humidified MOF-impregnated 13X pellets. The degradation on exposure to water can occur in atmosphere within a relatively short time period, making this far from ideal for use in a general respirator that would constantly be exposed to ambient conditions.

5.2.5 H_2S adsorption on MOFs vs. metal salts

To allow comparison with MOFs, one hybrid NV5/AbScents1000 hollow fibre was impregnated with 10% CuO and another was impregnated with 10% CuBTC. These were compared by dynamic H_2S challenge. This is shown Figure 5.14 a) and b).

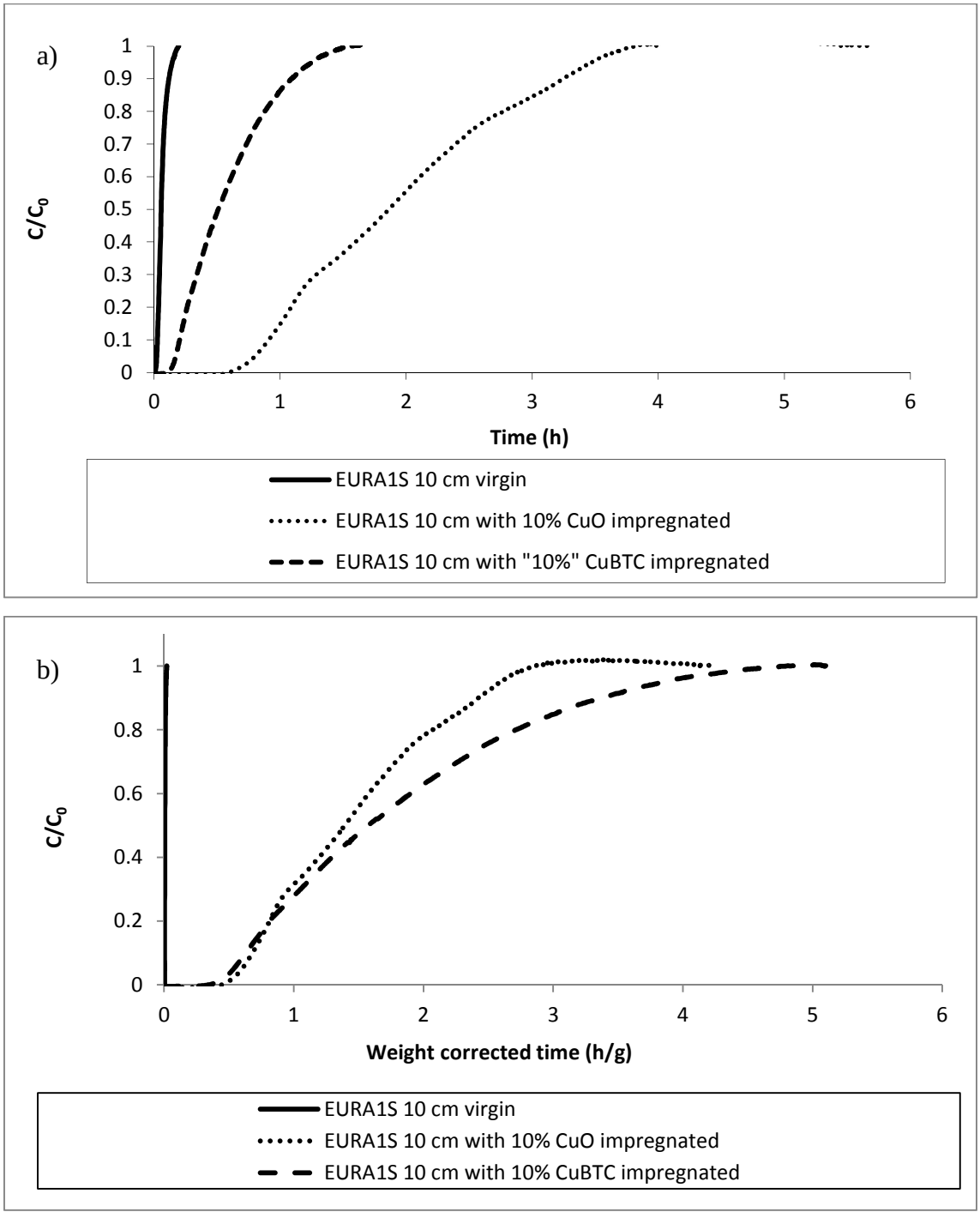

Figure 5.14. 800 ppm H_2S on virgin hybrid AbScents1000/NV5 carbon fibre, and the same impregnated with 10% CuO and "10%" CuBTC MOF. a) shows concentration over time, b) shows concentration over time/g of impregnant (or adsorbent, for control)

Figure 5.14 a) demonstrates that both CuBTC impregnation and CuO impregnation could increase breakthrough time and loading of the treated hybrid fibres, which had negligible adsorption of H_2S otherwise. However, when not corrected for weight, 10% CuO impregnation was superior to the MOF impregnated fibres. The reason for this was

associated with the impregnation process. During this process, 1.39 g of CuO were successfully impregnated onto the hybrid fibres, while only 0.324 g of CuBTC were impregnated, despite 1.2 g of the MOF being added to the fibres. CuBTC did not stick to the fibres very well, and a great deal of powder was lost from the fibre module even as it was set up for dynamic testing. When the breakthrough curves of the two different types of impregnant were compared, normalising the time by weight, shown in Figure 5.14 b) (i.e. time /1.388 for CuO, /0.324 for CuBTC, and /9.16 for the hybrid fibres), the control hybrid fibres were shown to adsorb negligible quantities of H_2S per weight. Meanwhile, the CuO and CuBTC had very similar breakthrough time/weight values, of 0.56 and 0.44 h/g respectively and breakthrough loadings 3.75 and 2.91 w/w% respectively. This would indicate that CuO was a superior fibre impregnant for removal of H_2S to CuBTC, not just in terms of water stability and cost but also in terms of H_2S uptake. The similar loadings were mostly likely due to the similar chemisorption reactions for the two, with copper sulphide forming in both cases, and resulting in irreversible breakdown in the crystalline structure in the case of the MOF.

5.2.6 Cyclohexane adsorption on MOFs vs. metal salts

Cyclohexane is not well adsorbed by metal salts, and no literature could be found to suggest CuBTC would adsorb it. As such, to whether there would be any interference in cyclohexane uptake caused by impregnating with MOFs or metal salts, dynamic vapour sorption was performed on samples of carbon impregnated with CuO and CuBTC. These isotherms were compared to a cyclohexane isotherm of an unimpregnated hybrid fibre sample, and MOF powder with results shown in Figure 5.15.

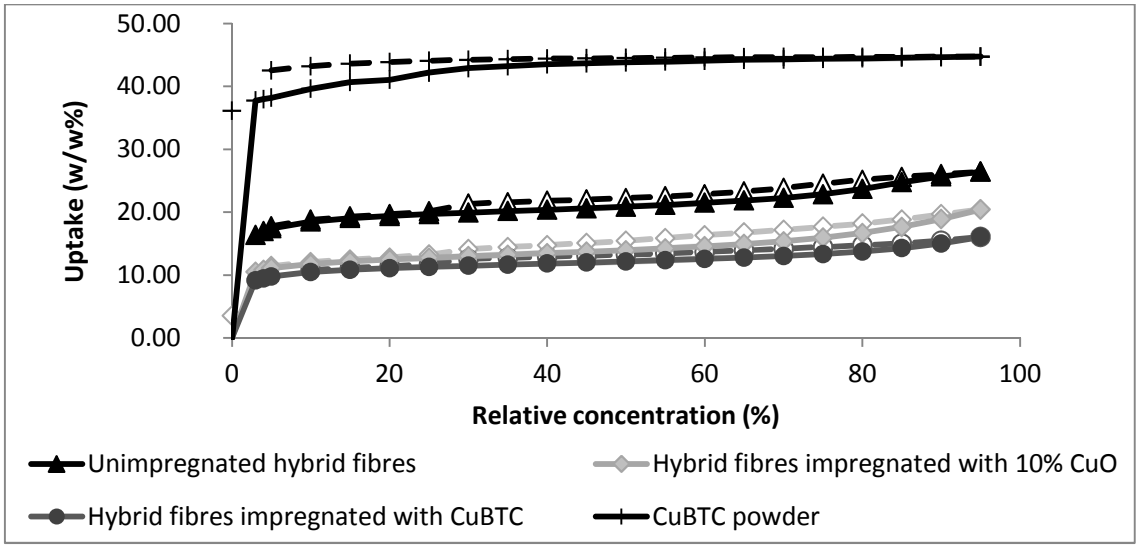

Figure 5.15. Cyclohexane dynamic vapour sorption on virgin and impregnated NV5 fibres, and of CuBTC powder (characterised at Dstl).

The metal salt CuO has no particular interaction with cyclohexane; as such it would not be expected to improve fibre adsorption of this contaminant. It would be expected to block access to the adsorbent in the fibre, however, resulting in lower loading at all concentrations. This was seen to be the case, in Figure 5.15, with cyclohexane loading decreasing from ~20% for an unimpregnated fibre to just over 10% for CuO impregnated fibres. This will be an important consideration when impregnating an adsorbent fibre for H_2S removal. Though H_2S removal can be greatly improved, adsorption of other contaminants may be reduced as a result. In the same manner, the CuBTC impregnated fibre, despite having a lower %wt impregnation than the CuO impregnated fibre, took up less cyclohexane at all concentrations than the CuO impregnated fibre. The CuBTC powder by itself was found to adsorb cyclohexane very well, with almost 40 w/w% loading. However, this performance was not seen in the impregnated fibre, which had only 10 w/w% loading. It is probable that due to its low density, the MOF covered a greater volume of the fibre than the relatively dense CuO, blocking access to the pores of the fibre. However, why the uptake of the impregnated fibre was so far below both the CuBTC and hybrid fibre only lines, even if it did block access to the porous structure of the fibre, is unclear.

5.2.7 Incorporation of pore forming agents into the adsorbent hollow fibre structure to increase porosity

5.2.7.1 Selecting a pore former

Three pore formers were initially spun into double layer NV5 carbon fibres, using a precursor mixture prepared by the methods described in Section 3.2.1.1, with 1% weight pore former included in the precursor mixture. The pore formers used were 'Licowax micropore C', 'Licowax PE 520' and 'Licowax SP'. During the spinning process, Licowax PE 520 could not be spun successfully, as it blocked the spinneret. Previous work suggests this may be as a result of its large particle size or tendency to clump. Water soluble pore formers were not selected for use, as their solubility in water would be likely to interfere with the spinning process and coagulation of the fibre. Following spinning, double layer standard bore 80% NV5 carbon with micropore C and Licowax SP fibres were successfully spun. The fibres with Licowax PE 520 could not successfully be spun. Both were bundled into 5 cm test modules and heated to 190°C to burn off the pore former.

Dynamic cyclohexane tests were performed, which were compared to a double layer NV5 carbon fibre without a pore former, shown in Figure 5.16, and calculated results shown in Table 5.6.

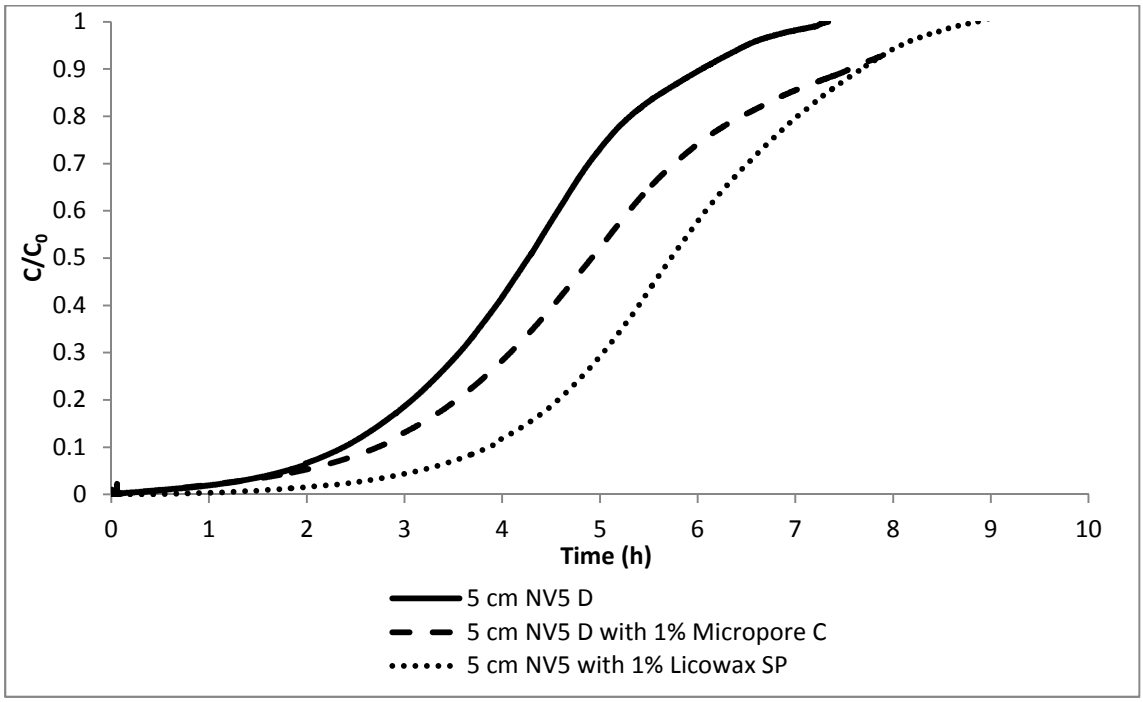

Figure 5.16. 1000 ppm 1 L/min cyclohexane breakthrough curves for 5 cm NV5 double layer fibres with and without pore formers.

Table 5.6. Breakthrough data for 1000 ppm 1 L/min cyclohexane dynamic challenge.

	Adsorbent wt (g)	T_b (h)	T_b loading (g)	T_b loading %	T_{eq} (hrs)	T_{eq} loading (g)	T_{eq} loading %	MTZ (cm	LUB (cm)
NV5 fibres	4.27	0.57	0.12	2.74%	7.34	0.86	20.20%	8.05	4.32
NV5 fibres/1% micropore C	4.61	0.89	0.18	3.94%	7.87	1.01	21.93%	7.07	4.09
NV5 fibres/1% Licowax SP	4.82	2.14	0.44	9.04%	9.02	1.17	24.39%	6.01	3.14

1% Licowax SP pore former significantly enhanced breakthrough time and loading, as well as increasing equilibrium loading, from just over 20% for the micropore C and standard fibre to 24.5% for the SP. In addition, mass transfer zone and length of unused bed were shortened. This was most likely due to increased porosity lowering transport resistances and improving adsorption kinetics.

These were further investigated with dynamic vapour sorption uptake tests using cyclohexane (Figure 5.17). The adsorption kinetics were more rapid on both the fibres with pore formers.

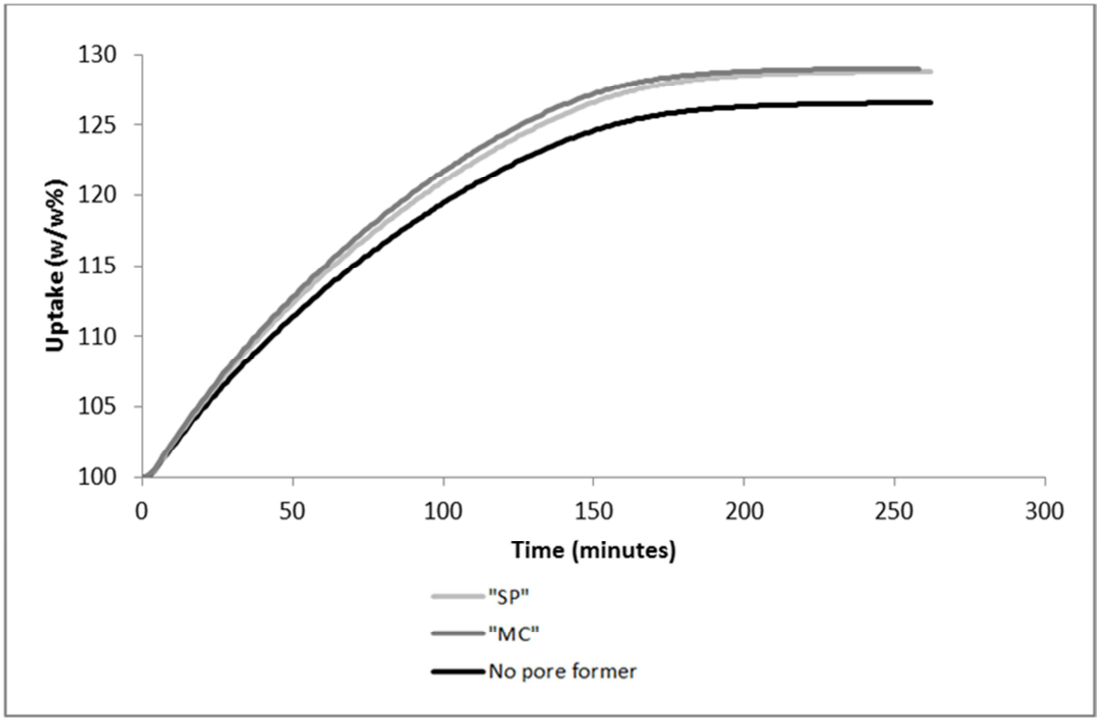

Figure 5.17. Cyclohexane uptake over time on NV5 carbon fibres with pore formers. SP = Licowax SP. MC = Micropore C (characterised at Dstl).

Fibres with pore formers had slightly greater uptake than those without pore formers. However, the two different pore formers were indistinguishable from each other, as seen in a cyclohexane isotherm (Figure 5.18).

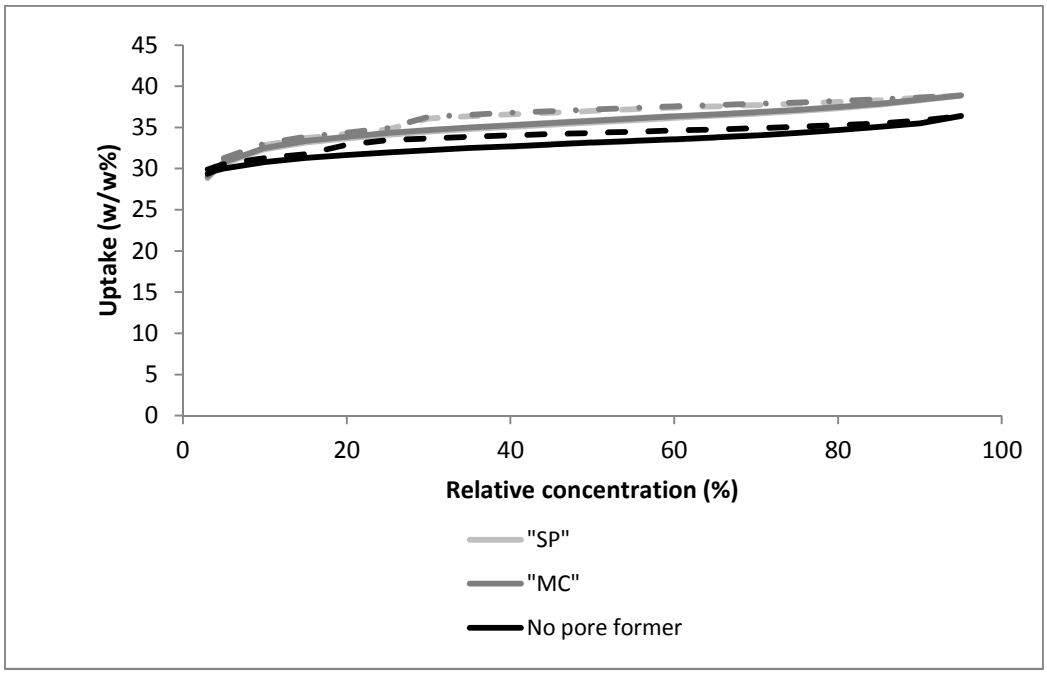

Figure 5.18. Cyclohexane isotherm of pore former fibres – 80% NV5 double layer standard bore. SP = Licowax SP. MC = Micropore C. SP pore former line is barely visible as it completely overlaps the MC line (characterised at Dstl).

Potential structural reasons for the improvements in uptake and adsorption kinetics were investigated by SEM. These are shown in Figure 5.19 and Figure 5.20. The two fibres were very similar in cross section, although the Licowax SP fibres appeared to have a more porous inner and outer wall than the Micropore C fibres. It is possible that improved breakthrough performance was seen with Licowax SP due to the uniform distribution of the pore former around the inner bore and outer wall, as opposed to micropore C, which distributed evenly through the structure, thus seeing similar isotherms but better breakthrough time.

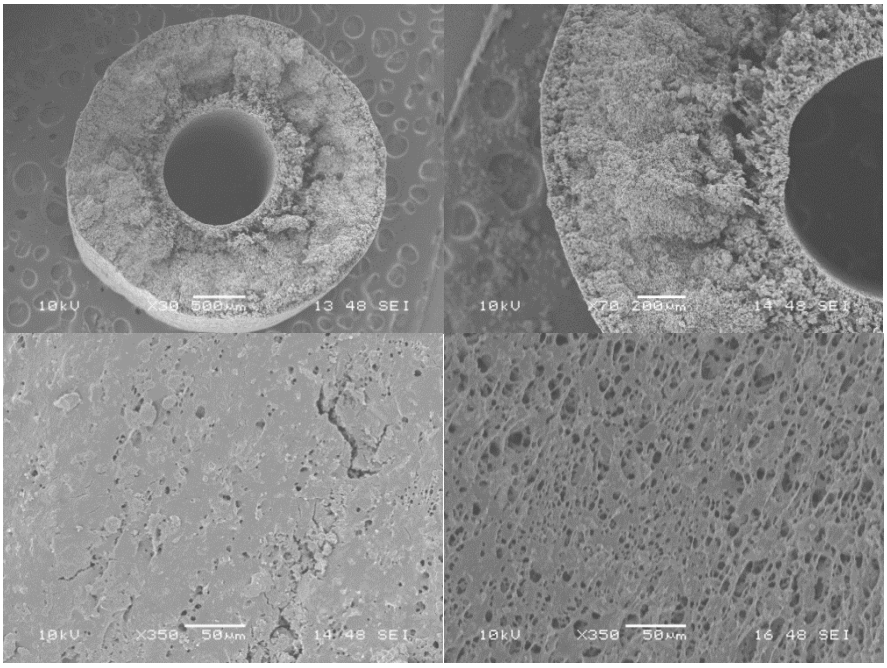

Figure 5.19. Micropore C fibres under SEM. Top: Cross section x 30 and x70. Bottom left: outside of fibre x350. Bottom right: fibre lumen x350.

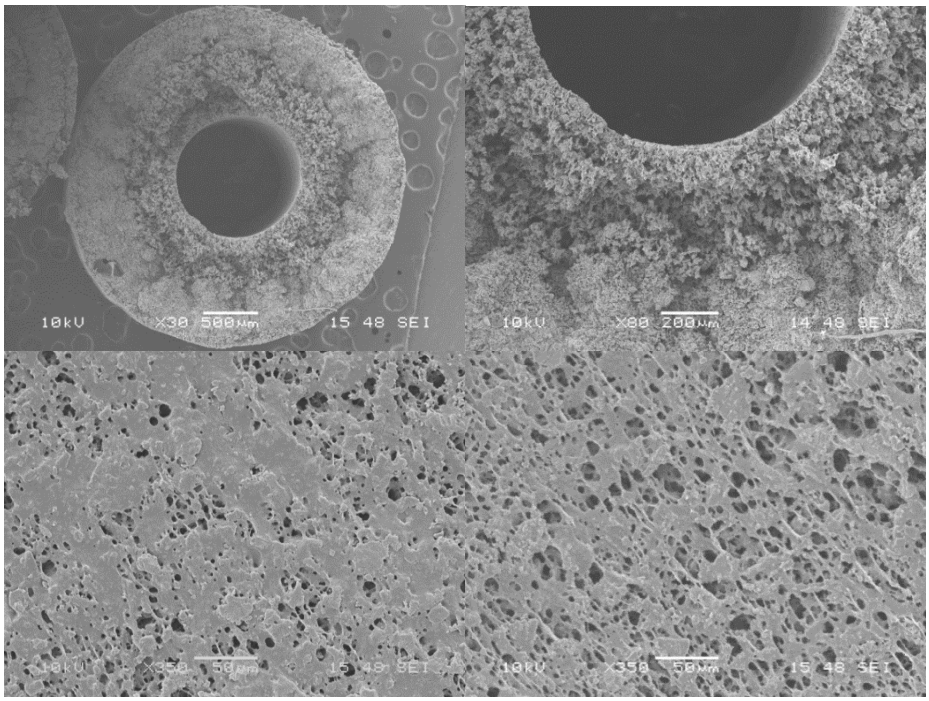

Figure 5.20. Licowax SP fibres under SEM. Top: Cross section x 30 and x80. Bottom left: outside of fibre x350. Bottom right: fibre lumen x350.

5.2.7.2 Licowax SP incorporated fibres for adsorption of cyclohexane

Fibres with Licowax SP pore former had higher and faster cyclohexane uptake than fibres with no pore former. The Licowax SP pore former showed greater improvements than the Micropore C, so was incorporated into hybrid fibres and dynamically challenged with 1 L/min 100 ppm cyclohexane, shown in Figure 5.21.

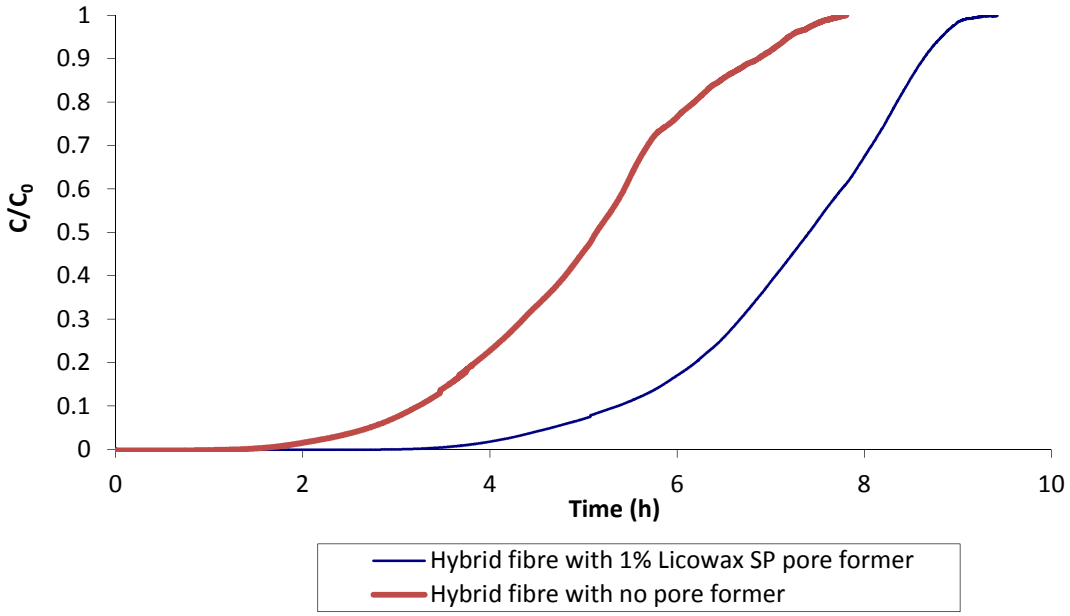

Figure 5.21. 1000 ppm 1 L/min dynamic cyclohexane test for 10 cm modules of 50/50 hybrid AbScents1000/NV5 carbon fibres with and without pore former.

Table 5.7. Breakthrough and equilibrium values for 1000 ppm 1 L/min dynamic cyclohexane test on 10 cm modules of 50/50 hybrid AbScents1000/NV5 carbon fibres with and without pore former.

	Adsorbent wt (g)	Breakthrough time (h)	Breakthrough loading (%)	Equilibrium time (h)	Equilibrium loading (%)	Length of unused bed (cm)	Mass transfer zone (cm)
Hybrid with no pore former	6.83	1.86	6.23%	7.81	15.12%	6.31	11.82
Hybrid with pore former	9.44	3.76	8.16%	9.42	15.66%	4.79	7.86

Figure 5.21 demonstrates that incorporating 1% Licowax SP pore former was sufficient to significantly increase breakthrough time over the fibre module with no pore former. It can be seen in Table 5.7 that the breakthrough loading was significantly increased for the module that included Licowax SP pore former, from 6.23 to 8.16%. However, the equilibrium loading was approximately the same for the two, indicating that while the

kinetics were improved, resulting in greater breakthrough time and hence loading, the overall capacity per weight was unchanged.

5.2.7.3 Licowax SP incorporated fibres for adsorption of ammonia

Given the improvements in cyclohexane uptake and kinetics seen in fibres with Licowax SP, it was also tested with ammonia. Licowax SP was incorporated at 1% wt into 80% hybrid NV5/AbScents1000 fibres with standard bore and single layer and tested dynamically with 1 L/min 800 ppm ammonia. The results are shown in Figure 5.22 and Table 5.8.

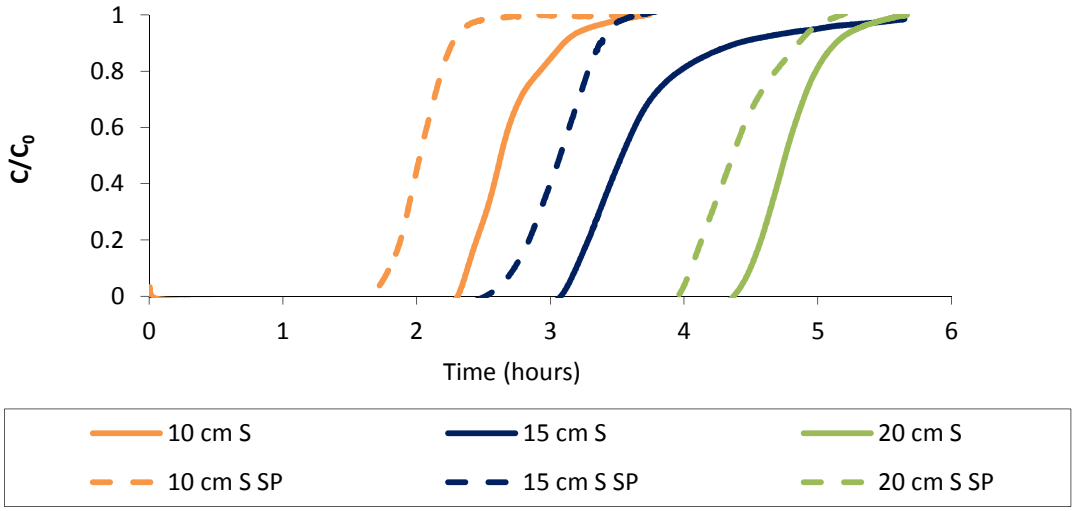

Figure 5.22. 800 ppm 1 L/min ammonia dynamic challenge on hybrid single layer standard bore fibres with and without pore former. The "S" after the length indicates single layer fibre. "S SP" indicates single layer with Licowax SP pore former.

Table 5.8. Breakthrough and equilibrium loading of ammonia on hybrid NV5/AbScents1000 fibres with and without pore former.

	Fibre with pore former	**Fibre without pore former**
Average breakthrough loading	0.67%	0.92%
Average equilibrium loading	0.76%	1.02%

Fibres incorporating pore formers, contrary to previous cyclohexane tests, showed a slight decrease in ammonia breakthrough time and loading when challenged. While the presence of Licowax SP greatly enhanced adsorption of cyclohexane on hybrid 50/50 NV5/AbScents1000 fibres, it hindered adsorption of ammonia.

5.3 Discussion

In this Chapter, a variety of techniques to enhance fibre adsorption were explored. In the previous Chapter, poor hydrogen sulphide adsorption was observed on all fibres, but this could be improved by impregnating the adsorbent with metal salts. There are many ways to impregnate granules, which were explored in the literature review, but only some of these are suitable for fibres. As an example, percolation adsorption would be difficult in the case of fibres, and was the technique used by the company Eurocarb to impregnate several samples, damaging them in the process. Suitable ways to include an impregnant in fibre modules were explored in this Chapter. Firstly, fibres were prepared using commercial impregnated carbons that had been ground down to powders. These were difficult to spin and required additional zeolite to stabilise the structure of the fibre, and this resulted in decreased loading by weight compared to an equivalent volume granular bed. Interestingly, fibres coated at Eurocarb with the adsorbents used on the RGE granules had a loading of 1.69%, which is very similar to that of the granules, so the fibre structure does not seem to introduce any inherent difference to available impregnant. In addition, the spinning process appeared to result in the loss of soluble salts, with no iodine detected in the fibre that should have been impregnated with KI. It is possible that exposure to water in the spinning process changed the impregnant such that the fibres spun from RGE carbon had higher loading. The potential loss or change of impregnants limits the possibility of spinning fibres from commercial carbons to those that have insoluble impregnants, such as CuO.

The method of incorporating metal salts into fibres was also investigated. CuO incorporation was not found to significantly enhance the breakthrough time or loading of the fibres. A granular bed with the same powder incorporated into it also showed no improvement in adsorption of H_2S over one without. This suggests that particle size and distribution of incorporated salts are likely to be the problem in this case. CuO is relatively dense, and so the small amount of dense large particles, added by percent weight, would not have spread well through the structure. They would also have a much

lower surface area than that of smaller particles. If evenly dispersed nanoparticles were used, this may make incorporation of metal salts more viable. However, these are expensive.

Fibres were also impregnated with metal salt after being spun. Excess soaking and dry impregnation were used in this Chapter successfully and found to outperform a sample that had been spray coated at Eurocarb. This is because most of the spray would coat the exterior of the fibre, while the contaminant would largely be on the interior of the fibres. In practical terms, this part of the fibre would be difficult to spray evenly. CuO impregnated fibres were prepared via several steps, which demonstrated the viability of impregnating fibres with insoluble salts in some cases. CuO impregnation was found to significantly enhance H_2S adsorption. As such, impregnating fibres after spinning was determined to be the best and most flexible way to impregnate adsorbent fibres with a range of salts, soluble or insoluble. While the use of an impregnated precursor to spin fibres is possible, this is limited to insoluble impregnants only, and some loss of adsorption will occur, most likely due to the presence of polymer in the fibre structure, which blocks access to some components (Nevell and Perera, 2011).

A metal organic framework impregnant, copper benzenetricarboxylate, was compared with a metal salt impregnant, copper (II) oxide. The crystalline structure of the MOF was confirmed by XRD. This MOF did not impregnate well on to the fibre. This poor adhesion has been observed in a previous study with clay monoliths (Küsgens *et al.*, 2010). To address this, Küsgens *et al* incorporated the MOF into the structure in large quantities. This solution is not possible for this work, as most MOFs are not stable in water and so would break down during the spinning process. Breakthrough tests comparing the 10% CuO loaded fibre to the 3% loaded CuBTC fibre showed similar breakthrough loading, of 2.91% wt impregnant for the CuBTC and 3.75% wt impregnant for the CuO, and 0.44 h/g impregnant breakthrough time for CuBTC and 0.56 h/g impregnant for CuO. Previous work suggests a loading of 92 mg/g H_2S on CuBTC (Petit *et al.*, 2010), which is higher than the value from this work of 31.25 mg/g, although they used a different synthesis technique (Millward and Yaghi, 2005) to produce their CuBTC. In their work they also performed XRD on CuBTC samples before and after exposure to H_2S and H_2O, which revealed the loss of crystalline structure after exposure to both gases (Petit *et al.*, 2010). However it should be noted that in their paper they assumed that

CuBTC was water stable. The work of Gul-E-Noor *et al.*, (2011) suggested that CuBTC decomposed when exposed to large quantities of water. However, as little decomposition was seen at low amounts (0.5 moles water) up to 60 days later and ambient humidity was all that was used by Petit *et al.*, it was assumed that H_2S was largely responsible for the loss in crystalline structure. A more recent study (Gutierrez-Sevillano *et al.*, 2013) has suggested that H_2S should not cause the breakdown of CuBTC in the presence of water, as the interaction between H_2O and CuBTC is much stronger than between H_2S and CuBTC. However, they suggested no mechanism for this interaction. Petit and Bandosz, 2012, suggested that the electron lone pair of the H_2S coordinates to the unsaturated copper sites on the CuBTC, forming CuS and resulting in the breakdown of the framework and subsequent loss of porosity. A similar interaction was suggested for CuBTC exposed to NH_3, with $Cu(NH_3)^{4+}$ as a product, again resulting in loss of porosity. These reactions were evidenced by the irreversible colour change of the MOF, which was also observed in this work.

One other area to consider is the effect of the impregnant on adsorption of other toxic gases of interest. Cyclohexane DVS tests were performed on CuO and CuBTC impregnated fibres and compared to unimpregnated fibre. CuO has no particular interaction with cyclohexane, and as such the uptake of the impregnated fibre was found to be lower in w/w% than the unimpregnated. This was because the CuO that was not contributing to adsorption of cyclohexane. It is in fact likely to block access to the pores of the fibre. One surprising observation was that the CuBTC adsorbed cyclohexane very well, up to 40 w/w% loading, while the CuBTC impregnated fibre took up very little cyclohexane – even less than the CuO impregnated fibre. Given the low % impregnation of CuBTC, and the fact that the MOF did not appear to break down during the cyclohexane isotherm, this is particularly surprising. Further tests to elucidate this will be necessary, and are discussed in the Future work Section.

No significant improvement was seen in adsorption of H_2S on CuBTC compared to CuO, and the CuBTC decomposed on exposure to H_2S and H_2O. Further, CuBTC did not enhance loading of other TICs, even though it would be expected to. Given these facts, metal salt impregnants were determined from this work to be superior for use on hollow fibre filters for respirators. While adsorption loading was similar for CuBTC and CuO, the CuO is lower in cost and simpler to impregnate than the CuBTC. However, future

work with MOF impregnants that will not decompose when exposed to common TICs should be evaluated on a case by case basis, taking into consideration the pitfalls associated with their use and consistency of results.

This Chapter also evaluated the use of pore formers to enhance adsorption of ammonia and cyclohexane on adsorbent hollow fibres. Pore formers have been used in previous work on adsorbent monolith structures, or monoliths for catalyst support (Baraton and Uvarova, 2001). In these applications a wide variety of pore formers can be used due to the high heat stability of ceramic monoliths. The options are more limited for polymer fibres, with no information available in the literature for use in adsorbent hollow fibres. Two waxes available from Clariant; a montan wax acid, Licowax S; and bis stearyl ethylenediamine, Licowax C (Clariant, 2012), were used, possibly for the first time, as pore formers in hollow fibres. They were suitable due to their low melting temperatures, resulting in the formation of pores throughout the fibre structure. This was found to enhance overall loading of cyclohexane on fibres as well as the speed of its uptake in Section 5.2.7.2. This was also reflected in breakthrough tests with longer breakthrough time and shorter mass transfer zones for cyclohexane tests. However, the opposite was seen to be the case when fibres with 1% wt pore former were dynamically challenged with ammonia. In general, higher ammonia uptake would be expected in smaller pores (Yu *et al.*, 2012). However, the Licowax S had the larger particle diameter of the pore formers tested. It is likely that the large pores it developed favoured adsorption of large molecules, such as cyclohexane but inhibited that of small molecules, such as ammonia. This characteristic could be useful for adsorption of other molecules with a bulky ring structure, but negative for smaller molecules. Licowax S was selected as a pore former to test extensively due to its excellent performance with cyclohexane but in future, to enhance the uptake of ammonia, the incorporation of other pore formers with smaller particle size may be helpful. For example the other pore former tested, Licowax C.

5.4 Conclusions

This Chapter has shown that adsorbent hollow fibres can be modified to include metal salts, which enhanced their adsorption performance over untreated fibres. The most effective method to do this was by impregnation of the fibres after spinning.

The possibility of using MOFs as impregnants was explored using CuBTC as a model and compared to a metal salt impregnant, CuO.

- Adsorbent pellets were successfully impregnated with this MOF, which enhanced their adsorption capacity for H_2S from 0.31% wt to 2.62%wt. However, this adsorption was greatly attenuated in the presence of even ambient levels of humidity.
- MOF CuBTC impregnated fibres had slightly lower H_2S loading than CuO impregnated fibres when corrected for weight (2.91 w.w% and 3.75 w/w% respectively). In addition, the adhesion of the MOF to the fibres was poor.
- CuBTC impregnated fibres had low uptake (10 w/w%) of cyclohexane despite the relatively high loading (40 w/w%) of cyclohexane on CuBTC powder.

Due to the effects of humidity and the cost, MOFs may not be ideal impregnants for adsorbent hollow fibres in respirators at present. Metal salt impregnation of adsorbent hollow fibres could be used to effectively tailor adsorbent fibres to sorb TICs that are not effectively removed by adsorbent alone, such as H_2S. However, they may interfere with adsorption of other TICs.

Incorporating pore formers into adsorbent hollow fibre structures was also investigated. Licowax S, a montanic wax acid, was found to enhance loading and uptake of large nonpolar molecules such as cyclohexane, but had a negative effect on adsorption of small polar molecules, reducing ammonia loading. Pore formers with different particle sizes (such as Licowax C) are likely to affect adsorption of different gases in different ways. Whether or not a pore former should be included, and what type, will vary depending upon the specific requirements of the respirator and should be factored into future design work.

6 Novel polymers of intrinsic microporosity for enhanced adsorption in adsorbent hollow fibres

6.1 Introduction

While polyethersulfone was typically used as the binder in adsorbent hollow fibres, some issues are associated with its use. These include a reduction in adsorption capacity per unit volume and slowed adsorption kinetics due to PES blocking access to adsorbent sites. Polymers of intrinsic microporosity (PIMs) offer an alternative to PES, with the potential to increase the adsorption of the composite fibre through use of a porous polymer support (Budd *et al.*, 2005b).

6.1.1 Polymers of intrinsic microporosity in adsorbent hollow fibres

PIMs are polymers with intrinsic microporosity, and further detail can be found in Section 2.1.6.2. In this Chapter, composite hollow fibres containing a microporous carbon (Eurocarb, UK, NV5 carbon) with either PES or PIM-1 as the polymer binder were prepared and characterised. Initially, composite fibres were prepared in a ratio of 40% polymer to 60% carbon (on a mass basis) as opposed to the standard 20% polymer to 80% adsorbent, in order to ensure they would successfully spin. Once this was successful, PIM fibres were prepared in the 20% polymer to 80% adsorbent ratio typical to the PES fibres tested in this study. The PIM and PES fibres were characterised by scanning electron microscopy and nitrogen, octane and water adsorption isotherms. Octane breakthrough tests were performed on the two different fibres types.

6.1.2 Adjusting the external coagulant in the spinning process

When fibres are spun, a dense layer forms where coagulation is occurring (Baker, 2012). In membranes, this is essential for a selective effect, however in adsorbent hollow fibres this is not ideal, as a dense skin will present a barrier for diffusion, causing resistance. The composition of the coagulating bore fluid, typically water, can be varied, for example by adding solvent. Solvent concentrations of 30-90% in the bore fluid have been reported to increase the inner porosity and even prevent the formation of a skin layer (Xu and Alsalhy Qusay, 2004). This is ideal for the inner skin of adsorbent hollow fibres, but could also be helpful on the external skin, as adsorption can also take place, particularly when wall effects are significant, as explored in Chapter 4. As such, methods to improve

adsorption kinetics on PIM-1 fibres were explored further by spinning fibres into an external coagulating fluid that was a 1:1 mixture of solvent:water by the techniques described in Section 3.2.1.3.

6.2 Results

6.2.1 Characterisation of PIM and PES composite fibres

6.2.1.1 Scanning electron microscopy

Macrovoids were apparent in the PES fibres (Figure 6.1 a) and b)). These are formed as the solvent (NMP) leaves the PES fibre during the spinning process. For the PIM-1 only fibres, a much denser structure was observed ((Figure 6.1 c) and d)). The structures of these fibres were affected strongly by the polymer to solvent ratio and the spinning process. This process has been refined for PES polymer fibres, with macrovoids or micropores intentionally formed to improve mass transfer and enhance the accessibility of the adsorbent. However, further refinement of the spinning parameters of the PIM-1 fibres is necessary to optimise the structure. The carbon composite fibre micrographs (Figure 6.2 a) and b)) show that the PES and microporous carbon particles were well mixed and macrovoids were present. On the other hand the PIM-1 composite fibres (Figure 6.2 c) and d)), appeared comparatively dense at low magnification.

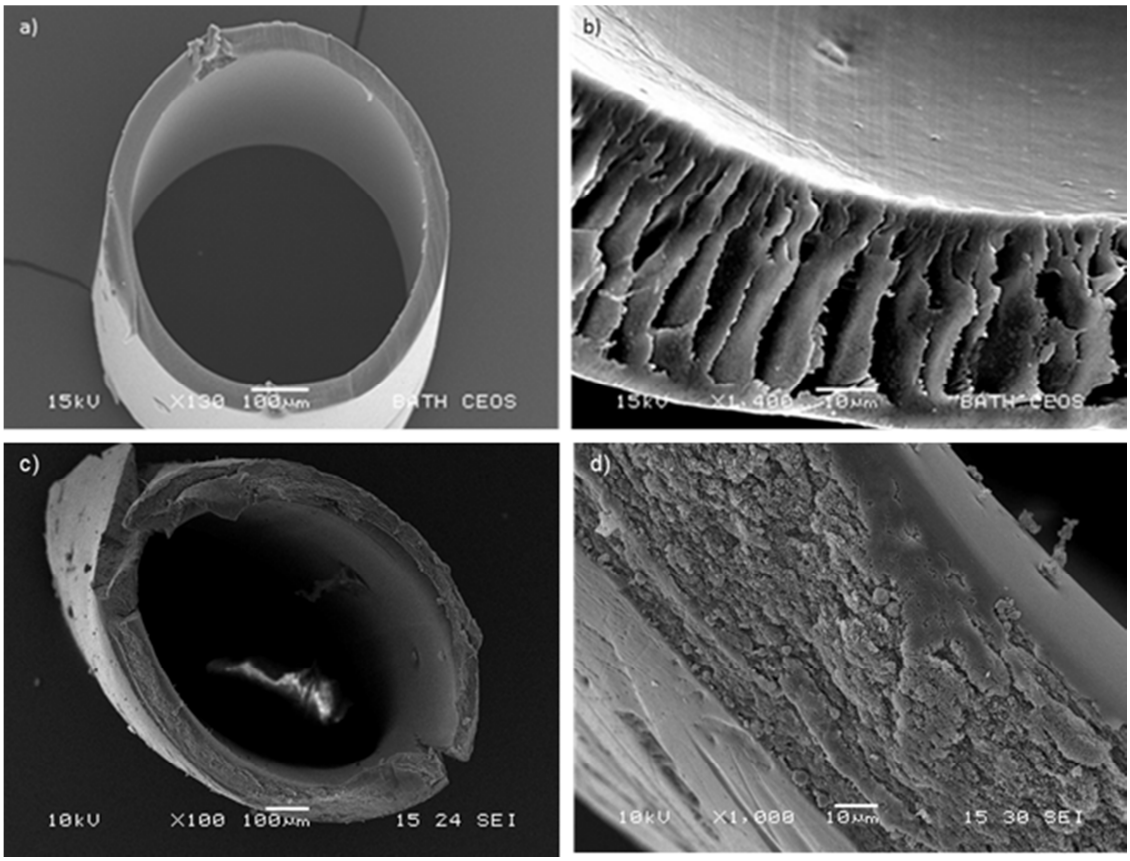

Figure 6.1. PES-only hollow fibre cross section a) x100 b) x1400. PIM-1-only hollow fibre cross section c) x100 d) x1000.

When examined at a higher magnification, activated carbon particles were seen embedded within the polymer matrix of the PES composite fibre (Figure 6.3 a)) and only those on the surface are visible, indicating that sorption capacity may be reduced as a result. Such coverage by the polymer binder could lead to underutilisation of adsorbent hollow fibre capacity due to high mass transfer resistance. A higher magnification of the fibre cross section shows that the inner walls of the PIM-1 composite fibres had a highly porous structure and individual carbon particles can be observed throughout the polymer matrix (Figure 6.3 b)). This suggests that due to the microporous nature of the PIM-1, vapour would be able to reach the entire fibre structure through these small channels.

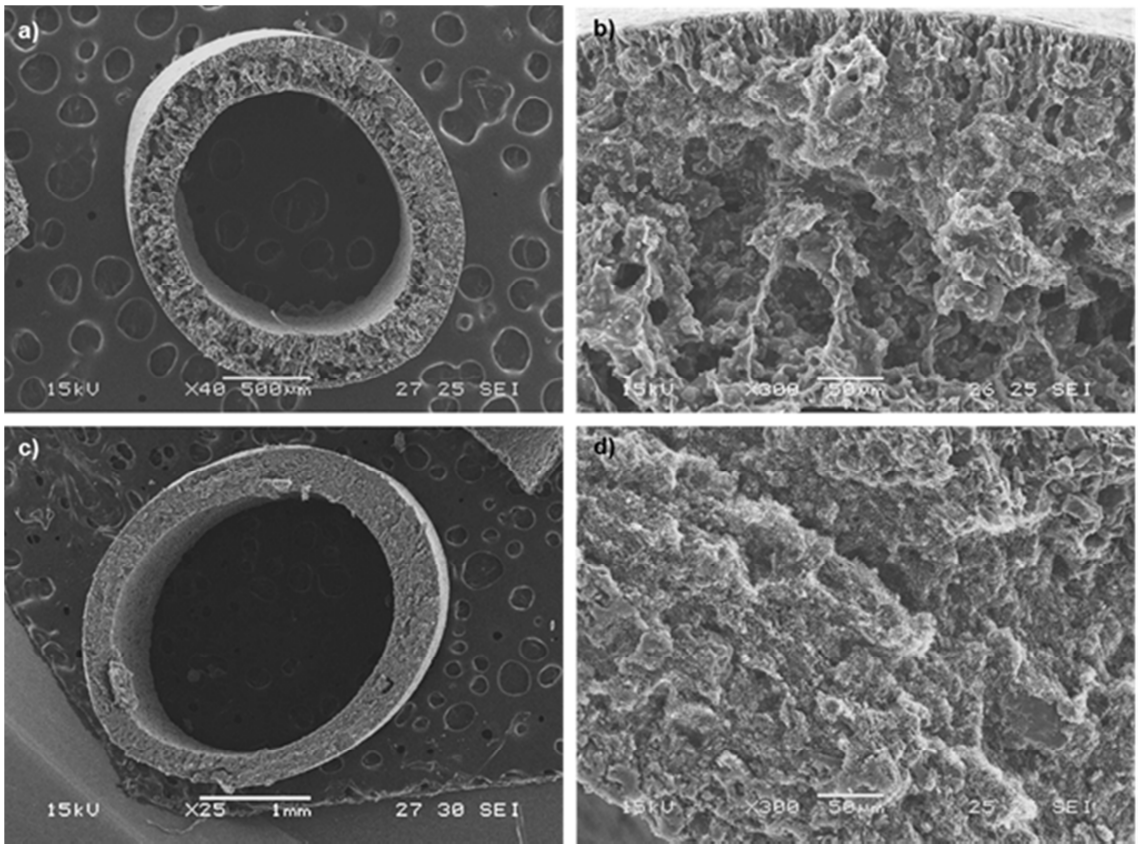

Figure 6.2. PES Composite hollow fibre a) cross section x40 b) cross section x 300; PIM-1 composite hollow fibre a) cross section x25, b) cross section x300.

As well as investigating the difference between PES and PIM-1 fibres, the preparation methods for PIM-1 fibres were studied. Soaking with methanol has been found to increase the gas permeability of PIM-1 (Budd *et al.*, 2008). As such, PIM-1 only fibre was spun directly into methanol and then some of this fibre was kept under methanol while the rest was transferred and stored under water. SEM images show the magnified cross section of these fibres in Figure 6.3 c) and d). While a highly porous nodular structure was clearly visible for the fibre kept under methanol, the fibre exposed to water showed a highly dense connected layer with agglomerated polymer particles formed in the structure. This would suggest that for optimal performance, PIM-1 fibres should be treated with methanol prior to testing.

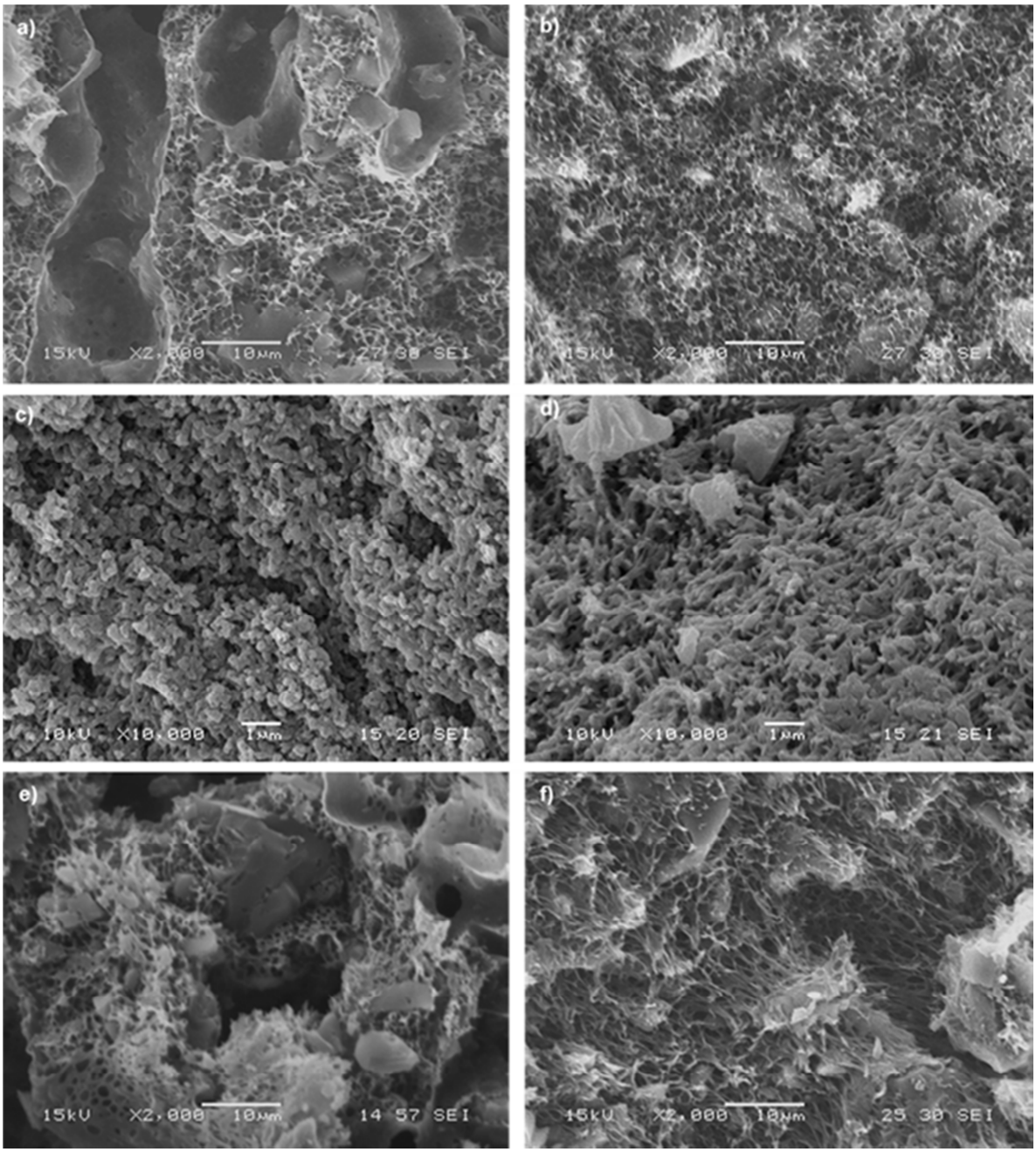

Figure 6.3. Inner walls of composite hollow fibres. a) PES composite hollow fibre x2000 b) PIM-1 composite hollow fibre x2000 demonstrating visible carbon particles c) x10000 magnification of the inner wall of a PIM-1 fibre stored under methanol d) x10000 magnification of the inner wall of a PIM-1 fibre stored under distilled water e) x2000 magnification of the inner wall structure of PES/carbon fibre heated to 190°C for 24 hours f) x2000 magnification of the structure of PIM/carbon fibre heated to 150°C for 24 hours.

In order to fully utilise these fibres for separation processes, heat treatment was required to remove any solvent or water remaining from the spinning process. The influence of this heat treatment on the freshly manufactured carbon/polymer fibre structures was investigated. The morphologies of carbon/PES and carbon/PIM composite hollow fibres

after heat treatment at 190 °C and 150 °C (Figure 6.3 e) and f) respectively), were compared with unheated fibres (Figure 6.3 a) and b) respectively). These images revealed that the morphology changed with the heat treatment conditions. As expected, for the PES fibres which were heat treated at 190 ºC, the polymer structure shrank and became nodular (Figure 6.3e). This suggests that a regeneration temperature of 190 ºC can enhance accessibility of carbon particle adsorption sites, which was confirmed by a slight increase in BET surface area from 836 to 885 m^2 g^{-1}. However, it is very important to keep the heat treatment temperature below the glass transition temperature of the polymer since the polymer will slowly degrade if the temperature goes beyond the T_g leading to loss of strength. The heated PIM-1 composite fibre (Figure 6.3f)), showed a different structure compared to the unheated structure (Figure 6.3).

6.2.1.2 Nitrogen isotherms

Nitrogen isotherms relating to PES materials are shown in Figure 6.4 and are typical for a non-porous material. PES fibre and powder had low apparent BET surface areas of 22 m^2 g^{-1} and 62 m^2 g^{-1} respectively. The PES powder showed unusual reverse hysteresis, with the desorption curve below the adsorption curve at high pressure. It is possible that this could be associated with the loss of excess free volume from the polymer during N_2 adsorption. The lower apparent porosity for the PES fibre suggests the fibre spinning process reduces the accessibility to the small degree of meso- and macroporosity demonstrated by the powdered material, consistent with the unconnected pores seen in the SEM micrographs (Figure 6.3 a and b). The isotherm for NV5 carbon was Type I according to IUPAC classification, typical for a predominantly microporous material, with BET surface area of 1634 m^2 g^{-1} (Figure 6.4). A comparison of the calculated isotherm for the weighted average for the PES composite fibre (in grey) with the measured isotherm, demonstrates that the nitrogen adsorption ratio of observed: predicted was ~ 0.81-0.87: 1 across the pressure range. This suggests that adsorption sites were being blocked by the presence of the polymer matrix.

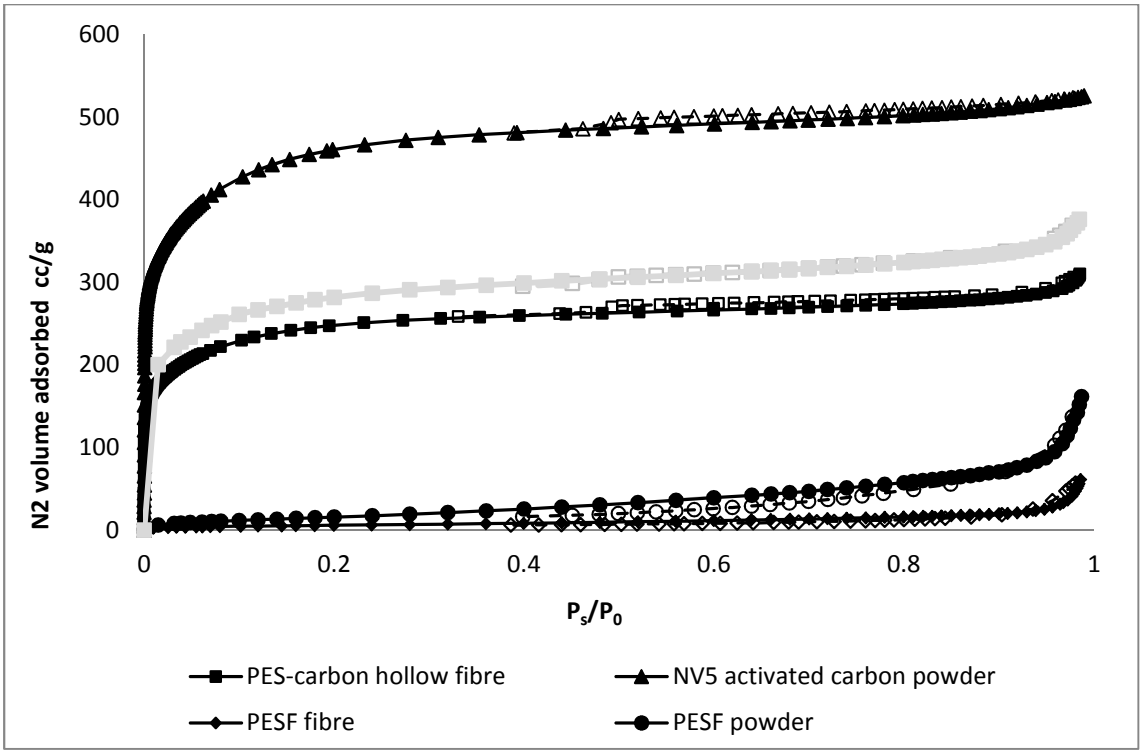

Figure 6.4. N_2 adsorption (filled shapes/solid line) and desorption (empty shapes/dashed line) isotherms at 77K. Lines in grey indicate weighted average isotherms for a 40:60 mix of PES fibre and NV5 carbon (characterised at University of Cardiff).

The N_2 isotherm of powdered PIM-1 (Figure 6.5) was consistent with that of a predominantly microporous material with a BET surface area of 720 m^2 g^{-1}. The pronounced hysteresis between adsorption and desorption isotherms was ascribed to swelling of the polymer as it adsorbed nitrogen (McKeown *et al.*, 2005). The N_2 isotherm of a 40: 60 mixture of PIM-1 and NV5 carbon powder, prepared by suspending the carbon in a THF solution of PIM-1 and removing the solvent under reduced pressure (Figure 6.5), is similar to the calculated isotherm based on the values for the two pure materials. The N_2 isotherm of the adsorbent hollow fibre composite of PIM-1 and NV5 carbon is shown in Figure 6.6. The weighted average of the nitrogen sorption isotherms of the pure materials was also plotted and this matched precisely the experimental isotherm for the composite fibre. This suggests there was no interference to the high sorption capacity of the NV5 carbon from the PIM-1 polymer, or from the adsorbent hollow fibre spinning process.

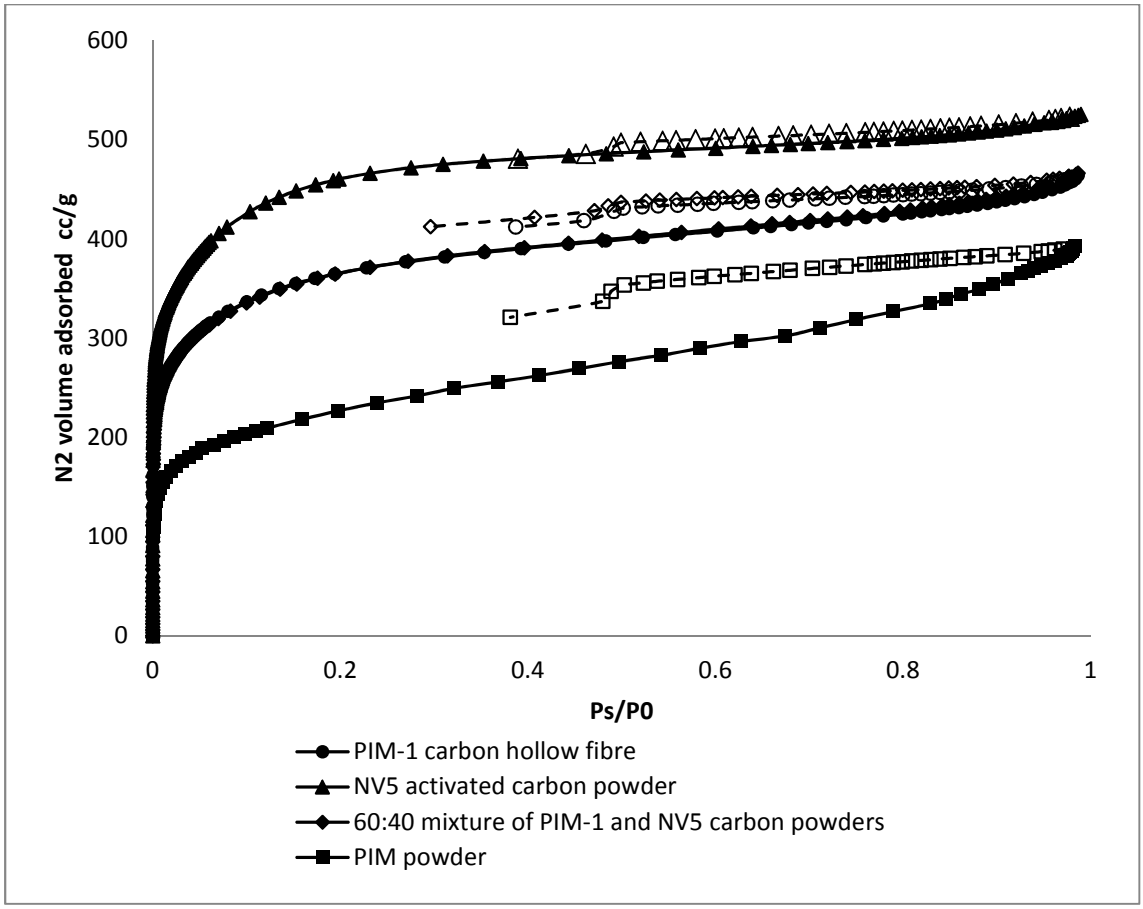

Figure 6.5. N_2 adsorption (filled shapes/solid line) and desorption (empty shapes/dashed line) isotherms at 77K. Note that the adsorption isotherms for PIM-1-carbon hollow fibre and 60:40 mixture of PIM-1 and NV5 carbon powders are superimposed (characterised at University of Cardiff).

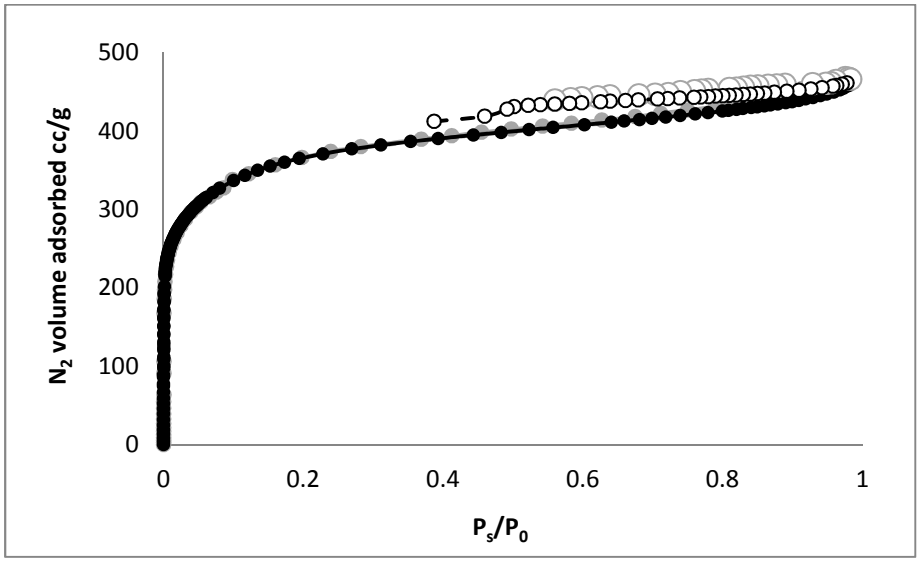

Figure 6.6. N_2 adsorption (filled shapes/solid line) and desorption (empty shapes/dashed line) isotherms at 77K PIM-1-carbon hollow fibre with a weighted average line for the composite fibre shown in grey. Note the isotherms are almost fully superimposed (characterised at University of Cardiff).

Theoretical surface area was determined in the same way as theoretical sorption. While the surface area of the PIM-1 composite fibre was as would be expected for a mixture of the two powders, the PES composite fibre showed significantly less surface area than would be anticipated and suggesting interference from PES. Importantly, the overall BET surface area of PIM-1/NV5 composite was much higher (1304 m^2 g^{-1}) that that of the PES/NV5 composite (885 m^2 g^{-1}).

Table 6.1 Theoretical and measured BET surface areas of adsorbent hollow fibres.

	PES/ NV5 fibre	**PIM/ NV5 fibre**
Weighted mean surface area (m^2 g^{-1})	1005	1300
Measured BET surface area (m^2 g^{-1})	885	1304

6.2.1.3 Octane isotherms

To confirm the observations from the nitrogen isotherms, octane adsorption isotherms at 298 K were determined for PES powder, PIM powder, NV5 carbon and composite hollow fibres of both polymers. Figure 6.7 shows the low octane adsorption of PES powder compared to the high adsorption capacity of NV5 carbon powder. The observed octane isotherm for the PES composite hollow fibre isotherm (Figure 6.7) was between that of the pure adsorbent and binder isotherms. However the calculated weighted average of adsorbent and binder was higher. The ratio of the observed line to the weighted average was ~0.82-0.86 across the whole isotherm, a number strikingly similar to the ratio observed for the nitrogen isotherms (~0.81-0.87) and to the ratio between calculated and observed BET surface area (0.88).

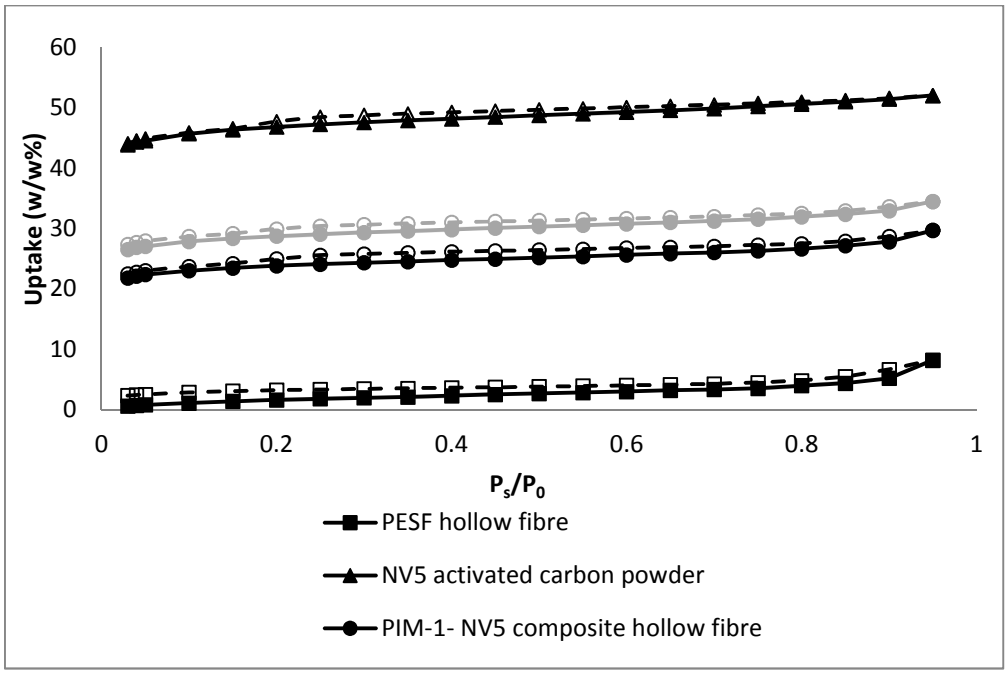

Figure 6.7. Octane adsorption (filled shapes/solid line) and desorption (empty shapes/dashed line) isotherms at 298 K. The weighted average isotherm for the hollow fibres is shown in grey (characterised at Dstl).

In contrast, the octane isotherm of PIM-1 (Figure 6.8) demonstrated a high uptake of octane, especially at higher pressures, which may be related to swelling. This suggests adsorption capacity may be improved by incorporating PIM-1 into adsorption beds intended to sorb organics. This performance is also reflected in the isotherm of the composite fibre (Figure 6.9), which had a high uptake, between that of the pure carbon and the PIM-1 isotherms. At saturation, the PIM-1/NV5 composite fibres sorbed almost twice as much octane as the PES/NV5 fibres. The octane isotherm of the PIM-1/NV5 composite hollow fibres was almost identical to the calculated weighted average derived from the octane isotherms of the pure materials, indicating that the PIM-1 polymer did not hinder the adsorptive performance of the carbon. The fact that the octane isotherm may be predicted so accurately by combining the individual PIM-1 isotherm and that of the adsorbent in the ratio at which they are combined could potentially be very useful for tailoring adsorbent hollow fibres with the desired uptake performance.

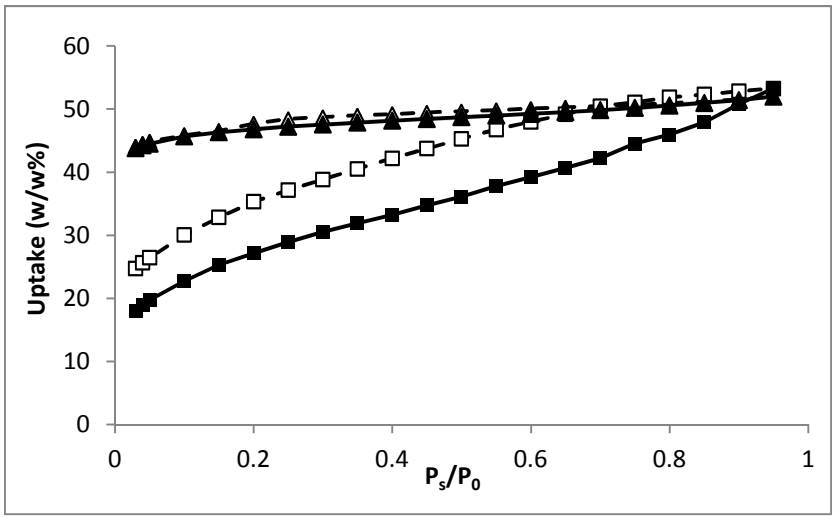

Figure 6.8. Octane adsorption (filled shapes/solid line) and desorption (empty shapes/dashed line) isotherms at 298 K (characterised at Dstl).

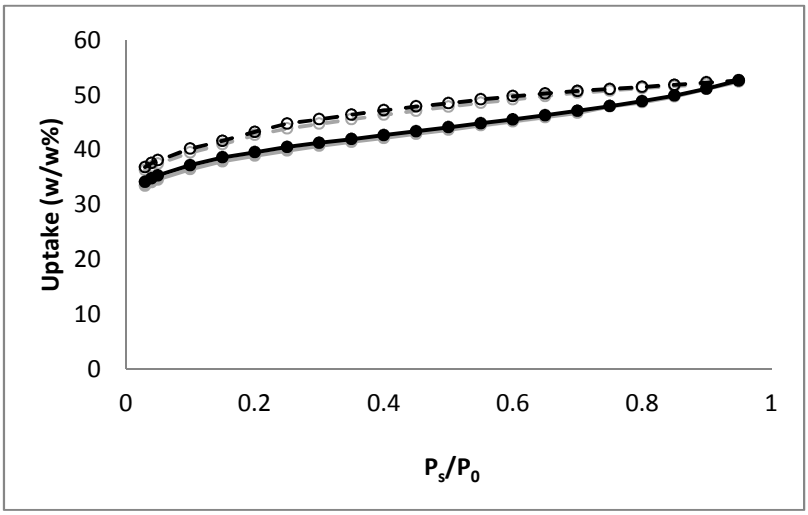

Figure 6.9. Octane adsorption (filled shapes/solid line) and desorption (empty shapes/dashed line) of PIM1: NV5 carbon composite hollow fibre at 298K. Observed adsorption is shown in black while weighted average adsorption is shown in grey. Note the isotherms are almost fully superimposed (characterised at Dstl).

6.2.1.4 Water isotherms

To further elucidate the structure of the composite fibres, water sorption isotherms were measured. The NV5 carbon took up a very high mass of water at high relative pressure, which was observed in both composite fibres. However, the composite PES fibre took up less than would be expected at high relative humidity (Figure 6.10). PIM-1 was shown to be hydrophobic even at high relative humidity in Figure 6.11, as has been found previously by different methods (Cheremisinoff, 2002). However, the adsorption of the composite fibres matched closely to the weighted average of the two components,

similar to octane. This may indicate greater connectivity between pores for the PIM-1 composite fibre than for the PES.

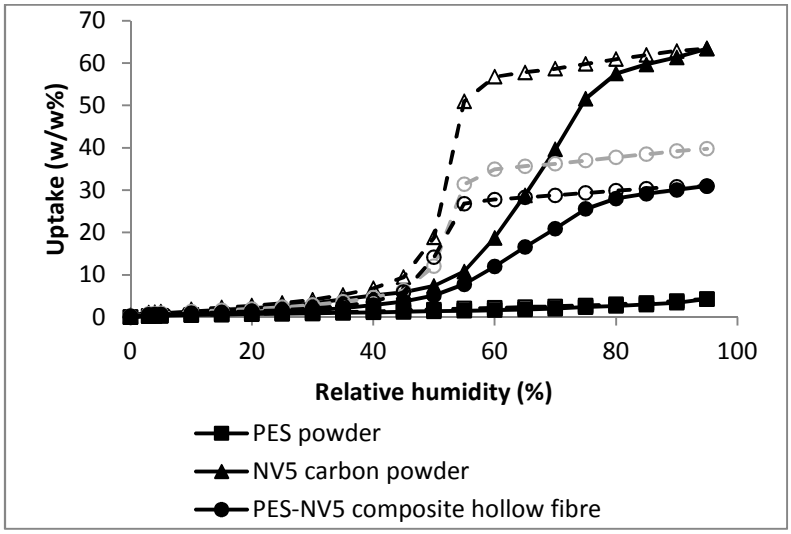

Figure 6.10. Water adsorption (filled shapes/solid line) and desorption (empty shapes/dashed line) isotherms at 298 K of NV5 carbon powder, PES powder and a PES-NV5 carbon composite hollow fibre. The weighted average isotherm for the hollow fibres is shown in grey (characterised at Dstl).

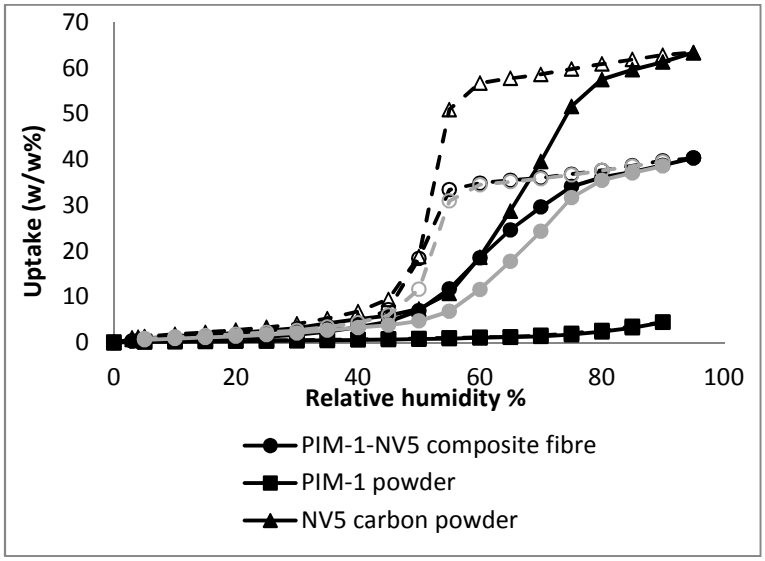

Figure 6.11. Water adsorption (filled shapes/solid line) and desorption (empty shapes/dashed line) isotherms at 298 K of NV5 carbon powder, PIM-1 powder and a PIM-1-NV5 carbon composite hollow fibre. The weighted average isotherm for the hollow fibres is shown in grey (characterised at Dstl).

6.2.2 Dynamic octane adsorption in PIM and PES composite fibres

A 1000 ppm octane breakthrough test was carried out at 0.25 L/min on a 2 x 5 cm module of PIM-1 fibres and PES fibres. This is shown in Figure 6.12. Note that these tests were not run to completion due to the limited quantity of octane available.

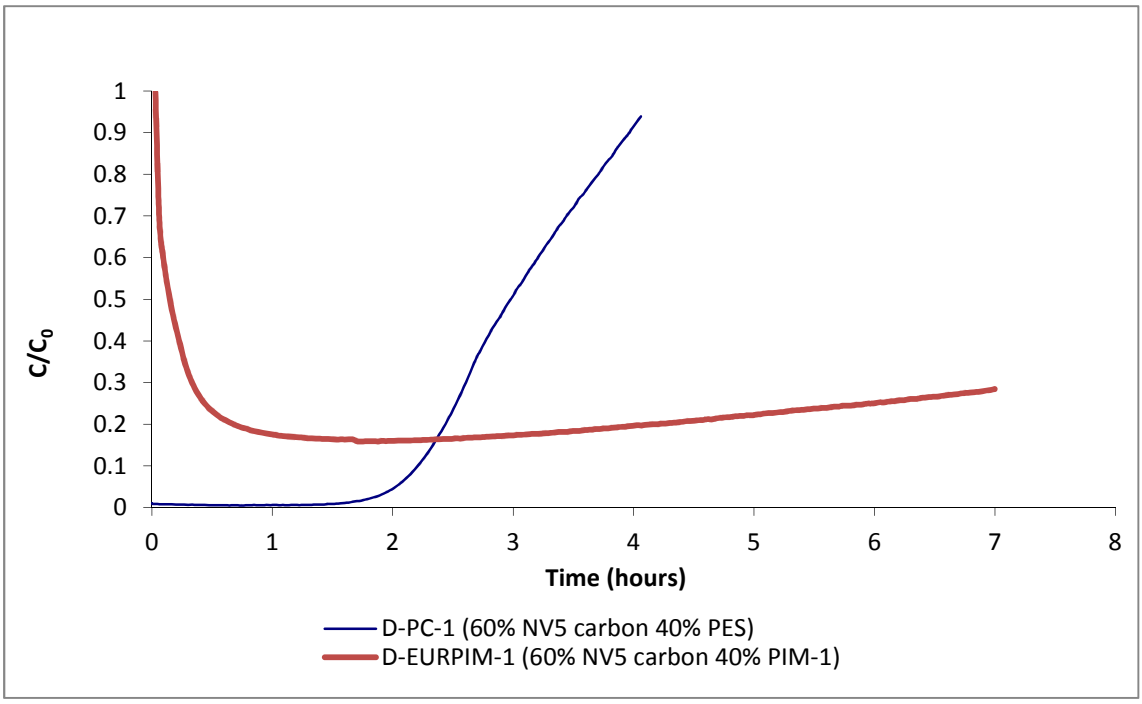

Figure 6.12. 0.25 L/min 1000 ppm octane dynamic challenge on PIM-1/NV5 and PES/NV5 hollow fibres.

Despite the improved loading observed in octane isotherms of PIM-1 fibres and full access to the adsorbent in the PIM fibres (Figure 6.7-Figure 6.9), greater adsorption performance in breakthrough challenge was observed in PES fibres. For PIM-1 fibres, the octane challenge concentration did not go down to 0 ppm (Figure 6.12), making it impossible to determine a 'breakthrough time'. The full curve was not completed for PIM fibres due to the low available quantity of octane. However, it was anticipated that the PIM fibres would eventually load very high quantities, as suggested by the isotherms.

A potential cause for this could be due to the gas bypassing the fibre bundle, which could occur due to the limited availability of PIM-1 fibres. Alternatively, PIM-1 could have poor adsorption kinetics for octane. Poor kinetics have been observed before on PIM-1 as a result of swelling due to water exposure, which was seen to reduce permeability in research carried out on membranes (Budd, 2013). This was thought to be addressed by exposing to methanol prior to testing, although in this case, this was not sufficient. The

hollow fibres were exposed to water while spinning, and as such a new method of spinning was developed to explore this issue.

6.2.3 Refining the spinning process for PES and PIM-1 fibres

Several ways to improve adsorption kinetics in PIM-1 fibres and potentially to improve access to adsorbent in PES fibres were investigated. Some fibres were spun into a solvent/water mixture and others into methanol in order to attempt to improve external porosity. The results are detailed in the Sections below.

6.2.3.1 Enhancing porosity of PES fibres

Initial tests were performed using PES fibres to refine the testing techniques. 50/50 hybrid NV5 carbon and AbScents1000 PES hollow fibres were spun into a measuring cylinder filled with a 50/50 water/NMP mix. This was to enhance the porosity of the outer layer of the fibre, which may in turn improve adsorption kinetics/capacity of adsorbent fibres by ensuring the outer layer of the adsorbent fibre is made use of, as illustrated in Figure 6.13. On the left, some gas travels into the interstitial space between the fibres but is forced down again as it cannot penetrate the thick outer wall of the fibres. On the right gas is able to enter the fibre structure through the more open outer wall where it can be adsorbed.

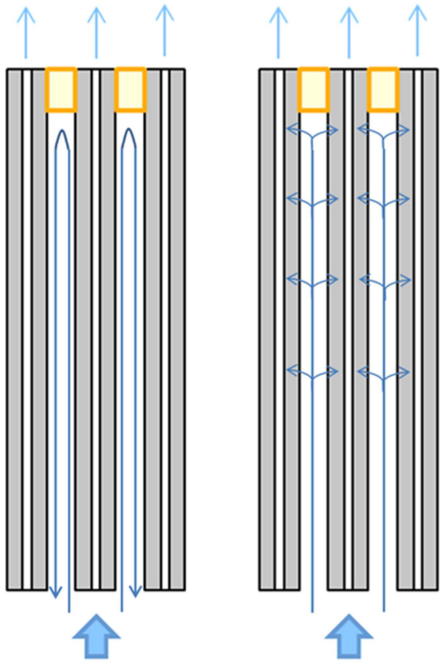

Figure 6.13. Diagram of possible flow pattern in fibre modules (fibres in grey) with blocked (orange) ends.

These were spun by the methods described in Section 3.2.1.3, into an external coagulating fluid of 50/50 water/NMP, similar to the internal coagulating fluid, with no air gap. This technique was used to delay the phase inversion of the fibre. The outer layer of a fibre prepared in this method was compared to one spun by the standard method, into water by SEM, shown in Figure 6.14.

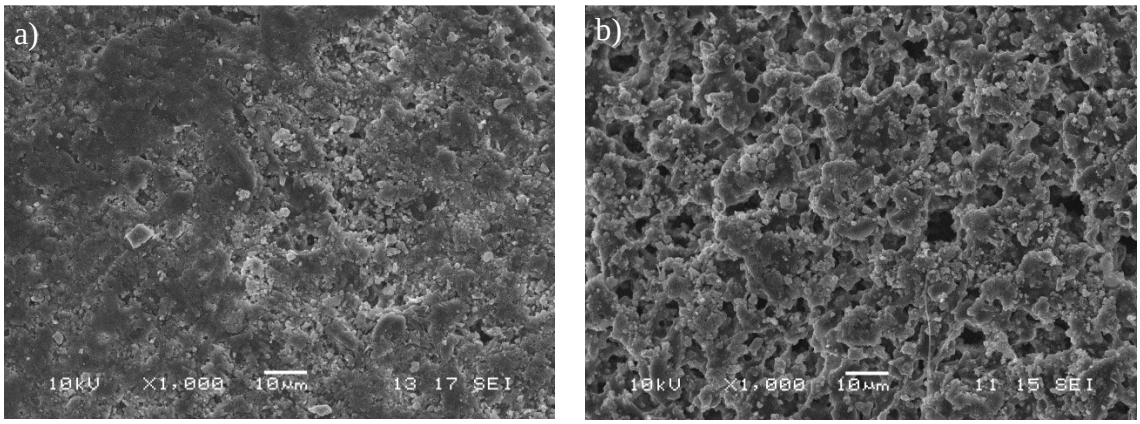

Figure 6.14. x1000 SEM of 20% PES: 80% adsorbent hybrid NV5 carbon/AbScents1000 fibre. a) outer wall of fibre spun into water. b) outer wall of fibre spun into water/solvent

The two outer skin layers were very different, with greater macroporosity seen on the outer layer of the fibre spun into the solvent/water mix compared to the fibre spun into water, which had a very smooth structure with few visible pores.

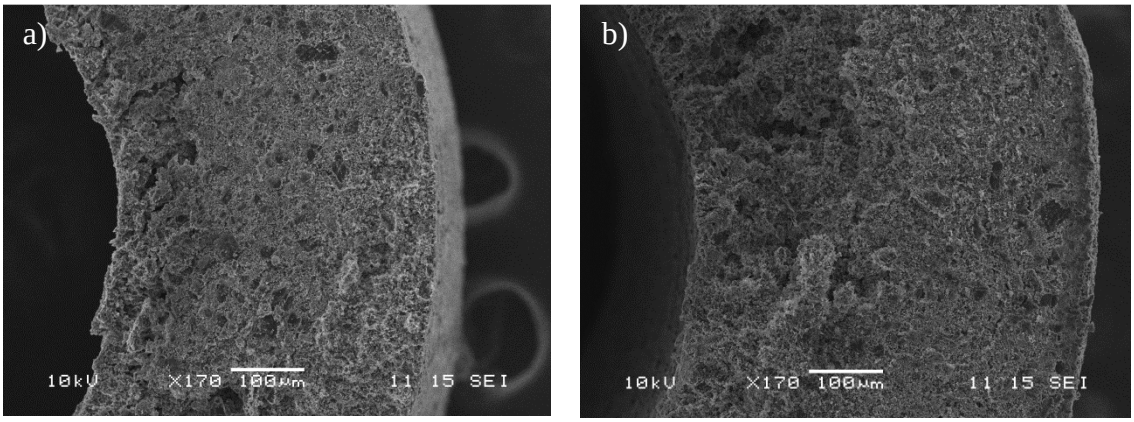

Figure 6.15. x170 SEM of 20% PES: 80% adsorbent hybrid NV5 carbon/AbScents1000 fibre. a) cross section of fibre spun into water. b) cross section of fibre spun into water/solvent

The cross sections of the two appeared similar, with no major changes to the fibre structure observed when spun into a solvent/water mix (Figure 6.15). The outer layer was examined more closely for the fibres spun into water and those spun into solvent/water.

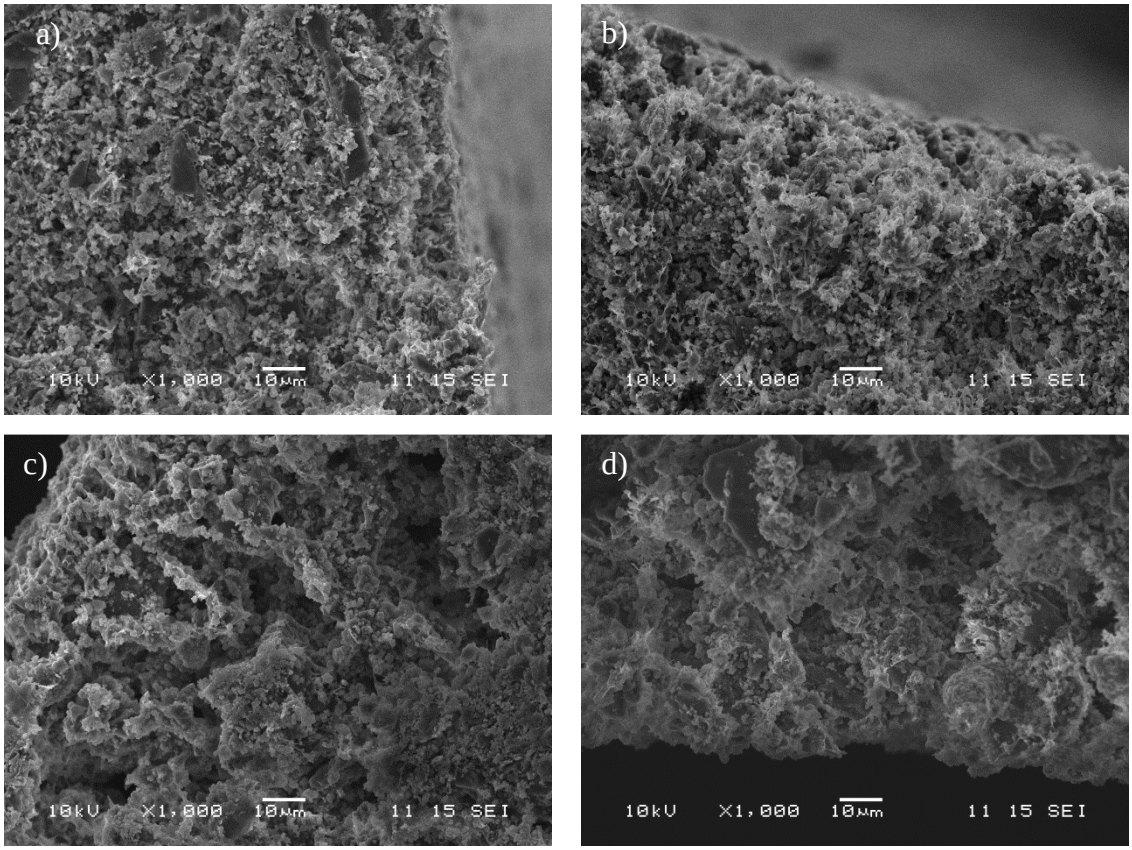

Figure 6.16. x1000 SEMs of 20% PES: 80% adsorbent hybrid NV5 carbon/AbScents1000 fibre. a) outside of cross section of fibre spun into water. b) inside of cross section of fibre spun into water. c) outside cross section of fibre spun into water/solvent. d) inside cross section of fibre spun into water/solvent.

As can be seen in Figure 6.16, there was very little difference visible between the two when examining the outside of the fibre cross sections, with, in both cases, less dense fibre structure around the inside of the cross section compared to that around the outer wall. It would seem that spinning into a solvent/water mix increased the number of macrovoids in the outer wall of the adsorbent hollow fibre without having a significant effect on the overall fibre structure, as shown in SEMs of the overall cross section.

The PES fibres spun into water and the water/solvent mix were compared by cyclohexane isotherm, to investigate rate of uptake and total capacity. Isotherms are shown in Figure 6.17.

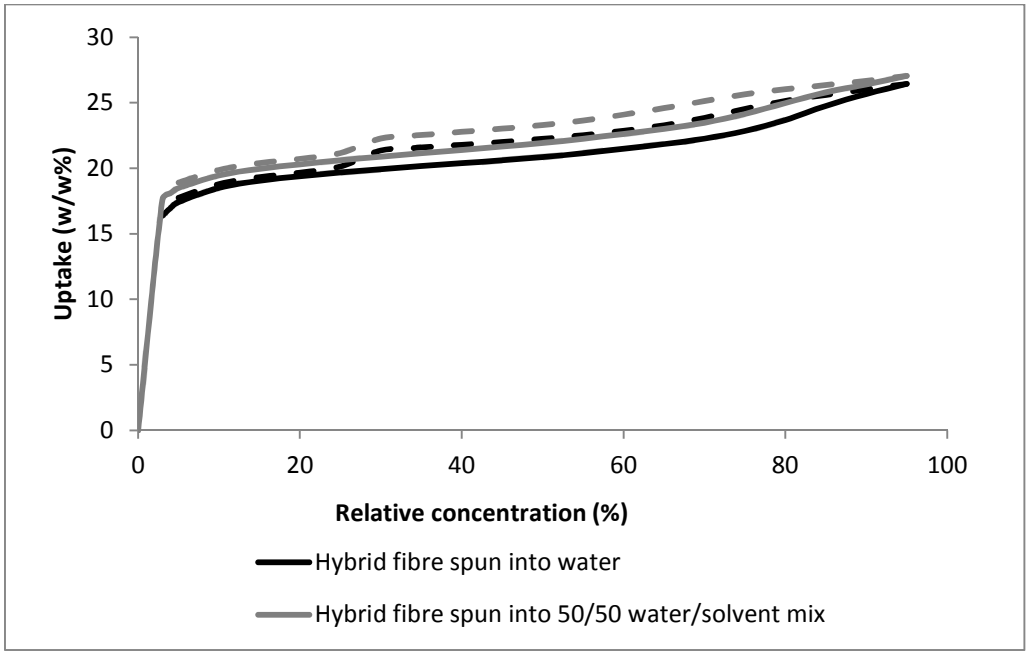

Figure 6.17. Cyclohexane isotherm of hybrid 20% PES 80% AbScents1000/NV5 carbon fibres spun into water and spun into a solvent water mix (characterised at Dstl).

While the lines were very close together, there was a notable increase in uptake for the fibres spun into the solvent/water mix, with higher cyclohexane uptake (w/w%) at lower relative concentrations until approximately the same overall uptake 26.4% on the water spun and 27.1% on the solvent/water spun. The uptake rates for the first points on the above isotherms were examined, and this is shown in Figure 6.18.

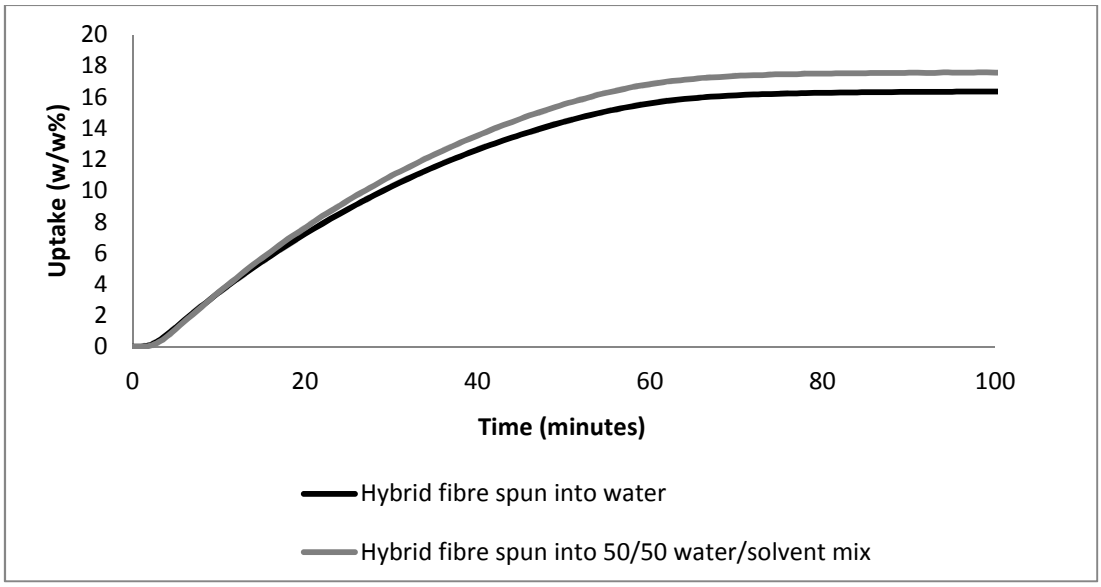

Figure 6.18. Cyclohexane uptake for the initial point of the isotherm of hybrid 20% PES 80% AbScents1000/NV5 carbon fibres spun into water and spun into a solvent water mix (characterised at Dstl).

The rate of cyclohexane uptake, shown in Figure 6.18, was slightly more rapid on the fibre spun into the 50/50 water/solvent mix. This was a result of the external spinning fluid. As the concentration gradient was lower between the fibre and the external coagulant, coagulation occurred more slowly, resulting in a more porous outer skin (Xu and Alsalhy Qusay, 2004). This was favourable for cyclohexane uptake rates, as shown in the isotherm. This is because cyclohexane molecules diffuse into the structure more easily with minimum resistance due to the porous structure of the adsorbent fibre. In addition, the difference in uptake rate was slight. Whether the altered spinning conditions will produce a fibre with favourable performance in a dynamic challenge set up, with gas largely exposed to the inner bore of the fibre rather than the outside, is not clear.

6.2.3.2 Preparing PIM-1 extruded cylinders in methanol

Earlier results in Section 6.2.2 suggested that exposure to methanol could improve porosity. To investigate this, an 80% PIM-1 hybrid (NV5/AbScents1000) precursor mixture was then prepared and extruded from a syringe into either:

1) A bath of methanol
2) A bath of tap water
3) Air

These formed three sets of cylinders of the adsorbent/polymer, of approximately 1.5 mm diameter. Those soaked in methanol and water had their baths refreshed three times each to fully remove the solvent, and were then dried by exposure to 1 L/min flow of dry nitrogen over one week, to avoid any additional exposure to moisture. The inside and outside of each of these cylinders was characterised by SEM to investigate the effects of the different spinning techniques.

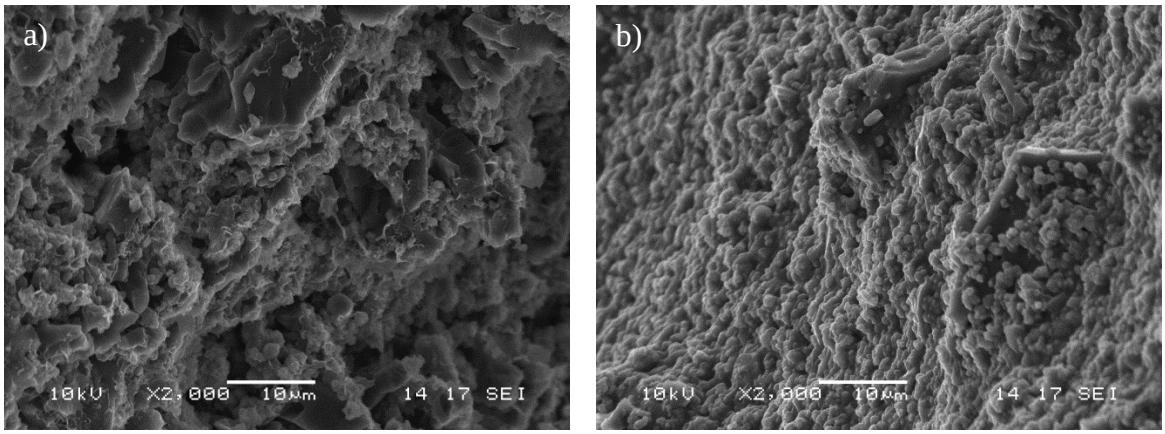

Figure 6.19. x2000 SEM of 20% PIM-1: 80% adsorbent hybrid NV5 carbon/AbScents1000 cylinder. a) interior of cylinders spun into air. b) exterior wall of cylinders spun into air.

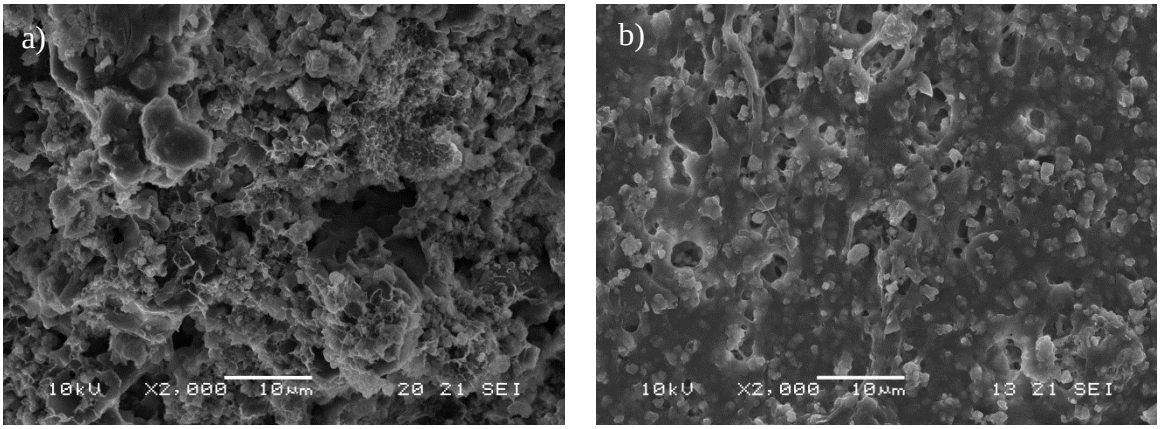

Figure 6.20. x2000 SEM of 20% PIM-1: 80% adsorbent hybrid NV5 carbon/AbScents1000 cylinder. a) interior of cylinders spun into water (x2000). b) exterior wall of cylinders spun into water (x2000).

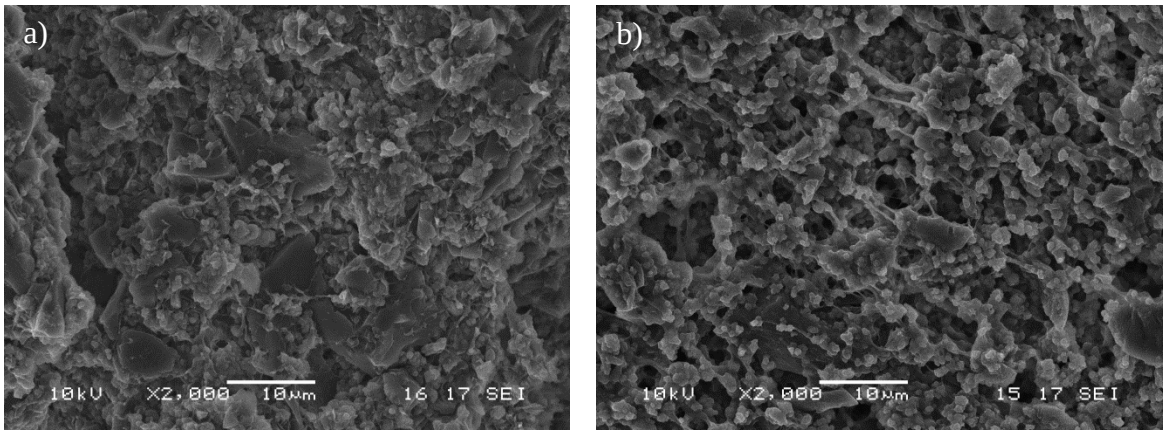

Figure 6.21. x2000 SEM of 20% PIM-1: 80% adsorbent hybrid NV5 carbon/AbScents1000 cylinder. a) interior of cylinders spun into methanol. b) exterior wall of cylinders spun into methanol (x2000).

The structures of all three sets of fibres (Figure 6.19 - Figure 6.21) were very different. For the cylinders dried in air, (Figure 6.19), large crystal-like particles (AbScents1000) were visible surrounded by smaller particles (the carbon and PIM-1). The exterior of the water-spun cylinder (Figure 6.20) was very smooth with few voids, indicating that water formed a skin on the PIM-1 cylinders, similar to the effect seen for PES fibres (Figure 6.14 left). When compared to the methanol extruded cylinders (Figure 6.21), a pronounced difference was observed. The exterior of the cylinders spun into methanol have large voids with a much more open structure and visible strings of polymer connecting the adsorbent particles. These were also visible on the interior of the cylinder. These string-like structures were not visible in the air spun fibres. However, extremely fine string structures could be observed on the fibres spun into water. These were examined at higher magnification in Figure 6.22.

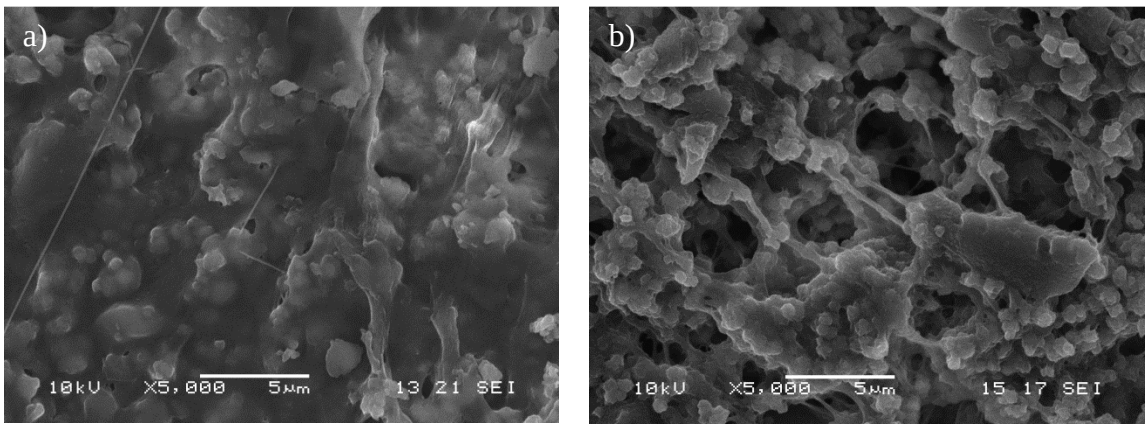

Figure 6.22. x5000 SEM of 20% PIM-1: 80% adsorbent hybrid NV5 carbon/AbScents1000 cylinder. a) exterior wall of cylinders extruded into water (x5000). b) exterior wall of cylinders extruded into methanol (x5000).

As can be seen in Figure 6.22, the string-like structures on the exterior of the water-spun cylinders were significantly thinner (~10 nm) than those on the exterior of the methanol spun cylinders. Also the difference between the macroporous structures was very obvious, with coagulation in methanol clearly a superior way to enhance the porosity of the PIM-1 fibre structure, over spinning into water.

The prevalence of the string-like structures in methanol-spun and water-spun fibres was investigated. These are shown in Figure 6.23 and Figure 6.24. The string-like structures on the water-spun cylinder were visible a short way into the structure of the cylinder structure, shown in Figure 6.23, although not all the way through, as was apparent from

the lack of them in the left image of Figure 6.20. This would indicate that the 'strings' could have been made as a result of the coagulation of the PIM-1 cylinders in water, and that the water travelled only a short distance into the structure, resulting in this effect. Meanwhile the string-like structures on the methanol extruded cylinders were present throughout the structure (Figure 6.24). This would indicate that the methanol was present all the way through the fibre structure, resulting in even coagulation throughout. This may be due to the hydrophobic nature of the PIM-1, which inhibits the permeation of the water through the cylinder structure, while methanol can easily travel through. If this was the case, this would be seen in other cylinders extruded with hydrophobic polymers, although it may be avoided in adsorbent hollow fibre production due to the bore, which was not present in the cylinders. Alternatively, this permeation could be prevented by the formation of a skin for the cylinders extruded into water (Figure 6.20 right).

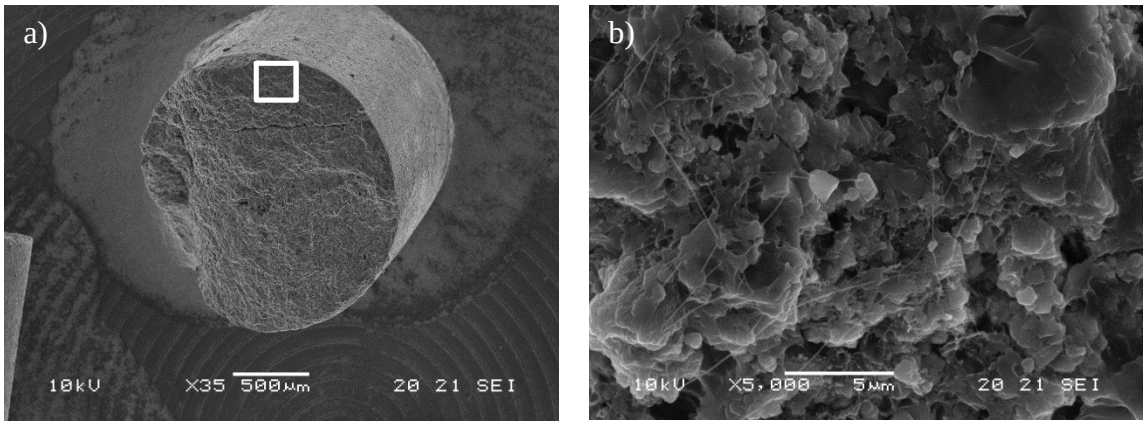

Figure 6.23. SEM of 20% PIM-1: 80% adsorbent hybrid NV5 carbon/AbScents1000 cylinder. a) cross section of cylinder extruded into water (x35). b) highlighted section of cylinder cross section spun into water (x2000).

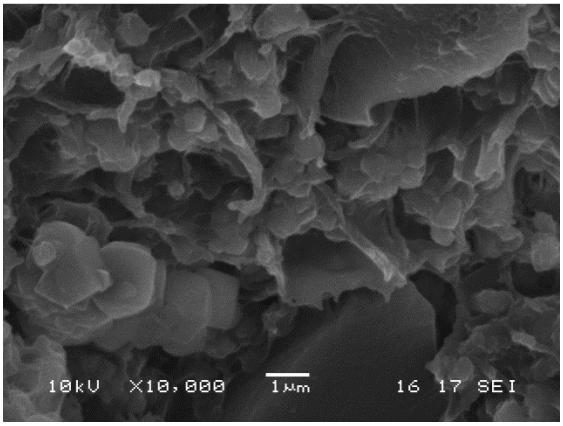

Figure 6.24. SEM of 20% PIM-1: 80% adsorbent hybrid NV5 carbon/AbScents1000 cylinder. Interior of methanol cylinder x10000.

The cyclohexane uptake of the cylinders extruded into methanol was compared with those of the cylinders extruded into water, to determine whether the different structures had a significant effect upon adsorption. This is shown in Figure 6.25.

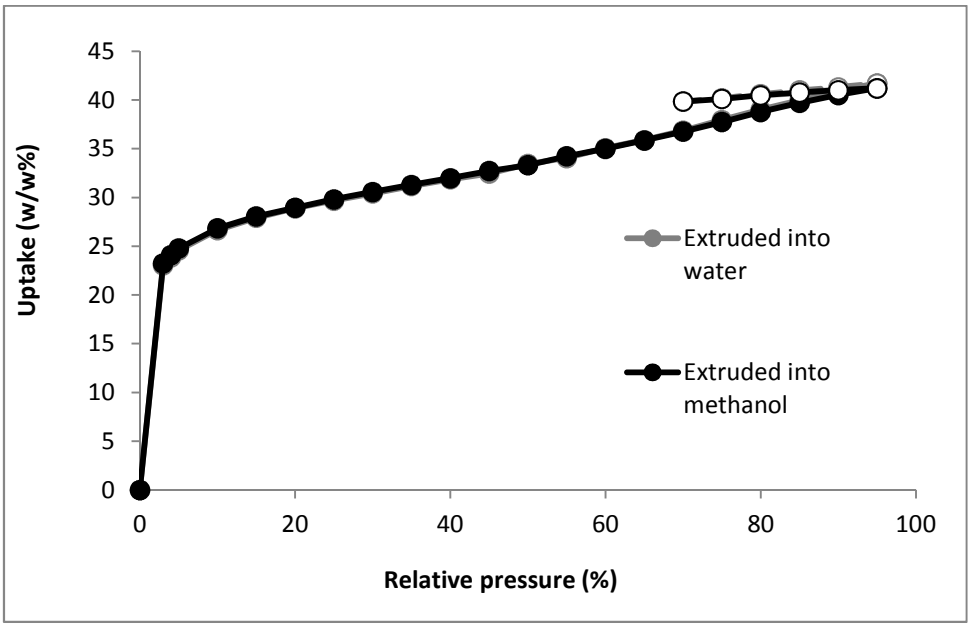

Figure 6.25. Cyclohexane uptake on 20% PIM-1: 80% adsorbent hybrid NV5 carbon/AbScents1000 cylinders spun into water and methanol (characterised at Dstl).

The two uptake lines overlap almost completely, both showing favourable isotherm types and with just over 40% uptake, but suggesting that there was very little difference in uptake caused by spinning into methanol rather than water. This is surprising, given the difference in fibre structures caused by exposure to water. The adsorption kinetics were investigated, by examining cyclohexane uptake rates on the first points of the above isotherms. This is shown in Figure 6.26.

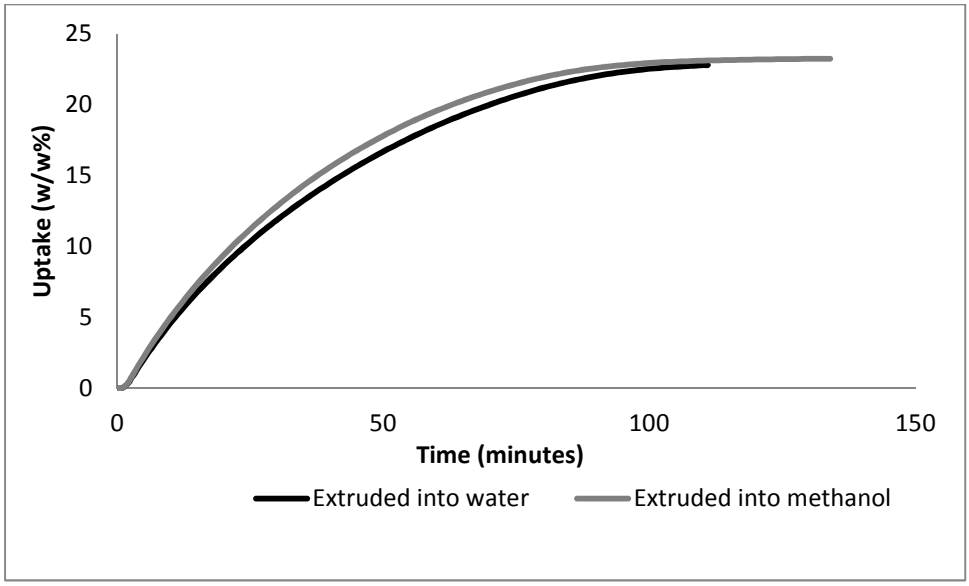

Figure 6.26. Cyclohexane uptake for the initial point of the isotherm on 20% PIM-1: 80% adsorbent hybrid NV5 carbon/AbScents1000 cylinders spun into water and methanol (characterised at Dstl).

Similar to the isotherms in in Figure 6.25, very little difference could be seen between the cylinders extruded into water and those extruded into methanol. This suggests that spinning into methanol would not be an advantageous change to make in the fibre spinning process in order to improve adsorption kinetics.

6.2.4 Preparing PIM-1 adsorbent hollow fibres

It is possible that there may not have been significant difference between cyclohexane uptake on fibres spun into methanol and those spun into water. As such in order to improve the macroporosity in the outer skin layer, PIM-1 hybrid fibres were prepared by spinning a 20% PIM-1 to 80% NV5/AbScents1000 fibre precursor mixture into a 50/50 water/THF mix. This was shown to be effective for PES fibres in Section 6.2.3.1, and may help to address the adsorption kinetic issues observed in Section 6.2.2. Due to limited availability of the PIM, an insufficient quantity of PIM-1 fibres was prepared to allow dynamic testing. PIM-1 fibres were successfully prepared, their structure was investigated by scanning electron microscopy and adsorption properties were investigated by cyclohexane isotherm.

In general, the PIM-1 fibres had a very dense structure throughout, observed by SEM in Figure 6.27, particularly when compared to the PES fibre structure. The outer layer showed very low porosity, shown by SEM in Figure 6.28, particularly when compared to

the outer structure of the PES fibres spun into a water/solvent mix, for example in Figure 6.14. The internal porosity was also low, seen in Figure 6.29. This was particularly clear when compared to the inner layer of a PES fibre, such as in Figure 5.19 amd Figure 5.20. This may be the reason that diffusion was slow in the PIM-1 fibres when compared to PES. This is similar to the effects observed on pellets in Chapter 4, where the lack of macrovoids resulted in slower kinetics and lower breakthrough loading per weight.

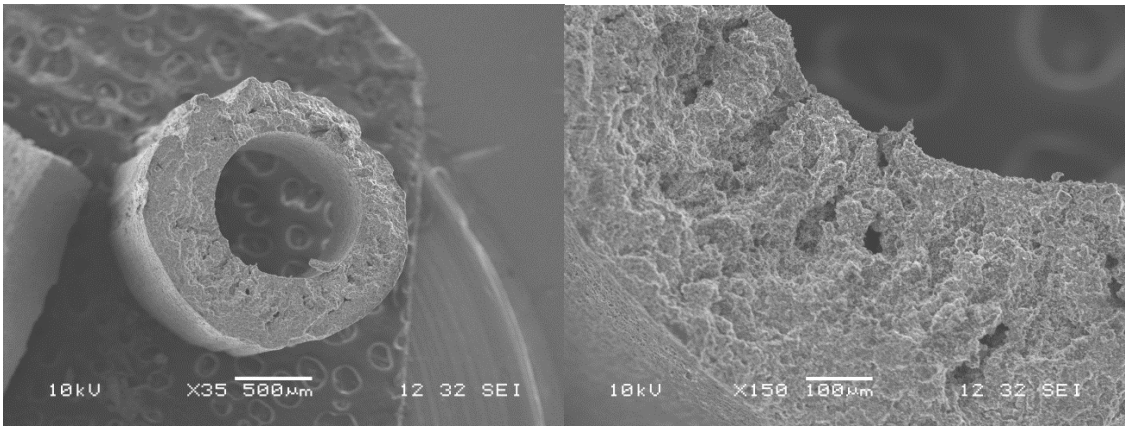

Figure 6.27. Cross section of PIM-1 fibre spun into 50/50 water/solvent mix. Left: x35. Right: x150.

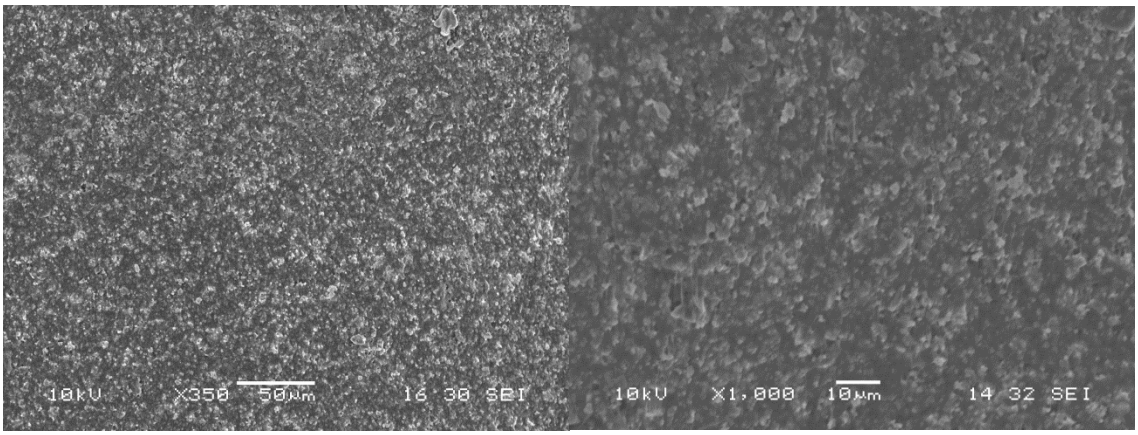

Figure 6.28. Outer wall of PIM-1 fibre spun into 50/50 water/solvent mix. Left: x350. Right: x1000.

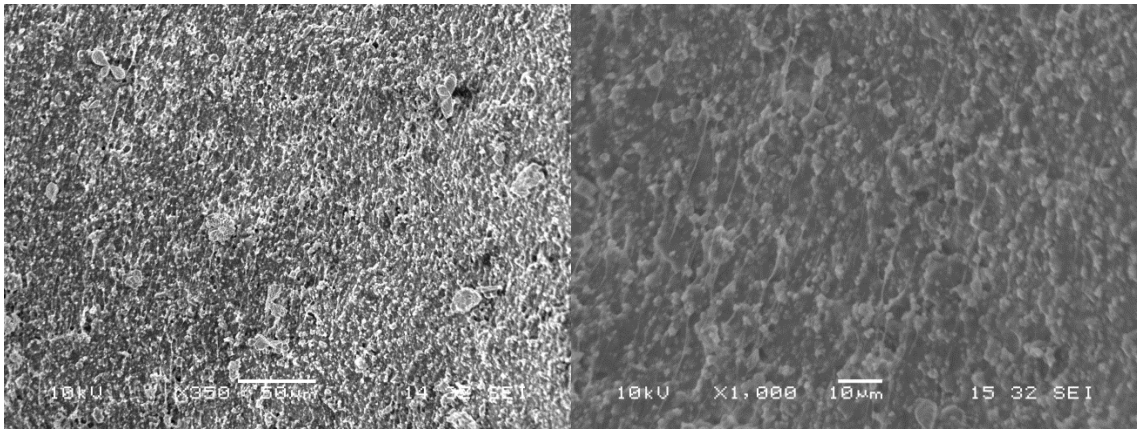

Figure 6.29. PIM-1 fibre spun into 50/50 water/solvent mix lumen wall. Left: x350. Right: x1000.

Cyclohexane isotherms were measured on the PIM-1 hybrid fibres and compared to PES hybrid fibres. The isotherm is shown in Figure 6.30, and the adsorption kinetics are explored by timing the uptake for the first point of the isotherm in Figure 6.31.

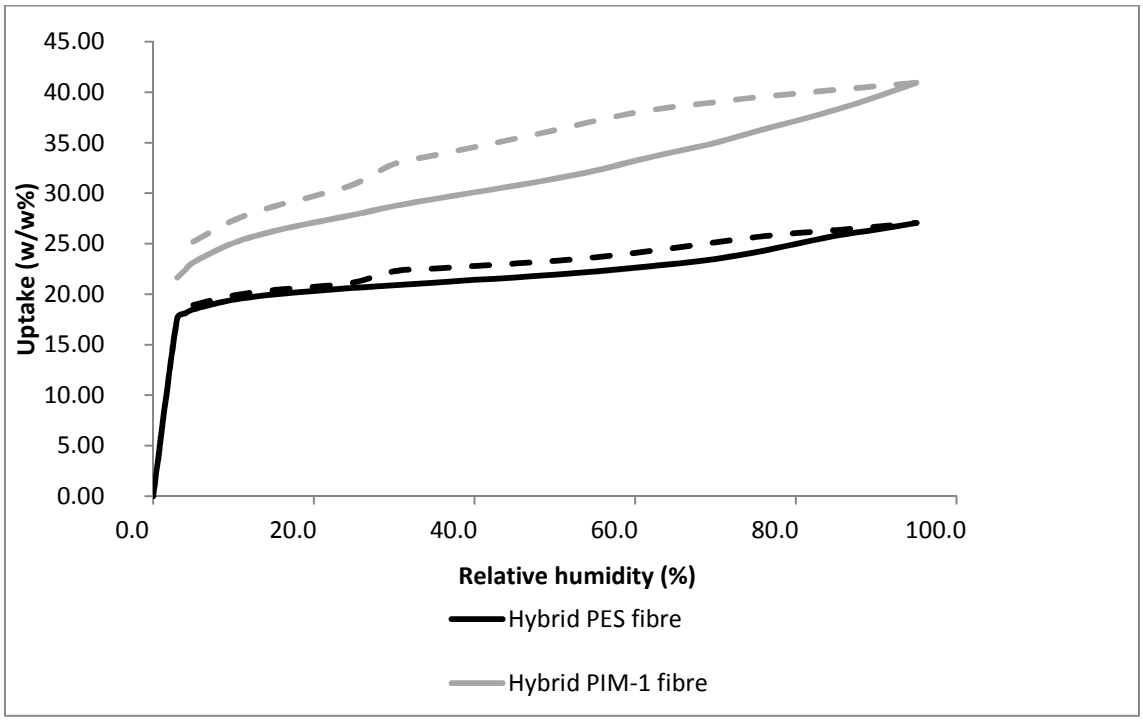

Figure 6.30. Cyclohexane isotherm of hybrid 20% PES 80% AbScents1000/NV5 carbon fibres and 20% PIM-1 80% AbScents1000/NV5 carbon fibres spun into a solvent water mix (characterised at Dstl).

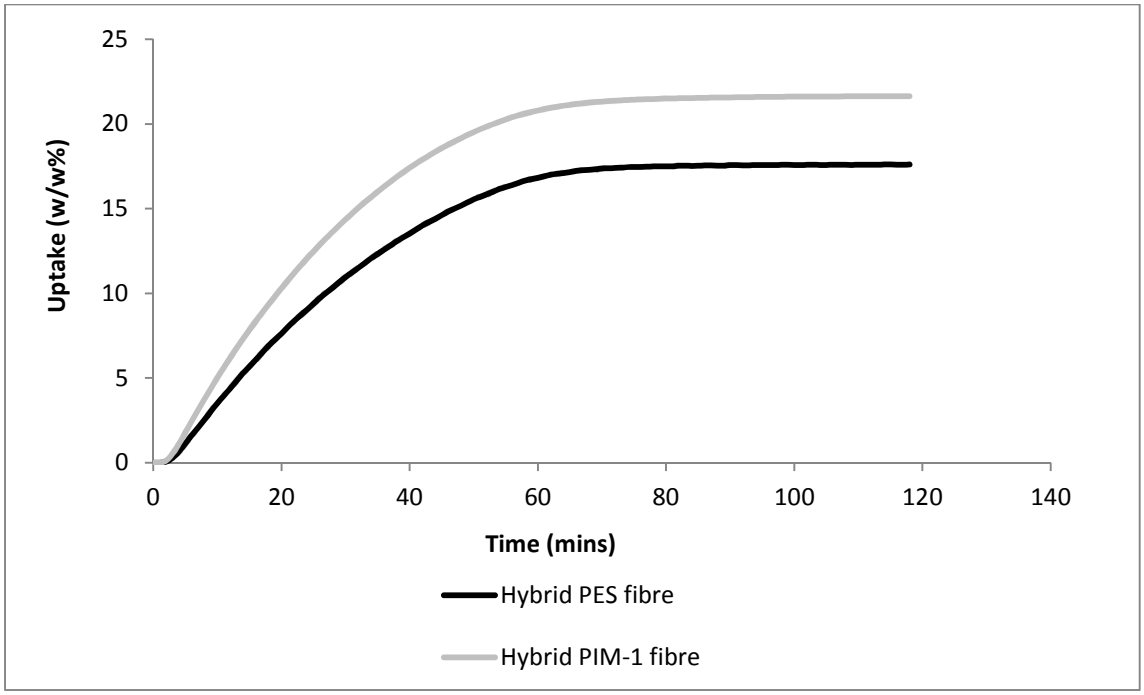

Figure 6.31. Cyclohexane uptake for the initial point of the isotherm of hybrid 20% PES 80% AbScents1000/NV5 carbon fibres and 20% PIM-1 80% AbScents1000/NV5 carbon fibres spun into a solvent water mix (characterised at Dstl).

Cyclohexane uptake was compared on 20% PIM-1 80% AbScents1000/NV5 hybrid fibres and the equivalent PES fibres, both of which having been spun into a 50/50 water/solvent mix. It is clear in Figure 6.30 that there was a significant increase in uptake, from 27.05 w/w% on the PES fibres to 40.94 w/w% on the PIM-1 fibres. This increase in uptake was expected, given the greater surface area of PIM-1 compared to PES, meaning the binder may have contributed to adsorption. However, this did not come at the cost of poor adsorption kinetics, as can be seen in Figure 6.31, with faster cyclohexane uptake observed on the PIM-1 fibres than the PES fibres. While dynamic cyclohexane challenge would be necessary to confirm these results, a PIM-1 hybrid fibre with high uptake of cyclohexane was successfully prepared with improved adsorption kinetics compared to the conventional PIM-1 fibres.

6.3 Discussion

Adsorbent hollow fibres were prepared for the first time replacing PES polymer with PIM-1. The structure of the PIM-1 was far more open than that of the PES, enabling adsorbent particles within the structure of the PIM-1 fibres to be seen by SEM. This was in keeping with the microporous nature of the PIM-1, and was reflected in nitrogen and

octane isotherm results, with the weighted average uptake of the components of the PIM-1 fibre equalling the observed uptake, and surface area able to be predicted from a weighted average of the components also. In contrast, a slight decrease was seen in the observed uptake and surface area of PES fibres compared to that of the weighted averages. The reason for this was that PES covered the adsorbent in the fibre, blocking adsorbate access. While the PIM-1 also covers the adsorbent, it has an intrinsically porous structureand will allow adsorbate to pass through. This confirmed the results seen in Chapter 4, in which bentonite pellets had higher cyclohexane uptake than the PES fibres, and suggests that the loss in equilibrium loading for cyclohexane (but not ammonia) was not inherent to the fibre structure, but was a result of the PES binder. One of the causes may be due to PES being a hydrophilic polymer, while the PIM-1 is organophilic, meaning cyclohexane cannot easily diffuse through the PES by solution diffusion while it can through the PIM-1. It may be interesting to observe ammonia isotherms on the two types of hollow fibres prepared, although the equipment was not available to carry out an ammonia uptake test in this project. However, dynamic octane breakthrough challenge revealed poor kinetics on PIM-1 fibres compared to the PES fibres, despite higher octane w/w% uptake and a more porous structure. There are several possible reasons:

- PIM-1 has lower density than PES due to its microporous structure. As such a greater volume of PIM makes up the fibre precursor mixture meaning adsorbent was covered more thoroughly than in a PES fibre. As the pores of the PIM are very small, it takes time for large molecules, such as octane or cyclohexane, to reach the adsorbent through these small pores.

- PIM-1 has an unusual interaction with water. Though PIM-1 is hydrophobic, as indicated by the water isotherms, traces of water can be strongly adsorbed, which significantly reduces permeability, which could be counteracted by post-treatment with methanol (Budd *et al.*, 2008), although in this study, treatment with methanol did not appear to improve adsorption kinetics. In addition, traces of water with other solvents can have a strong effect, such as gelation of the polymer. This was somewhat indicated by the water isotherm Figure 6.11, in which PIM-1 itself was hydrophobic up to high humidity, but the hybrid PIM-1 fibre took up slightly

more water than the weighted average of the components. However, these effects have not yet been fully explored (Budd, 2013).

- It can be difficult to fully remove organic solvents from PIM-1 due to its high affinity for organics. The developers of PIM-1 suggested soaking it in methanol non-solvent to fully displace the solvent, and then allow the methanol to evaporate with heat/vacuum. This was performed in all cases for the PIM fibres. For the sample spun into methanol, no particular improvement in uptake was observed over that spun into water. As such, pending further investigation, residual solvent was not considered to be an issue in this work.

By spinning PES fibres into a solvent/water mixture, it was possible to increase porosity of the outer surface of the fibres and accelerate the adsorption uptake rate of cyclohexane. This is because decreasing the concentration gradient of the external coagulant decelerates liquid-liquid demixing, enhancing porosity (Xu and Alsalhy Qusay, 2004). When this was applied to PIM-1 fibres, the introduction of solvent to the coagulant bath did not appear to induce significant porosity in the outer layer of the fibre structure when examined by SEM. Reasons for this could be the strong interaction between PIM-1 and the organic solvent, resulting in extremely delayed liquid-liquid demixing and therefore a particularly dense, spongy structure (Kesting, 1971). Alternatively this could be due to the tendency of PIM-1 to experience unusual effects when exposed to a mixture of solvent and water (Budd, 2013), especially as the lumen wall of the PIM-1 fibre showed poor porosity, while this was not observed to be the case for PES fibres. Despite the apparently low porosity, cyclohexane uptake isotherms revealed a high uptake of cyclohexane (47.05%) on the PIM-1 hybrid fibres spun into a solvent/water mixture, with a faster uptake rate than an equivalent PES fibre. This demonstrates the viability of preparing PIM-1 hybrid fibres with good cyclohexane uptake rate. Dynamic cyclohexane challenge on a module of the PIM-1 hybrid fibres could confirm these results, however this will require the scaling up of the PIM-1 fibre spinning process in order to produce a large enough volume to test in this manner. If flow through tests showed slow uptake, in spite of the isotherm results, there are several other possible parameters that could be adjusted to improve the macrovoidal structure of the fibre and porosity of the skins. These include the use of pore formers to open up the PIM-1 fibre structure, or other additives, such as PVP to induce hydrophilicity in the fibre to aid coagulation, or ethanol to develop

greater porosity (Liu *et al.*, 2003). Another option to improve porosity on the fibre exterior, would be to spin the fibres with a large air gap (Liu *et al.*, 2003). One final option is that the PIM-1 fibre precursor mixture had low viscosity, meaning it left the spinneret rapidly, which could result to an increase in the density of the outer wall of the fibre (Chung *et al.*, 2000). This could be addressed by adjusting the ratio of polymer: solvent: adsorbent in future work.

At present, PIM-1 is an expensive polymer that is not yet commercially available, so there was difficulty acquiring enough to prepare large volumes of PIM-1 fibres for detailed investigation. As such, despite high contaminant loadings, there are still potential concerns about the uptake rate of some gases (e.g. octane) on PIM-1 fibres. In addition, the price of PIM-1 respirator filters would be very high, and there may be a reduction in permeability associated with the PIM-1 interacting with atmospheric water (Budd *et al.*, 2008). While the adsorption loadings of cyclohexane and octane were greatly increased by replacing the PES in adsorbent fibres with PIM-1, at present PIM-1 fibres are not suitable for use in respirator filters without further investigation.

6.4 Conclusion

Adsorbent hollow fibres were prepared using a polymer of intrinsic microporosity for the first time. As a result of replacing the conventional polyethersulfone with adsorptive PIM-1:

- Overall improvements were made to the fibre surface area and loading of organics octane and cyclohexane.
- The adsorption isotherms of N_2, octane and cyclohexane for PIM-1/carbon fibre could be predicted accurately using the individual isotherms of its constituent parts, while for PES the observed values were lower than predicted from this weighted average.

This indicates that the PES matrix obstructed access to the incorporated adsorbent whereas PIM-1 allowed access to all of the sorption sites of the carbon and provided additional sorption sites.

Though replacing the PES in fibres with PIM-1 could greatly enhance the overall loading of the fibres, allowing full use of the adsorbent to be made, this is at the cost of adsorption rate. The PIM-1 fibres were found to be dense and adsorb octane slowly, with instant breakthrough, compared to 2 hours in PES fibres. This makes PIM-1 fibres impractical for use in a respirator, where high breakthrough loading is important. As such, several attempts were made to enhance the adsorbate uptake speed on PIM-1:

- PIM-1 cylinders were extruded into water and methanol, but this was not found to greatly affect the uptake rate.
- PIM-1 fibres spun using a 50/50 solvent/water mixture as the external coagulant as well as the internal coagulant. SEM images did not show any improvement in the porosity of the structure, but cyclohexane isotherms demonstrated good cyclohexane loading (47.05%) at a faster uptake rate than an equivalent PES fibre.

Further research into the interactions between PIM-1, solvent and water will be necessary to understand these relationships better.

7 Incorporating adsorbent hollow fibres into respirator cartridges: novel respirator design

7.1 Introduction

This Section draws together results of the previous Sections to present several potential candidate designs for future respirators incorporating adsorbent hollow fibres. In order to design fibre modules for use in respirators, several key factors have been taken into consideration. These include:

- Protection from toxic gases (breakthrough time)
- Breathing resistance (pressure drop)
- Mass of the filter
- Size of the filter

To provide optimal protection, a respirator cartridge must balance these factors. Obviously, the greatest possible protection from toxic gases is highly desired, however in order to provide this the size, weight, pressure drop and other such factors of the filter, collectively referred to as the burden, would become impossible to tolerate as a user. The levels of protection required as well as the limits to the factors affecting the user are stated in BSI regulations (BSI, 2008). The protection levels required from toxic chemicals are shown in Table 12.3 in Appendix 6, and the maximum allowable breathing resistance gases (P1 for a low capacity filter, P2 for a medium capacity filter and P3 for a high capacity filter) in Table 7.1.

Table 7.1. Maximum allowable breathing resistance in filters for removal of NH_3, H_2S and cyclohexane, adapted from BSI, (2008).

Filter type and class	Maximum resistance (mbar)	
P1	1.6	6.1
P2	1.7	6.4
P3	2.2	8.2

BSI regulations for mass and size are given below:

1) Mass: The maximum mass of filter for a half mask is 300 g, and for a full face mask is 500 g.
2) Size: No specification is given for filter size, although it should be ergonomic and take into account the interaction between the wearer and the mask.

The potential of adsorbent fibre filters to fulfil these requirements will be considered in this Chapter.

7.1.1 Measuring and modelling pressure drop in respirator filters

For optimum comfort, a respirator should provide the lowest possible resistance at the average human breathing rate of 6 L/min and up to the maximum voluntary ventilation, between 125 and 170 L/min (Barrett *et al.*, 2009). The maximum resistances allowed by BSI regulations are 160 Pa for a low capacity filter at 30 L/min, and 610 Pa at 95 L/min (BSI, 2008). In order to fully explore the pressure drop at these high flow rates, it was necessary to use a pressure drop model.

The pressure drop of adsorbent hollow fibres and of carbon granules was measured and compared from 0 to 5 L/min flow rates by the techniques shown in Section 3.2.6. Reynolds numbers were calculated for granular beds and adsorbent hollow fibre modules in order to determine suitable models, and calculated data were compared to the pressure drop results.

7.1.2 Modelling breakthrough time for respirator filters using the Wheeler-Jonas equation

A respirator filter is likely to be exposed to a range of conditions, such as challenge gas concentration and flow rate. These conditions will affect the breakthrough time. As such, a model that considered breakthrough time in different conditions was a necessity for respirator design.

The Wheeler-Jonas model, equation given below, is the simplest option for modelling experimental data. Many of the breakthrough curves observed have been almost symmetrical and fit the shape of the Wheeler-Jonas equation more closely than the linear

driving force equation, as discussed in the Literature Review, (Section 2.2.4). The fit of the Wheeler-Jonas equation compared to the experimental results, and its potential use as a tool in respirator design will be investigated in this Chapter. The Wheeler-Jonas equation is given below:

$$t_b = \frac{M.W_e}{Q.c_0} - \frac{W_e\,.p_b}{k_v.c_0}\,.\ln\frac{c_0 - c_b}{c_b} \qquad (22)$$

While W_e and k_v values can theoretically be determined using the equations given in the literature review, they can also be determined empirically using several experiments. By changing a variable, such as the weight of the module, *M* (Wood and Moyer, 1989). If the module weight is plotted against the breakthrough time, a straight line will be obtained, as shown below, and W_e and k_v can be calculated using the intercept and slope of the graph. Using the basic equation for a straight line graph compared to the Wheeler-Jonas equation:

$$y = m_1\,x_1 + \,c_1$$

where
m_1 = slope
c_1 = intercept
$y = t_b$
x_1 = weight of module M

When applied to the Wheeler-Jonas equation:

$$m_1 = \frac{W_e}{Q.c_0} \quad \rightarrow \quad W_e = m_1.Q.c_0$$

$$c_1 = \frac{\rho_b.W_e}{k_v.c_0}\ln\frac{c_0}{c_b} \quad \rightarrow \quad k_v = \frac{\rho_b.W_e}{c.c_0}\ln\frac{c_0}{c_b}$$

Alternatively, the inverse of the flow rate may be plotted against breakthrough time, which should result in another linear graph, in which:

$$y = m_2\,x_2 + \,c_2$$

where
m_2 = slope

c_2 = intercept
$y = t_b$ (h)
x_2 = 1/Q (1/min)
M = Weight of module (g)

Therefore:

$$m_2 = \frac{W_e M}{c_0} \quad \rightarrow \quad W_e = \frac{m_2 . c_0}{M}$$

$$c_2 = \frac{\rho_b . W_e}{k_v . c_0} \ln \frac{c_0}{c_b} \quad \rightarrow \quad k_v = \frac{\rho_b . W_e}{k_v . c_0} \ln \frac{c_0}{c_b}$$

$$c_1 = c_2$$

These W_e and k_v values are specific to particular gas/adsorbent combinations. When they have been determined, they can be used in the Wheeler-Jonas equation with other variables changed, such as weight, flow rate and challenge gas concentration. This allows prediction of breakthrough time to be made for a variety of environmental conditions.

Theoretically, other sets of data can be calculated from the Wheeler-Jonas model. The full breakthrough curve can be plotted, to determine whether the observed breakthrough curve matches the predicted Wheeler-Jonas breakthrough curve:

$$t = \frac{\rho_b . W_e}{C_0} \left[\frac{z}{u} - \frac{1}{k_v} \ln \frac{C_0 - C}{C} \right] \tag{23}$$

where
z = axial distance in the bed (cm)
C = local concentration in bed

This can be rearranged to obtain C/C_0.

$$\ln \frac{c_0 - c}{c} = k_v \left(\frac{z}{u} - \frac{c_0 . t}{\rho_b W_e} \right)$$

If we take:

$$k_v\left(\frac{z}{u}-\frac{c_0.t}{\rho_b W_e}\right)=x$$

then:

$$\frac{c}{c_0}=e^{\frac{1}{x+1}} \tag{24}$$

This can be plotted to give the breakthrough front as it travels through the bed at different times, with an example shown in Figure 7.1

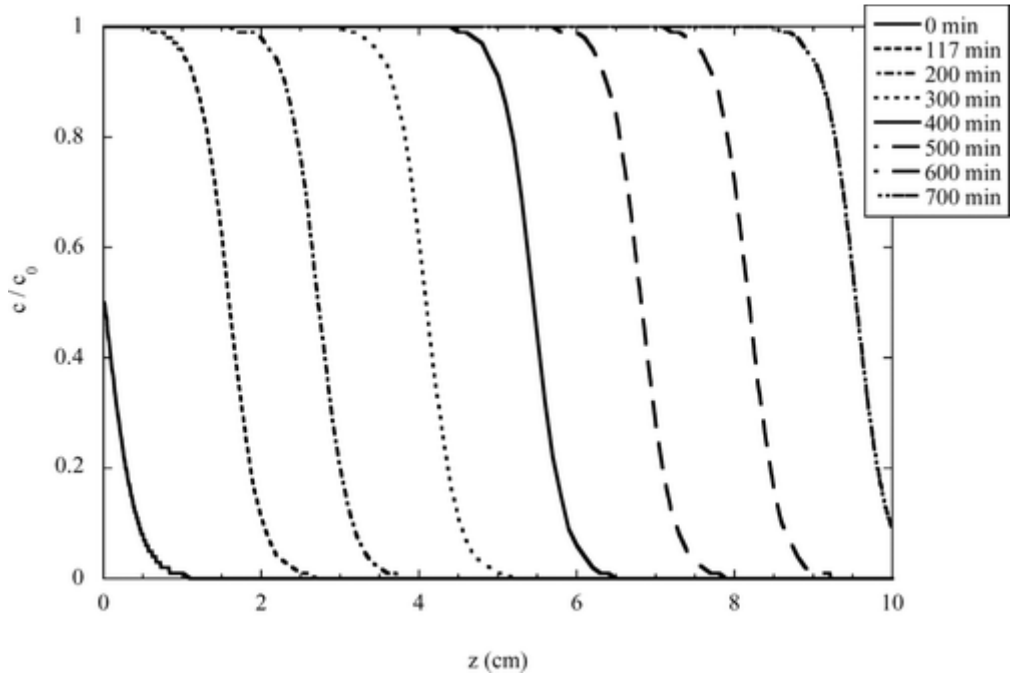

Figure 7.1. A developed Wheeler-Jonas adsorption front moving through a granular bed, from Grévillot *et al.*, (2011).

The stoichiometric time can also be predicted, by assuming infinite k_v:

$$t_s=\frac{M.W_e}{Q.c_0} \tag{25}$$

The length of mass transfer zone (LMTZ) can also be predicted from the Wheeler-Jonas equation, using:

$$\text{LMTZ}=2\frac{u}{k_v}ln\frac{1-x}{x} \tag{26}$$

where

x = the breakthrough concentration as a fraction of the feed concentration

u = superficial velocity (cm min^{-1}).

This can also be rearranged to determine the equilibrium time. Given:

$$\text{LMTZ} = \frac{L}{t_s}(t_{eq} - t_b)$$

then:

$$t_{eq} = \frac{t_s \text{LMTZ}}{L} + t_b$$

The Wheeler-Jonas model offers a way to calculate many important values needed in filter design without the need to do a large number of experiments.

Dynamic 800 ppm 1 L/min NH_3 challenges were carried out on 80% AbScents1000, NV5 and hybrid AbScents1000/NV5 fibres from 5-25 cm in length, double and single layer, and including a pore former. At least three module lengths were tested for each type of fibre. Dynamic 1000 ppm cyclohexane challenges were performed on the same types of fibres but fixing the length at 10 cm and varying the flow rate from 1 to 3 L/min. The flow rates selected depended on the speed of breakthrough, as in some cases breakthrough occurred instantly. Three different flow rates with non-zero breakthrough times were tested. When inputting values to the Wheeler-Jonas equation, the breakthrough time was standardised by dividing by the mass of the fibre module, giving a breakthrough time per gram of adsorbent. For ammonia tests, W_e and k_v were calculated from a graph of module weight against breakthrough time. For cyclohexane tests, W_e and k_v were calculated from a graph of the inverse of flow rate against breakthrough time. W_e and k_v were determined for each fibre/gas combination and used to calculate breakthrough time for different flow rates or weights. For example, ammonia data were used to predict breakthrough time for a different flow rate, and cyclohexane data were used to predict breakthrough time for a bed of a different weight. The challenges for which breakthrough time was predicted were then performed to confirm the accuracy of the model in different challenge conditions. The calculations and values are provided in Appendix 7.

7.1.3 Performance indices for respirator filters

The weight and volume of a respirator filter are important when considering user burden. Due to their high voidage, hollow fibres have low density. This means that a hollow fibre filter will have a significantly lower weight than an equivalent volume granular filter. As

such, to get the best adsorption performance, an adsorbent hollow fibres filter will require a reasonably large volume, making volume a limiting factor. A granular bed is denser by comparison, and pressure drop will increase when the volume is increased. As such particle size, weight and pressure drop are limiting factors for granular filters. Granular and adsorbent hollow fibre modules were compared in terms of breakthrough time and loading relative to volume, weight and pressure drop to give performance indices.

7.1.4 Candidate mask design

The results from previous Sections were combined to predict breakthrough times, weights and pressure drops of a potential respirator gas filter suggested by Dstl.

7.2 Results and discussion

7.2.1 Modelling pressure drop in hollow fibre and granular test modules

Hollow fibre bore sizes were determined to be 0.84, 1.04 and 1.20 mm respectively for 'small', 'medium' and 'large' bore modules using ImageJ to measure photos of fully prepared fibres. An example of the calculations carried out to determine pressure drop is given in Appendix 2. To select suitable pressure drop models, Reynolds numbers were calculated to determine whether flow was laminar or turbulent. The flow rates at which flow begins to transition and at which it becomes fully turbulent are shown in Table 7.2. The calculations and Reynolds numbers are shown in Appendix 12.2.1.

Table 7.2. Approximate flow rates for transitional and fully turbulent flow to occur in 2 cm diameter modules.

Module type	Transitional flow (L/min)	Fully turbulent flow (L/min)
Empty	33	87
Granular bed	0.1	18
Small bore adsorbent hollow fibres	48	126
Standard bore adsorbent hollow fibres	75	141
Large bore monolith	109	298

Table 7.2 demonstrates that the adsorbent hollow fibres will have a laminar flow regime at greater flow rates than even the empty test module. This is due to the narrow channels through which the gas travels, and so higher superficial velocity with lower channel diameter. This suggests that Hagen-Poiseuille model will be a suitable model for the pressure drop up to the point where flow becomes fully turbulent for hollow fibres. Flow is not laminar in granular beds at flow rates greater than 0.1 L/min, meaning the Ergun equation is a suitable model. The Reynolds numbers for different types of module as flow rate increases are shown in Figure 7.2.

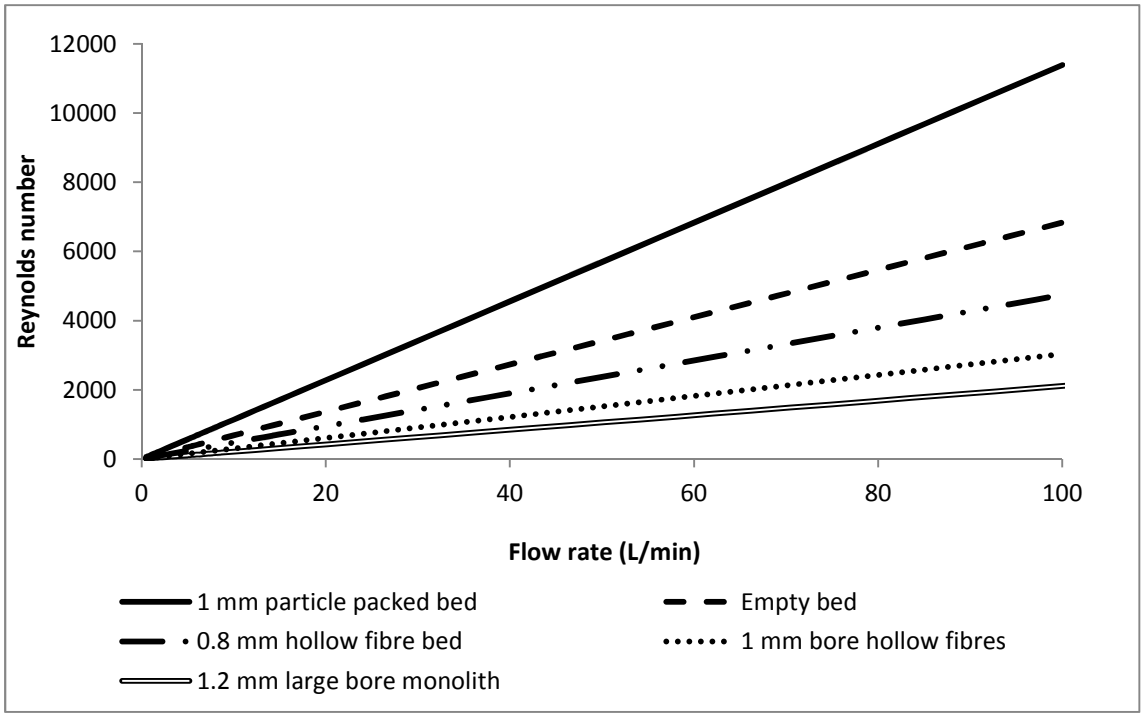

Figure 7.2. Reynolds numbers as flow rate increases in three different modules.

Given these results, the Hagen-Poiseuille model is suitable for adsorbent hollow fibres up to high flow rates, and the Ergun model, for granular beds. The pressure drop per length for these two models is shown in Figure 7.3.

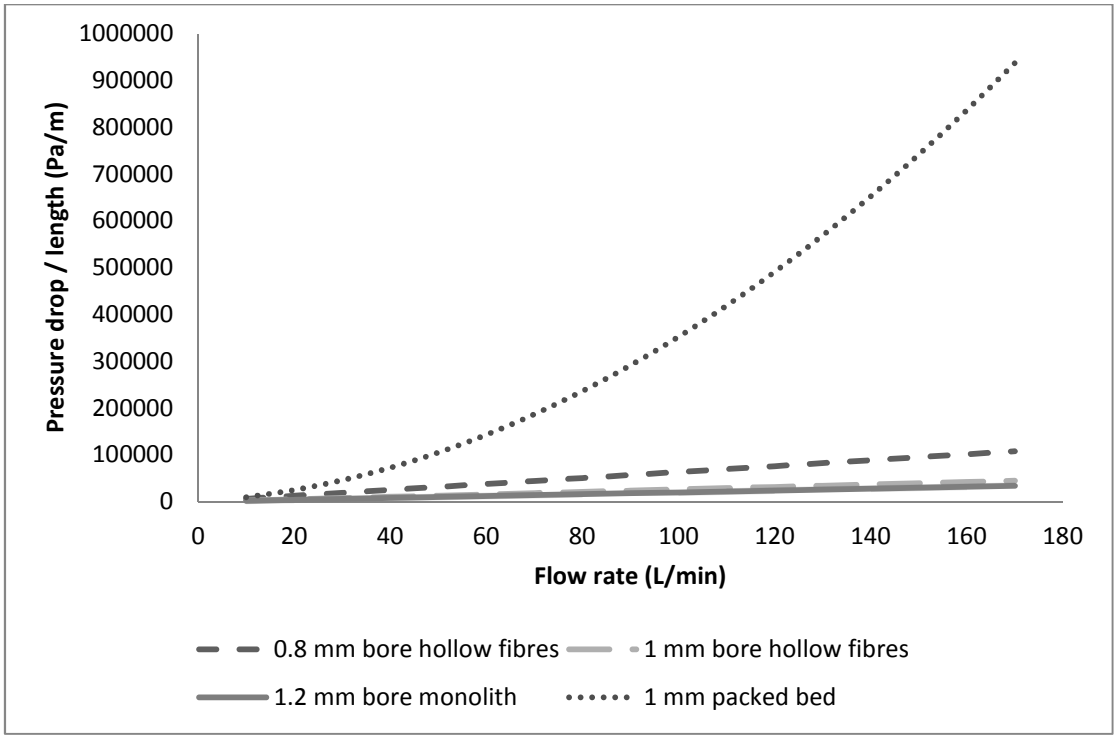

Figure 7.3. Projected pressure drops per length for a 2cm diameter module containing adsorbent hollow fibres, monolith or granular bed.

The Hagen-Poiseuille model provides a far lower pressure drop at all flow rates compared to the Ergun model, with a greater decrease as flow rates increase. As an extreme example, a 1 metre standard bore adsorbent hollow fibre module, following the Hagen-Poiseuille model, would have a lower pressure drop than a 5 cm module following the Ergun model at the highest flow rates. While a straight 1 m long tube on a respirator would be quite cumbersome, the lower pressure drop would allow incorporation of corners or coils (with their higher associated pressure drop) into future respirator design.

Values generated from the Hagen-Poiseuille model were plotted against the measured $\Delta P/L$ values for the adsorbent hollow fibres to see how well they fit, shown in the figures below.

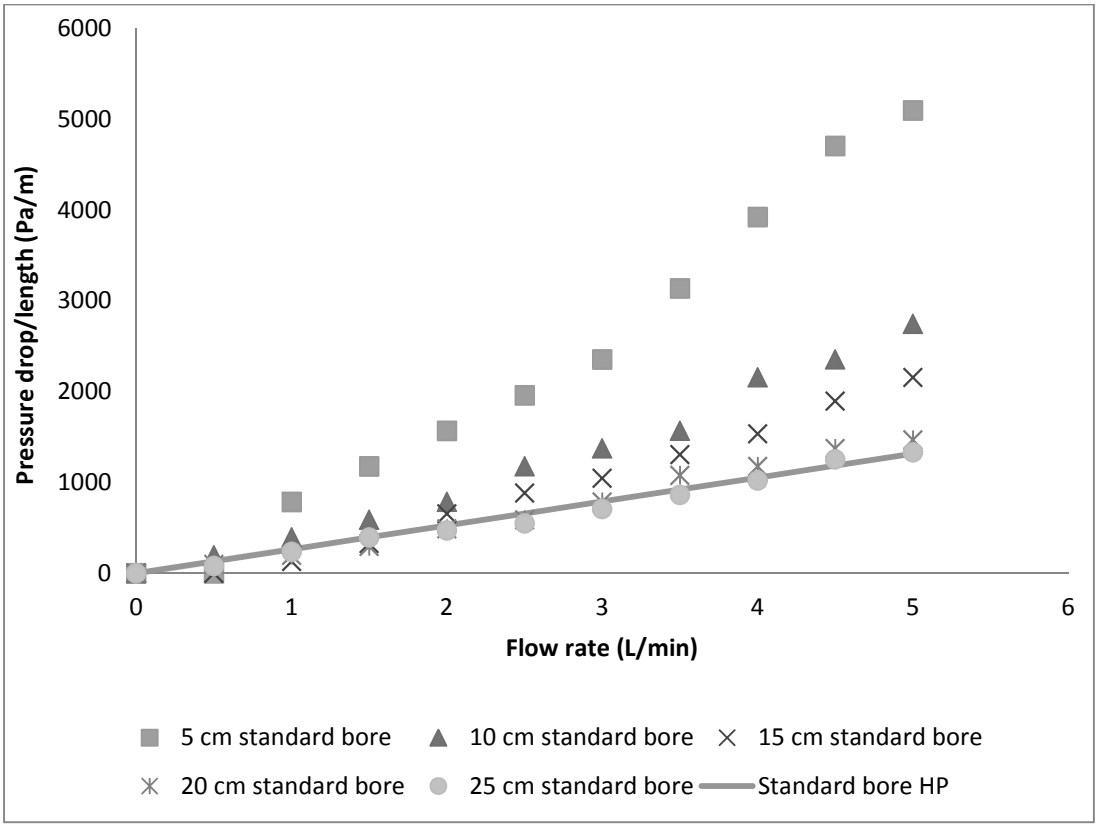

Figure 7.4. ΔP/L values calculated from experimental pressure drop values of different length standard bore fibre modules compared to the Hagen Poiseuille model.

Figure 7.4 clearly shows that for standard bore fibres, the model closely matched the lines of ΔP/L calculated for the 20 and 25 cm standard bore hollow fibre modules, verifying that the model is a reasonable fit to calculate pressure drops for adsorbent hollow fibre modules at flow rates up to approximately 140 L/min.

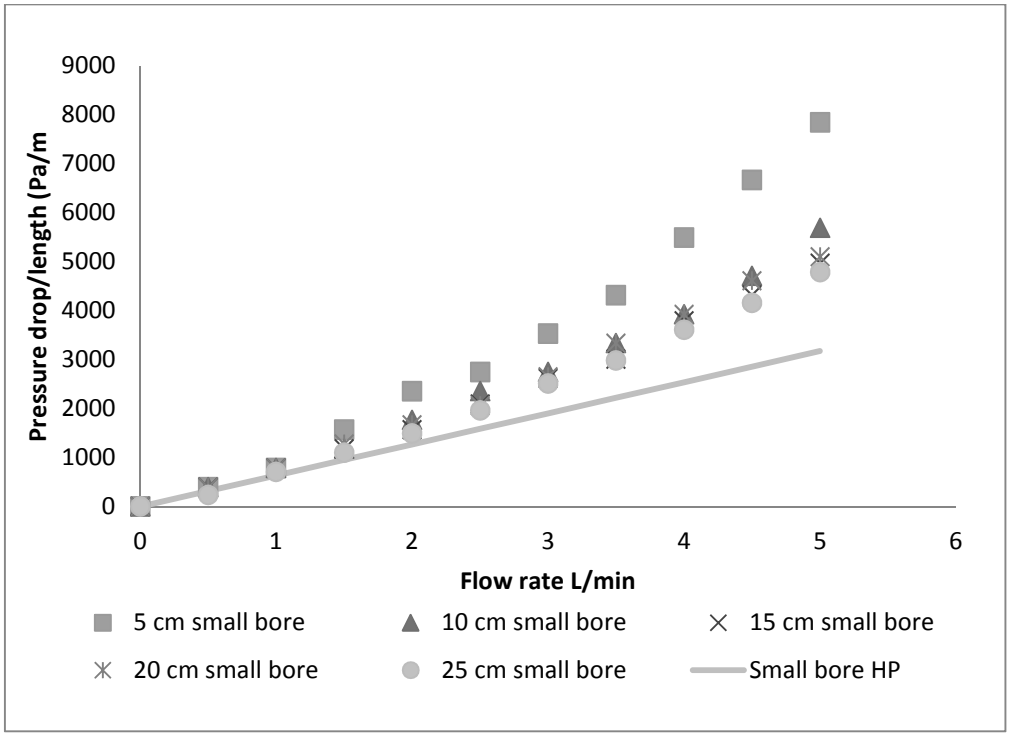

Figure 7.5. ΔP/L values calculated from experimental pressure drop values of different length small bore fibre modules compared to the Hagen Poiseuille model.

In Figure 7.5, for small bore fibres, it was observed that although the ΔP/L values stabilise for 10 cm beds or longer there is a noticeable difference from the Hagen-Poiseuille model as flow rate increases. This suggests entrance effects as a result of the particularly narrow bores of the adsorbent hollow fibres result in higher pressure drop than would be predicted by the Hagen-Poiseuille equation.

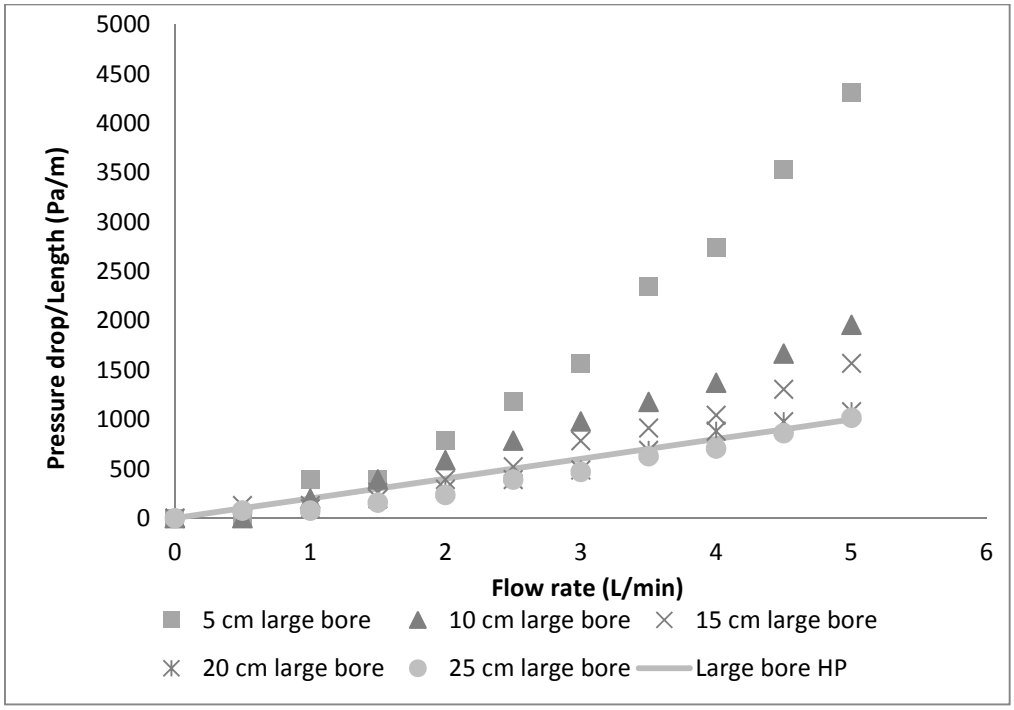

Figure 7.6. ΔP/L values calculated from experimental pressure drop values of different length large bore monolith modules compared to the Hagen Poiseuille model.

Figure 7.6 shows that the Hagen-Poiseuille model fit the curves reasonably well for the 20 and 25 cm long large circular bore monoliths modules, but not the lower lengths. Similar to the fibres, this disparity with the lower lengths is most likely a result of entrance effects. This is supported by the fact that at lower flow rates, the model fits more closely for the shorter length monoliths, with differences occurring when flow rate becomes greater, resulting in more severe entrance effects.

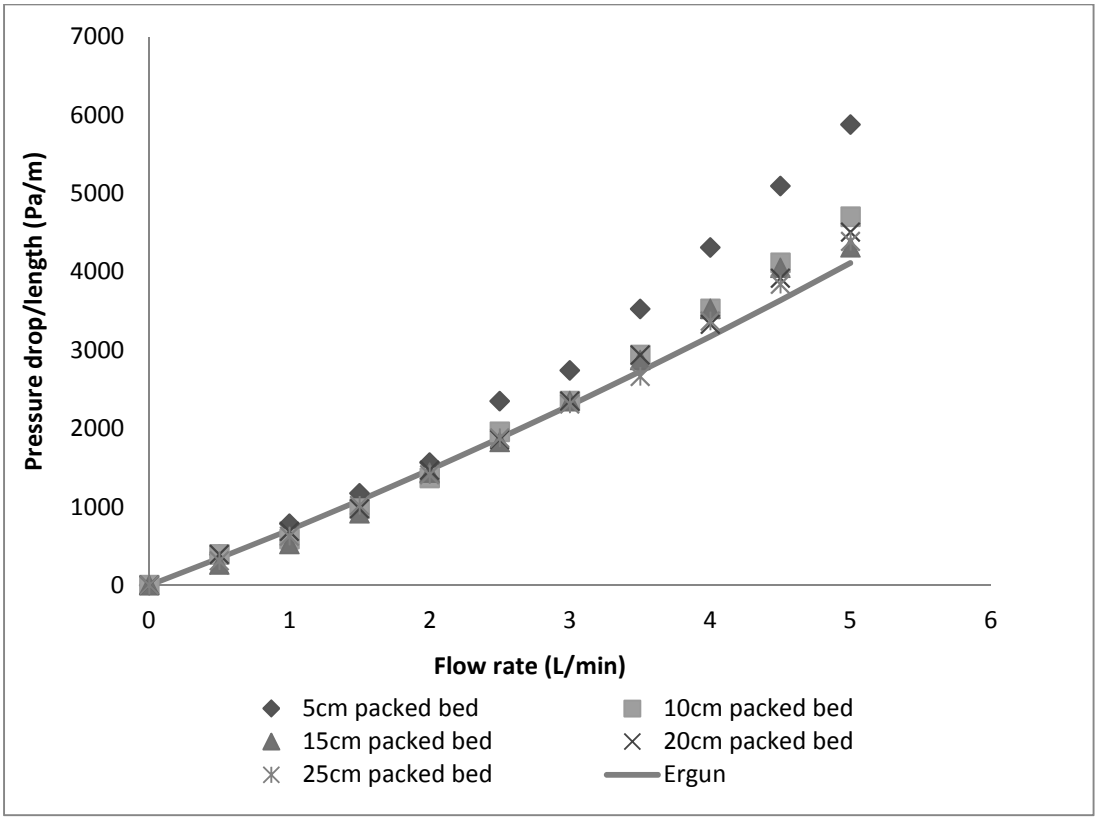

Figure 7.7. ΔP/L values calculated from experimental pressure drop values of different length granular bed modules compared to the Ergun model.

As can be seen in Figure 7.7 the Ergun model fit the pressure drop/length values for 15, 20 and 25 cm beds packed with granules. Entrance effects were observed, similar to the fibre and monoliths, but it is also possible that these results could be altered by wall effects. Wall effects are significant when the diameter of the module/ diameter of the particle is < 40 (Winterberg and Tsotsas, 2000). In this case, the module diameter was 20 mm and the largest particle diameter was 1 mm. 20/1 = 20. However, it has been observed in the literature that the Ergun model will fit when module diameter/particle diameter > 10 relatively accurately (Winterberg and Tsotsas, 2000). As such wall effects were not considered significant in this case.

7.2.2 Modelling breakthrough performance and other module characteristics using the Wheeler-Jonas equation

7.2.2.1 Ammonia by weight

Fibre modules were challenged with ammonia and their breakthrough times plotted against their weight. The results are shown in Figure 7.8, Figure 7.9 and Figure 7.10. A

linear trend was observed for AbScents1000 and hybrid fibres, with increasing breakthrough time as weight increased. This was less clear for the NV5 fibres, in Figure 7.8, largely due to the low values of breakthrough time, meaning an error of a few seconds could translate to a significant change in the gradient of the line.

In this study, single layer fibres had greater breakthrough time than double layer fibres, except in the case of NV5 fibres, where the difference was very small. The relationship between breakthrough time and module weight was linear and a trend line could be fit. However, the 5 cm long modules that were tested did not fit well on the trend lines. Given the pressure drop results, it is likely that entrance effects had an effect on breakthrough time for the 5 cm beds. As such, the points were not included.

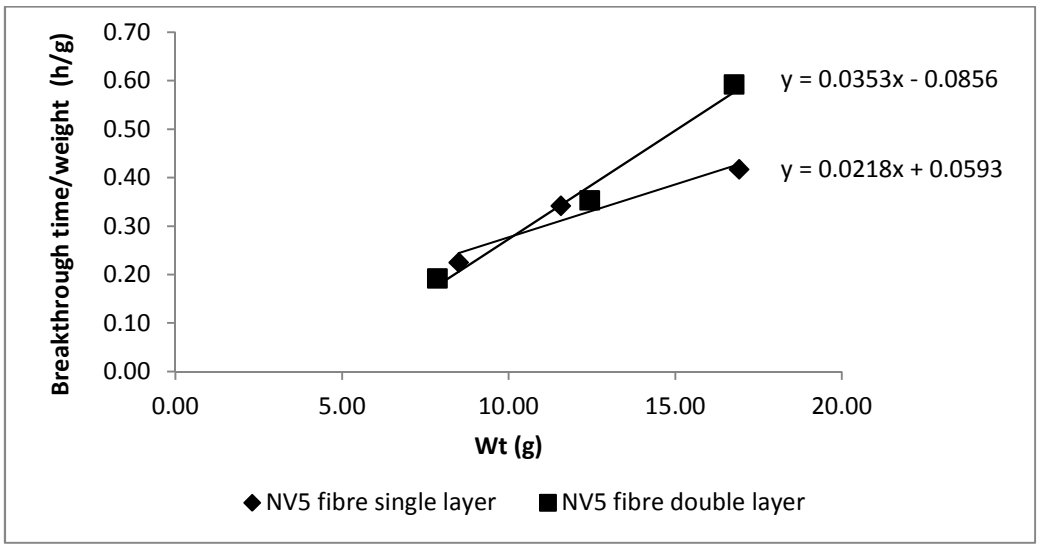

Figure 7.8. Weight plotted against breakthrough time/weight for 800 ppm 1 L/min ammonia challenge on NV5 carbon fibres.

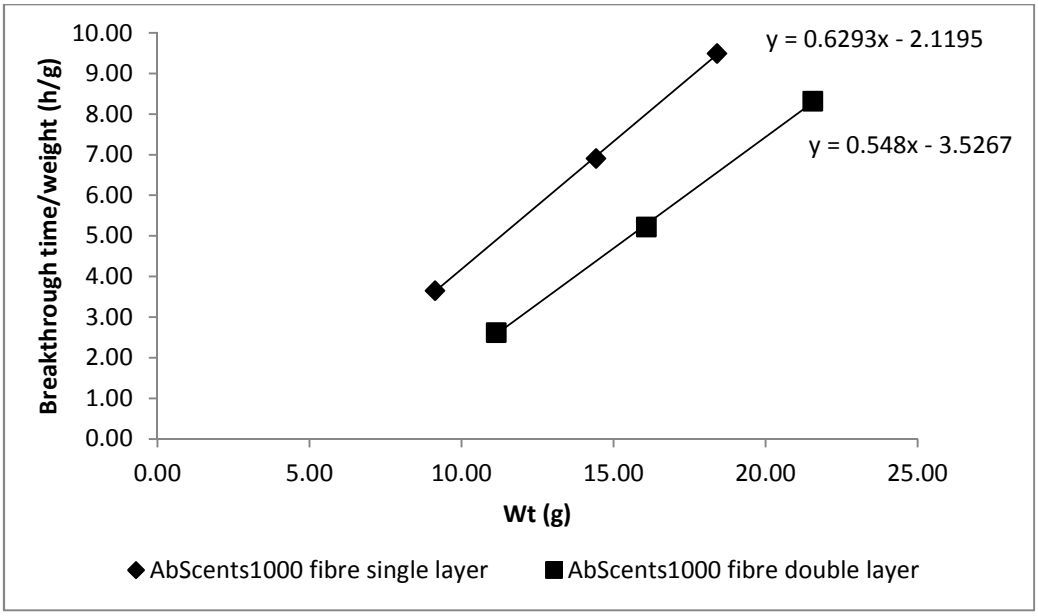

Figure 7.9. Weight plotted against breakthrough time/weight for 800 ppm 1 L/min ammonia challenge on AbScents1000 fibres.

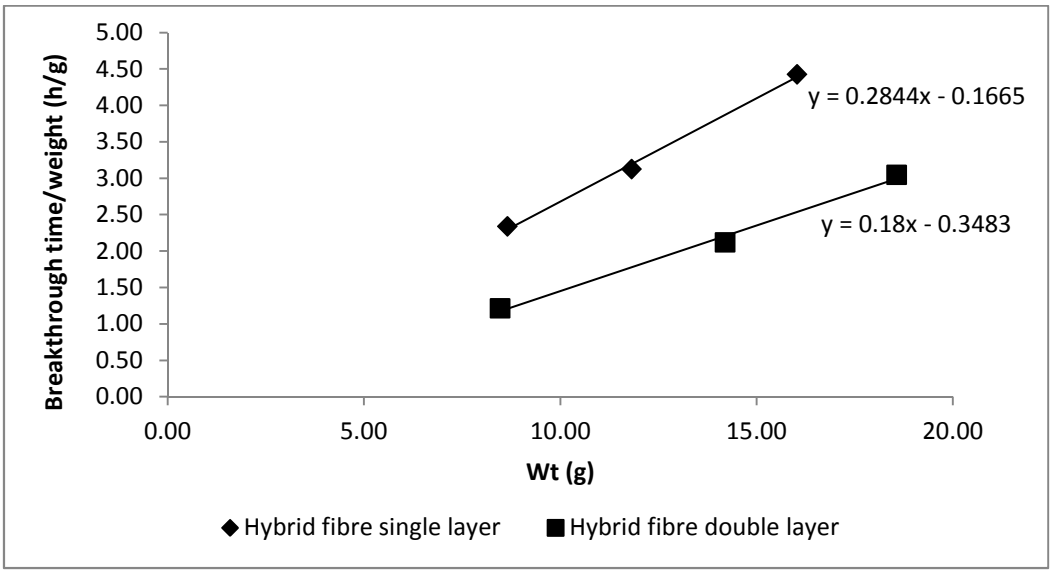

Figure 7.10. Weight plotted against breakthrough time/weight for 800 ppm 1 L/min ammonia on hybrid fibres.

Using the gradients shown in the figures above, k_v and W_e were calculated and used in the Wheeler-Jonas equation to predict breakthrough times. One example of data generated from the model for hybrid fibres is shown in Table 7.3 for hybrid fibres.

Table 7.3. Breakthrough times predicted using Wheeler-Jonas equation for hybrid fibres exposed to 800 ppm 1 L/min ammonia, using W_e of 0.0094 g/g.

Length (cm)	Adsorbent weight (g)	Density (g/cm^3)	k_v (min^{-1})	Experimental Breakthrough time (min)	Predicted breakthrough time (min)	**Difference (%)**
5.00	3.97	0.25	1670.64	58.83	58.66	**0.29**
10.00	8.65	0.28	1819.14	140.17	138.16	**1.43**
15.00	11.82	0.25	1656.63	187.50	191.96	**-2.38**
20.00	16.04	0.26	1685.44	265.50	263.54	**0.74**

Table 7.3 demonstrates that breakthrough time could be predicted accurately from the Wheeler-Jonas model. Using appropriate W_e and k_v values, it should be possible to predict the breakthrough time for different module weight and flow rates.

Theoretically Wheeler-Jonas can also be used to calculate t_s, t_{eq} and LMTZ. Examples of these predictions are shown for the single layer hybrid fibre. Calculations for stoichiometric time are shown in Table 7.4, equilibrium time in Table 7.5 and for the LMTZ in Table 7.6.

Table 7.4. Stoichiometric times predicted using Wheeler-Jonas for hybrid fibres with 800 ppm 1 L/min ammonia.

Length (cm)	Adsorbent weight (g)	t_s (min)	Predicted t_s (min)	**Difference (%)**
5.00	3.97	75.43	67.79	**-10.12%**
10.00	8.65	161.66	147.64	**-8.67%**
15.00	11.82	215.23	201.67	**-6.30%**
20.00	16.04	287.71	273.58	**-4.91%**

The accuracy of the stoichiometric times calculated using the Wheeler-Jonas equation is lower than for the breakthrough time in all cases. The difference between predicted and calculated t_s was 10% or less at all lengths, and decreased as the length/weight of the fibre module increased. This suggests the model will be more accurate for fibres of greater weight/length.

Table 7.5. Equilibrium time calculated from Wheeler-Jonas equation for single layer hybrid fibres with 800 ppm 1L/min ammonia.

Length (cm)	Adsorbent wt (g)	Actual t_{eq} (min)	Predicted t_{eq} (min)	**Difference (%)**
10.00	8.65	214.60	224.33	**+4.34%**
15.00	11.82	287.65	289.67	**+0.70%**
20.00	16.04	334.51	340.00	**+1.62%**

The predicted equilibrium time, shown in Table 7.5 was relatively accurate, with a difference of less than 5% in each case. In all cases, the predicted equilibrium time was higher than the actual breakthrough time.

Table 7.6. LMTZ calculated from Wheeler-Jonas equation for single layer hybrid fibres with 800 ppm 1L/min ammonia.

Length (cm)	Adsorbent weight (g)	Predicted MTZ (cm)	Observed MTZ (cm)	**Difference (%)**
5.00	3.97	5.86	1.46	**-75.04%**
10.00	8.65	5.21	1.34	**-74.22%**
15.00	11.82	7.13	1.47	**-79.33%**
20.00	16.04	5.18	1.45	**-72.02%**

The length of the adsorption front should not change, and so the LMTZ should be the same in each sample. This was reflected in the predicted lengths in Table 7.6. However, the predicted LMTZs were very different to the actual LMTZs for the adsorbent hollow fibres. This supports the observation from the pressure drop tests that there were entrance effects until the fibre length reached 20 cm in length, and as such the weight reached a certain point. This demonstrates that the Wheeler-Jonas equation does not model well LMTZ for ammonia on hybrid fibres. For AbScents1000, single layer fibres, tests were performed on 5 to 25 cm long modules and used to predict LMTZ, shown in Table 7.7. In general, while the predicted LMTZ was fairly consistent, the measured MTZ from the tests varied significantly. This was most likely due to the difficulty in selecting an equilibrium time from the breakthrough tests. As equilibrium time was selected subjectively, this affected the stoichiometric time and as such the observed LMTZ.

Table 7.7. LMTZ calculated from Wheeler-Jonas equation for single layer AbScents1000 fibres challenged with 1 L/min 800 ppm ammonia.

Length (cm)	Weight (g)	Predicted MTZ (cm)	Observed MTZ (cm)	**Difference (%)**
5	4.79	4.13	2.95	**40.15%**
10	9.13	4.34	3.85	**12.68%**
15	14.42	4.12	4.22	**-2.33%**
20	18.40	4.30	5.47	**-21.29%**
25	24.09	4.11	4.45	**-7.74%**

While the measured breakthrough times and those predicted from the Wheeler-Jonas equation were similar, it is clear that they diverge more for stoichiometric and equilibrium times and it helps explain why there is a difference in calculated LUB and MTZ. In addition, as the length of fibre increased, the difference between measured and predicted breakthrough curves became proportionally smaller.

7.2.2.2 Modelling breakthrough time for cyclohexane challenge using flow rate

Breakthrough tests at changing flow rates can be used to obtain the constants for the Wheeler-Jonas model. Breakthrough time ($y = t_b$) was plotted against 1/ the flow rate ($x = 1/Q$). Figure 7.11, Figure 7.12 and Figure 7.13 show the linear graphs of breakthrough time against 1/flow rate for hybrid fibres, AbScents1000 fibres and NV5 fibres respectively.

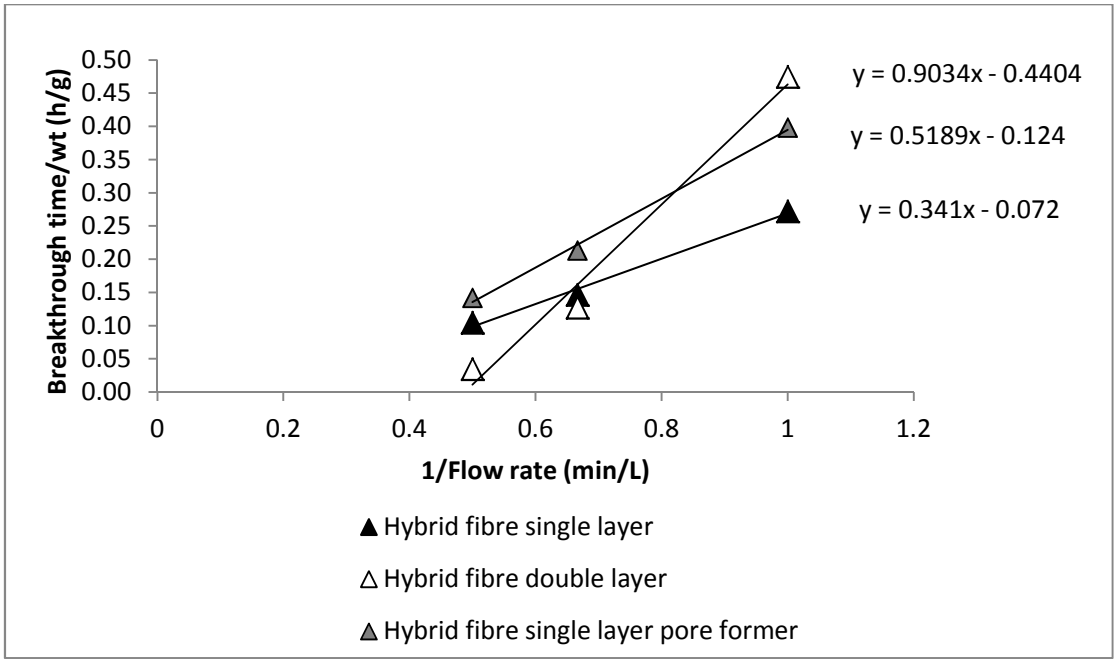

Figure 7.11. Breakthrough times for 1000 ppm 1 L/min cyclohexane on 80% hybrid fibres, plotted against 1 / flow rate.

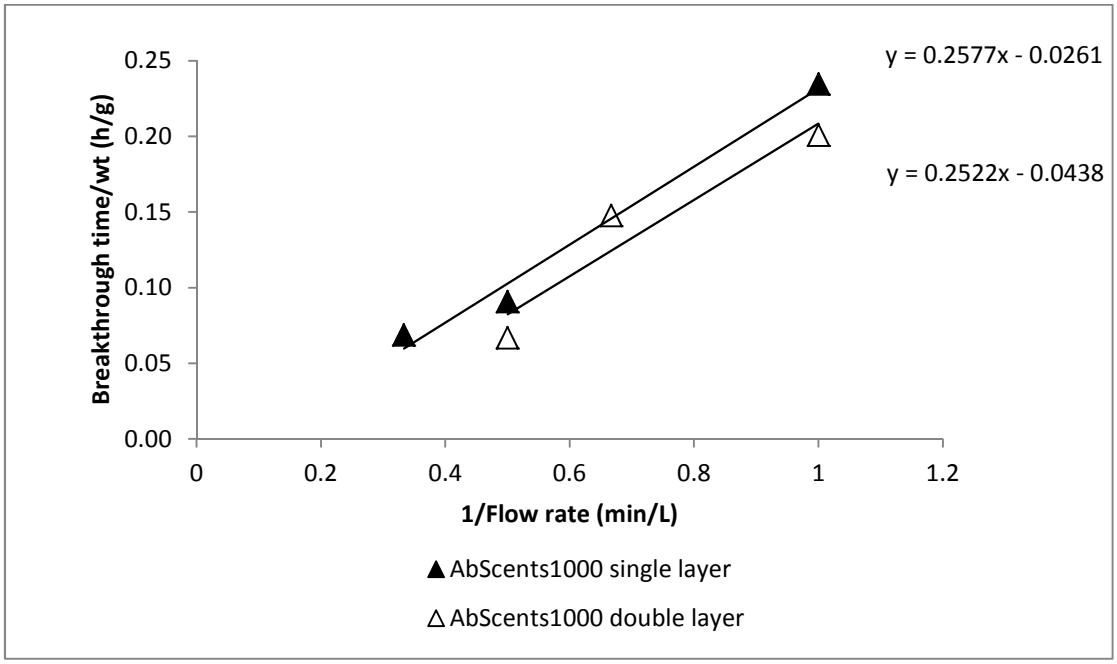

Figure 7.12. Breakthrough times for 1000 ppm 1 L/min cyclohexane on 80% AbScents1000 fibres, plotted against 1 / flow rate.

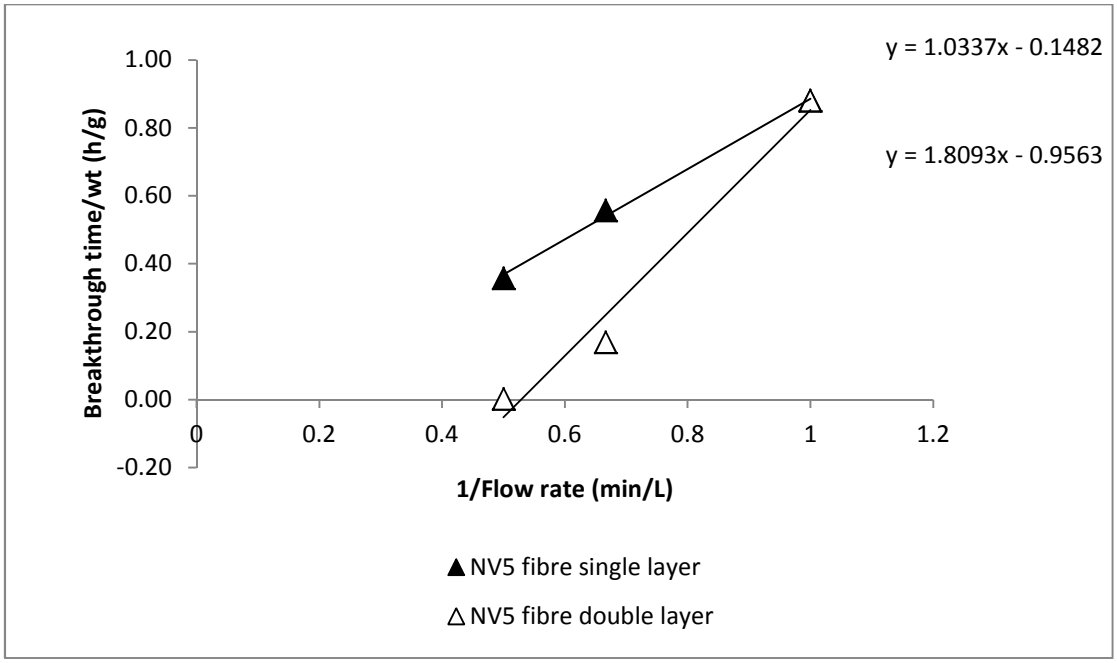

Figure 7.13. Breakthrough times for 1000 ppm 1 L/min cyclohexane on 80% NV5 fibres, plotted against 1 / flow rate.

As flow rate increased, the breakthrough time decreased. The trend between 1/flow rate and breakthrough time was linear. For the hybrid fibres, clear trend lines could be drawn. However, for the AbScents1000 fibres, these trend lines were less accurate. This is attributed to the poor affinity of cyclohexane for AbScents1000, most likely due to its small pore size. As such the breakthrough times on these fibres were low, especially as flow rate increased and residence time decreased. The poor fit of the line will affect the W_e and k_v values, and so reduce accuracy of any model derived from this graph.

Breakthrough times were predicted for single layer hybrid fibres exposed to 1000 ppm cyclohexane at 1, 1.5 and 2 L/min using W_e of 0.0080 g/g. These are shown in Table 7.8. The breakthrough times for single layer 80% NV5 fibres exposed to 1000 ppm cyclohexane at 1, 1.5 and 2 L/min using We of 0.025 g/g is shown in Table 7.9.

Table 7.8. Breakthrough times for 1000 ppm cyclohexane predicted using Wheeler-Jonas equation for single layer hybrid fibres using W_e of 0.025 g/g.

Flow rate (L/min)	Adsorbent weight (g)	Density (g/cm^3)	k_v (min^{-1})	Breakthrough time (min/g)	Predicted breakthrough time (min/g)	**Difference (%)**
1	6.83	0.22	543	16.32	16.15	**1.06**
1.5	10.17	0.32	809	8.77	9.33	**-6.37**
2	9.19	0.29	731	6.28	5.92	**5.68**

Table 7.8 shows relatively good agreement between predicted and actual breakthrough times for 1000 ppm cyclohexane on hybrid fibres, with the greatest % difference of 6.37%. These predicted breakthrough times were less accurate than those predicted for ammonia on hybrid fibres. This is most likely due to the smaller breakthrough times/g. For example, a difference of 0.56 min/g breakthrough time/weight for 10 cm fibres at 1.5 L/min in Table 7.8 resulted in a 6.37% difference, while a difference of 2.01 min/g in Table 7.3 gave a difference of 1.43%. As expected, when breakthrough times are lower, a greater amount of error was introduced. This is verified by the predictions in Table 7.9.

Table 7.9. Breakthrough times predicted using Wheeler-Jonas equation for single layer 80% NV5 fibres exposed to 1000 ppm 1-2 L/min cyclohexane using W_e of 0.025 g/g (measured equilibrium loading from experiments 0.024 g/g).

Flow rate (L/min)	Adsorbent weight (g)	Density (g/cm^3)	k_v (min^{-1})	Breakthrough time (min/g)	Predicted breakthrough time (min)	**Difference (%)**
1	8.82	0.28	1070	52.81	53.15	**-0.65**
1.5	8.00	0.25	970	33.43	32.48	**2.85**
2	8.48	0.27	1030	21.47	22.14	**-3.11**

As shown in Table 7.9, the difference between predicted and observed breakthrough time for a flow rate of 1.5 L/min was just over 1 min/g, which was only a 2.85% difference compared to the 64% difference in the hybrid fibres for the reasons stated above.

Most cyclohexane tests could not be run to completion, making a detailed comparison of predicted and observed stoichiometric times, equilibrium times, and MTZ impossible. For AbScents1000 single layer fibres, all tests were run to completion, due to shorter breakthrough times. However, due to these short values, greater errors were calculated, with +/- 10% difference between predicted and actual breakthrough times. This suggests that the Wheeler-Jonas model is suitable for predicting breakthrough times for ammonia and cyclohexane on hollow fibres, so long as the fibres are greater than 5 cm in length. Predicted values will be more accurate for fibres with higher breakthrough time/weight.

7.2.2.3 Testing applicability of the Wheeler-Jonas model to adsorbent hollow fibre filters

To confirm the applicability of the Wheeler-Jonas model for predicting the breakthrough times for adsorbent hollow fibre filters, the constants determined in the previous Section were used to predict:

1) Breakthrough time of dynamic ammonia challenge on 15 cm single layer 80% AbScents1000 fibres at 3 L/min, shown in Table 7.10.
2) Breakthrough time of dynamic cyclohexane challenge on 15 cm single layer 80% hybrid fibres at 1 L/min, shown in Table 7.11.
3) Breakthrough time of dynamic cyclohexane challenge on 15 cm single layer 80% NV5 fibres at 1 L/min, shown in Table 7.12.

Table 7.10. Predicting breakthrough times for 800 ppm 3 L/min ammonia challenge on 15 cm fibres using kinetic data from 1 L/min ammonia challenge.

Flow rate (cm^3/s)	Adsorbent wt (g)	t_b (min/g)	Density (g/cm^3)	1/Q (s/cm^3)	W_e (g/g)	k_v (1/min)	Predicted t_b (min/g)	**Difference (%)**
3000	14.02	6.85	0.30	3.33E-04	0.02	532.67	6.55	**4.27**

Table 7.11. Predicting breakthrough time for 1000 ppm 1 L/min cyclohexane challenge on 15 cm hybrid fibres, calculated using data from 1-2 L/min cyclohexane challenge.

Flow rate (cm^3/s)	Adsorbent wt (g)	t_b (min/g)	Density (g/cm^3)	W_e (g/g)	k_v (1/min)	Predicted t_b (min/g)	**Difference (%)**
1000	3.7952	10.27614	0.24	0.018428	6.04E+02	7.06	**31.31**

Table 7.12. Predicting breakthrough time for 1000 ppm 1 L/min cyclohexane challenge on 15 cm NV5 carbon fibres, calculated using data from 1-2 L/min cyclohexane challenge.

Flow rate (cm^3/s)	Adsorbent wt (g	t_b (min/g)	Density (g/cm^3)	W_e (g/g)	k_v (1/min)	Predicted t_b (min/g)	**Difference (%)**
1000	4.77	28.05	0.30	0.04	1156.68	24.69	**11.99**

The k_v and W_e values for ammonia on AbScents1000 fibres were those calculated for 800 ppm ammonia at 1 L/min (Table 7.3). Breakthrough time was predicted using the flow rate, rather than the weight of the fibres as was used previously. The calculated breakthrough time of 6.55 min/g was very similar to the experimental breakthrough time of 6.85 min/g (<5% difference).

The k_v and W_e values calculated from cyclohexane on hybrid NV5/AbScents1000 fibres (Table 4.8) were used to predict 1000 ppm cyclohexane breakthrough on these fibres. In the case, the fibre weight was used to calculate breakthrough time, rather than flow rate as was done previously. As can be seen in Table 7.11, the error was higher than in the ammonia predictions. 3 min/g error on a 4 g fibre is small in practical terms, but large proportionally. For the NV5 fibres, the k_v and W_e values for cyclohexane on NV5 fibres were used to predict 1000 ppm cyclohexane breakthrough on these fibres. As shown in Table 7.12, the error was smaller, 12%. These errors were most likely a product of the wall and entrance effects affecting the shorter fibre beds, particularly at higher flow rates. Nevertheless, these results demonstrate the viability of the Wheeler-Jonas to give an approximate estimate of the breakthrough time in minutes/weight adsorbent.

7.2.3 Overall performance of adsorbent hollow fibres compared to granular beds

Adsorption indices of breakthrough time and loading per weight, pre pressure drop and per volume of the module were calculated for single and double layer hybrid NV5/AbScents1000 fibres and hybrid NV5/AbScents1000 pellets. These were calculated as the breakthrough time and loading divided by the weight, pressure drop and volume of the module. These are compared in Table 7.13 and Table 7.14 with data bars indicating the relative size of the value in each column.

Table 7.13. 800 ppm 1 L/min ammonia adsorption performance indices of hybrid 20% PES 40% AbScents1000 40% NV5 fibres to hybrid 20% bentonite 40% AbScents1000 40% NV5. S indicates single layer fibres.

Module	Breakthrough time/wt (h/g)	Breakthrough loading/wt (g/g)	Breakthrough time/pressure drop (h/Pa)	Breakthrough loading/pressure drop (g/Pa)	Breakthrough time/volume (h/cm^3)	Breakthrough loading/volume (g/cm^3)
10 cm hybrid pellets	0.208	0.007	0.047	0.002	0.088	0.003
10 cm hybrid fibres S	0.270	0.009	0.060	0.002	0.074	0.003

Table 7.14. 1000 ppm 1 L/min cyclohexane adsorption performance indices of hybrid 20% PES 40% AbScents1000 40% NV5 fibres to hybrid 20% bentonite 40% AbScents1000 40% NV5. S indicates single layer fibres, D indicates double layer.

Module	Breakthrough time/wt (h/g)	Breakthrough loading/wt (g/g)	Breakthrough time/pressure drop (h/Pa)	Breakthrough loading/pressure drop (g/Pa)	Breakthrough time/volume (h/cm^3)	Breakthrough loading/volume (g/cm^3)
10 cm hybrid pellets	0.957	0.197	0.213	0.044	0.399	0.082
10 cm hybrid fibres S	0.272	0.062	0.048	0.011	0.059	0.014

For ammonia adsorption, the data shown in Table 7.13 demonstrates that single layer fibres had greater breakthrough time and loading in respect to weight and pressure drop, but lower breakthrough time and loading in respect to the volume of the module. The higher breakthrough time and loading of the pellets in respect to volume was due to the higher density of the module, which also confirms why the pellets performed less well in regards to their pressure drop and weight.

For the cyclohexane adsorption, shown in Table 7.14, hybrid pellets outperformed the PES hollow fibres in all cases. While the adsorbent hollow fibres had a reasonable breakthrough time of 1.49 hours, the pellets had such a long breakthrough time, 12.54 hours, that they would always excel in the performance indices. The relatively poor performance of the adsorbent hollow fibres must be associated with one of the two main differences between the two: the binder used or the flow of the gas through the bed. PES

blocks access to the adsorbent structure, as was discussed in Chapter 6, which particularly seemed to negatively affect adsorption of the large cyclohexane molecules. It is likely that this problem for adsorbent hollow fibres could be mitigated by using a PIM as the binder rather than PES.

7.2.4 Candidate mask design and performance

One potential candidate cartridge design suggested by Dstl was a rectangular chin bar cartridge: 1 cm wide, 10 cm long and 6 cm high with a diagram shown in Figure 7.14. Two of these would be used in a mask. Breakthrough time, loading and pressure drop were calculated for 800 ppm 1 L/min ammonia and 1000 ppm 1 L/min cyclohexane at 5 L/min (average human breathing rate) on two cartridges prepared from single layer hybrid 20% PES 40% AbScents1000 40% NV5 fibres this size.

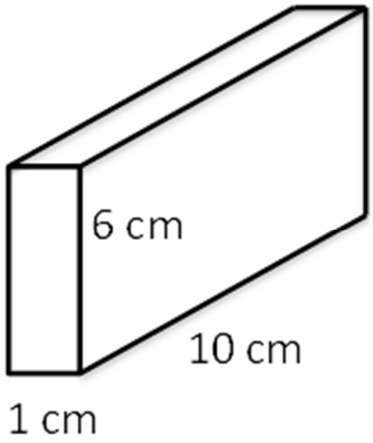

Figure 7.14. Potential future respirator chin bar cartridge

With a volume of 60 cm^3 and density of the hybrid fibres approximately 0.26 g/cm^3, the weight of one cartridge would be 15.6 g. Assuming flow rate will distribute evenly between both cartridges, each will be exposed to a 2.5 L/min flow rate.

For 800 ppm ammonia, W_e was determined to be 0.024 g/g and k_v to be 4254.14 /min. This gives a breakthrough time of 256.11 minutes. If flow is evenly distributed through both cartridges, breakthrough should occur through both simultaneously at this point.

For 1000 ppm cyclohexane, W_e was determined to be 0.0080 g/g and k_v to be 650 /min. This gives a breakthrough time of 203.75 minutes.

According to BSI regulations (2008), the minimum breakthrough time for 0.1% volume (1000 ppm) cyclohexane is 70 minutes, and for the same concentration of ammonia, 50 minutes. Though no flow rate is specified, assuming an average breathing rate of 5 L/min, the projected hollow fibre cartridge breakthrough time comfortably exceeds both of these breakthrough times.

Modelling pressure drop:

The area occupied by a single layer standard bore hollow fibre is 2.81 x10^{-6} m^2 and the area of the module is 6 cm^2 or 0.0006 m^2. This will be occupied by 213 fibres. The total lumen area is 0.00014 cm^2. The voidage is therefore 0.0006 m^2/0.00014 cm^2, or 0.22.

Using the Hagen-Poiseuille equation:

$$\frac{\Delta P}{L} = \frac{32\mu}{d^2}\left(\frac{v}{\epsilon_0}\right)$$

Superficial velocity v = flow rate (m^3/s) / area of module = (2.5 / 1000 / 60) / 0.0006 = 0.069 m/s. Viscosity of nitrogen μ = 1.84x10^{-5} Pa·s. Therefore:

$$\Delta P = \frac{32\ \times 1.84 \times 10^{-5}}{(9.0 \times 10^{-4})^2}\left(\frac{0.069}{0.22}\right) \times 0.1$$

This gives a pressure drop of 22.13 Pa for a 10 cm module.

The equivalent for a granular bed, according to the Ergun equation, would be:

$$\Delta P = L\left(\frac{150u\mu(1-\varepsilon)^2}{\varepsilon^3 d_p^2} + \frac{1.75(1-\varepsilon)\rho u^2}{\varepsilon d_p}\right)$$

$$\Delta P = L\left(\frac{150 \times 0.069 \times 1.84 \times 10^{-5}(1-0.4)^2}{0.4^{3\times}0.0016^2} + \frac{1.75(1-0.4) \times 1.19 \times 0.069^2}{0.4 \times 0.0016}\right)$$

This gives a pressure drop of 40.49 Pa, double that of the equivalent adsorbent hollow fibre. If the flow rate was increased to 90 L/min, or 45 L/min through each filter, the pressure drop in the fibre module would be 420.52 Pa and for the granular bed it would be 717.10 Pa.

According to the BSI regulations (2008), the maximum allowed breathing resistance is 610 Pa at 95 L/min. As such, the breathing resistance of the novel cartridge with an adsorbent hollow fibre filter is allowable, while with a pellet filter, it would be too high.

The maximum allowable mass of the filter is 500 g for a full face mask. The hollow fibre filters weigh 15.6 g each, making the combined weight of 31.2 g far below the maximum allowable weight.

The small size of the cartridges makes them ergonomic for inclusion in a helmet design. However, if greater weight filters were developed (up to 250 g each) there would certainly be concerns, as the volume of each filter would be 962 cm^3!

7.3 Discussion

This Chapter investigated the overall applicability of adsorbent hollow fibres in respirator cartridges, focusing on models to simulate more realistic challenge conditions than those in the labs. The Hagen-Poiseuille model has successfully been used to measure pressure drop in fibres by Bhandari *et al.* (2010) and Feng *et al.* (1998). The Hagen-Poiseuille equation was found to simulate the pressure drop in adsorbent hollow fibres well in this work, but only once the length of the fibre was greater than 20 cm, for a 2 cm diameter module. This is most likely due to entrance and wall effects. These are likely to be in effect in the current military cartridges, as these have a greater diameter than length, but will make modelling at higher flow rates more complicated for adsorbent hollow fibre modules. The pressure drops in the granular beds tested were simulated well by the Ergun equation once the column was longer than 15 cm in length, for the same reasons as for the fibres. However, the dispersive effects of the granular beds counteracted some of the entrance effects, hence the effectiveness at lower aspect ratio. As flow rate increases, the improvement in pressure drop of an adsorbent hollow fibre cartridge over a granular cartridge will increase due to the linear Hagen-Poiseuille equation compared to the exponential Ergun equation. Laminar flow takes place in standard bore hollow fibres up to high flow rates. This is due to the large number of small diameter bores in the hollow fibre modules. Turbulent flow in adsorbent hollow fibres could still be encountered in respirators, and in this case, a different model that explains turbulent flow in pipes would be necessary to predict pressure drop.

The Wheeler-Jonas model was used to predict the breakthrough times of fibre beds, using empirical data from several experiments to determine W_e and k_v values. This worked relatively well, giving accurate breakthrough times +/- several minutes in either direction. However, when used to predict stoichiometric time, equilibrium time and mass transfer zone, the error grew larger and larger. This suggests that the Wheeler-Jonas equation is most accurate for determining breakthrough time in adsorbent hollow fibres. This was similar to what was found by Bell *et al.* (2012), with the Wheeler-Jonas equation fitting the adsorption curve of their hollow fibre cartridge from C/C_0 0.08 to 0.88, although breakthrough occurred at C/C_0 of 0.03 in the case of their research. Problems in predicting values other than t_b arose because the Wheeler-Jonas does not take into account any resistances or isotherm data. The modelled Wheeler-Jonas curve was far sharper than the experimental breakthrough curves of the adsorbent hollow fibres. The equation also only applies to symmetrical breakthrough curves, which was not always the case for adsorbent hollow fibres, some giving asymmetric curves that more closely matched the curve given by the linear driving force equation (Grévillot *et al.*, 2011). As resistance is reduced in adsorbent hollow fibres, for example, by spinning into a water solvent mix (Chapter 6), the difference between the breakthrough curve and that given by the Wheeler-Jonas equation may be smaller, meaning stoichiometric time, equilibrium time and mass transfer zone could be more accurately predicted. Alternatively, the linear driving force model may give more accurate predictions, given the results in Bell *et al.* (2012). However, one problem would be that obtaining full isotherms of a range of toxic industrial chemicals, or even nerve agents, would be difficult.

Performance indices were calculated for adsorbent hollow fibres and pellets, in terms of their breakthrough time and loading compared to their weight, pressure drop and volume. Adsorbent hollow fibres were found to give favourable indices in terms of adsorption per weight and pressure drop for ammonia adsorption, but were unfavourable in all regards for cyclohexane adsorption. This is due to the extremely high uptake of cyclohexane on the pellets compared to the fibres, and indicates a potential problem with organic adsorption on the adsorbent hollow fibres. By volume, the adsorption on pellet module was superior to the fibre module, due to the higher density of pellets. If fibres were packed more densely, this could begin to improve their performance index in terms of

adsorption per volume, but would weaken their performance with respect to adsorption per weight and pressure drop.

In terms of future design, one particular example suggested by Dstl was a 1 x 10 x 6 cm rectangular gas mask filter for incorporation into the chin bars of a helmet. Two of these would be used, one on each side. The current S10 gas mask has only one filter, but a greater number of filters would improve the flow properties. As breakthrough time is proportional to 1/flow rate, it can drop very rapidly as flow rate increases. As such, by distributing the flow through several different cartridges it can be reduced accordingly. Due to the lower weight of fibres this would be possible without heavily weighing down the user. It is also important to consider that while PES has good mechanical strength, the fibres are vulnerable to crushing or snapping. By incorporating the respirator within a helmet, the user will not have to wear a separate helmet and mask and the incorporated fibres will be protected from mechanical stress by the helmet. Pressure drop in the candidate respirator filter was modelled using the Hagen-Poiseuille equation breakthrough time for ammonia and cyclohexane at the concentrations stated in BSI was modelled using the Wheeler-Jonas equation. At an average human breathing rate of 5 L/min, a breakthrough time of approximately 256 minutes was predicted for ammonia and 204 minutes for cyclohexane. These well exceed the times given in the BSI (2008) as well as the other physical parameters for a mask. This suggests that, even though adsorbent hollow fibres may have lower breakthrough times than pellets, they are still suitable for use in cartridges, and will have a lower pressure drop in the set size.

7.4 Conclusion

Pressure drop in adsorbent hollow fibres greater than 20 cm in length could be predicted using the Hagen-Poiseuille model as flow rate was increased from 1-5 L/min. This model suggests that adsorbent hollow fibres are a favourable alternative to granular beds at high flow rates. However, the practical implications of such a long filter must be considered.

Ammonia and cyclohexane challenge breakthrough times on adsorbent hollow fibres could be predicted using the Wheeler-Jonas equation with empirically determined kinetic parameters. This was confirmed to allow predictions for changing:

- Flow rate

- Bed weight

Using the empirical values determined in this chapter, the Wheeler-Jonas equation should hypothetically be able to predict breakthrough time in these particular hollow fibres for changing:

- Adsorbent concentration
- Module density

Performance indices were determined for granular beds of pellets and fibres based on their breakthrough time and loading per pressure drop, weight and volume:

- For cyclohexane breakthrough challenge, the adsorbent hollow fibres performed poorly compared to the granular bed in all cases.
- For ammonia breakthrough challenge, the adsorbent hollow fibres had improved breakthrough time per Pascal and gram.

The Hagen-Poiseuille and Wheeler-Jonas equations were used to predict pressure drop and breakthrough time for a candidate respirator filter. Breakthrough times of over 200 minutes for 5 L/min ammonia and cyclohexane challenge, assuming even flow between both cartridges, and a pressure drop of 40 Pa at a 5 L/min breathing rate were predicted. This suggested that adsorbent hollow fibres are viable for use in a respirator according to BSI regulations, despite their unfavourable performance index for cyclohexane adsorption.

8 Future work

Throughout this project a number of avenues of research taking advantage of the adsorbent hollow fibre structure have been investigated. In some cases, basic experimentation was carried out but further research will be necessary to fully explore the area. This has resulted in a several potential future projects based on this work, some of which are elaborated in this Section.

Gas travels down the bore of hollow fibres in a linear path as opposed to the tortuous path taken through a granular bed. This presents the opportunity to develop a 'residual service life indicator' (RSLI) for a fibre filter. This would be some transformation, such as a colour change, that indicates when adsorption has taken place and so how far the adsorption front has travelled along the filter. Experimentation was carried out using thermochromic paint incorporated into the fibre precursor mixture to take advantage of the exothermic nature of adsorption. While this retained effectiveness after the spinning process, the temperature change was not sensitive enough to indicate the adsorption front, and further, after the adsorption front had passed, the fibres would return to their original colour. In hot or cold ambient conditions, there would be interference.

Figure 8.1. Hollow fibres soaked in flavin anthocyanin derived from boiled red cabbage.

An alternative method using a pH indicator either in the adsorbent hollow fibre precursor mixture or as a coating was considered and brief experimentation using a pH indicator derived from boiled red cabbage was found to be effective at detecting acid or alkali gases, shown in Figure 8.1. The centre is the colour of the fibre after soaking. The lowermost left fibre has had 1M hydrochloric acid dripped onto it with the two above changing pink as a result of the hydrochloric avid vapour released. The right side of the fibres changed green after exposure to 1M sodium hydroxide liquid. Obviously this would not detect neutral gases (i.e. organics), providing a potential sense of false security in military applications, but could be suitable in industry, where the specific contaminant gas is known. Alternatively,

some PIMs change colour when exposed to organics and could potentially be used in combination. This work could be refined further in future.

Further opportunities exist in investigating gas flow, such as higher or lower flow rates. In addition studying flow distribution between two columns could unveil any interesting interactions or bias in flow between columns. In addition, testing with combined challenge gases (e.g. ammonia and hydrogen sulphide at the same time), to determine which are adsorbed preferentially and whether there are likely to be any interactions on the adsorbent could have interesting results, although in practice it would be difficult to prepare such an experiment due to difficulties with detectors.

The BSI regulations used to inform the selection of TICs also include a separate category for sulphur dioxide. Dynamic tests or isotherms with this particular gas, and particularly its interaction with impregnants, which are likely to be necessary for full removal, would be useful future work in filter design. In addition, isotherms with ammonia or hydrogen sulphide could be measured, as the equipment was not available during this project. This would enable linear driving force modelling to be performed and compared to the Wheeler-Jonas modelling. Breakthrough challenge tests could also be run for further TICs of interest, as these fibres could potentially be used in industry as well as in the military.

Chapter 4 investigated the effect of changing the bore size of the fibres, and on the whole, it was determined that larger bore size resulted in lower pressure drop, as did reducing the fibre size. Further investigation could be done in this area to find an optimal bore size and diameter for the fastest adsorption kinetics, taking into account other concerns, such as fibre strength and the need for specialised spinning equipment. Similarly, the BSI regulations detail a method of testing cartridge strength that was not available for this work. As such, mechanical tests of the strengths of fibre cartridges could be carried out in future.

This report focused on a relatively few different adsorbents, impregnants and polymers, as the key aim was to explore the applicability of adsorbent hollow fibres in respirator applications and look for patterns and models in adsorption. As such, further optimisation of the adsorbent and impregnating chemicals, alone or in combination, would allow targeting of adsorbent hollow fibre cartridges to specific TICs, while changing polymers

and further exploring the area of PIMs may result in greater accessibility to the fibre (as explored in Chapter 6) or improve or weaken mechanical strength. In addition, previous work has indicated that lower polymer content may enhance adsorbent accessibility (Nevell and Perera, 2011). As such, developing methods to spin fibres with up to 90% adsorbent could prove useful, as could exploring lower adsorbent content to enhance fibre strength.

Gas mask cartridges undergo extensive testing before use, including an ageing test. This was not explored extensively in this project due to time constraints, as ageing a cartridge for a year was not feasible within the timescale.

Finally, in order to examine the practicality of introducing fibres to respirators and associated pitfalls or advantages, a prototype mask could be prepared in future, incorporating the adsorbent hollow fibres in best possible configuration. This would enable practical tests of comfort as well as effectiveness in the field, as well as potentially resulting in a new product at the end of the project.

9 Overall Conclusions

The project aim was to develop novel hollow fibre modules with low pressure drop for use in respirator filters, and tailor them to remove toxic industrial chemicals, while following EU regulations for stability and performance.

This aim has been met by fulfilling each of the objectives described below:

The objectives and how they were met, are given below:

- Determine the optimal adsorbents for removal of the model gases ammonia, hydrogen sulphide and cyclohexane, and prepare these as adsorbent hollow fibres.

  A literature review suggested carbon and zeolites are good adsorbents for cyclohexane and ammonia respectively. A range of such adsorbents was screened. From these, AbScents1000, a high silica zeolite, and NV5 carbon, a microporous carbon, were selected as candidate adsorbents. This was due to their ability to sorb ammonia and cyclohexane without severe negative effects from competition with water, which would hinder the use of more hydrophilic zeolites. No untreated adsorbents were found to adequately sorb hydrogen sulphide.

- Optimise the hollow fibre structure for the greatest adsorption uptake, fastest adsorption kinetics and lowest pressure drop.

  Fibres developed to complete the previous objective were dynamically challenged with ammonia and cyclohexane to explore different fibre structures. It was found that:

  - Thin walled single layer fibres adsorbed ammonia faster than thick walled (double or single layer).
  - Thick walled fibres adsorbed cyclohexane faster than thin walls. However, as flow rate was increased beyond 2 L/min, the thin walled fibres had higher breakthrough time than double layer.

  The average human breathing rate is greater than 2 L/min, meaning that thin walled fibres are likely to have higher breakthrough time than thick walled fibres at higher flow rates. As such thin walled fibres were selected for potential use in a respirator filter.

From pressure drop tests, it was found that fibres with 1 mm bores had lower pressure drop than those with 0.8 mm bore. As such, the larger bore fibres were selected for further testing.

Overall the fibres developed to meet this objective were thin walled fibres with 1 mm bores.

- Explore ways to enhance adsorption using additives, such as metal salts, metal organic frameworks and pore formers.
  Hybrid fibres were treated by including metal salts, metal organic frameworks and pore forming agents.

  The simplest and most effective method to include a metal salt was found to be by impregnating the adsorbent fibre after it had been spun. 10%wt impregnated copper oxide was found to greatly enhance the adsorption of H_2S on adsorbent hollow fibres.

  The metal organic framework CuBTC (also known as HKUST-1 or MOF-199) slightly improved H_2S adsorption on adsorbent hollow fibres. However it was difficult to impregnate and broke down on exposure to H_2S. As a result, MOF impregnated fibres loaded no more H_2S than the CuO impregnated fibres in terms of %wt. CuBTC was concluded not to be a impregnant for hollow fibres. The problems encountered are likely to extend to other MOFs, though some may be suitable for impregnation on fibres if they are stable on exposure to the contaminants and ambient water.

  Incorporation of pore forming agents, specifically 1%wt montanic acid wax (Licowax SP), was found to increase the breakthrough time of cyclohexane on hollow fibres, but to decrease the breakthrough time of ammonia. Other pore formers and other ratios of pore former may have different effects on fibre structure and need to be studied further.

- Investigate an alternative microporous polymer for use as the binder in hollow fibres.

  The use of PES binder in the hollow fibres was found to decrease overall cyclohexane uptake of the fibres. As such, a polymer of intrinsic microporosity, PIM-1, was used instead of PES. This increased overall uptake of octane and cyclohexane due to the adsorption on the PIM-1.

  Despite improved access to the adsorbent within the polymer matrix and higher overall uptake, PIM-1 fibres had slow uptake of octane (instant breakthrough on dynamic challenge). Methods to enhance uptake rate were explored. However none of these approaches were found to significantly improve the porosity of the fibres or affect the uptake rate. As such, while PIM-1 or other microporous polymers have the potential to fully realise the adsorbent potential of the fibres, they slow down adsorption kinetics. This is impractical for use in a respirator filter, where a long breakthrough time is necessary.

- Model pressure drop and breakthrough time for a candidate novel hollow fibre respirator filter using the data collected.

  Pressure drop and breakthrough time were modelled on a candidate cartridge using the Hagen-Poiseuille and Wheeler-Jonas equations respectively, with accurate breakthrough time (+/- ~10%) and pressure drop performance calculated. These models will assist in future hollow fibre filter design.

- Develop performance indices that will allow comparison of adsorbent hollow fibre and conventional granular adsorbent performance relative to their weight and pressure drop.

  Granular beds and adsorbent hollow fibres were compared in terms of their adsorption in relation to their weight, volume and pressure drop.

  - For cyclohexane, adsorbent hybrid pellets had superior pressure drop, weight and volume indices.
  - For ammonia, adsorbent hybrid pellets had inferior weight and pressure drop indices (though superior volume performance).

These indices enabled fair comparison of hollow fibre and granular modules, despite different weights and pressure drops.

To fulfil the aim of this project and demonstrate the potential of adsorbent hollow fibres to be used in respirators, a future hollow fibre filter design was tested. The Wheeler-Jonas equation was used to predict ammonia and cyclohexane breakthrough time at 5 L/min flow rate. The breakthrough time for was 256.11 minutes for ammonia and 203.75 minutes for cyclohexane. These exceed the BSI regulations of 60 minutes breakthrough, as well as the pressure drop requirement.

In conclusion, this project has demonstrated the viability of preparing adsorbent hollow fibres for future respirator filters. This work is intended to demonstrate the flexibility and viability of adsorbent hollow fibres and to be used as a spring board for future investigations.

10 Author's publications

Jeffs, C.A. Smith, M.W., Stone, C.A., Bezzu, C. G., Msayib, K.J., McKeown, N.B., Perera, S.P, 2013. A polymer of intrinsic microporosity as the active binder to enhance adsorption/separation properties of composite hollow fibres. *Microporous and Mesoporous Materials,* 170, 105-112.

Jeffs, C.A. Smith, M.W., Stone, C.A., Crittenden, B.D., Perera, S.P, 2013. Hybrid Hollow Fibres with Enhanced Adsorption Capacity and Reduced Pressure Drop. *Third International Conference on Multifunctional, Hybrid and Nanomaterials,* Sorrento. Poster presentation.

Jeffs, C.A. Smith, M.W., Stone, C.A., Crittenden, B.D., Perera, S.P, 2013. Low pressure drop respirator gas filters using adsorbent hollow fibres as an alternative to granular adsorbents. *Journal of the International Society of Respiratory Protection,* 30, 21-30.

11 References

Águeda, V.I., Crittenden, B.D., Delgado, J.A. & Tennison, S.R. 2011. Effect of channel geometry, degree of activation, relative humidity and temperature on the performance of binderless activated carbon monoliths in the removal of dichloromethane from air. *Separation and Purification Technology,* 78**,** 154-163.

Aigueperse, J., Mollard, P., Devilliers, D., Chemla, M., Faron, R., Romano, R. & Cuer, J.P. 2000. Fluorine compounds, inorganic. *Ullmann's encyclopedia of industrial chemistry.* Wiley-VCH Verlag GmbH & Co. KGaA.

Alves, B.R. & Clark, A.J. 1986. An examination of the products formed on reaction of hydrogen cyanide and cyanogen with copper, chromium (6+) and copper-chromium (6+) impregnated activated carbons. *Carbon,* 24**,** 287-294.

Ameloot, R., Liekens, A., Alaerts, L., Maes, M., Galarneau, A., Coq, B., Desmet, G., Sels, B.F., Denayer, J.F.M. & De Vos, D.E. 2010. Silica–mof composites as a stationary phase in liquid chromatography. *European Journal of Inorganic Chemistry,* 2010**,** 3735-3738.

An, H., Feng, B. & Su, S. 2013. Effect of monolithic structure on co2 adsorption performance of activated carbon fiber–phenolic resin composite: A simulation study. *Fuel,* 103**,** 80-86.

Atkinson, J.D., Fortunato, M.E., Dastgheib, S.A., Rostam-Abadi, M., Rood, M.J. & Suslick, K.S. 2011. Synthesis and characterization of iron-impregnated porous carbon spheres prepared by ultrasonic spray pyrolysis. *Carbon,* 49**,** 587-598.

ATSDR. 2006. *Toxfaqs™ for hydrogen sulfide* [Online]. Atlanta: GA: Agency for Toxic Substances & Disease Registry. Available: http://www.atsdr.cdc.gov/toxfaqs/tf.asp?id=388&tid=67 [Accessed 23/08/13].

Auerbach, I., Miller, W.R., Kuryla, W.C. & Gehman, S.D. 1958. A diffusivity approach for studying polymer structure. *Journal of Polymer Science,* 28**,** 129-150.

Avon. 2011. *Nh15 data sheet* [Online]. Wiltshire, UK: Avon Rubber plc. Available: http://www.avon-rubber.com/Downloads/protection-row-datasheets/AVP%20NH15%20Data%20Sheet%20A4%206pp%20WEB3.pdf [Accessed 28/03/2013].

Bagreev, A., Bandosz, T.J., Adib, F. & Turk, A. 2000. Unmodified versus caustics-impregnated carbons for control of hydrogen sulfide emissions from sewage treatment plants. *Environmental Science & Technology,* 34**,** 1069-1074.

Bagreev, A., Bandosz, T.J. & Locke, D.C. 2001a. Pore structure and surface chemistry of adsorbents obtained by pyrolysis of sewage sludge-derived fertilizer. *Carbon,* 39**,** 1971-1979.

Bagreev, A., Bashkova, S., Locke, D.C. & Bandosz, T.J. 2001b. Sewage sludge-derived materials as efficient adsorbents for removal of hydrogen sulfide. *Environmental Science & Technology,* 35**,** 1537-1543.

Bagreev, A., Katikaneni, S., Parab, S. & Bandosz, T.J. 2005. Desulfurization of digester gas: Prediction of activated carbon bed performance at low concentrations of hydrogen sulfide. *Catalysis Today,* 99**,** 329-337.

Baker 1992. Activated carbon. *In:* Raymond Eller Kirk (ed.) *Kirk-othmer encyclopedia of chemical technology.* Hoboken: NJ: John Wiley & Sons, Incorporated.

Baker, R. 2012. *Membrane technology and applications*: Wiley.

Baker, R.W. 2004. *Membrane technology and applications - 2nd ed.* , Chichester, UK: John Wiley & Sons Ltd.

Bandosz, T.J. 2002. On the adsorption/oxidation of hydrogen sulfide on activated carbons at ambient temperatures. *Journal of Colloid and Interface Science,* 246**,** 1-20.

Bandosz, T.J. & Petit, C. 2009. On the reactive adsorption of ammonia on activated carbons modified by impregnation with inorganic compounds. *Journal of Colloid and Interface Science,* 338**,** 329-345.

Barascu, A., Kullmann, J., Reinhardt, B., Rainer, T., Roggendorf, H., Dubiel, M. & Enke, D. 2012. Preparation of porous glass monoliths with an aligned pore system via stretch forming. *Journal of the American Ceramic Society,* 95**,** 3013-3015.

Baraton, M.I. & Uvarova, I.V. 2001. *Functional gradient materials and surface layers prepared by fine particles technology*: Springer.

Barrett, K.E., Barman, S.M., Boitano, S. & Brooks, H. 2009. *Ganong's review of medical physiology, 23rd edition*: McGraw-Hill Publishing.

Barzin, J., Feng, C., Khulbe, K.C., Matsuura, T., Madaeni, S.S. & Mirzadeh, H. 2004. Characterization of polyethersulfone hemodialysis membrane by ultrafiltration and atomic force microscopy. *Journal of Membrane Science,* 237**,** 77-85.

Bekkum, H., Flanigen, E.M. & Jansen, J.C. 1991. *Introduction to zeolite science and practice*: Elsevier.

Bell, J.G., Angus, K., Todd, C. & Thomas, K.M. 2012. Functional hollow fiber adsorbent materials with a self-regulating composite outer layer for gas purification with energy efficient electrothermal regeneration. *Industrial & Engineering Chemistry Research,* 52**,** 1335-1351.

Berens, A.R. & Hopfenberg, H.B. 1982. Diffusion of organic vapors at low concentrations in glassy pvc, polystyrene, and pmma. *Journal of Membrane Science,* 10**,** 283-303.

Bhandari, D.A., Bessho, N. & Koros, W.J. 2010. Hollow fiber sorbents for desulfurization of natural gas. *Industrial & engineering chemistry research,* 49**,** 12038-12050.

Blanco, J., Martin, M.P., Knapp, C. & Alvarez, E. 2000. Adsorption of traces of chlorinated aromatic hydrocarbons: Design parameters for monolithic adsorbents *Environmental Engineering Science,* 17**,** 215-219.

Blomfield, G.A. & Little, L.H. 1973. Chemisorption of ammonia on silica. *Canadian Journal of Chemistry,* 51**,** 1771-1781.

Boedeker. 2013. *Material selection guide* [Online]. Texas, USA: Boedeker. [Accessed 14/5/13].

Borrelli, J. 2007. *Bioterrorism: Prevention, preparedness and protection*: Nova Science Pub Incorporated.

Britt, D., Tranchemontagne, D. & Yaghi, O.M. 2008. Metal-organic frameworks with high capacity and selectivity for harmful gases. *Proceedings of the National Academy of Sciences,* 105**,** 11623-11627.

Broehmer, M. 19/03/13 2013. *RE: Aw: 130319 - licowax s p - particle size - university of bath.* Type to Jeffs.

Brown, W.R. & Park, G.S. 1970. *Journal of Paint Technology,* 42**,** 16.

Brunauer, S., Emmett, P.H. & Teller, E. 1938. Adsorption of gases in multimolecular layers. *Journal of the American Chemical Society,* 60**,** 309-319.

BSI 2008. Respiratory protective devices - gas filter(s) and combined filter(s) - requirements, testing, marking. BSI.

Budd, P. 28/2/13 2013. *RE: Pim-1 'cylinders' email.* Type to Jeffs.

Budd, P.M., Elabas, E.S., Ghanem, B.S., Makhseed, S., McKeown, N.B., Msayib, K.J., Tattershall, C.E. & Wang, D. 2004a. Solution-processed, organophilic membrane derived from a polymer of intrinsic microporosity. *Adv. Mater.,* 16**,** 456-459.

Budd, P.M., Ghanem, B., Msayib, K., McKeown, N.B. & Tattershall, C. 2003. A nanoporous network polymer derived from hexaazatrinaphthylene with potential

as an adsorbent and catalyst support. *Journal of Materials Chemistry,* 13**,** 2721-2726.

Budd, P.M., Ghanem, B.S., Makhseed, S., McKeown, N.B., Msayib, K.J. & Tattershall, C.E. 2004b. Polymers of intrinsic microporosity (pims): Robust, solution-processable, organic nanoporous materials. *Chemical Communications,* 10**,** 230-231.

Budd, P.M., McKeown, N.B. & Fritsch, D. 2005a. Free volume and intrinsic microporosity in polymers. *Journal of Materials Chemistry,* 15**,** 1977-1986.

Budd, P.M., McKeown, N.B., Ghanem, B.S., Msayib, K.J., Fritsch, D., Starannikova, L., Belov, N., Sanfirova, O., Yampolskii, Y. & Shantarovich, V. 2008. Gas permeation parameters and other physicochemical properties of a polymer of intrinsic microporosity: Polybenzodioxane pim-1. *Journal of Membrane Science,* 325**,** 851-860.

Budd, P.M., Msayib, K.J., Tattershall, C.E., Ghanem, B.S., Reynolds, K.J., McKeown, N.B. & Fritsch, D. 2005b. Gas separation membranes from polymers of intrinsic microporosity. *Journal of Membrane Science,* 251**,** 263-269.

Busmundrud, O. 1993. Vapour breakthrough in activated carbon beds. *Carbon,* 31**,** 279-286.

Calgon. 2006. *Sulfusorb 8 impregnated granular activated carbon* [Online]. Pittsburgh, USA: Calgon Carbon Corporation. Available: http://www.calgoncarbon.com/carbon_products/documents/Sulfusorb8GAC.pdf [Accessed 11/09/2012 2012].

Callister, W.D. 2007. *Materials science and engineering: An introduction*: John Wiley & Sons.

Caretti, D.M., Scott, W.H., Johnson, A.T., Coyne, K.M. & Koh, F. 2001. Work performance when breathing through different respirator exhalation resistances. *AIHAJ - American Industrial Hygiene Association,* 62**,** 411-415.

CDC. 1994. *Documentation for immediately dangerous to life or health concentrations (idlhs)*
cyclohexane [Online]. Atlanta, GA: CDC. Available: http://www.cdc.gov/niosh/idlh/110827.html [Accessed 14/9/12].

Chemviron, C. 2013. *Chemviron carbon: Defence applications* [Online]. Feluy, Belgium: Calgon Carbon Corporation. [Accessed 03/05/13].

Cheremisinoff, N.P. 2002. *Handbook of water and wastewater treatment technologies,* Oxford, UK: Butterworth-Heinemann.

Choi, D.-Y., Lee, J.-W., Jang, S.-C., Ahn, B.-S. & Choi, D.-K. 2008. Adsorption dynamics of hydrogen sulfide in impregnated activated carbon bed. *Adsorption,* 14**,** 533-538.

Chui, S.S.-Y., Lo, S.M.-F., Charmant, J.P.H., Orpen, A.G. & Williams, I.D. 1999. A chemically functionalizable nanoporous material [cu3(tma)2(h2o)3]n. *Science,* 283**,** 1148-1150.

Chung, T.-S., Qin, J.-J. & Gu, J. 2000. Effect of shear rate within the spinneret on morphology, separation performance and mechanical properties of ultrafiltration polyethersulfone hollow fiber membranes. *Chemical Engineering Science,* 55**,** 1077-1091.

Clariant. 2012. *Licowax®, ceridust®, licolub®, licomont®, licocene®: General leaflet: Waxes* [Online]. Muttenz, Switzerland: Clariant International Ltd. Available: http://www.clariant.com/C12576850036A6E9/A958505C28F2D54EC1257A4C003F392B/$FILE/DA8048E.pdf [Accessed 08/05/2013].

Collins, J.J. 1967. The lub/equilibrium section concept for fixed-bed adsorption. *AICHE journal Chemical Engineering Progress Symposium Series,* 63**,** 31-35.
Crittenden, B. 2010. Adsorption resistances. *CE40030 Lecture Notes.* Bath: University of Bath.
Crittenden, B., Patton, A., Jouin, C., Perera, S., Tennison, S. & Echevarria, J.A.B. 2005. Carbon monoliths: A comparison with granular materials. *Adsorption,* 11**,** 537-541.
Crittenden, B.a.T., W.J. 1998. *Adsorption technology and design,* Oxford: UK: Butterworth-Heinemann.
Dangi, G., Jetwani, A., Somani, R., Bajaj, H., Jasra, R. & Sethia, G. 2010. Equilibrium and dynamic adsorption of carbon monoxide and nitrogen on zsm-5 with different sio2/al2o3 ratio separation science and technology. *Separation science and technology,* 45**,** 413-420.
Doughty, D.T., Knebel, W.J., Cobes, J.W. 1996. *Chromium-free impregnated activated universal respirator carbon for adsorption of toxic gases and/or vapors in industrial applications*. US patent application 97,423.
Dyer, A. 1988. *An introduction to zeolite molecular sieves*: J. Wiley.
Empower-Materials. 2005. *Organic pore formers* [Online]. Newark, DE: Empower Materials. Available: http://www.empowermaterials.com/download/application/organic%20pore%20formers_Apr%2005.pdf [Accessed 22/02/13].
EPA 1995. Ap-42, compilation of air pollutant emission factors.
Ergun, S. 1952. Fluid flow through packed columns. *Chemical Process Engineering,* 48**,** 89-94.
Feng, X.S., Pan, C.Y., McMinis, C.W., Ivory, J. & Ghosh, D. 1998. Hollow-fiber-based adsorbers for gas separation by pressure-swing adsorption. *AIChE journal,* 44**,** 1555-1562.
Férey, G. 2008. Hybrid porous solids: Past, present, future *Chemical Society reviews,* 37**,** 191-214.
Fortier, H., Westreich, P., Selig, S., Zelenietz, C. & Dahn, J.R. 2008. Ammonia, cyclohexane, nitrogen and water adsorption capacities of an activated carbon impregnated with increasing amounts of zncl2, and designed to chemisorb gaseous nh3 from an air stream. *Journal of Colloid and Interface Science,* 320**,** 423-435.
Garcia, C.L. & Lercher, J.A. 1992. Adsorption of h2s on zsm5 zeolites. *Journal of physical chemistry,* 96**,** 2230-2235.
Gascon, J., Aguado, S. & Kapteijn, F. 2008. Manufacture of dense coatings of cu-3(btc)(2) (hkust-1) on alpha-alumina. *Microporous and mesoporous materials,* 113**,** 132-138.
George, S.C. & Thomas, S. 2001. Transport phenomena through polymeric systems. *Progress in Polymer Science,* 26**,** 985-1017.
Golden, C.M.A., Golden, T.C. & Battavio, P.J. 2005. *Multilayered adsorbent system for gas separations by pressure swing adsorption*. US patent application.
Goodfellow. 2013. *Goodfellow on-line interactive catalog* [Online]. Huntingdon, England: Goodfellow. Available: http://www.goodfellow.com/catalogue/GFCatalogue.php?Language=A [Accessed 14/5/13].
Greathouse, J.A. & Allendorf, M.D. 2006. The interaction of water with mof-5 simulated by molecular dynamics. *Journal of the American Chemical Society,* 128**,** 10678-10679.

Grévillot, G., Marsteau, S. & Vallières, C. 2011. A comparison of the wheeler-jonas model and the linear driving force at constant-pattern model for the prediction of the service time of activated carbon cartridges. *Journal of Occupational and Environmental Hygiene,* 8**,** 279-288.

Gul-E-Noor, F., Jee, B., Poppl, A., Hartmann, M., Himsl, D. & Bertmer, M. 2011. Effects of varying water adsorption on a cu3(btc)2 metal-organic framework (mof) as studied by 1h and 13c solid-state nmr spectroscopy. *Physical Chemistry Chemical Physics,* 13**,** 7783-7788.

Guo, J., Xu, W.S., Chen, Y.L. & Lua, A.C. 2005. Adsorption of nh3 onto activated carbon prepared from palm shells impregnated with h2so4. *Journal of Colloid and Interface Science,* 281**,** 285-290.

Guo, X.J., Tak, J.K. & Johnson, R.L. 2009. Ammonia removal from air stream and biogas by a h2so4 impregnated adsorbent originating from waste wood-shavings and biosolids. *Journal of hazardous materials,* 166**,** 372-376.

Gutierrez-Sevillano, J.J., Martin-Calvo, A., Dubbeldam, D., Calero, S. & Hamad, S. 2013. Adsorption of hydrogen sulfide on metal-organics frameworks. *RSC Advances*.

Haber, J., Block, J.H. & Delmon, B. 1995. Manual of methods and procedures for catalyst characterization (technical report). *Pure and Applied Chemistry,* 67**,** 1257-1306.

Hagen, G. 1839. Ueber die bewegung des wassers in engen cylindrischen röhren. *Annalen der Physik,* 122**,** 423-442.

Haslego, C. 2010. *Hollow fiber membranes* [Online]. US: Cheresources. Available: http://www.cheresources.com/content/articles/separation-technology/hollow-fiber-membranes [Accessed 04/09/13].

Heck, R.M., Gulati, S. & Farrauto, R.J. 2001. The application of monoliths for gas phase catalytic reactions. *Chemical Engineering Journal,* 82**,** 149-156.

Helminen, J., Helenius, J., Paatero, E. & Turunen, I. 2000. Comparison of sorbents and isotherm models for nh3-gas separation by adsorption. *AIChE journal,* 46**,** 1541-1555.

Helminen, J., Helenius, J., Paatero, E. & Turunen, I. 2001. Adsorption equilibria of ammonia gas on inorganic and organic sorbents at 298.15 k. *Journal of chemical and engineering data,* 46**,** 391-399.

Hincal, F. & Erkekoglu, P. 2006. Toxic industrial chemicals (tics) - chemical warfare without chemical weapons. *Fabad J. Pharm. Sci.,* 31**,** 220-220.

HSDB. 2005. *Hazardous substances data bank: Cyclohexane* [Online]. Available: http://toxnet.nlm.nih.gov/cgi-bin/sis/search/a?dbs+hsdb:@term+@DOCNO+60 [Accessed 14/9/12].

HSDB. 2006. *Hazardous substances data bank: Ammonia* [Online]. Bethesda: MD: United States Library of Medicine. Available: http://toxnet.nlm.nih.gov/cgi-bin/sis/search/f?./temp/~sBrs5p:1 [Accessed 24/5/11].

Huang, C.C., Chen, C.H. & Chu, S.M. 2006. Effect of moisture on h2s adsorption by copper impregnated activated carbon. *Journal of hazardous materials,* 136**,** 866-873.

IUPAC. 2012. *Compendium of chemical terminology gold book* [Online]. International Union of Pure and Applied Chemistry. Available: http://goldbook.iupac.org/PDF/goldbook.pdf [Accessed 23/08/15].

Jhung, S.H., Yoon, J.W., Hwang, J.-S., Cheetham, A.K. & Chang, J.-S. 2005. Facile synthesis of nanoporous nickel phosphates without organic templates under microwave irradiation. *Chemistry of materials,* 17**,** 4455-4460.

Jonas, L.A. & Rehrmann, J.A. 1973. Predictive equations in gas adsorption kinetics. *Carbon,* 11**,** 59-64.
Jonas, L.A. & Rehrmann, J.A. 1974. The rate of gas adsorption by activated carbon. *Carbon,* 12**,** 95-101.
Kerr, G.T. & Johnson, G.C. 1960. Catalytic oxidation of hydrogen sulfide to sulfur over a crystalline aluminosilicate. *The Journal of Physical Chemistry,* 64**,** 381-382.
Kesting, R.E. 1971. *Synthetic polymeric membranes,* New York: Mc-Graw Hill.
Kim, D., Caruthers, J.M. & Peppas, N.A. 1993. Penetrant transport in crosslinked polystyrene. *Macromolecules,* 26**,** 1841-1847.
Kim, J.H. & Lee, K.H. 1998. Effect of peg additive on membrane formation by phase inversion. *Journal of membrane Science,* 138**,** 153-163.
Kusgens, P., Siegle, S. & Kaskel, S. 2009. Crystal growth of the metal-organic framework cu-3(btc)(2) on the surface of pulp fibers. *Advanced Engineering Materials,* 11**,** 93-95.
Küsgens, P., Zgaverdea, A., Fritz, H.-G., Siegle, S. & Kaskel, S. 2010. Metal-organic frameworks in monolithic structures. *Journal of the American Ceramic Society,* 93**,** 2476-2479.
Langmuir, I. 1918. The adsorption of gases on plane surfaces of glass, mica and platinum. *Journal of the American Chemical Society,* 40**,** 1361-1403.
Leatt, A. 2011. *RE: Mechanism of hydrogen sulphide adsorption on eurocarb rge and sac impregnated carbons.* Type to Jeffs.
Li, G., Singh, R., Li, D., Zhao, C., Liu, L. & Webley, P.A. 2009. Synthesis of biomorphic zeolite honeycomb monoliths with 16 000 cells per square inch. *Journal of Materials Chemistry,* 19**,** 8372-8377.
Li, N.N., Fane, A.G., Ho, W.S.W. & Matsuura, T. 2011. *Advanced membrane technology and applications*: Wiley.
Li, Y. & Yang, R.T. 2007. Gas adsorption and storage in metal−organic framework mof-177. *Langmuir,* 23**,** 12937-12944.
Li, Y.Y. 1998. *Air separation with monolithic adsorbents.* University of Bath.
Li, Y.Y., Perera, S.P. & Crittenden, B.D. 1998. Zeolite monoliths for air separation part 2: Oxygen enrichment, pressure drop and pressurization. *Chemical Engineering Research & Design,* 76**,** 931-941.
Liu, Y., Koops, G.H. & Strathmann, H. 2003. Characterization of morphology controlled polyethersulfone hollow fiber membranes by the addition of polyethylene glycol to the dope and bore liquid solution. *Journal of Membrane Science,* 223**,** 187-199.
Lodewyckx, P. & Vansant, E.F. 1999. Influence of humidity on adsorption capacity from the wheeler-jonas model for prediction of breakthrough times of water immiscible organic vapors on activated carbon beds. *American Industrial Hygiene Association Journal,* 60**,** 612-617.
Lodewyckx, P. & Vansant, E.F. 2000. Estimating the overall mass transfer coefficient kv of the wheeler-jonas equation: A new and simple model. *AIHAJ - American Industrial Hygiene Association,* 61**,** 501-505.
Lodewyckx, P. & Verhoeven, L. 2003. Using the modified wheeler–jonas equation to describe the adsorption of inorganic molecules: Chlorine. *Carbon,* 41**,** 1215-1219.
Lodewyckx, P., Wood, G.O. & Ryu, S.K. 2004. The wheeler–jonas equation: A versatile tool for the prediction of carbon bed breakthrough times. *Carbon,* 42**,** 1351-1355.
Loera-Serna, S., Oliver-Tolentino, M.A., de Lourdes López-Núñez, M., Santana-Cruz, A., Guzmán-Vargas, A., Cabrera-Sierra, R., Beltrán, H.I. & Flores, J. 2012. Electrochemical behavior of [cu3(btc)2] metal–organic framework: The effect of the method of synthesis. *Journal of Alloys and Compounds,* 540**,** 113-120.

Machado, P.S.T., Habert, A.C. & Borges, C.P. 1999. Membrane formation mechanism based on precipitation kinetics and membrane morphology: Flat and hollow fiber polysulfone membranes. *Journal of Membrane Science,* 155**,** 171-183.

Massey, B. & Ward-Smith, J. 1998. *Mechanics of fluids 7th ed.* , UK: Nelson Thornes.

McCabe, W.L., Smith, J.C. & Harriott, P. 2005. *Unit operations of chemical engineering,* New York: McGraw-Hill.

McKeown, N.B. & Budd, P.M. 2010. Exploitation of intrinsic microporosity in polymer-based materials. *Macromolecules,* 43**,** 5163-5176.

McKeown, N.B., Budd, P.M., Msayib, K.J., Ghanem, B.S., Kingston, H.J., Tattershall, C.E., Makhseed, S., Reynolds, K.J. & Fritsch, D. 2005. Polymers of intrinsic microporosity (pims): Bridging the void between microporous and polymeric materials. *Chemistry- A European Journal,* 11**,** 2610-2620.

Meeyoo, V., Lee, J.H., Trimm, D.L. & Cant, N.W. 1998. Hydrogen sulphide emission control by combined adsorption and catalytic combustion. *Catalysis Today,* 44**,** 67-72.

Meeyoo, V., Trimm, D.L. & Cant, N.W. 1997. Adsorption-reaction processes for the removal of hydrogen sulphide from gas streams. *Journal of chemical technology and biotechnology,* 68**,** 411-416.

Millward, A.R. & Yaghi, O.M. 2005. Metal−organic frameworks with exceptionally high capacity for storage of carbon dioxide at room temperature. *Journal of the American Chemical Society,* 127**,** 17998-17999.

Milton. 1959. *Molecular sieve adsorbents*. US patent application.

Mirasol, F. 2010. *Us chemical profile: Cyclohexane* [Online]. Reed Business Information Ltd. Available: http://www.icis.com/Articles/2010/12/06/9416634/us-chemical-profile-cyclohexane.html [Accessed 9/10/12 2012].

Mueller, U., Schubert, M., Teich, F., Puetter, H., Schierle-Arndt, K. & Pastre, J. 2006. Metal-organic frameworks - prospective industrial applications. *Journal of materials chemistry,* 16**,** 626-636.

Nakamura, T., Kawasaki, N., Hirata, M., Oida, Y. & Tanada, S. 2002. Adsorption of hydrogen sulfide by zinc-containing activated carbon. *Toxicological & Environmental Chemistry,* 82**,** 93-98.

Nevell, J. 2009. Development of a compact novel adsorbent hollow fibre for oxygen production: Transfer report. University of Bath.

Nevell, J. & Perera, S. 2011. Novel adsorbent hollow fibres for oxygen concentration. *Adsorption,* 17**,** 273-283.

Nickolov, R.N. & Mehandjiev, D.R. 2004. Comparative study on removal efficiency of impregnated carbons for hydrogen cyanide vapors in air depending on their phase composition and porous textures. *Journal of Colloid and Interface Science,* 273**,** 87-94.

NIOSH 2010. *Niosh pocket guide to chemical hazards,* Atlanta: GA: CDC.

Omata, K., Mazaki, H., Yagita, H. & Fujimoto, K. 1990. Preparation of nickel-on-active carbon catalyst by cvd method for methanol carbonylation. *Catalysis Letters,* 4**,** 123-127.

Omnexus. 2013. *Polymer properties* [Online]. SpecialChem. Available: http://www.omnexus.com/tc/polymerselector/polymerprofiles.aspx [Accessed 15/03/13].

Pan, C.Y. & McMinis, C.W. 1992. *Hollow fiber bundle element*. Canada patent application.

Patcas, F.C., Garrido, G.I. & Kraushaar-Czarnetzki, B. 2007. Co oxidation over structured carriers: A comparison of ceramic foams, honeycombs and beads. *Chemical Engineering Science,* 62**,** 3984-3990.

Patton, A., Crittenden, B.D. & Perera, S.P. 2004. Use of the linear driving force approximation to guide the design of monolithic adsorbents. *Chemical Engineering Research and Design,* 82**,** 999-1009.

Pelfrey, S. 2011. The dual cavity respirator - an alternative to paprs. University of Bath.

Perera, S.P. & Tai, C.C. 2009. *Hollow fibres*. United States patent application 20090305871.

Peterson, G. 2008. Evaluation of mof-74, mof-177, and zif-8 for the removal of toxic industrial chemicals. Edgewood.

Peterson, G.W., Wagner, G.W., Balboa, A., Mahle, J., Sewell, T. & Karwacki, C.J. 2009. Ammonia vapor removal by cu3(btc)2 and its characterization by mas nmr. *The Journal of Physical Chemistry C,* 113**,** 13906-13917.

Petit, C. & Bandosz, T.J. 2009. Mof–graphite oxide composites: Combining the uniqueness of graphene layers and metal–organic frameworks. *Advanced Materials,* 21**,** 4753-4757.

Petit, C. & Bandosz, T.J. 2012. Exploring the coordination chemistry of mof-graphite oxide composites and their applications as adsorbents. *Dalton Transactions,* 41**,** 4027-4035.

Petit, C., Karwacki, C., Peterson, G. & Bandosz, T.J. 2007. Interactions of ammonia with the surface of microporous carbon impregnated with transition metal chlorides. *The Journal of Physical Chemistry C,* 111**,** 12705-12714.

Petit, C., Mendoza, B. & Bandosz, T.J. 2010. Hydrogen sulfide adsorption on mofs and mof/graphite oxide composites. *Chemphyschem,* 11**,** 3678-84.

Pichon, A. & James, S.L. 2008. An array-based study of reactivity under solvent-free mechanochemical conditions-insights and trends. *CrystEngComm,* 10**,** 1839-1847.

Poiseuille 1846. *Recherches expérimentales sur le mouvement des liquides dans les tubes de très-petits diamètres,* Paris.

Polcaro, A.M., Palmas, S. & Dernini, S. 1993. Role of catalyst characteristics in electrocatalytic hydrogenation: Reduction of benzaldehyde and acetophenone on carbon felt/palladium electrodes. *Industrial & Engineering Chemistry Research,* 32**,** 1315-1322.

Potoczna-Petru, D. & Krajczyk, L. 1995. Microstructure evolution of co particles supported on carbon induced by oxidation-reduction treatment. *Journal of Materials Science Letters,* 14**,** 1294-1297.

Pritchard, J.D. 2011. *Hpa compedium of chemical hazards: Ammonia* [Online]. London, UK: Health Protection Agency. Available: http://www.hpa.org.uk/webc/HPAwebFile/HPAweb_C/1194947367219 [Accessed 14/9/12 2012].

Qin, J.-J. & Chung, T.-S. 2004. Effects of orientation relaxation and bore fluid chemistry on morphology and performance of polyethersulfone hollow fibers for gas separation. *Journal of Membrane Science,* 229**,** 1-9.

Qin, J.-J., Wang, R. & Chung, T.-S. 2000. Investigation of shear stress effect within a spinneret on flux, separation and thermomechanical properties of hollow fiber ultrafiltration membranes. *Journal of Membrane Science,* 175**,** 197-213.

Radovic, L.R. & Rodriguez-Reinoso, F. 1997. *Carbon materials in catalysis,* New York: Dekker.

Rajhans, G.S., Bhawani, P. Patak 2002. *Practical guide to respirator usage in industry,* USA: Butterworth-Heinemann.

Rakow, N.A., Wendland, M.S., Trend, J.E., Poirier, R.J., Paolucci, D.M., Maki, S.P., Lyons, C.S. & Swierczek, M.J. 2010. Visual indicator for trace organic volatiles. *Langmuir,* 26**,** 3767-3770.

Ren, X.H., Stapf, S. & Blümich, B. 2005. Magnetic resonance visualisation of flow and pore structure in packed beds with low aspect ratio. *Chemical Engineering & Technology,* 28**,** 219-225.

Rezaei, F. & Webley, P. 2009. Optimum structured adsorbents for gas separation processes. *Chemical Engineering Science,* 64**,** 5182-5191.

Rezaei, F. & Webley, P. 2010. Structured adsorbents in gas separation processes. *Separation and Purification Technology,* 70**,** 243-256.

Rhodes, M. 2008. *Introduction to particle technology*: Wiley.

Richardson, J.F., Harker, J.H. & Backhurst, J.R. 2002. *Coulson and richardson's chemical engineering volume 2 - particle technology and separation processes (5th edition),* Amsterdam: Elsevier.

Rouquerol, J., Rouquerol, F. & Sing, K. 1999. *Absorption by powders and porous solids: Principles, methodology and applications*: Elsevier Science & Technology.

Rousseau, R.W. 1987. Handbook of separation process technology. John Wiley & Sons.

Ruthven, D.M. 2000. *Adsorption, fundamentals*: John Wiley & Sons, Inc.

Ruthven, D.M. & Thaeron, C. 1996. Performance of a parallel passage adsorbent contactor. *Gas Separation & Purification,* 10**,** 63-73.

Schneider, W. & Diller, W. 2000. Phosgene. *Ullmann's encyclopedia of industrial chemistry*. Wiley-VCH Verlag GmbH & Co. KGaA.

Schubert, M., Mueller, U., Hesse, M. & Diehlmann, U. 2012. *Process for preparing porous metal-organic framework materials*. United States patent application 8115024.

Schüth, F., Sing, K.S.W. & Weitkamp, J. 2002. *Handbook of porous solids,* Weinheim: Wiley-VCH.

Schweitzer, P.A. 1997. *Handbook of separation techniques for chemical engineers,* New York ; London: McGraw-Hill.

Scott-Safety. 2011. *General service respirator english brochure* [Online]. Lancashire, UK: Scott Safety. Available: https://www.scottsafety.com/en/emea/DocumentandMedia1/Marketing/ProductLiteratureandCatalogs/Brochures/GSR_Brochure_English_72dpi.pdf [Accessed 22/02/13].

Seader, J.D., Henley, E.J. & Roper, D.K. 1998. *Separation process principles*: John Wiley & Sons.

Seader, J.D., Henley, E.J. & Roper, D.K. 2010. *Separation process principles*: John Wiley & Sons.

Shirazi, L., Jamshidi, E. & Ghasemi, M.R. 2008. The effect of si/al ratio of zsm-5 zeolite on its morphology, acidity and crystal size. *Crystal Research and Technology,* 43**,** 1300-1306.

Singh, B., Saxena, A., Srivastava, A.K. & Vijayaraghavan, R. 2009. Impregnated carbon based catalyst for protection against carbon monoxide gas. *Applied Catalysis B: Environmental,* 88**,** 257-262.

Smith, J.W.H., Westreich, P., Smith, A.J., Fortier, H., Croll, L.M., Reynolds, J.H. & Dahn, J.R. 2010. Investigation of copper oxide impregnants prepared from various precursors for respirator carbons. *Journal of Colloid and Interface Science,* 341**,** 162-170.

Smith, M.W. 2011. Activated carbon for military respiratory protection – past, present and future. University of Bath.

Solvay. 2011. *Radel®, veradel®, acudel® design guide – english [online]* [Online]. USA: Solvay Plastics. Available: http://www.solvayplastics.com/sites/solvayplastics/EN/Solvay%20Plastics%20Literature/DPG_Radel_Veradel_Acudel_Design_Guide_EN.pdf [Accessed 15/06/2012].

Stern, S.A. & Trohalaki, S. 1990. Fundamentals of gas diffusion in rubbery and glassy polymers. *Barrier polymers and structures.* American Chemical Society.

Sullivan, J.B. & Krieger, G.R. 1992. *Hazardous materials toxicology: Clinical principles of environmental health*: Williams & Wilkins.

Suzin, Y., Nir, I. & Kaplan, D. 2000. The effect of flow pattern on adsorption of dimethyl methyl phosphonate in activated carbon beds and canisters. *Carbon,* 38**,** 1129-1133.

Tamon, H., Kitamura, K. & Okazaki, M. 1996. Adsorption of carbon monoxide on activated carbon impregnated with metal halide. *AIChE journal,* 42**,** 422-430.

Tao, W., Yang, T., Chang, Y., Chang, L. & Chung, T. 2004. Effect of moisture on the adsorption of volatile organic compounds by zeolite. *Journal of Environmental Engineering,* 130**,** 1210-1216.

Tolles, E.D. 1989. *Method and apparatus for removing cyanogen chloride from air*. US patent application.

ToolingU. 2012. *Materials training: Principles of injection molding 255* [Online]. Available: http://www.toolingu.com/definition-500255-54083-molecular-orientation.html [Accessed 20/05/13].

Tucker, J. 2007. *War of nerves : Chemical warfare from world war i to al qaeda,* New York: Anchor Books.

Ulbricht, M. 2006. Advanced functional polymer membranes. *Polymer,* 47**,** 2217-2262.

van Bekkum, H. 2001. *Introduction to zeolite science and practice*: Elsevier.

Verhoeven, L. & Lodewyckx, P. 2001. Using the wheeler-jonas equation to describe adsorption of inorganic molecules: Ammonia.

Verschueren, K. 2001. Handbook of environmental data on organic chemicals (4th edition). John Wiley & Sons.

Wheeler, A. & Robell, A.J. 1969. Performance of fixed-bed catalytic reactors with poison in the feed. *Journal of Catalysis,* 13**,** 299-305.

Wickramasinghe, S.R., Semmens, M.J. & Cussler, E.L. 1992. Mass transfer in various hollow fibre geometries. *Journal of Membrane Science,* 69**,** 235-250.

Williams, J.L. 2001a. Monolith structures, materials, properties and uses. *Catalysis Today,* 69**,** 3-9.

Williams, J.L. 2001b. Monolith structures, materials, properties and uses. *Catalysis Today,* 69**,** 3-9.

Winterberg, M. & Tsotsas, E. 2000. Impact of tube-to-particle-diameter ratio on pressure drop in packed beds. *AIChE Journal,* 46**,** 1084-1088.

Wood, G.O. & Lodewyckx, P. 2003. An extended equation for rate coefficients for adsorption of organic vapors and gases on activated carbons in air-purifying respirator cartridges. *AIHA Journal,* 64**,** 646-650.

Wood, G.O. & Moyer, E.S. 1989. A review of the wheeler equation and comparison of its applications to organic vapor respirator cartridge breakthrough data. *American Industrial Hygiene Association Journal,* 50**,** 400-407.

Wood, G.O. & Stampfer, J.F. 1993. Adsorption rate coefficients for gases and vapors on activated carbons. *Carbon,* 31**,** 195-200.

Wu, L.-C., Chang, T.-H. & Chung, Y.-C. 2007. Removal of hydrogen sulfide and sulfur dioxide by carbons impregnated with triethylenediamine. *Journal of the Air & Waste Management Association,* 57**,** 1461-1468.

Xu, Z.-L. & Alsalhy Qusay, F. 2004. Polyethersulfone (pes) hollow fiber ultrafiltration membranes prepared by pes/non-solvent/nmp solution. *Journal of Membrane Science,* 233**,** 101-111.

Yaghi, O.M., O'Keeffe, M., Ockwig, N.W., Chae, H.K., Eddaoudi, M. & Kim, J. 2003. Reticular synthesis and the design of new materials. *Nature,* 423**,** 705-714.

Yang, R.T. 1997. *Gas separation by adsorption processes*: Imperial College Press.

Yu, D., Ghosh, P. & Snurr, R.Q. 2012. Hierarchical modeling of ammonia adsorption in functionalized metal-organic frameworks. *Dalton Transactions,* 41**,** 3962-3973.

Yuan, W., Garay, A.L., Pichon, A., Clowes, R., Wood, C.D., Cooper, A.I. & James, S.L. 2010. Study of the mechanochemical formation and resulting properties of an archetypal mof: Cu3(btc)2 (btc = 1,3,5-benzenetricarboxylate). *CrystEngComm,* 12**,** 4063-4065.

Zacher, D., Shekhah, O., Woll, C. & Fischer, R.A. 2009. Thin films of metal-organic frameworks. *Chemical Society reviews,* 38**,** 1418-1429.

Zhao, X.S., Ma, Q. & Lu, G.Q.M. 1998. Voc removal: Comparison of mcm-41 with hydrophobic zeolites and activated carbon. *Energy & fuels,* 12**,** 1051-1054.

12 Appendices

12.1 Appendix 1

12.1.1 Breakthrough curves for ammonia adsorbent screening tests

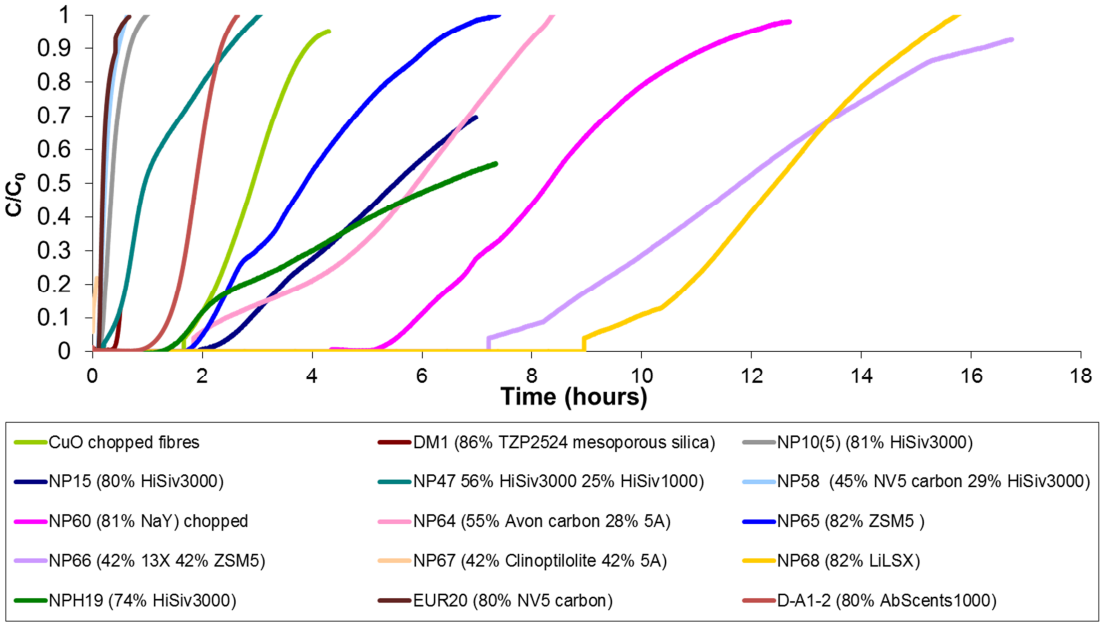

Figure 12.1. 800 ppm 1 L/min dynamic tests with ammonia to screen and select adsorbents

12.1.2 Breakthrough curves for hydrogen sulphide adsorbent screening tests

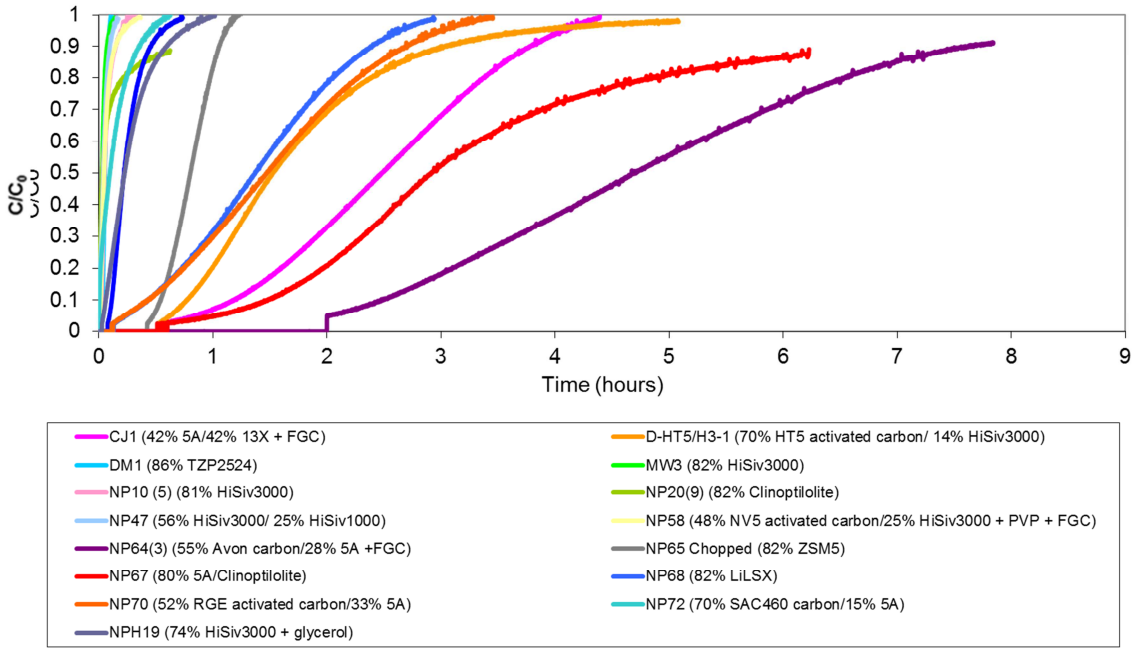

Figure 12.2. 800 ppm 1 L/min dynamic tests with hydrogen sulphide to screen and select adsorbents

12.1.3 Breakthrough curves for cyclohexane adsorbent screening tests

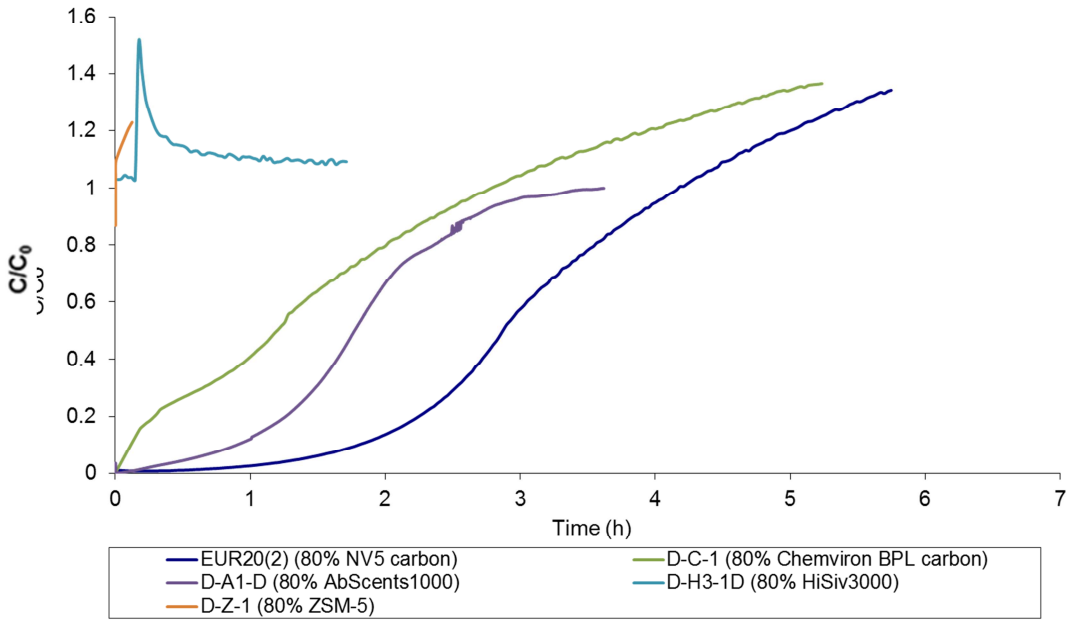

Figure 12.3. Dynamic tests with cyclohexane, showing problem with FID sensor resulting in C/C0 > 1.

12.2 Appendix 2

12.2.1 Calculation of Reynolds numbers

Viscosity of nitrogen at room temperature and 1 atm:	1.840×10^{-5} Pa.S
Fluid density of nitrogen at room temperature and 1 atm:	1.185 kg/m^3
Area of the column (2 cm diameter):	3.142×10^{-4} m^2
Area of a single standard bore hollow fibre (1 mm diameter):	7.854×10^{-7} m^2
Area of 45 standard bore hollow fibres (1mm diameter):	3.534×10^{-5} m^2

The test module is a 5 cm long cylindrical stainless steel pipe with a 2 cm diameter. When testing pressure drop, nitrogen gas is used at a range of flow rates. The granular bed is made up of granules approximately 1 mm, with a voidage of 0.4 (Richardson *et al.*, 2002). As an example, we will consider flow rates of 0.5 L/min and 100 L/min as examples of high and low. The fluid density of nitrogen at room temperature is 1.185 kg/m^3 and its viscosity is 1.840×10^{-5} Pa.S. For an empty column, superficial velocity must be calculated. For 0.5L/min:

$0.5 / 1000 / 60 = 8.33 \times 10^{-6}$ m^3/sec

The superficial velocity = u = Q/A where A is the cross sectional area (m^2)

In this case, the diameter is 2cm = 0.02m. Cross sectional area = $\pi r^2 = \pi \times 0.01^2 = 0.0001 \pi$ m^2

$u = 8.33 \times 10^{-6} / 0.0001 \pi$

u = 0.0265 m/s (for 0.5 L/min)

$$Re = \frac{1.185 \times 0.0265 \times 0.020}{1.840 \times 10^{-5}} = 34.13$$

34.13 is significantly less than 2300, and so flow through the empty module is laminar at 0.5 L/min.

Using the same calculations as above, u = 5.305 m/s for 100 L/min flow rate. In this case, Re = 6833. This is greater than 4000 and so flow is fully turbulent. Transitional flow occurs when the flow rate is 1.786 m/s (just over 30 L/min) in an empty module of 2cm diameter.

Granular bed

For a granular bed:

$$Re = \frac{1.185 \times 0.03 \times 0.02}{(1.840 \times 10^{-5}) \times (1 - 0.4)} = 56.94$$

Re = 56.94 which is lower than 2000, so for a granular bed of this voidage at a flow rate of 0.5 L/min, flow is laminar. However, at 100 L/min, Re becomes 11388, which is fully turbulent. Transition from laminar to transitional occurs at ~20 L/min

Hollow fibres

For the 'standard' bore hollow fibres, the diameter of each fibre bore is 1 mm (or 0.001m). When considering the superficial velocity in this case, assuming the gas flows only through fibre lumen (of which there are ~45), the area available for gas flow is 45 x $0.0005^2\pi$ = 0.00001125 π = 3.534×10^{-5} m^2. As such following the working above, the superficial velocity at 0.5 L/min is 0.236 m/s, and at 100 L/min is 47.157 m/s. As only the fibre lumen area is available for gas flow, the 'diameter' for the Reynolds equation is taken as 1 mm (the fibre lumen diameter).

$$Re = \frac{1.185 \times 0.236 \times 0.001}{(1.840 \times 10^{-5})} = 15.185$$

By the same principle, at 100 L/min, Re = 3037. The lower value is significantly below 2300, meaning flow will be laminar at low flow rates. At 100 L/min, the flow rate is in a transition between laminar and turbulent. In fact, using this system, flow does not become fully turbulent until the flow rate reaches 141 L/min.

12.3 Appendix 3

12.3.1 Sample breakthrough curve calculations

This Section works through a sample calculation for 5cm Chemviron BPL granules, challenged under dynamic conditions with 800 ppm 1L/min H_2S. The breakthrough curve is shown in Figure 12.4.

c_0=800 ppm

To work out total loading in the module (g), c_0 must be in g/m^3

By ideal gas law:

PV = nRT

n=PV/RT

P = pressure (pascals)
V= volume (m^3)
n= number of moles (mol)
R= gas constant 8.314
T= temperature (K)

In this experiment:

800 ppmv = 800 cm^3/m^3

To convert this into g/m^3

P = 1 x 10^5 pascals
V= 1cm^3 = 1x10^{-6} m^3
n= number of moles
R= 8.314 J/K/mol
T= 296.15 K
Molecular weight of H_2S = 34.081 g/mol

n = (1x10^5)(1x10^{-6}) /(8.314 x 296.15) = 4.06 x 10^{-5} mol/cm^3

Mw of hydrogen sulphide = 34.081 g/mol

1 cm^3 of H_2S weighs 34.081 x 4.06x10^{-5} = 0.0014 g

For 800 cm^3/m^3, c_0= 800 x 0.0014 = 1.11 g/m^3

Carbon granules are 100% sorbent with no binder, therefore adsorbent weight = 9.93g.

Table 12.1. Section from calculations for 5cm Chemviron BPL challenged with 800ppm 1L/min H_2S.

t (s)	t (h)	Concentration (ppm)	c/c_0	Area under the graph between t_n and $t_{(n-1)}$
$=t_1$	$= t_1/3600$	$=c_1$	$=c_1/c_0$	
$=t_2$	$= t_2/3600$	$=c_2$	$=c_2/c_0$	$=0.5 \times (t_2-t_1)\times ((c/c_0)_1+(c/c_0)_2)$
$=t_n$	$= t_n/3600$	$=c_n$	$=c_n/c_0$	$=0.5 \times (t_n-t_{n-1})\times ((c/c_0)_n+(c/c_0)_{(n-1)})$
7045	1.956944	786	0.9825	0.001364
7050	1.958333	786	0.9825	0.001365
7055	1.959722	786	0.9825	0.001365
7060	1.961111	784	0.98	0.001363
7065	1.9625	785	0.98125	0.001362
7070	1.963889	787	0.98375	0.001365
7075	1.965278	786	0.9825	0.001365
7080	1.966667	786	0.9825	0.001365

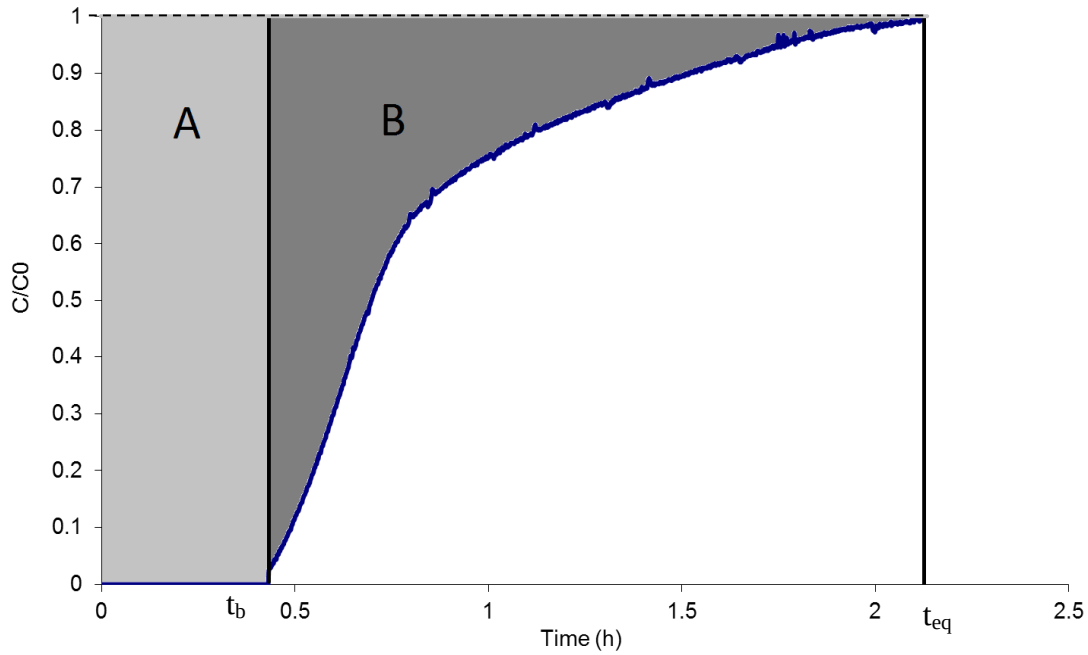

Figure 12.4. Dynamic challenge of Chemviron BPL granules with 800ppm H_2S at 1L/min.

Breakthrough loading of the module (g) is equivalent to shaded area A in Figure 12.4.

To calculate breakthrough loading:

t_b= 0.43 hours

Total area under graph at breakthrough = 1.74×10^{-5}

Loading at breakthrough (g) = Flow rate (m^3/min) x c_0 (g/m^3) x (area above graph at breakthrough time – area under graph at breakthrough time)

where area above is determined by the area of a square t_bx1 on Figure 12.4 and area beneath the graph is determined by trapezoidal rule up to t_b

$$\int_0^T f(t)dt \approx (t_2 - t_1) \times \left(\left(\frac{c}{c_0} \right)_1 + \left(\frac{c}{c_0} \right)_2 \right)$$

where t_2 and t_1 are times at 5 second intervals and $(c/c_0)_2$ and $(c/c_0)_1$ their respective concentration/initial concentration.

Loading at breakthrough (g) = 0.001 x 1.11 x (25.8-1.74×10^{-5}) = 0.029g in a module

Loading at breakthrough (%wt) = 0.029/9.93 *100 = 0.29% wt

Equilibrium loading of the module (g) is proportional to shaded area A + B in Figure 12.4.

To calculate equilibrium loading:

t_{eq}= 2.12 hours

Area under graph at equilibrium = 1.28

Loading at equilibrium (g) = Flow rate (m^3/min) x c_0 (g/m^3) x (total area of graph at equilibrium time – area under graph at equilibrium time)

Where area above is determined by the area of a square t_{eq}x1 on Figure 12.4 and area beneath the graph is determined by trapezoidal rule up to t_{eq} as above.

Loading at equilibrium (g) = 0.001 x 1.11 x (127.2-1.28) = 0.056g in a module

Loading at equilibrium (%wt) = 0.056/9.93*100 = 0.57% wt

12.4 Appendix 5

12.4.1 Hollow fibre spinning conditions

Table 12.2. List of the composition and spinning conditions of hollow fibres used in this report. SmB = Small bore. StB = Standard bore. Fibres marked with a * were prepared by Thomas Richards.

Fibre name	Adsorbent	Polymer: adsorbent wt ratio	Polymer : solvent wt ratio	Air gap (cm)	Bore fluid %NMP	Single/ double layer	Bore diameter
NP09 (38)*	13X	18 PESF: 82 13X	19.4 : 80.6	0	30	Double	SmB
NP20 (8)*	Clinoptilolite	18 PESF: 82 Clinoptilolite	1 : 4	"	50	"	"
NP60*	NaY	18.75 PESF : 81.25 NaY	14.4 : 85.6	"	0	"	"
NP61*	NaY/13X	20 PESF : 47.9 NaY: 32.1 13X	17.4 : 82.6	"	50	"	"
NP62*	Clinoptilolite/13X	15 PESF : 68.3 Clinoptilolite: 16.7 13X	18.5 : 81.5	"	60	"	"
NP63*	5A	16 PESF : 84 5A	16 : 84	"	50	"	"
NP63 (2)*	5A/13X	16 PESF : 42 5A: 42 13X	16 : 84	"	"	"	"
NP64*	Avon carbon/5A	17 PESF: 55 Avon: 28 5A	17 : 83	"	"	"	"
NP64 (3)	Avon/5a/hydrocerol BIH	17 3000P: 55 Avon: 28 5A	15 : 85	"	"	"	"
NP65*	ZSM-5	18 PESF: 82 ZSM-5	20 : 80	3.5	"	"	"
NP66*	ZSM-5/13X	16 PESF: 42 13x: 42 ZSM-5	20 : 80	0 and 3	"	"	"
NP67*	5A/Cli	16 PESF: 42 Cli: 42 5A	20 : 80	0	"	"	"
NP68	Zeosorb 2100 (LiLSX)	18 PESF: 82 LiLSX	20 : 80	"	"	"	"
NP69	Zeosorb 62 (13X)	18 PESF: 82 13X	18 : 82	3	"	"	"
NP70	RGE12X20 carbon/5A	15 3000P: 52 RGE: 33 5A	13 : 87	0	50	Double	"
NP72	SAC460 carbon/ 5A	15 3000P: 70 sac460: 15 5A	17 : 83	"	"	"	"

13X standard bore*	13X	18 PESF : 82 13X	19.4 : 80.6	“	“	“	“
13X small bore*	13X	18 PESF : 82 13X	19.4 : 80.6	“		“	“
CJ1	5A/13X/fine grain cellulose	15 PESF : 42.5 5A: 42.5 13X 5A	16 : 84	“	“	“	“
CJ2	Zeosorb 2210/fine grain cellulose	15 PESF: 85 Zeosorb 2210 + 1% cellulose fine grain sieved to 35 microns	15 : 85	“	“	“	“
CJ3	5A/fine grain cellulose	14.85 PESF : 84.15% 5A: 1 Fine grain cellulose sieved to 35 microns	16 : 84	“	“	“	“
CJ4	Zeosorb 2100 (LiLSX)/MOF-199 powder	15 3000P: 75 LiLSX : 10 MOF-199	18 : 82	5/0	30	Single	“
RLB-CO21*	13X	11 PESF: 86 13X: 2.5 Micropore C	12 : 88	“	“	“	“
RLB-CO22*	13X	12 PESF: 87 13X: 1.2 Cellulose fine grain	12.2 : 87.8	“	“	“	“
NP10(5)*	HiSiv3000	19 PESF: 81 HiSiv3000		“	“	“	StB
NP47*	HiSiv1000/HiSiv3000	19PESF : 25 HiSiv1000 : 56 HiSiv3000	18 : 82	“	“	“	SmB
NP58(3)*	NV5 carbon/HiSiv3000/PVP10/PVP58 +2% fine grain cellulose	18 PESF 48 NV5: 29HISIV3000: 2PVP10: 3PVP58	13 : 87	2	“	“	“
DM1	TZP2524 (mesoporous silica)	14 3000P: 86 TZP2524	16 : 84	0	“	“	“
DHT5/H3-1	HT5 12x20 carbon	16 3000P:70 HT5 :14 HiSiv3000	13 : 87	“	“	“	“
EUR20	NV5 carbon	20 3000P : 80 NV5 carbon	15 : 85	“	“	“	“
EUR30	NV5 carbon	30 3000P : 80 NV5 carbon	15 : 85	“	“	“	“
D-H3-1*	HiSiv3000 + micropore	18 PESF: 82 HiSiv3000	15 : 85	0	“	Single/ double	StB

	C						
D-EUR20-1	NV5 carbon	20 PES: 80 NV5 carbon	14 : 86	0	“	Single/ double	StB/SmB
D-A1-1	AbScents 1000	20 PES: 80 AbScents1000	12.5 : 87.5	0	“	Single/ double	StB
D-EURA1-1	NV5 carbon/ AbScents 1000	20 PES: 40 NV5 carbon: 40 AbScents1000	12.5 : 87.5	0	“	Single/double	StB

12.5 Appendix 6

12.5.1 BSI respirator gas filter regulations

Table 12.3. Test conditions and gas capacity required of A, B, E and K gas filters (note 1, 2, 3 refer to level of protection, with 3 as the highest) (BSI, 2008).

Type and class	Test gas	Minimum breakthrough time at test condition	Test gas concentration in air		Breakthrough concentration
		min	% by volume	mg/l	ml/m^3
A 1	Cyclohexane (C_6H_{12})	70	0,1	3,5	10
B 1	Chlorine (Cl_2)	20	0,1	3,0	0,5
	Hydrogen sulphide (H_2S)	40	0,1	1,4	10
	Hydrogen cyanide (HCN)	25	0,1	1,1	10 [a]
E 1	Sulphur dioxide (SO_2)	20	0,1	2,7	5
K 1	Ammonia (NH_3)	50	0,1	0,7	25
A 2	Cyclohexane (C_6H_{12})	35	0,5	17,5	10
B 2	Chlorine (Cl_2)	20	0,5	15,0	0,5
	Hydrogen sulphide (H_2S)	40	0,5	7,1	10
	Hydrogen cyanide (HCN)	25	0,5	5,6	10 [a]
E 2	Sulphur dioxide (SO_2)	20	0,5	13,3	5
K 2	Ammonia (NH_3)	40	0,5	3,5	25
A 3	Cyclohexane (C_6H_{12})	65	0,8	28,0	10
B 3	Chlorine (Cl_2)	30	1,0	30,0	0,5
	Hydrogen sulphide (H_2S)	60	1,0	14,2	10
	Hydrogen cyanide (HCN)	35	1,0	11,2	10 [a]
E 3	Sulphur dioxide (SO_2)	30	1,0	26,6	5
K 3	Ammonia (NH_3)	60	1,0	7,0	25

[a] C_2N_2 may sometimes be present in the effluent air. The total concentration of (C_2N_2 + HCN) shall not exceed 10 ml/m^3 at breakthrough.

12.6 Appendix 7

12.6.1 Example calculations for Wheeler-Jonas equation: ammonia

The Wheeler-Jonas equation is:

$$t_b = \frac{M.W_e}{Q.c_{in}} - \frac{W_e.p_b}{k_v.c_{in}}.\ln\frac{c_{in}-c_{out}}{c_{out}} \quad (27)$$

(Jonas and Rehrmann, 1973; Wheeler and Robell, 1969)

where

t_b= breakthrough time to reach c_{out} (min)

M= weight of carbon bed (g)

W_e = equilibrium adsorption capacity (g/g carbon)

Q = volumetric flow rate (g/cm^3)

p_b = bulk density of carbon bed (g carbon/cm^3)

k_v = overall adsorption rate coefficient (min^{-1})

c_{in}=contaminant concentration in air (g/cm^3)

The weights of the different length hybrid single layer fibres with SP pore former and their breakthrough times are shown in Table 12.4. These are plotted in Figure 12.4.

Table 12.4. Breakthrough time for 800 ppm 1 L/min ammonia challenge on single layer hybrid fibres with SP pore former.

Fibre	Length (cm)	Weight (g)	Breakthrough time (h)
DEURA1S 10	10	8.65	2.34
DEURA1S 15	15	11.82	3.12
DEURA1S 20	20	16.04	4.43

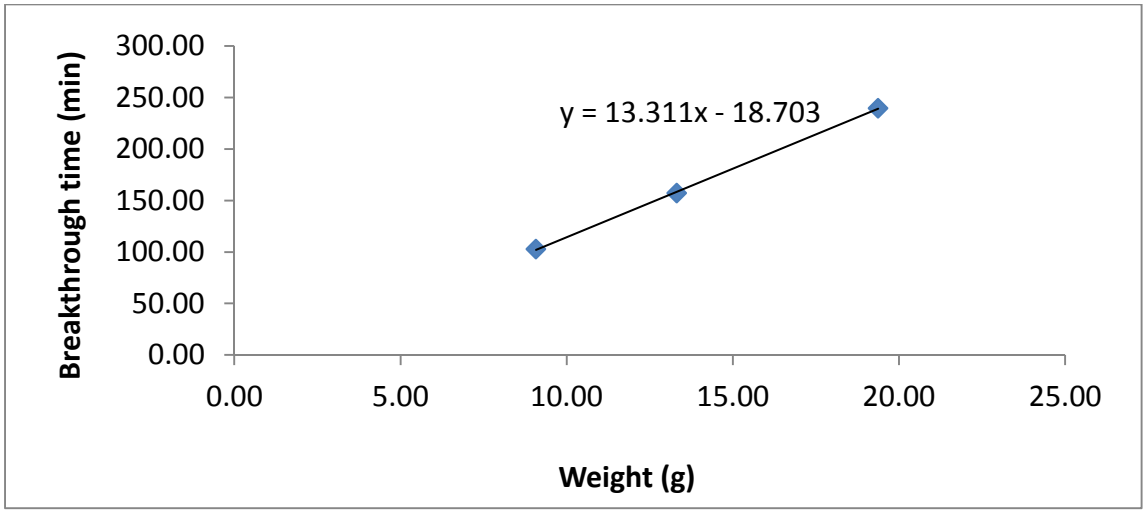

Figure 12.5. Breakthrough time against weight for 800 ppm 1 L/min ammonia on single layer hybrid fibres with SP pore former.

The slope of the graph is 13.311 and the intercept is -18.703. Using these values, with density of a 10 cm module:

$$W_e = m_1 . Q . C_0$$

$$W_e = 13.311 \times 1000 \times (5.53 \times 10^{-7}) = 0.0074$$

$$k_v = \frac{\rho_b . W_e}{c . C_0} \ln \frac{C_0}{C_x}$$

$$k_v = \frac{0.29 \times 0.0074}{(-18.703 \times 5.53 \times 10^{-7})} \ln \frac{5.53 \times 10^{-7}}{1.73 \times 10^{-8}} = 712.46$$

These values can then be substituted into the Wheeler-Jonas equation.

$$t_b = \frac{9.07 \times 0.0074}{1000 \times 5.53 \times 10^{-7}} - \frac{0.0074 \times 0.29}{712.46 \times 5.53 \times 10^{-7}} \times \ln \frac{5.53 \times 10^{-7} - 1.73 \times 10^{-8}}{1.73 \times 10^{-8}} = 102.26$$

In this case, the measured breakthrough time is 102.83 minutes. The difference is ((102.83-102.26)/102.83) x 100 = 0.56%.

12.6.2 Example calculations for Wheeler-Jonas equation: cyclohexane

The flow rates of the different length hybrid single layer fibres with SP pore former and their breakthrough times are shown in Table 12.5. These are plotted in Figure 12.4. In this case, breakthrough time was corrected for weight variations, by dividing the breakthrough time by weight.

Table 12.5. Breakthrough time for 1000 ppm 1 L/min cyclohexane challenge on single layer hybrid fibres with SP pore former.

Fibre	Length (cm)	Weight (g)	Breakthrough time (h)
DEURA1S SP 10	1	9.44	3.76
DEURA1S SP 10	1.5	9.00	1.92
DEURA1S SP 10	2	9.16	1.30

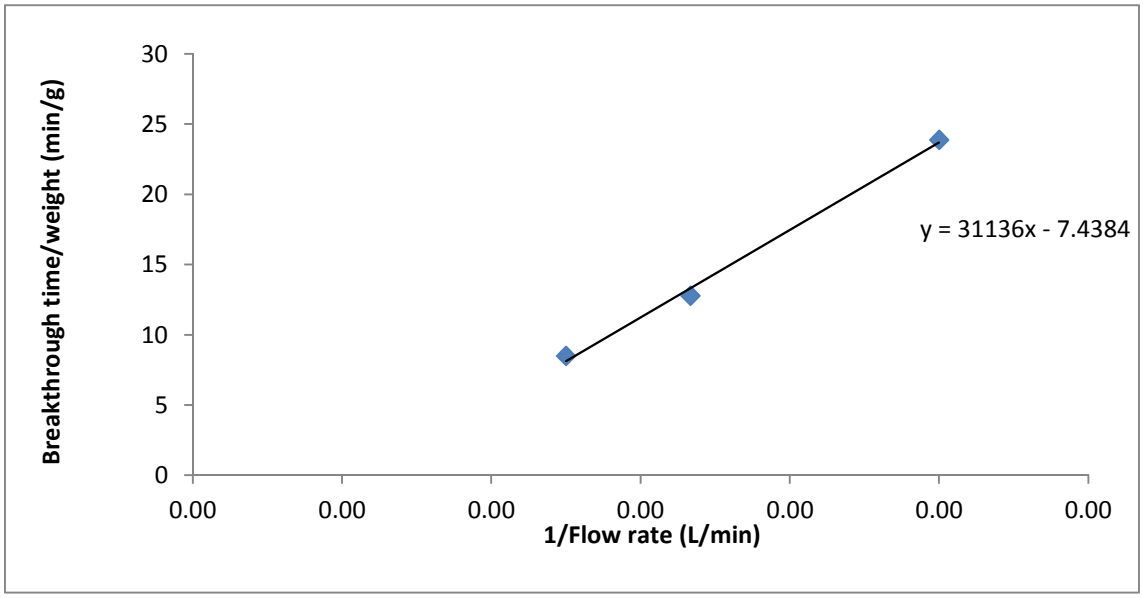

Figure 12.6. Breakthrough time corrected for weight against 1/flow rate for 1000 ppm 1 L/min cyclohexane on single layer hybrid fibres with SP pore former.

Using data for the 10 cm fibre:

$$W_e = \frac{m_2 . C_0}{M}$$

$$W_e = \frac{31136 \times 3.42 \times 10^{-6}}{9.44} = 0.012$$

$$k_v = \frac{\rho_b . W_e}{c . C_0} \ln \frac{C_0}{C_x}$$

$$k_v = \frac{0.3 \times 0.012}{-7.4384 \times 3.42 \times 10^{-6}} \ln \frac{3.42 \times 10^{-6}}{3.42 \times 10^{-8}} = 629$$

Putting these into the Wheeler-Jonas equation:

$$t_b = \frac{9.44 \times 0.012}{Q \times 3.42 \times 10^{-6}} - \frac{0.012 \times 0.3}{629 \times 3.42 \times 10^{-6}} \times \ln \frac{3.42 \times 10^{-6} - 3.42 \times 10^{-8}}{3.42 \times 10^{-8}}$$
$$= 23.71$$

The predicted breakthrough time is 23.71 min/g or 223.76 minutes, and the observed breakthrough time was 23.88 min/g or 225.33 minutes, meaning the difference is 0.7%.